

University of Windsor

## Scholarship at UWindor

---

Electronic Theses and Dissertations

Theses, Dissertations, and Major Papers

---

5-11-2018

# Machine Learning based Early Fault Diagnosis of Induction Motor for Electric Vehicle Application

Eshaan Ghosh  
*University of Windsor*

Follow this and additional works at: <https://scholar.uwindsor.ca/etd>

---

### Recommended Citation

Ghosh, Eshaan, "Machine Learning based Early Fault Diagnosis of Induction Motor for Electric Vehicle Application" (2018). *Electronic Theses and Dissertations*. 7446.  
<https://scholar.uwindsor.ca/etd/7446>

This online database contains the full-text of PhD dissertations and Masters' theses of University of Windsor students from 1954 forward. These documents are made available for personal study and research purposes only, in accordance with the Canadian Copyright Act and the Creative Commons license—CC BY-NC-ND (Attribution, Non-Commercial, No Derivative Works). Under this license, works must always be attributed to the copyright holder (original author), cannot be used for any commercial purposes, and may not be altered. Any other use would require the permission of the copyright holder. Students may inquire about withdrawing their dissertation and/or thesis from this database. For additional inquiries, please contact the repository administrator via email ([scholarship@uwindsor.ca](mailto:scholarship@uwindsor.ca)) or by telephone at 519-253-3000ext. 3208.

# **Machine Learning based Early Fault Diagnosis of Induction Motor for Electric Vehicle Application**

By

Eshaan Ghosh

A Dissertation

Submitted to the Faculty of Graduate Studies  
through the Department of Electrical and Computer Engineering  
in Partial Fulfillment of the Requirements for  
the Degree of Doctor of Philosophy  
at the University of Windsor

Windsor, Ontario, Canada

© 2018 Eshaan Ghosh

**MACHINE LEARNING BASED EARLY FAULT DIAGNOSIS OF INDUCTION  
MOTOR FOR ELECTRIC VEHICLE**

By

Eshaan Ghosh

APPROVED BY:

---

R. Karki, External Examiner  
University of Saskatchewan

---

C. Novak  
Department of Mechanical, Automotive & Materials Engineering

---

M. Khalid  
Department of Electrical & Computer Engineering

---

J. Wu  
Department of Electrical & Computer Engineering

---

N. C. Kar, Advisor  
Department of Electrical & Computer Engineering

30<sup>th</sup> April 2018

## DECLARATION OF CO-AUTHORSHIP/PREVIOUS PUBLICATIONS

I hereby declare that this dissertation incorporates material that is result of joint research, as follows: This dissertation includes the outcome of publications which also have co-authors who are / were graduate students or post-doctoral fellows supervised by Dr. Narayan Kar. In all cases, only primary contributions of the author towards these publications are included in this dissertation. The contribution of co-authors was primarily through the provision of assistance in experimentation and analysis. For Chapter 2, I am one of the co-authors, only sections with my contribution is included. I am aware of the University of Windsor Senate Policy on Authorship and I certify that I have properly acknowledged the contribution of other researchers on my dissertation and have obtained written permission from each of the co-author(s) to include the above material(s) in my dissertation. I certify that, with the above qualification, this dissertation, and the research to which it refers, is the product of my own work. This dissertation includes selected sections and extended work of research conducted in twelve original papers that have been published / submitted for publication in peer reviewed IEEE Transactions and IEEE International Conferences, as follows:

Dissertation Chapter	Publication title/full citation	Publication status
2	A. Mollaeian, <b>E. Ghosh</b> , H. Dhulipati, J. Tjong and N. C. Kar, "3-D Sub-Domain Analytical Model to Calculate Magnetic Flux Density in Induction Machines with Semi-closed Slots Under No-Load Condition," <i>IEEE Transactions on Magnetics</i> , vol. 53, no. 6, pp. 1-5, June 2017.	Published
3	<b>E. Ghosh</b> , F. Ahmed, M. M. Sangdehi and N. C. Kar, "Temperature Influenced Online Stator Resistance Estimation Using an Improved Swarm Intelligence Technique for Induction Machine," in the Proc. of <i>2015 IEEE Transportation Electrification Conference and Expo (ITEC)</i> , Dearborn, MI, 2015, pp. 1-6	Published

3	<b>E. Ghosh</b> , F. Ahmed, A. Mollaeian, J. Tjong and N. C. Kar, "Online Parameter Estimation And Loss Calculation Using Duplex Neural-Lumped Parameter Thermal Network for Faulty Induction Motor," in the Proc. of <i>2016 IEEE Conference on Electromagnetic Field Computation (CEFC)</i> , pp. 1-1, Miami, FL, 2016.	Published
4	<b>E. Ghosh</b> , S. Mukundan, H. Dhulipati, and N. C. Kar, "Design of Harmonics Analysis Block for Faulty Induction Motor Using Magnetic Equivalent Circuit and Observer Search Coil," to be submitted to <i>IET Electric Power Application</i> , 2018	To be Submitted
5	<b>E. Ghosh</b> , A. Mollaeian, W. Hu and N. C. Kar, "A Novel Control Strategy for Online Harmonic Compensation in Parametrically Unbalanced Induction Motor," <i>IEEE Transactions on Magnetics</i> , vol. 52, no. 7, pp. 1-4, July 2016.	Published
6	<b>E. Ghosh</b> , A. Mollaeian, S. Kim, J. Tjong and N. C. Kar, "Intelligent Flux Predictive Control Through Online Stator Inter-Turn Fault Detection for Fault-Tolerant Control of Induction Motor," in the Proc. of <i>2017 IEEE International Conference on Industrial Technology (ICIT)</i> , pp. 306-311, Toronto, ON, 2017.	Published
7	<b>E. Ghosh</b> , A. Mollaeian, S. Kim, J. Tjong and N. C. Kar, "DNN-Based Predictive Magnetic Flux Reference for Harmonic Compensation Control in Magnetically Unbalanced Induction Motor," <i>IEEE Transactions on Magnetics</i> , vol. 53, no. 11, pp. 1-7, Nov. 2017.	Published
8	<b>E. Ghosh</b> , and N. C. Kar "Prediction of Magnetic Flux Reference using DMG Machine Learning for Fault-tolerant Control of Magnetically Unbalanced Induction Motor"	To be Patented

I certify that I have obtained a written permission from the copyright owners to include the above published materials in my dissertation. I certify that the above material describes work completed during my registration as graduate student at the University of Windsor.

I declare that, to the best of my knowledge, my dissertation does not infringe upon anyone's copyright nor violate any proprietary rights and that any ideas, techniques, quotations, or any other material from the work of other people included in my dissertation, published or otherwise, are fully acknowledged in accordance with the standard referencing practices. Furthermore, to the extent that I have included copyrighted material that surpasses the bounds of fair dealing within the meaning of the Canada Copyright Act, and have included copies of such copyright clearances to the appendix of this dissertation. I declare that this is a true copy of my dissertation, including any final revisions, as approved by my dissertation committee and the Graduate Studies office, and that this dissertation has not been submitted for a higher degree to any other University or Institution.

## **ABSTRACT**

Electrified vehicular industry is growing at a rapid pace with a global increase in production of electric vehicles (EVs) along with several new automotive cars companies coming to compete with the big car industries. The technology of EV has evolved rapidly in the last decade. But still the looming fear of low driving range, inability to charge rapidly like filling up gasoline for a conventional gas car, and lack of enough EV charging stations are just a few of the concerns. With the onset of self-driving cars, and its popularity in integrating them into electric vehicles leads to increase in safety both for the passengers inside the vehicle as well as the people outside. Since electric vehicles have not been widely used over an extended period of time to evaluate the failure rate of the powertrain of the EV, a general but definite understanding of motor failures can be developed from the usage of motors in industrial application. Since traction motors are more power dense as compared to industrial motors, the possibilities of a small failure aggravating to catastrophic issue is high. Understanding the challenges faced in EV due to stator fault in motor, with major focus on induction motor stator winding fault, this dissertation presents the following:

1. Different Motor Failures, Causes and Diagnostic Methods Used, With More Importance to Artificial Intelligence Based Motor Fault Diagnosis.
2. Understanding of Incipient Stator Winding Fault of IM and Feature Selection for Fault Diagnosis
3. Model Based Temperature Feature Prediction under Incipient Fault Condition
4. Design of Harmonics Analysis Block for Flux Feature Prediction
5. Flux Feature based On-line Harmonic Compensation for Fault-tolerant Control
6. Intelligent Flux Feature Predictive Control for Fault-Tolerant Control
7. Introduction to Machine Learning and its Application for Flux Reference Prediction
8. Dual Memorization and Generalization Machine Learning based Stator Fault Diagnosis

*“When something is important enough, you do it even if the odds are not in your favor.”*

– Elon Musk

This dissertation is dedicated to those who get doubted upon, the weaker section, the underdogs, but still choose to dream big and fight for their dream.

Be inspired and inspire others around you!

Stay hungry, Stay foolish!

MAY THE FORCE BE WITH YOU



## ACKNOWLEDGEMENTS

To say that this dissertation is “by Eshaan Ghosh” is overstating. This dissertation would certainly never exist without the significant contribution of a lot of people.

I would like to thank my parents for their relentless support physically, mentally and emotionally despite all odds and adversities. Their unwavering faith in me has been exemplary and their prayers to almighty and blessings has given me that inner strength. I would not have been able to reach wherever I am today without them being there by my side. I would like this dissertation to be my humble gift to them. To my father wanting me to be an engineer while my mother wanting me to be doctor, I did both!

I would like to thank Dr. Jagdish Pathak and Mrs. Chhanda Pathak who introduced me to Dr. Narayan Kar and helping me in broadening my mental horizon.

To whatever I am today from the first day at University of Windsor, the greatest influence on me during this period, has been my supervisor and guide Dr. Narayan C. Kar. I would like to thank him for having given me this opportunity and platform to mold myself into a researcher. His constant motivation, pushing boundaries of hard work, charisma and exuding positivity all the time is infectious. His constant reminder of ‘good things happen to good people’ is just an example of his positivity that I shall carry with me forever. CHARGE Labs and his research program has the best resources and people which has helped me to develop novel ideas and implement them. He has not only made a researcher out of me but also a leader, team player, good communicator and a patient man.

A special thanks to Dr. Novak, Dr. Mohammed Khalid and, Dr. Jonathan Wu for being my committee members and to Dr. Rajesh Karki, for serving as my external examiner for this doctoral degree.

I would like to thank ‘soon to be Dr.’ Aida Mollaeian for being a wonderful colleague, friend, and a sister that I never had. Together we have been able to test our novel concepts and establish them. I would like thank Ms. Shruthi Mukundan for her help, and support as a friend apart from the technical assistance for my research. Thanks to Ms. Himavarsha Dhulipati who has been a great friend and support through the rollercoaster ride of my doctoral candidate life. Also, I would like to extend my thanks to Dr. Anas Labak, Dr. K. Lakshmi Varaha Iyer, Dr. Xiaomin Lu, Brian Esteban, Debarshi Biswas and all the

members of CHARGE Labs. I have learnt a lot from them which I have incorporated in both my professional and personal life. I would also like to thank Mr. Andrew Jenner, who is the manager of technical support at University of Windsor, for helping me to build several test setups and solve mechanical issues of systems quickly and efficiently.

I would like to sincerely thank late Dr. Voiko Loukanov who had given me the opportunity to work as an intern at D&V Electronics Ltd. for a year. Dr. Veliko Velikov, for being the much needed technical mentor who not only made me have a deeper understanding of solving technical issues, putting novelty in a production unit and introducing me to the concept of how to implementation of academic research knowledge into manufacturing units. I would also like to extend my thanks to all the other staff members and engineers at D&V Electronics Ltd. for helping me develop the industrial bend of mind and personality.

A special appreciation and thanks to Ms. Vridula Soni for being the support in my life that I received more than I could have asked for and for her deep faith and care for me.

Last but not the least, I would like to thank Elon Musk, the real life ironman, for being a true inspiration for me. His electric car company TESLA Inc. has not only been a game changer in the automotive sector but also is the reason why the research done in this dissertation gets to prove its point.

# TABLE OF CONTENT

<b>Declaration of Co-Authorship/Previous Publications .....</b>	<b>iii</b>
<b>Abstract .....</b>	<b>vi</b>
<b>Dedication .....</b>	<b>vii</b>
<b>Acknowledgements .....</b>	<b>viii</b>
<b>List of Tables .....</b>	<b>xiii</b>
<b>List of Figures.....</b>	<b>xiv</b>
<b>Chapter 1: Introduction .....</b>	<b>1</b>
1.1. <i>Overview of Electric Vehicles in Canadian Market.....</i>	1
1.2. <i>Background of Faults Occurring in Electric Motors for EVs.....</i>	6
1.3. <i>Fault Occurrences and Diagnostic Methods .....</i>	9
1.4. <i>Machine Learning based Fault Diagnosis .....</i>	14
1.5. <i>Research Contribution of this Dissertation.....</i>	15
1.6. <i>Organization of this Dissertation Highlighting Research Contributions .....</i>	16
1.7. <i>References .....</i>	18
<b>Chapter 2: Understanding of Incipient Stator Winding Fault of IM And Feature             Selection for Fault Diagnosis .....</b>	<b>25</b>
2.1. <i>Introduction.....</i>	25
2.2. <i>Electromagnetic Design of Electric Motor using Field Equations .....</i>	25
2.3. <i>Structural Design of Laboratory IM in FEA software .....</i>	28
2.4. <i>Performance Analysis of IM under Different Operating Conditions .....</i>	33
2.5. <i>Fundamentals of Heat Transfer in Electric Machines .....</i>	35
2.6. <i>Feature Selection for Developing Machine Learning for Fault Diagnosis .....</i>	38
2.7. <i>References .....</i>	39
<b>Chapter 3: Model Based Temperature Feature Prediction under Incipient Fault             Condition.....</b>	<b>40</b>
3.1. <i>Introduction.....</i>	40
3.2. <i>Mathematical Model of Copper Rotor Induction Motor.....</i>	41
3.3. <i>Investigation of Online Stator Resistance using Thermal Resistance .....</i>	43
3.4. <i>Calculation of Stator Resistance Using Particle Swarm Optimization.....</i>	46
3.5. <i>Numerical Investigation of Copper Rotor Induction Motor.....</i>	49

3.6.	<i>Re-Modelling of Faulty IM for DNLTN Method .....</i>	52
3.7.	<i>Duplex Neural — Lumped Thermal Network Development.....</i>	55
3.8.	<i>Experimental Validation of Proposed Novel Duplex Network.....</i>	57
3.9.	<i>Proposed Duplex Model Result Analysis .....</i>	59
3.10.	<i>Conclusion.....</i>	61
3.11.	<i>References .....</i>	61
<b>Chapter 4: Design of Harmonics Analysis Block for Flux Feature Prediction .....</b>		64
4.1.	<i>Introduction .....</i>	64
4.2.	<i>Modelling of Harmonics Analysis Block .....</i>	65
4.3.	<i>Experimental Verification of Proposed Harmonic Block .....</i>	71
4.4.	<i>Result Analysis of the Proposed Harmonic Block for Flux Feature Prediction .....</i>	73
4.5.	<i>Conclusion.....</i>	74
4.6.	<i>References .....</i>	75
<b>Chapter 5: Flux Feature based On-line Harmonic Compensation for Fault-tolerant Control.....</b>		76
5.1.	<i>Introduction .....</i>	76
5.2.	<i>Modelling of Harmonic Compensation Block .....</i>	76
5.3.	<i>Experimental Validation of Proposed Harmonic Compensation Drive.....</i>	79
5.4.	<i>Analysis of Time and Spatial Harmonics .....</i>	82
5.5.	<i>Conclusion.....</i>	86
5.6.	<i>References .....</i>	86
<b>Chapter 6: Intelligent Flux Feature Predictive Control for Fault-Tolerant Control</b>		88
6.1.	<i>Introduction .....</i>	88
6.2.	<i>Stator Flux Reference IM Model .....</i>	88
6.3.	<i>Development of Proposed Flux-Oriented Control .....</i>	89
6.4.	<i>Intelligent Swarm Optimization for Reference Flux Calculation.....</i>	95
6.5.	<i>Investigation of ALIM with Stator Winding Fault Using FEM .....</i>	97
6.6.	<i>Numerical and Experimental Investigation of Proposed Control.....</i>	100
6.7.	<i>Conclusion.....</i>	101
6.8.	<i>References .....</i>	102

<b>Chapter 7: Introduction to Machine Learning and its Application for Flux</b>	
<b>Reference Prediction</b> .....	103
7.1. <i>Introduction</i> .....	103
7.2. <i>Modelling of IM with UMP for DNN</i> .....	103
7.3. <i>Machine Learning for Flux Prediction</i> .....	107
7.4. <i>Experimental Validation of Proposed Novel DNN based Harmonic</i> <i>Compensation Block</i> .....	111
7.5. <i>Investigation Using Finite Element Model</i> .....	112
7.6. <i>Proposed Deep Neural Network Predictive Model Result Analysis</i> .....	115
7.7. <i>Conclusion</i> .....	118
7.8. <i>References</i> .....	119
<b>Chapter 8: Dual Memorization and Generalization Machine Learning based Flux</b>	
<b>Reference Prediction for Fault Diagnosis</b> .....	120
8.1. <i>Introduction</i> .....	120
8.2. <i>IM Model with Stator Winding Fault for DMG-ML</i> .....	120
8.3. <i>Motor Condition in-terms of Flux under Fault Condition</i> .....	124
8.4. <i>Dual Memorization and Generalization Machine Learning for Magnetic Flux</i> <i>Reference Estimation</i> .....	127
8.5. <i>Experimental Validation and Result Analysis</i> .....	143
8.6. <i>Conclusion</i> .....	147
8.7. <i>References</i> .....	147
<b>Chapter 9: Conclusion and Suggested Future Work</b> .....	149
9.1. <i>Conclusion</i> .....	149
9.2. <i>Future Work</i> .....	151
<b>Appendix A: Abbreviations</b> .....	152
<b>Appendix B: List of Publications</b> .....	154
<b>Appendix C: List of Industrial Projects and Scholarships</b> .....	157
<b>Appendix D: Permission for Using IEEE Publications</b> .....	159
<b>Vita Auctoris</b> .....	168

## LIST OF TABLES

TABLE 1.1 COMMERCIALY AVAILABLE ELECTRIFIED VEHICLES .....	5
TABLE 1.2 SURVEY RESULTS OF INDUCTION MOTOR FAILURE RATE .....	8
TABLE 1.3 OFFLINE TECHNIQUES FOR FAULT DETECTION .....	11
TABLE 1.4 ONLINE TECHNIQUES FOR FAULT DETECTION .....	12
TABLE 1.5 MACHINE LEARNING TECHNIQUES FOR FAULT DETECTION .....	15
TABLE 2.1 WINDING DISTRIBUTION IN THE STATOR OF THE IM UNDER STUDY .....	29
TABLE 2.2 PARAMETERS OF THE ALUMINUM ROTOR INDUCTION MOTOR UNDER TEST.....	33
TABLE 3.1 CRIM DATA SHEET .....	42
TABLE 3.2 STEADY STATE TEMPERATURE RISE AT 1,500 RPM.....	46
TABLE 3.3 EQUIVALENT CIRCUIT PARAMETERS OF CRIM .....	49
TABLE 8.1 VARIATION IN FLUX IN 3-PHASES FOR HEALTHY AND FAULTY IM UNDER FEA .....	125

# LIST OF FIGURES

Fig. 1.1. Overview of an electric vehicle. (a) Layout of Tesla Model S powertrain. (b) Physical layout of Tesla Model S with motor, controller and battery pack [7]. ..	3
Fig. 1.2. Electric motors used in current electric vehicles. (a) Cross section of Volkswagen e-Golf permanent magnet motor. (b) Smart Electric permanent magnet motor with in-motor controller. (c) Ford Focus Electric interior permanent magnet motor with gearbox. ....	4
Fig. 1.3. Classification of induction motor faults. ....	7
Fig. 1.4. Distribution of various fault occurrences in industrial induction motor. ....	7
Fig. 1.5. General overlay of any fault diagnostic method for electric motors. ....	8
Fig. 2.1. Stator slot dimension as measured to be used as inputs for FEA design.....	30
Fig. 2.2. Rotor slot dimensions as measured and used as input for FEA designing. ....	30
Fig. 2.3. Faulty IM under test. (a) Rotor cross-section to understand and find the dimensions of the rotor slots. (b) Opened stator for dimension measurement. (c) Just the rotor taken out of the motor. (d) Complete faulty IM. (e) Rotor placed inside the stator. ....	31
Fig. 2.4. 2-D FEA modelling of the 7.5 hp motor. ....	32
Fig. 2.5. 3-D FEA modelling of the motor under investigation.....	32
Fig. 2.6. The stator current waveform as generated in FEA software. (a) Healthy IM. (b) IM with incipient stator winding fault. ....	34
Fig. 2.7. The induced voltage in the windings of all the phases of IM. (a) Healthy IM. (b) IM with incipient stator winding fault. ....	34
Fig. 2.8. The flux linkage as generated in the windings of all the phases of IM. (a) Healthy IM. (b) IM with incipient stator winding fault. ....	34
Fig. 2.9. Torque generated in IM with incipient fault has more torque ripple when compared with the healthy IM condition. ....	35

Fig. 2.10. Temperature rise in Faulty IM. (a) CFD analysis. (b) Experimental results. ..	38
Fig. 3.1. The investigated motor under test. (a) Stator. (b) Rotor.....	41
Fig. 3.2. Schematic representation of the experimental test setup.....	44
Fig. 3.3. Machine under test and instrumentation layout.....	44
Fig. 3.4. Measured temperature over a period of time with & without cooling fan. ....	45
Fig. 3.5. Flowchart to show each step of process used in finding stator resistance.....	48
Fig. 3.6. Convergence diagram of the IPSO for the CRIM. ....	50
Fig. 3.7. Comparative results for IM under investigation. (a) With fan cooling as obtained from the experimental setup and the output of the PSO. (b) Without fan cooling as obtained from the experimental setup and the output of the PSO. ....	51
Fig. 3.8. The power flow and losses as generated in the induction motor.....	54
Fig. 3.9. Schematic flow of novel DNLTN method for parameter and loss estimation. ..	55
Fig. 3.10. Design of neural network used in application of parameter estimation. ....	56
Fig. 3.11. Proposed lumped parameter thermal network for the fault IM. ....	57
Fig. 3.12. Set up for experimental validation of the proposed duplex neural-lumped thermal network. ....	58
Fig. 3.13. Comparison of experimental and duplex model based change in stator resistance.....	59
Fig. 3.14. Motor thermal condition as measured using IR sensor. (a) Distribution of temperature over various parts of the motor with the image of IM as x-axis to indication the locations. (b) DC load motor remains cool unlike the faulty IM indicating that fault cause undue heat at same ambient conditions. (c) Faulty IM before starting the experiment. (d) Faulty IM condition after 30 minutes of operation. ....	60
Fig. 4.1. MEC network as used for the proposed modelling. ....	65
Fig. 4.2. Search coil placed on the phase of detected unbalance .....	66



Fig. 4.3. MEC network as used for the proposed modelling. ....	67
Fig. 4.4. MEC network variation due to inter-turn fault. ....	68
Fig. 4.5. Comparative results of flux obtained from MEC and OSC. (a) Healthy IM flux. (b) Faulty IM flux. ....	72
Fig. 4.6. Real time flux harmonic analysis of (a) Healthy motor condition (b) Faulty motor condition. ....	74
Fig. 5.1. Set up for experimental validation of the proposed compensation drive. ....	78
Fig. 5.2. Proposed novel control strategy with harmonic compensation block. ....	79
Fig. 5.3. Search coil placed on the phase of detected fault. ....	80
Fig. 5.4. Behavior of electromagnetic torque (a) Ripples caused in the unbalanced IM. (b) Decrease in ripples after balancing the IM. ....	82
Fig. 5.5. The air gap magnetic flux density for healthy and unstable condition. ....	83
Fig. 5.6. Magnetic flux distribution for the IM. (a) Normal condition. (b) Unbalanced condition. ....	83
Fig. 5.7. Back EMF voltage as measured using search coil. (a) Eccentric condition of 157 mV for fundamental, 185 mV for harmonics. (b) After using the control 130 mV for fundamental, 137 mV for harmonics. ....	84
Fig. 5.8. The current waveform of the IM as measured. (a) Eccentric condition. (b) After using the control. (c) Reference flux input for the control. (d) Transient performance during speed change. ....	85
Fig. 6.1. Search coil placed on the phase of detected unbalance. ....	90
Fig. 6.2. Schematic flow for stator inter-turn fault detection with stator-flux oriented control. ....	94
Fig. 6.3. Set up for experimental validation of the proposed fault tolerant control drive. ....	95
Fig. 6.4. Flowchart presenting the how the proposed algorithm uses to the best value of flux in order to predict accurately. ....	96

Fig. 6.5. Fast Fourier Transformation of the current flowing through the stator windings for ALIM with (a) No winding fault. (b) Small stator winding fault. ....	98
Fig. 6.6. Study of magnetic flux distribution for ALIM. (a) Normal operating condition. (b) With small stator winding fault on phase A. ....	99
Fig. 6.7. Current waveform for ALIM (a) with incipient stator winding fault (b) after the proposed control has been implemented. ....	100
Fig. 6.8. The back EMF voltage as measured using the search coil. (a) With stator inter-turn fault (b) After proposed control has been implemented. ....	101
Fig. 6.9. Comparative experimental flux waveform of flux with stator-inter-turn fault (red), predicted reference flux (black), modified flux after the control (blue) to present how the flux waveform is modified. ....	101
Fig. 7.1. Schematic flow of novel DNN based harmonic compensation method. ....	104
Fig. 7.2. The current and voltage waveforms of faulty IM at (a) Rated load. (b) Rated speed. ....	105
Fig. 7.3. Various types of machine learning techniques. ....	107
Fig. 7.4. Design of neural network used in application of harmonic compensation. ....	108
Fig. 7.5. DNN based prediction results. (a) Regression plot for output vs target flux density. (b) Regression plot for output vs target current. (c) Fitness plot for flux density. (d) Performance plot of DNN upto 77 epoch. ....	110
Fig. 7.6. Experimental setup to investigate the proposed DNN predictive method. ....	111
Fig. 7.7 . Magnetic flux vector distribution for IM in normal and unbalanced condition. ....	113
Fig. 7.8. Scalar and Vector distribution of magnetic flux density. (a) Healthy IM. (b) Faulty IM. ....	113
Fig. 7.9. Air-gap flux density over one pole pair. (a) Radial flux density. (b) Tangential flux density for both healthy and faulty condition flux density. (c)	

Electromagnetic torque fluctuation as shown due to deviation of IM from its healthy condition to stator.....	115
Fig. 7.10. Real time flux harmonic analysis. (a) Healthy motor condition. (b) Faulty motor condition.....	116
Fig. 7.11. Experimental validation. (a) Flux density at rated load for faulty IM (b) Flux density at rated speed for faulty IM. (c) Uniformity in current waveform after DNN predictive model implementation. (d) Comparison of experimental and DNN predictive harmonic.....	118
Fig. 8.1. Schematic flow of novel DMG-ML based flux reference and fault prediction.....	121
Fig. 8.2. Experimental analysis of faulty IM indicating (a) Current and voltage waveform at rated speed of 1,750 rpm with faulty phase A. (b) Magnetic flux density at rated speed. (c) Current and voltage at rated load of 70 Nm with faulty phase A. (d) Magnetic flux density at rated load.....	122
Fig. 8.3. FEA modelling of IM under test for understanding of the motor in healthy and unhealthy conditions. (a) Cross-sectional cut of rotor for design purpose. (b) 3D FEA Model.....	126
Fig. 8.4. Flux linkage as observed using finite element method to evaluate flux variation in different conditions. (a) Healthy IM. (b) Fault IM. ....	126
Fig. 8.5. Variation in scalar and vector magnetic flux density. (a) Healthy IM. (b) IM with inter-turn fault. ....	127
Fig. 8.6. Event classification for a set of features.....	129
Fig. 8.7. Statistical understanding of model fitting.....	130
Fig. 8.9. Confusion Matrix for statistical measurement of results.....	134
Fig. 8.10 Types of Regression model relationships.....	136
Fig. 8.11. Evaluating regression model. (a) When histogram is close to 0 with a definite pattern. (b) When histogram is close to 0 with no apparent pattern. ....	137
Fig. 8.12. Differentiating between outliers in terms of leverage and influence.....	138

Fig. 8.13. Deep Neural Network with dense embedding.....	139
Fig. 8.14. Dual memorization and generalization machine learning used for flux prediction. ....	141
Fig. 8.15. Complete flow of dual memorization and generalization machine learning..	142
Fig. 8.16. Experimental setup using faulty IM for voltage and current feature extraction for input along with flux input for validation of DMG-ML. ....	144
Fig. 8.17. DMG–ML metrics determining (a) Progressive Recall. (b) Progressive Precision. (c) Progressive Accuracy variation over repetitive iteration. ....	146
Fig. 8.18. DMG–ML based results. (a) Flux values as measured experimentally as well as during different training conditions and variation. (b) Comparison of magnetic flux reference at rated speed, and 10 Nm load. (c) Comparison of magnetic flux reference 300 rpm and rated load.....	147

# CHAPTER 1

## INTRODUCTION

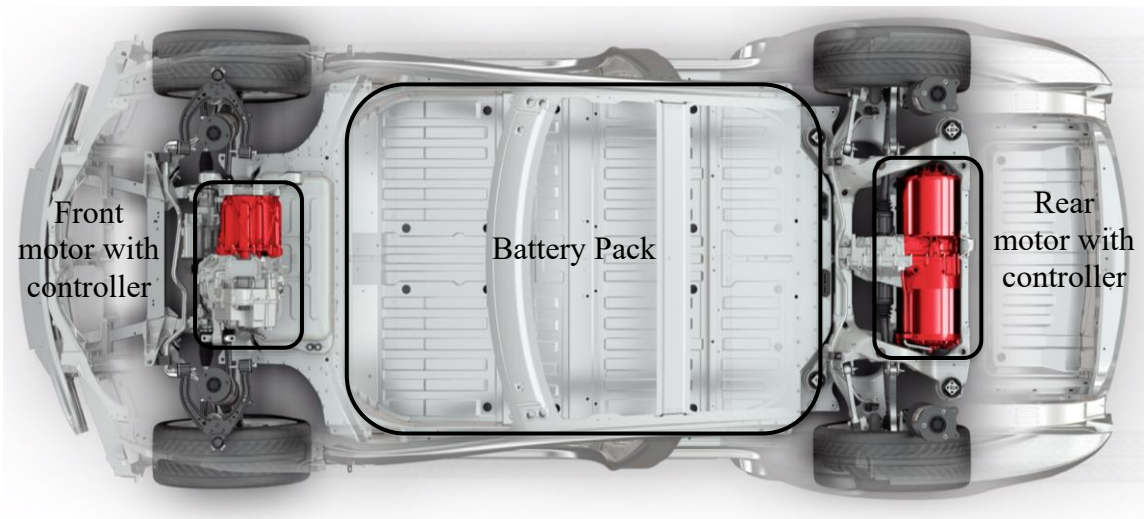
During the recent few years, due to increase in geo-political awareness, affordable pricings, significant incentives from the government, cheaper cost to run has lead to increase in sales and production of electric vehicles (EVs). It is being predicted that if this current electric car revolution continues, by 2025, EVs will be as cheap as gasoline cars and by 2038, EV sales shall surpass internal combustion engine cars [1]. Although the basic concept of electric vehicle dates back to 1800s, EVs have not been able to cater to the needs of commercial usage like gasoline cars have been. Thus, although the technology is not new, the commercialization of EVs is fairly new and has not reached the maturity of gasoline cars. Thus, the kind of problems that might occur in the long term usage of EVs are at their primitive stages. There are mechanics every where to fix any kind of issues arising in gasoline vehicles. But when it comes to EVs, according to market survey more than 90% of mechanic car repair shops are not ready or have enough capabilities to fix problems arising in an electric motor run vehicle. With an alarming production ramp up of EVs some of which are autonomous at the same time, it is important to understand and prevent any faults that might occur in the powertrain of EVs in future for safety of the passengers. As more EVs are being used commercially, some of these EVs might have a fault occurring due to manufacturing defect, irrational usage, long-term wear and tear or unprecedented circumstances, which are inevitable.

### *1.1. Overview of Electric Vehicles in Canadian Market*

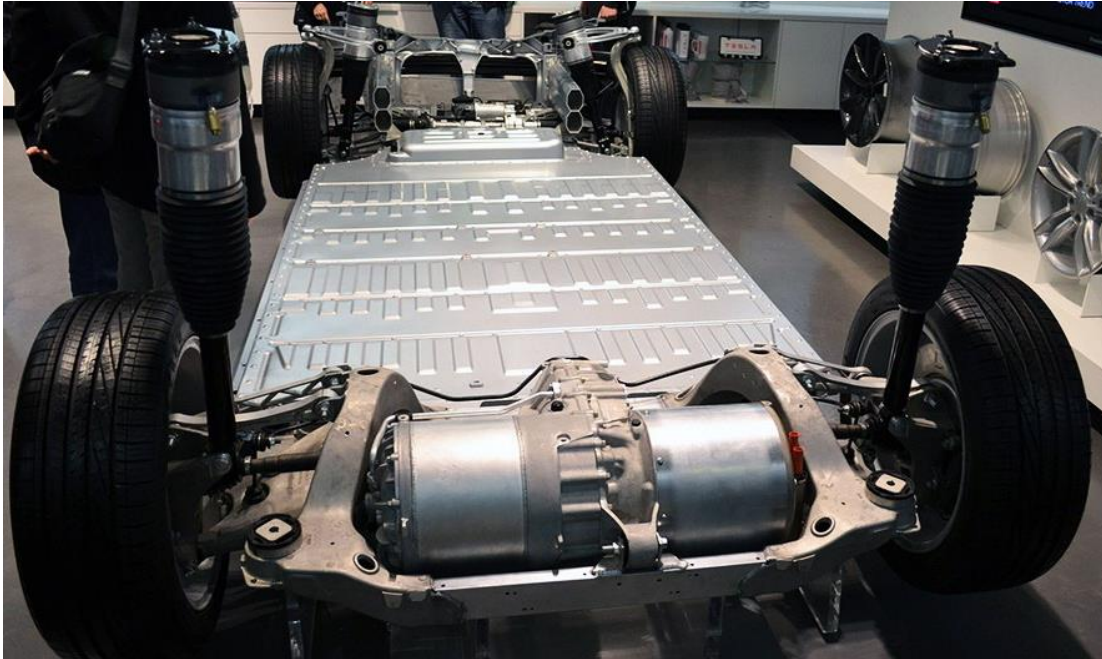
With the modern paradigm shift to electric vehicles from the conventional gas cars, a lot of research is being done. Most of the research concentration is being put into making the batteries last longer, and designing electric machines of high performance efficiency complemented by highly efficient control drive. This is done for optimized operation of the motor and adequate amount of battery usage by having least amount of losses produced in the whole drivetrain. Since the world is moving more and more to artificial intelligence and self-driving cars, electric cars are the favourite of manufacturers considering it is much easier to have a complete electric system starting from the LIDAR for self-driving to the

control of the vehicle programmed into a high processing microcontroller to an electric motor. This new revolution of paradigm shift from combustion engine vehicles to hybrid and electric cars and also to self-driving cars, is here to stay [2]-[4]. With cars like Tesla Model S and Model X being highly efficient on ‘fuel’, highest 0-60mph pick up, having fast charging, are aesthetically designed; the auto car industry has moved to attract customers with such features. Companies such as General Motors, Ford, Mercedes Benz, BMW, Volkswagen and Toyota are now moving into developing such electric vehicles. A comparative study of different EVs has been done in Table 1.1. 0-60 acceleration has been considered in mph unit since it is a standard. Vehicles such as Nissan Leaf and Ford Focus Electric have been around for a while but it could not attract the general mass because of the fear of losing charge while driving and not being able to ‘refuel’ (charge the batteries) the car as it would be to do with a conventional gas car [5]. A lot of research is being done in order to alleviate the fears of the masses and making electric cars cheaper, better looking and faster charging. But down the lane, these electric motor driven vehicles can have the same fault issues as the industrial motors get that have been running continuously for several years. Thus, this dissertation investigates in solving such fault occurrences that might occur in the electric motor while the car is being driven, for the safety of the driver and the passengers. For better understanding, it is important to understand the structure of an electric vehicle. A sample image of Tesla Model S as shown in Fig. 1.1 has been used to understand the structure. An electric vehicle mainly consists of an electric motor, a battery pack, a battery management system, a controller unit for the motor and a main control overlooking the vehicle dynamics [6]. Sometimes, it might have 2 motors in the vehicle to make it an all-wheel drive (AWD). As it can be seen in Fig. 1.1(a), in the front is the electric motor which is an induction motor in this case with its controller. Various electric motors used in other commercial electric vehicles have been shown in Fig. 1.2. Similarly, the back has a motor and a control unit consisting of the control and inverter stack which can be seen in Fig. 1.1 (b). In the center, below the seats, the battery pack is placed, since it has two advantages as it does not occupy space in the back or front of the car and the whole vehicle has a lower center of gravity making it more stable while driving. The placement of battery pack in the car varies from one car manufacturer to another. Since, the electric motor is the heart of an electric vehicle, a healthy motor condition

determines the best operating condition of the motor, proper driving experience and safety of driver and co-passengers. In the case of any fault occurrence in the motor while the vehicle is being driven it will cause the passengers to be stranded in the middle of nowhere.



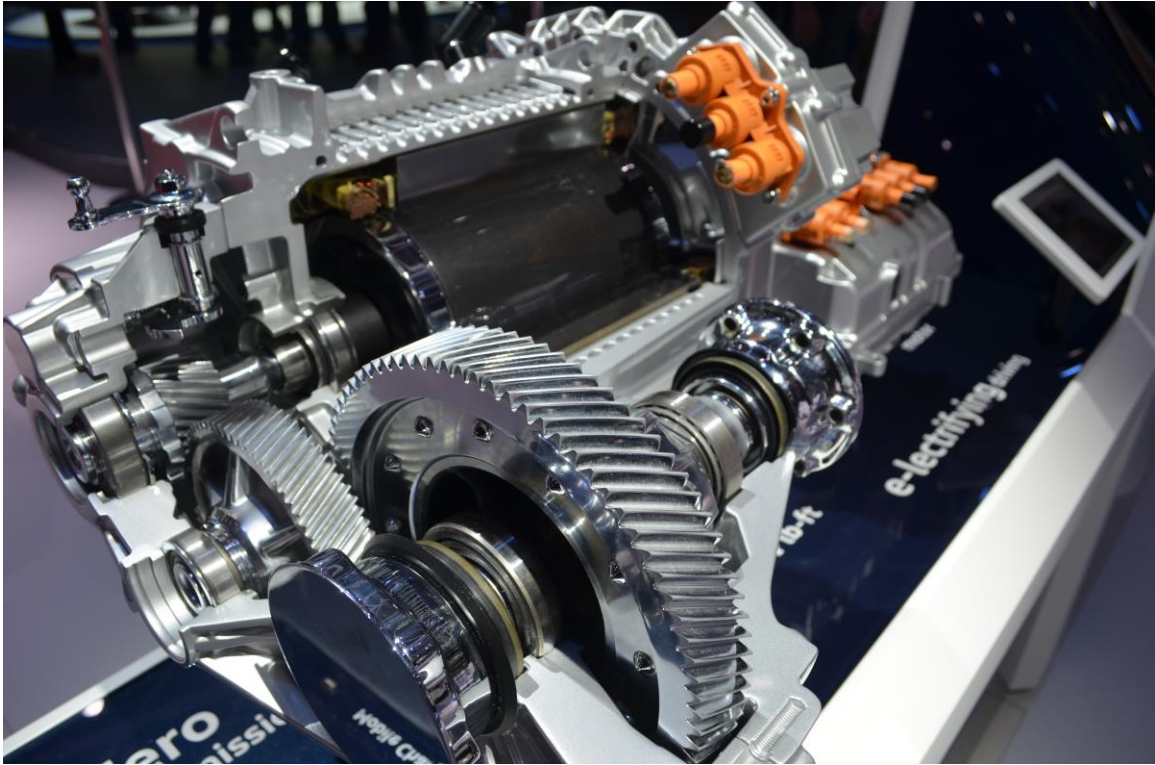
(a)



(b)

Fig. 1.1. Overview of an electric vehicle. (a) Layout of Tesla Model S powertrain. (b) Physical layout of Tesla Model S with motor, controller and battery pack [7].





(a)



(b)



(c)

Fig. 1.2. Electric motors used in current electric vehicles. (a) Cross section of Volkswagen e-Golf permanent magnet motor. (b) Smart Electric permanent magnet motor with in-motor controller. (c) Ford Focus Electric interior permanent magnet motor with gearbox.



TABLE 1.1

COMMERCIALLY AVAILABLE ELECTRIFIED VEHICLES [8] – [10]

<b>Car Model</b>	<b>Price (CAD)</b>	<b>Range (km)</b>	<b>0-60 mph</b>	<b>Motor Type</b>	<b>Motor Size (kW)</b>	<b>Torque (Nm)</b>
Smart forTwo Electric	\$28,800	109	9.8	Synchronous	60	160
Ford Focus Electric	\$31,498	185	10.1	Permanent Magnet	107	249
Kia Soul Electric	\$35,395	150	11.8	Permanent Magnet	81	157
Hyundai IONIQ Electric	\$35,649	177	8.1	Interior Permanent Magnet	88	295
Nissan Leaf	\$35,998	172	10.2	Permanent Magnet	80	157
Volkswagen e-Golf	\$36,355	134	10.4	Permanent Magnet	100	290
Tesla Model 3 (Base)	\$40,000	350	4.6	Permanent Magnet	228	563
Chevrolet Bolt	\$42,895	383	6.5	Permanent Magnet	150	160
BMW i3	\$48,750	183	7.1	Permanent Magnet	127	249
Tesla Model S (75D)	\$95,350	210	2.5	Induction	193	249
Tesla Model X (75D)	\$108,100	381	2.9	Induction	193	249
Tesla Model S (P100D)	\$174,700	507	2.28	Dual Induction	193+375	249+649
Tesla Model X (P100D)	\$188,300	465	2.4	Dual Induction	193+376	249+650
Fiat 500e (US only)	USD \$31,800	135	8.7	Permanent Magnet	83	200
Mercedes B250e (US only)	USD \$39,900	140	7.9	Permanent Magnet	87	187

## *1.2. Background of Faults Occurring in Electric Motors for EVs*

The invention of induction motor (IM) in 1888 by Nikola Tesla has been by far one of the simplest and most rugged machines for conversion of alternating current electrical energy to mechanical energy [11]. Since then IM has been widely used in various industrial, commercial as well as automotive applications. With the advent of power electronics and their implementations for control of AC electric motor since the 1960s, the popularity of usage of IM increased exponentially. But that doesn't mean that AC machines like IM and permanent magnet synchronous motor (PMSM) are immune to any kind of failure. Since IM and PMSM act as the main prime mover for many industrial applications, any kind of failure occurrence leads to stopping the motor to clear the fault. Thus, losing on production time and reduced productivity. With increase in use of IMs and PMSMs in EVs, such kind of fault occurrence would mean the risk of safety of passengers as well as the inconvenience cause by the need to stop the car, possibly at an inconvenient time and place. Since there is always the probability of sudden motor failure, continuous online condition monitoring and diagnostic are vital issues of electric machines to be done to vastly improve the reliability, maintainability and safety of EVs.

Electric motor faults can be broadly categorised as electrical and mechanical faults. Any kind of bearing, shaft, other eccentricity or loading fault are classified as mechanical faults. Other kind of faults like stator winding burn, broken rotor bar, broken end-rings, and drive based faults are classified as electrical fault. The classification of faults is shown in Fig. 1.3. As per IEEE-IAS and EPRI surveys [12], [13] shown in Table 1.2, it can be said that bearing fault is the highest occurring fault. Just after bearing fault, stator winding fault can be rightly said as the second highest fault occurrence at approximately 37%. More than 90% of the stator fault are related to stator windings. Considering, bearing is a mechanical fault, stator winding fault can be rightfully assumed as the highest electrical fault occurrence. It has been indicated in [14], that time taken for a single turn stator winding fault to develop into a critical fault in a conventional 20 hp induction motor is less than 2 seconds. Thus, the risk of stator winding inter-turn fault occurrence in a 504 hp motor of a Tesla Model S is much greater. If the various faults are visualised as shown in Fig. 1.4, it can be seen that stator fault is the highest electric fault occurrence in any motor. Thus, this dissertation has primarily been focused on stator fault.

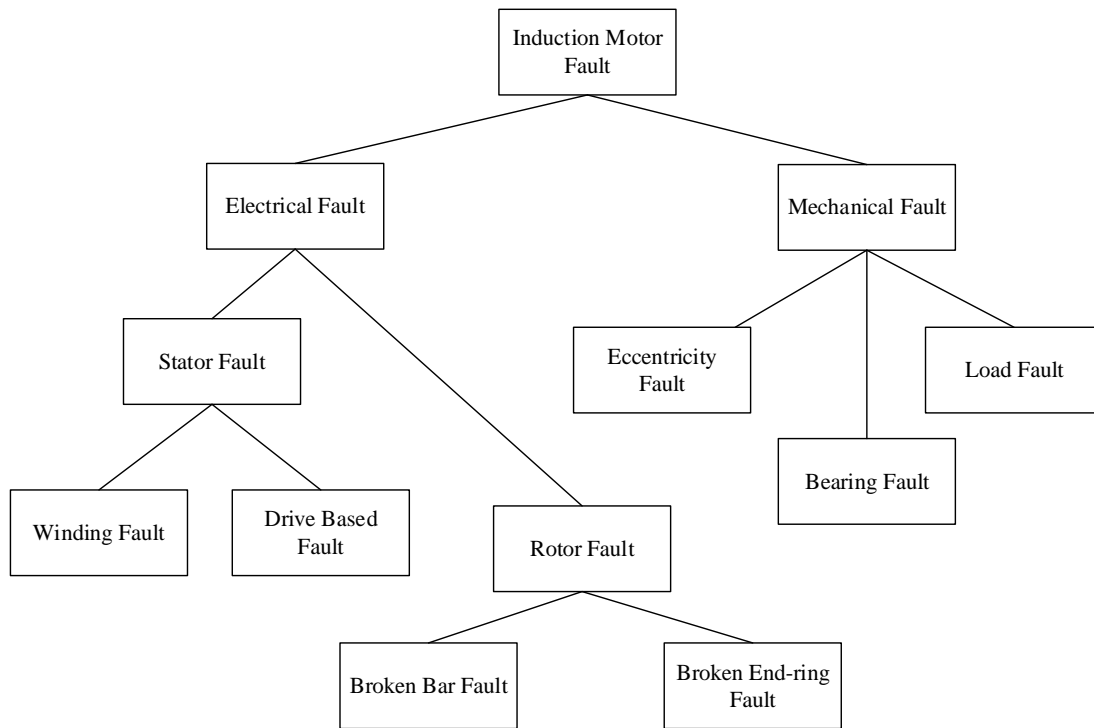


Fig. 1.3. Classification of induction motor faults.

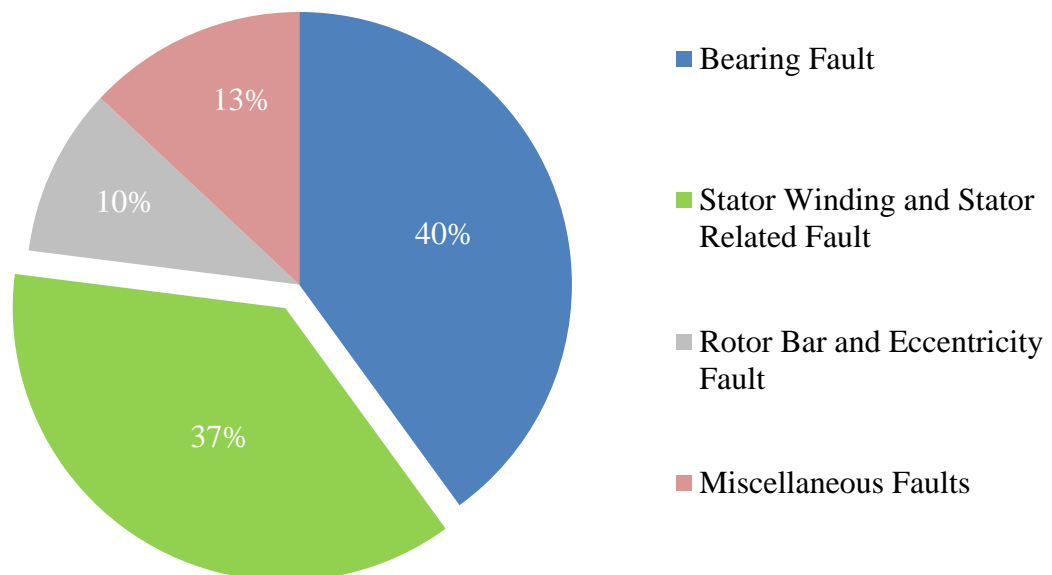


Fig. 1.4. Distribution of various fault occurrences in industrial induction motor.

TABLE 1.2

SURVEY RESULTS OF INDUSTRIAL INDUCTION MOTOR FAILURE RATE [12], [13]

Component	IEEE-IAS Survey (% of failure)	EPRI Survey (% of failure)
Bearing	44	41
Stator	26	36
Rotor	8	9
Miscellaneous	22	14

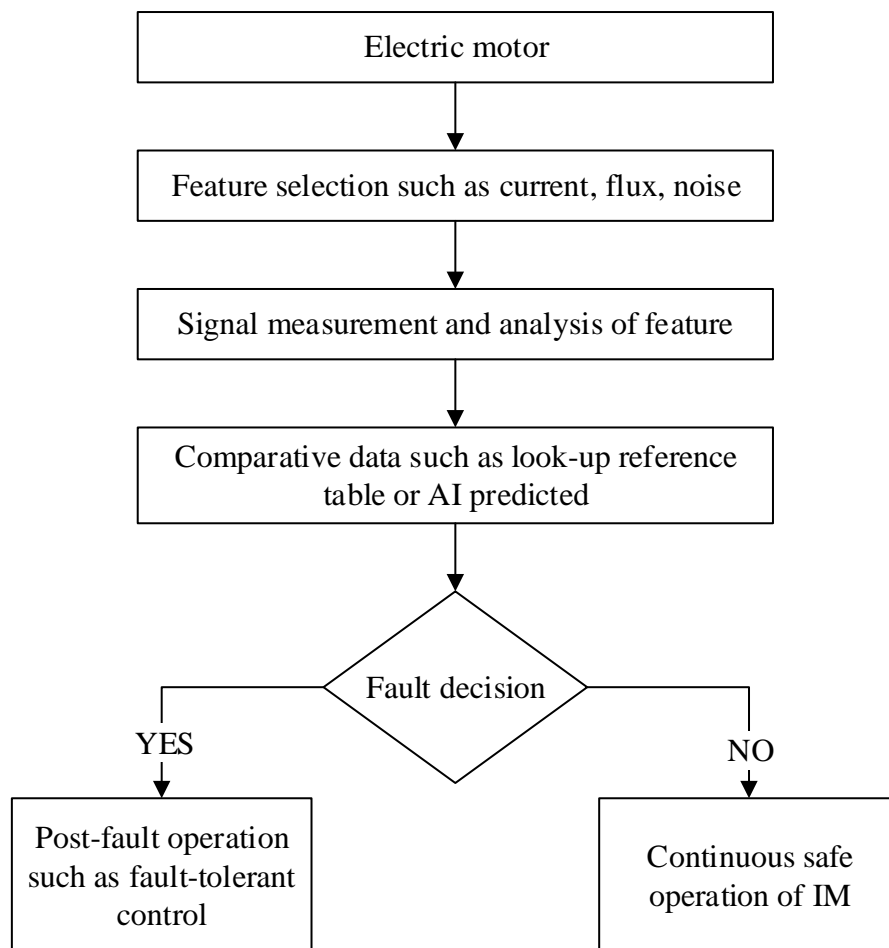


Fig. 1.5. General overlay of any fault diagnostic method for electric motors.

### *1.3. Fault Occurrences and Diagnostic Methods*

Various fault diagnosis methods have been developed depending on the type of method or sensor used or by the reason the fault happened. Most of background study relates to motor faults in general and not specific to EV application. The process of fault detection to data processing and post fault detection general methodology has been shown in Fig 1.5. Fault diagnostic methods can be classified based on the cause or method used as follows:

#### 1. Based on the **Fault Cause**:

- (a) **Thermal**: Due to thermal stresses, the motor is subject to thermal aging which means the motor in EV might need to be changed in a few years. An increase in temperature leads to lower performance of the machine reducing the life span of the insulation of the machine. A simple rule of thumb can be considered where a  $10^{\circ}$  increase in temperature can decrease motor insulation life by 50%. Other side effects caused by thermal stress is thermal overloading which occurs due to variation in voltage, unbalance in phase voltages, excess motor loading, improper cooling of the motor and variation in ambient temperature. For example, a small increase in voltage unbalance has an huge effect on the winding temperature. Thereby exposing the windings to various faults [15], [16].
- (b) **Electrical**: The types of electrical faults can be due to phase-to-ground, phase-to-phase, and turn-to-turn faults leading to short circuit or open circuit winding, overvoltage and, under voltage problems. An unbalanced supply from the inverter side is also a huge cause of electrical stress to increase in the motor of the EV powertrain. Tracking and corona effect arise at operating voltages above 600 V which vastly effects the automotive drive system performance. At those high voltages the transient voltage conditions leads to deterioration of stator insulation ad case various line-to-line or, line-to-ground faults. With usage of power electronics based drive units, the voltage transients subjected onto the motor are continuous and more during motor start-stop [17]-[20].
- (c) **Mechanical**: The most common mechanical faults are bearing failure, rotor-shaft misalignment and shaft deflection which can directly affect the wheels of the EV. These can happen due to continuous usage and time, manufacturing defect or some

unavoidable circumstances. There are several other mechanical stress like loose rotor balancing weights, loose rotor fan blades, improper tubing or collapse of cooling pipe inside the motor, and loose parts striking the motor while the car is being driven [21]-[25].

- (d) **Environmental:** Environmental conditions affecting the system when used in extreme situations, contamination, increase in humidity, hostile chemicals, or any unwanted radiations can be categorized as environmental or ambient stress. Existence of contamination particles can lead to reduction in heat dissipation, thereby increasing the thermal deterioration of the motor. If those contaminations are conducting, then a thin layer of that material can lead to surface currents and electrical tracking, leading to additional electrical stress to be applied on the motor. Destructive chemicals can degrade the insulation, or windings or the core material and make it more vulnerable to mechanical stresses. To avoid such environmental faults, the motor should be kept clean and dry internally, as well as externally, to avoid the influence of any kind of moisture, chemicals, and foreign particles, or develop motors with new advanced material which are more resilient [26]-[28].

## 2. Based on **Sensor Application and Installation:**

- (a) **Invasive:** Placement of sensors inside the motor for detection purpose, such as the application of RTDs or flux sensors placed right inside the motor for continuous monitoring of the condition of the running motor. The advantage of this method is that the health condition monitoring is extremely accurate [29].
- (b) **Non-Invasive:** Sensors outside the motor such as current sensor is used for fault diagnosis which does not involve tampering with the already manufactured motor. Using such non-invasive sensor, the data collected is processed accordingly to figure out the fault condition of the motor. This method of estimation is not so accurate but the amount of sensors required are less and non-intrusive [30].

## 3. Based on **Test Method** used:

- (a) **Offline Testing:** Motor needs to be removed from the vehicle and then checked for fault developed. This method of testing is the oldest method to date. Various research done in [31]-[40] has been tabulated in Table 1.3.

TABLE 1.3

## OFFLINE TECHNIQUES FOR FAULT DETECTION [31] – [40]

Core Technique	Methodology	Diagnostic Results
Winding Resistance Test	Detection of shorted turns	<ul style="list-style-type: none"> <li>• Ease of operation</li> <li>• Detects only fault</li> </ul>
Insulation Resistance Test	Detection of phase-to-ground insulation	<ul style="list-style-type: none"> <li>• Ease of operation</li> <li>• Can be used for both stator and rotor winding</li> <li>• Temperature sensitive</li> </ul>
Polarization Index	Detections of contaminations and phase to ground fault	<ul style="list-style-type: none"> <li>• Ease of operation</li> <li>• Less sensitive than insulation resistance test</li> </ul>
DC High-Pot Test	DC based phase to ground insulation detection	<ul style="list-style-type: none"> <li>• Ease of operation</li> <li>• More predictive than insulation resistance and polarization index method</li> <li>• If test is successful, insulation of the winding is fine</li> <li>• If test fails, a fault is detected</li> </ul>
AC High-Pot Test	Phase to ground insulation detection using AC	<ul style="list-style-type: none"> <li>• Better than DC high-pot test but more difficult to test</li> </ul>
Surge Test	Turn-to-turn insulation failure	<ul style="list-style-type: none"> <li>• Ideal for finding insulation fault</li> <li>• Cannot find fault due to grounding error</li> <li>• Destructive for the motor</li> </ul>
Offline Partial Discharge	Deterioration of phase-to-ground and turn-to-turn fault detection	<ul style="list-style-type: none"> <li>• Gives proper results</li> <li>• Not applicable for low voltage machines</li> </ul>

Dissipation Factor	Phase-to-ground and phase-to-phase insulation deterioration detection	<ul style="list-style-type: none"> <li>• Regular basis observation needed to get data over period of time</li> <li>• Can determine the exact cause of deterioration</li> </ul>
Inductive Impedance	Phase-to-ground and phase-to-phase insulation ground detection	<ul style="list-style-type: none"> <li>• Easily affected by contaminations and impurities</li> <li>• Not so easy in operation</li> </ul>
Terminal Voltage Signature Analysis	Turn-to-turn fault detection	<ul style="list-style-type: none"> <li>• Analysis is independent of unbalanced supply voltage</li> <li>• Can be done only after switching off</li> </ul>

(b) **Online Testing:** The EV need not be stopped for checking the motor for fault. It can continue running as any fault occurrence will be indicated. Online methods of condition monitoring are growing and continuous research is being done to improve the methods. Research done as in [41]-[50] has been summarised in Table 1.4.

TABLE 1.4  
ONLINE TECHNIQUES FOR FAULT DETECTION [41] – [50]

Core Technique	Methodology Implemented	Results Obtained
Motor Current Signature Analysis (MCSA)	Analysis of stator current spectrum	<ul style="list-style-type: none"> <li>• 3rd order harmonic was observed in the event of stator turn fault.</li> <li>• However, saturation of magnetic material and unbalanced source supply also cause increase in 3rd harmonics.</li> </ul>
	Shorted stator turns as a search coil	Observed stator currents at the terminal voltage of machine just after switching it off. But, it cannot provide continuous monitoring.
	Stator power analysis	AC components of power signal could detect stator turn fault for severity more than 5%.



	Phase shifts	<ul style="list-style-type: none"> <li>• Magnitude of phase shifts between the line current and phase voltage was observed indicating the stator turn fault.</li> <li>• Immune to source unbalance.</li> </ul>
	Park's vector approach & extended Park's vector approach	<ul style="list-style-type: none"> <li>• Degree of ellipticity and major axes orientation of the pattern was used to determine the stator turn</li> <li>• Fault severity and the faulty phase.</li> </ul>
Sequence Component	Current/voltage sequence components	<ul style="list-style-type: none"> <li>• Negative sequence current/voltage and voltage negative/positive sequence components were used to detect stator turn faults accurately.</li> <li>• However, it is affected by asymmetries like unbalance supply voltage and machine saturation etc.</li> </ul>
	Sequence impedance	<ul style="list-style-type: none"> <li>• Effect of unbalanced source on negative sequence current has been eliminated in seq.</li> <li>• Impedance method.</li> </ul>
	High frequency signal injection	<ul style="list-style-type: none"> <li>• High frequency signals were injected for turn fault detection due to its immunity to negative seq. component.</li> </ul>
Air-gap Torque	Air-gap torque frequency components	<ul style="list-style-type: none"> <li>• Air-gap torque being sensitive to stator turn fault was applied.</li> <li>• Non-zero angular frequency of the torque showed the faulty situation.</li> </ul>
Temperature Monitoring	Thermal model and parameter based approaches	<ul style="list-style-type: none"> <li>• Temperature estimation techniques based on solving analytical lumped circuit, according to the variation of the resistance, was employed to detect stator winding fault.</li> </ul>

	Embedded temperature detector	<ul style="list-style-type: none"> <li>• Metallic sensors were used to measure the local temperature which showed rise corresponding to the faulty condition.</li> </ul>
	Thermal images	<ul style="list-style-type: none"> <li>• Infrared thermal images based on image processing were used to detect stator turns short circuit.</li> </ul>
Artificial Intelligence	Expert system, fuzzy, neural network, genetic algorithm etc.	<ul style="list-style-type: none"> <li>• AI techniques such as ES, NN, fuzzy, GA etc. employed for fault detection have been found advantageous as well as more accurate.</li> </ul>

#### *1.4. Machine Learning based Fault Diagnosis*

As the background study presented in Section 1.3 relates more to faults and fault diagnosis occurring in motors in general for all applications, it is important to understand that such slow methodologies cannot be applied for EVs since a fault incidence can compromise the safety of the passengers in the fraction of a second. Thus fast, and reliable machine learning methodologies are needed to prevent fault in EV application. Many researchers have worked on statistical fault diagnosis, mild machine learning algorithm and hybrid neural network based algorithms to find faults in motor faster, with higher precision and accuracy. Not much work has been done in the field of machine learning based fault diagnosis although during recent times, there has been an inevitable increase in development of machine learning algorithms for software applications. Just 5 years back such processing power was not possible in microcontrollers or computers to process humongous data produced by the system. But still some work has been done as shown in the Table 1.5. The most commonly used machine learning methodology is using artificial neural networks (ANN) and various forms of ANN such as back-propagation neural networks, regression based neural network, hybrid neural network and fuzzy logic. As shown in the Table 1.5, all the various machine learning techniques are either mild or hybrid or computationally slow so not feasible to implement in a controller to be used in a vehicle but highly feasible for industrial application based purposes where time is not extremely crucial in term of the time between fault occurrence and damage done.

TABLE 1.5  
MACHINE LEARNING TECHNIQUES FOR FAULT DETECTION

Machine Learning Techniques Used	Ref. Number
High-breakdown statistical techniques which acts as a supervised classifier	[51]
Hybrid of artificial immune and support vector machines	[52]
Unsupervised Learning with Softmax regression and sparse filtering	[53]
Hybrid Fuzzy Min Max-Classification and Regression Tree model for supervised learning	[54], [55]
Hybrid Statistical and Neural Network for feature extraction/reduction	[56], [57]
Kalman Filter based pattern recognition	[58]
Adaptive Neural-Fuzzy	[59], [60]
Self-organizing-map based radial-basis-function network	[61]
Unsupervised Neural Network based	[62]

### *1.5. Research Contribution of this Dissertation*

As per the background study done, it clearly indicates that fault diagnosis is best when used with machine learning when it comes to EV application since they have higher predictive capabilities with increased accuracy and precision in considerable smaller period of time as opposed to other methods as shown in Table 1.3 and 1.4. So major objectives of this dissertation has been to investigate the stator winding fault occurrence at incipient stage before it leads to a catastrophic fault, propose faster methods of fault diagnosis and thereby creating a fault-tolerant drive system for an EV. For all of this, a few machine learning based fault detection method has been developed and implemented to find the feasibility and the usage of features to detect fault faster and classify the motor health condition as per the detected fault. Since this method needs to operate on a chip placed inside a vehicle, the algorithm to detect fault has to be faster than any present methodology, highly intuitive in nature, should not create a false alarm, work in collaboration with other

algorithms that will be used in self-driving technology. In this dissertation the findings of model based fault diagnosis has been presented using scaled down laboratory motors with similar characteristics as a traction motor. Then the idea of model based was moved to artificial neural network based predictive results. Since ANN in single layer is not so intuitive in prediction, multiple layers such as deep neural network has been used to predict better but that increased the time of training and the algorithm became much computational intensive. Eventually using the basic knowledge of statistical mathematics and the intuitive nature of deep neural nets, a dual memorization and generalization machine learning algorithm has been developed which changes itself on-time to adapt and process data faster when needed and higher accuracy. This algorithm uses, adaptive gradient decent, improvised regression and classification methodologies, deep neural networks and other regularization algorithms in one machine learning algorithm. This has been explained in details in chapter 4 along with the results.

### *1.6. Organization of this Dissertation Highlighting Research Contributions*

This dissertation including the introduction chapter has 9 chapters that presents the research conducted and the novel contributions made to this field of work to achieve the overall objectives. The chapters are organised as follows:

Chapter 2 discusses the performance of a motor in a traction application with incipient stator fault from finite element analysis (FEA) point of view. Two motors have been designed in an FEA software – one healthy and the other faulty, analysed and simulated to achieve similar results obtained from the experimental results. The study in chapter helped in defining the features which are essential for fault diagnosis and later using it for developing the machine learning algorithm.

Chapter 3 describes the methods used to understand how temperature can be used as one of the features for fault diagnosis of the motor in the EV. Initially, the motor temperature rise is monitored over a period of time and how it affects the parameters of the motor especially stator resistance. To achieve a more predictive temperature based fault diagnosis, a lumped thermal model has been proposed which has been coupled with artificial neural network to predict temperature of the motor and diagnose fault based on that predicted temperature.

Chapter 4 introduces how flux can be used as a feature for fault diagnosis. Since the value of flux reference is a direct input into the drive control of a motor in the powertrain of the EV, designing a block which can help in continued motor operation even after the occurrence of incipient stator fault. The design of this novel harmonics block has been explained here.

Chapter 5 uses the novel harmonics block as designed in Chapter 4 to develop a more fault-tolerant motor control for traction application. This harmonic compensation based control has been implemented on a 7.5 hp induction motor (IM) which has previously detected stator winding fault. It has been shown how this novel fault-tolerant control has helped in continued operation of the motor with better performance than a control without fault-tolerant capabilities.

Chapter 6 extends the work done in Chapter 5 by introducing an intelligent swarm optimization based flux reference prediction since in traction application the prediction needs to be fast. This has greatly improved the computational time and also the faulty motor is ready before the incipient fault occurs by observing the trend in change of parameters.

Chapter 7 introduces machine learning algorithm and a deep neural network has been developed in order to predict flux reference more efficiently accurately as compared to the swarm optimization method. Due to machine learning algorithm, the improvement in flux predictions have been noted and shown how it helps in developing a smarter, artificial intelligent based fault-tolerant motor control.

Chapter 8 shows the final work of the development of a better, faster, more accurate and precise dual memorization and generalization machine learning algorithm which has been a significant improvement in the previous algorithms used for predicting fault using different features. It has also been a big improvement as compared to the other flux predictive fault-tolerant controls as per literature review.

Chapter 9 is the conclusive chapter summarizing the different tasks that have been achieved which led to the final development of a machine learning based flux prediction for a fault-tolerant control. The future work has been shown so as to continue this work into a well defined artificial intelligence based motor control.

## 1.7. References

- [1] J. Shankleman, "The Electric Car Revolution Is Accelerating," Bloomberg Businessweek Publication, Jul. 2017
- [2] B. Muller and G. Meyer, "Electric Vehicle Systems Architecture and Standardization Needs," Springer Publications, Feb. 2015
- [3] C. Chen and K.T. Chau, "Modern Electric Vehicle Technology," Oxford University Press, 2001
- [4] J. Larminie, "Electric Vehicle Technology Explained," Wiley Publication, 2003
- [5] Electric Vehicle Market, "<https://cleantechnica.com/>" Accessed on January 21, 2018
- [6] Layout of Tesla Model S, "<https://www.tesla.com/models>"
- [7] Information about Tesla Model S design and specifications, "[https://en.wikipedia.org/wiki/Tesla\\_Model\\_S](https://en.wikipedia.org/wiki/Tesla_Model_S)"
- [8] Electric car sales values at "<https://electricdrive.org>"
- [9] Electric vehicles available in Canadian market and prices of respective cars, "<https://www.fleetcarma.com/electric-vehicles-currently-available-in-canada/>," Accessed on February 10, 2018
- [10] Prices of Electric vehicles available in Canadian market "<http://www.autotrader.ca>" Accessed on January 30, 2018
- [11] B. Johnston, and N. Tesla, "My Inventions: The Autobiography of Nikola Tesla," Experimenter Publishing Company, Inc., 1919
- [12] S. Karmakar, S. Chattopadhyay, M. Mitra, and S. Sengupta, "Induction Motor Fault Diagnosis," Springer Publications, April 2016
- [13] S. Grubic, J. M. Aller, B. Lu, and T. G. Habetler, "A Survey on Testing and Monitoring Methods for Stator Insulation Systems of Low-Voltage Induction Machines Focusing on Turn Insulation Problems," *IEEE Transactions on Industrial Electronics*, vol. 55, no. 12, pp. 4127-4136, Dec. 2008.
- [14] G. M. Joksimovic, and J. Penman, "The Detection of Inter-turn Short Circuits in the Stator Windings of Operating Motors," *IEEE Transactions on Industrial Electronics*, vol. 47, no. 5, pp. 1078-1084, Oct 2000.

- [15] A. H. Bonnett, and G. C. Soukup, "Cause and Analysis of Stator and Rotor Failures in Three-phase Squirrel-cage Induction Motors," *IEEE Transactions on Industry Applications*, vol. 28, no. 4, pp. 921-937, Jul/Aug 1992.
- [16] J. P. G. de Abreu, and A. E. Emanuel, "Induction Motor Thermal Aging Caused by Voltage Distortion and Imbalance: Loss of Useful Life and its Estimated Cost," *IEEE Transactions on Industry Applications*, vol. 38, no. 1, pp. 12-20, Jan/Feb 2002.
- [17] H. Henao, C. Demian, and G. A. Capolino, "A Frequency-domain Detection of Stator Winding Faults in Induction Machines Using an External Flux Sensor," *IEEE Transactions on Industry Applications*, vol. 39, no. 5, pp. 1272-1279, Oct. 2003.
- [18] S. B. Lee, R. M. Tallam, and T. G. Habetler, "A Robust, On-line Turn-fault Detection Technique for Induction Machines based on Monitoring the Sequence Component Impedance Matrix," *IEEE Transactions on Power Electronics*, vol. 18, no. 3, pp. 865-872, May 2003.
- [19] R. M. Tallam, T. G. Habetler, and R. G. Harley, "Stator Winding Turn-fault Detection for Closed-loop Induction Motor Drives," *IEEE Transactions on Industry Applications*, vol. 39, no. 3, pp. 720-724, May-June 2003.
- [20] J. Yun, K. Lee, K. W. Lee, S. B. Lee, and J. Y. Yoo, "Detection and Classification of Stator Turn Faults and High-Resistance Electrical Connections for Induction Machines," *IEEE Transactions on Industry Applications*, vol. 45, no. 2, pp. 666-675, March-april 2009.
- [21] A. M. Knight, and S. P. Bertani, "Mechanical Fault Detection in a Medium-sized Induction Motor Using Stator Current Monitoring," *IEEE Transactions on Energy Conversion*, vol. 20, no. 4, pp. 753-760, Dec. 2005.
- [22] L. Frosini, C. Harlişca, and L. Szabó, "Induction Machine Bearing Fault Detection by Means of Statistical Processing of the Stray Flux Measurement," *IEEE Transactions on Industrial Electronics*, vol. 62, no. 3, pp. 1846-1854, March 2015.
- [23] R. R. Schoen, T. G. Habetler, F. Kamran, and R. G. Bartfield, "Motor Bearing Damage Detection Using Stator Current Monitoring," *IEEE Transactions on Industry Applications*, vol. 31, no. 6, pp. 1274-1279, Nov/Dec 1995.

- [24] S. B. Chaudhury, M. Sengupta, and K. Mukherjee, "Experimental Study of Induction Motor Misalignment and its Online Detection through Data Fusion," *IET Electric Power Applications*, vol. 7, no. 1, pp. 58-67, Jan. 2013.
- [25] O. A. Omitaomu, M. K. Jeong, A. B. Badiru, and J. W. Hines, "Online Support Vector Regression Approach for the Monitoring of Motor Shaft Misalignment and Feedwater Flow Rate," *IEEE Transactions on Systems, Man, and Cybernetics, Part C (Applications and Reviews)*, vol. 37, no. 5, pp. 962-970, Sept. 2007.
- [26] L. Lin, A. Kang, J. Song, Z. Lei, Y. Zhao, and C. Feng, "Influences of Humidity and Temperature on Oil Contamination Discharge of HV Motor Stator Windings," *IEEE Transactions on Dielectrics and Electrical Insulation*, vol. 23, no. 5, pp. 2695-2703, October 2016.
- [27] M. Levesque, E. David, C. Hudon, and M. Belec, "Contribution of humidity to the evolution of slot partial discharges," *IEEE Transactions on Dielectrics and Electrical Insulation*, vol. 19, no. 1, pp. 61-75, February 2012.
- [28] C. Li, J. Song, L. Lin, Z. Lei, W. Su, and X. Bi, "Effects of Vapor with Different Chemical Properties on Corona Partial Discharges of Stator Windings," *IEEE Transactions on Dielectrics and Electrical Insulation*, vol. 21, no. 3, pp. 964-972, June 2014.
- [29] D. Shah, S. Nandi, and P. Neti, "Stator-Interturn-Fault Detection of Doubly Fed Induction Generators Using Rotor-Current and Search-Coil-Voltage Signature Analysis," *IEEE Transactions on Industry Applications*, vol. 45, no. 5, pp. 1831-1842, Sept.-Oct. 2009.
- [30] M. Cuevas, R. Romary, J. P. Lecoite, and T. Jacq, "Non-Invasive Detection of Rotor Short-Circuit Fault in Synchronous Machines by Analysis of Stray Magnetic Field and Frame Vibrations," *IEEE Transactions on Magnetics*, vol. 52, no. 7, pp. 1-4, July 2016.
- [31] S. Grubic, J. M. Aller, B. Lu and T. G. Habetler, "A Survey on Testing and Monitoring Methods for Stator Insulation Systems of Low-Voltage Induction Machines Focusing on Turn Insulation Problems," *IEEE Transactions on Industrial Electronics*, vol. 55, no. 12, pp. 4127-4136, Dec. 2008.



- [32] G. C. Stone, H. G. Sedding, B. A. Lloyd and B. K. Gupta, "The Ability of Diagnostic Tests to Estimate the Remaining Life of Stator Insulation," *IEEE Transactions on Energy Conversion*, vol. 3, no. 4, pp. 833-841, Dec 1988.
- [33] G. C. Stone, "Recent Important Changes in IEEE Motor and Generator Winding Insulation Diagnostic Testing Standards," *IEEE Transactions on Industry Applications*, vol. 41, no. 1, pp. 91-100, Jan.-Feb. 2005.
- [34] IEEE Recommended Practice for Testing Insulation Resistance of Electric Machinery - Redline," *IEEE Std 43-2013 (Revision of IEEE Std 43-2000)*, vol., no., pp.1-75, March 6 2014
- [35] T. Emery, "Stator Winding Performance Testing when using AC and DC Voltages,"in the Proc. of *2014 IEEE Electrical Insulation Conference (EIC)*, pp. 363-367, Philadelphia, PA, 2014.
- [36] X. Huang, T. G. Habetler, R. G. Harley, and E. J. Wiedenbrug, "Using a Surge Tester to Detect Rotor Eccentricity Faults in Induction Motors," *IEEE Transactions on Industry Applications*, vol. 43, no. 5, pp. 1183-1190, Sept.-Oct. 2007.
- [37] G. C. Stone, "A Perspective on Online Partial Discharge Monitoring for Assessment of the Condition of Rotating Machine Stator Winding Insulation," *IEEE Electrical Insulation Magazine*, vol. 28, no. 5, pp. 8-13, September-October 2012.
- [38] T. J. Kang, J. Kim, S. B. Lee, and C. Yung, "Experimental Evaluation of Low-Voltage Offline Testing for Induction Motor Rotor Fault Diagnostics," *IEEE Transactions on Industry Applications*, vol. 51, no. 2, pp. 1375-1384, March-April 2015.
- [39] B. Kim, K. Lee, J. Yang, S. B. Lee, E. J. Wiedenbrug, and M. R. Shah, "Automated Detection of Rotor Faults for Inverter-Fed Induction Machines Under Standstill Conditions," *IEEE Transactions on Industry Applications*, vol. 47, no. 1, pp. 55-64, Jan.-Feb. 2011.
- [40] S. Nandi, and H. A. Toliyat, "Novel Frequency-Domain-Based Technique to Detect Stator Inter-turn Faults in Induction Machines using Stator-Induced Voltages after Switch-Off," *IEEE Transactions on Industry Applications*, vol. 38, no. 1, pp. 101-109, Jan/Feb 2002.

- [41] W. T. Thomson, and M. Fenger, "Current Signature Analysis to Detect Induction Motor Faults," *IEEE Industry Applications Magazine*, vol. 7, no. 4, pp. 26-34, Jul/Aug 2001.
- [42] M. El Hachemi Benbouzid, "A Review of Induction Motors Signature Analysis as a Medium for Faults Detection," *IEEE Transactions on Industrial Electronics*, vol. 47, no. 5, pp. 984-993, Oct 2000.
- [43] Z. Hou, J. Huang, H. Liu, M. Ye, Z. Liu, and J. Yang, "Diagnosis of Broken Rotor Bar Fault in Open- and Closed-Loop Controlled Wye-Connected Induction Motors Using Zero-Sequence Voltage," *IET Electric Power Applications*, vol. 11, no. 7, pp. 1214-1223, Aug. 2017.
- [44] D. Wu, X. Wu, L. Su, X. Yuan, and J. Xu, "A Dual Three-Level Inverter-Based Open-End Winding Induction Motor Drive with Averaged Zero-Sequence Voltage Elimination and Neutral-Point Voltage Balance," *IEEE Transactions on Industrial Electronics*, vol. 63, no. 8, pp. 4783-4795, Aug. 2016.
- [45] B. M. Ebrahimi, J. Faiz and M. J. Roshtkhari, "Static-, Dynamic-, and Mixed-Eccentricity Fault Diagnoses in Permanent-Magnet Synchronous Motors," *IEEE Transactions on Industrial Electronics*, vol. 56, no. 11, pp. 4727-4739, Nov. 2009.
- [46] J. Hey, A. C. Malloy, R. Martinez-Botas, and M. Lampérth, "Online Monitoring of Electromagnetic Losses in an Electric Motor Indirectly Through Temperature Measurement," *IEEE Transactions on Energy Conversion*, vol. 31, no. 4, pp. 1347-1355, Dec. 2016.
- [47] J. A. Ramirez-Nunez, L. A. Morales-Hernandez, R. A. Osornio-Rios, J. A. Antonino-Daviu, and R. J. Romero-Troncoso, "Self-Adjustment Methodology of a Thermal Camera for Detecting Faults in Industrial Machinery," in the Proc. of *42nd Annual Conference of the IEEE Industrial Electronics Society*, pp. 7119-7124, Florence, 2016.
- [48] F. Filippetti, G. Franceschini, C. Tassoni, and P. Vas, "Recent Developments of Induction Motor Drives Fault Diagnosis Using AI Techniques," *IEEE Transactions on Industrial Electronics*, vol. 47, no. 5, pp. 994-1004, Oct 2000.
- [49] F. J. Lin, Y. C. Hung, J. C. Hwang, and M. T. Tsai, "Fault-Tolerant Control of a Six-Phase Motor Drive System Using a Takagi–Sugeno–Kang Type Fuzzy Neural

- Network With Asymmetric Membership Function," *IEEE Transactions on Power Electronics*, vol. 28, no. 7, pp. 3557-3572, July 2013.
- [50] A. Gandhi, T. Corrigan, and L. Parsa, "Recent Advances in Modeling and Online Detection of Stator Interturn Faults in Electrical Motors," *IEEE Transactions on Industrial Electronics*, vol. 58, no. 5, pp. 1564-1575, May 2011.
  - [51] L. A. García-Escudero, O. Duque-Perez, M. Fernandez-Temprano, and D. Morinigo-Sotelo, "Robust Detection of Incipient Faults in VSI-Fed Induction Motors Using Quality Control Charts," *IEEE Transactions on Industry Applications*, vol. 53, no. 3, pp. 3076-3085, May-June 2017.
  - [52] I. Aydin, M. Karakose, and E. Akin, "Artificial Immune based Support Vector Machine Algorithm for Fault Diagnosis of Induction Motors," in the Proc. of *2007 International Aegean Conference on Electrical Machines and Power Electronics*, pp. 217-221, Bodrum, 2007.
  - [53] Y. Lei, F. Jia, J. Lin, S. Xing, and S. X. Ding, "An Intelligent Fault Diagnosis Method Using Unsupervised Feature Learning Towards Mechanical Big Data," *IEEE Transactions on Industrial Electronics*, vol. 63, no. 5, pp. 3137-3147, May 2016.
  - [54] M. Seera, and C. P. Lim, "Online Motor Fault Detection and Diagnosis Using a Hybrid FMM-CART Model," *IEEE Transactions on Neural Networks and Learning Systems*, vol. 25, no. 4, pp. 806-812, April 2014.
  - [55] M. Seera, C. P. Lim, D. Ishak, and H. Singh, "Fault Detection and Diagnosis of Induction Motors Using Motor Current Signature Analysis and a Hybrid FMM-CART Model," *IEEE Transactions on Neural Networks and Learning Systems*, vol. 23, no. 1, pp. 97-108, Jan. 2012.
  - [56] T. Boukra, A. Lebaroud, and G. Clerc, "Statistical and Neural-Network Approaches for the Classification of Induction Machine Faults Using the Ambiguity Plane Representation," *IEEE Transactions on Industrial Electronics*, vol. 60, no. 9, pp. 4034-4042, Sept. 2013.
  - [57] M. D. Prieto, G. Cirrincione, A. G. Espinosa, J. A. Ortega, and H. Henao, "Bearing Fault Detection by a Novel Condition-Monitoring Scheme Based on Statistical-

- Time Features and Neural Networks," *IEEE Transactions on Industrial Electronics*, vol. 60, no. 8, pp. 3398-3407, Aug. 2013.
- [58] O. Ondel, E. Boutleux, E. Blanco, and G. Clerc, "Coupling Pattern Recognition with State Estimation Using Kalman Filter for Fault Diagnosis," *IEEE Transactions on Industrial Electronics*, vol. 59, no. 11, pp. 4293-4300, Nov. 2012.
- [59] M. S. Ballal, Z. J. Khan, H. M. Suryawanshi, and R. L. Sonolikar, "Adaptive Neural Fuzzy Inference System for the Detection of Inter-Turn Insulation and Bearing Wear Faults in Induction Motor," *IEEE Transactions on Industrial Electronics*, vol. 54, no. 1, pp. 250-258, Feb. 2007.
- [60] D. Fuessel, and R. Isermann, "Hierarchical Motor Diagnosis Utilizing Structural Knowledge and a Self-Learning Neuro-Fuzzy Scheme," *IEEE Transactions on Industrial Electronics*, vol. 47, no. 5, pp. 1070-1077, Oct 2000.
- [61] S. Wu, and T. W. S. Chow, "Induction Machine Fault Detection Using SOM-based RBF Neural Networks," *IEEE Transactions on Industrial Electronics*, vol. 51, no. 1, pp. 183-194, Feb. 2004.
- [62] J. F. Martins, V. F. Pires, and A. J. Pires, "Unsupervised Neural-Network-Based Algorithm for an On-Line Diagnosis of Three-Phase Induction Motor Stator Fault," *IEEE Transactions on Industrial Electronics*, vol. 54, no. 1, pp. 259-264, Feb. 2007.

## CHAPTER 2

# UNDERSTANDING OF INCIPIENT STATOR WINDING FAULT OF IM AND FEATURE SELECTION FOR FAULT DIAGNOSIS

### 2.1. *Introduction*

To understand what an incipient stator winding fault looks like in a motor, it is essential to understand fault occurrence from the design point of view. Since winding fault is a fault which occurs in the motor itself and not in any of the power electronics components, design overview of a healthy and faulty IM has been presented in this chapter to understand the various aspects and the motor performance. To do so, the induction motor under test has been develop in a finite element analysis (FEA) software. Two identical motors have been used for this. One is the healthy motor on which various experiments have been done before cutting the motor into half to understand the design and recreate it in FEA. The other one is the fault IM which has been developed from the healthy IM FEA to match with the real IM under test.

### 2.2. *Electromagnetic Design of Electric Motor using Field Equations*

FEA has been proven an effective tool for precise electric machine simulation and analysis considering time and space harmonics [1], [2]. The focus of this section is a brief description of electromagnetic analysis via finite element method to compute the vector fields and forces acting in induction machine, and therefore a brief review of the FEA technique is necessary. Only the two-dimensional (2D) FEA technique is briefly reviewed in this section. The three-dimensional (3D) FEA technique is based upon similar principles, but with more complex differential equations due to the additional dimension. The dynamics of electromagnetic fields are modeled using Maxwell's equations.

$$\nabla \times \vec{E} = -\frac{\partial \vec{B}}{\partial t} \quad (2.1)$$

$$\nabla \times \vec{B} = \mu \vec{J} + \mu \epsilon \frac{\partial \vec{E}}{\partial t} \quad (2.2)$$

$$\nabla \cdot \vec{E} = \frac{\rho}{\epsilon} \quad (2.3)$$

$$\nabla \cdot \vec{B} = 0 \quad (2.4)$$

where  $E$  is the electric field,  $B$  is the flux density,  $J$  is the current density,  $\rho$  is the charge density,  $\epsilon$  is the permittivity of the material, and  $\mu$  is the permeability of the material. In electric machines,  $\mu J$  is considered, while the rest of the term is generally very small, and is neglected. Therefore, in most of electric machines it is neglected and (2.2) is approximated. To derive a partial differential equation to model machines, a magnetic vector potential  $A$  is often defined and subsequently substituted into (2.2), which yields,

$$\nabla \times v(\nabla \times \vec{A}) = \vec{J} \quad (2.5)$$

where  $v$  is magnetic reluctivity equal to  $1/\mu$ . In electric machines, the uniformity along the  $z$ -axis enables one to model the machine in two dimensions. Assuming the vector fields can be modeled in two-dimensions, vector potential is assumed to be in  $Z$  coordinate as

$$\vec{A} = A_z \hat{z} \quad (2.6)$$

where  $Z$  is the unit vector of the  $Z$ -axis. Moreover,  $A_z$  is not a function of  $z$ . Hence,

$$\nabla \times \vec{A} = \frac{\partial A_z}{\partial y} \hat{x} - \frac{\partial A_z}{\partial x} \hat{y} \quad (2.7)$$

Equation 2.5 becomes

$$\left[ \frac{\partial}{\partial x} v \left( \frac{\partial A_z}{\partial x} \right) + \frac{\partial}{\partial y} v \left( \frac{\partial A_z}{\partial y} \right) \right] \hat{z} = -\vec{J} \quad (2.8)$$

In the machine, the current density vector  $J$  is also in the  $Z$  direction, and (2.8) is converted to Poisson's equation

$$\frac{\partial}{\partial x} v \left( \frac{\partial A_z}{\partial x} \right) + \frac{\partial}{\partial y} v \left( \frac{\partial A_z}{\partial y} \right) = -J_z \quad (2.9)$$

In the FEA, the planar structure being modeled is divided into numerous elements. These are often triangles in 2D FEA. The three vertices of a triangle are called nodes. Within each triangle,  $\gamma$  is assumed to be constant. In addition, the magnetic vector potential within each triangle is assumed to be a linear combination of the three nodal potentials of the triangle [3]. Starting with (2.9), for the stator and rotor assuming that the current density results from winding excitations and induced voltage from stator respectively where induced electric fields are neglected, upon applying the finite element method, the magnetic vector potential at each node is obtained by solving an algebraic equation

$$SA = I \quad (2.10)$$

where the global stiffness matrix  $S$  is an  $n \times n$  matrix that contains components that are a function of the material properties, and element geometries,  $A$  is the unknown  $n \times 1$  vector of nodal potentials,  $I$  is an  $n \times 1$  vector representing nodal currents

$$I = [I_1 \quad I_2 \quad \cdots \quad I_n]^T \quad (2.11)$$

The individual nodal current is represented by

$$I_j = \sum_{\text{All triangles containing node } j} \frac{J_k \Delta_k}{3}, \quad j \in [1, n] \quad (2.12)$$

$k$  is the index number of a triangle containing node  $j$ ,  $J_k$  is the current density of triangle  $k$ , and  $\Delta k$  is the area of triangle  $k$ . After calculating  $A$ , the flux density within each element can be also obtained using (2.5). The accuracy of the FEA solution is a function of the number of elements used in the discretization. Generally, a large number of elements are required to have a satisfactorily and accurate result for induction machines. This means equation (2.10) is of relatively large order, which imposes significant computational load for constructing and solving the equation. Therefore, FEA requires much more

computational effort compared with lumped-parameter models and MEC to satisfy the accuracy of the analysis.

Using the magnetic field calculated in FEA, the electromagnetic force and torque are calculated from the computed flux densities or magnetic potentials. To calculate the force and torque within FEA, several numerical techniques have been applied such as Lorenz force, Maxwell stress tensor or global co-energy methods. FEA is a useful modeling method to accurately predict machine performance, but its intense computational effort limits its application. Therefore, research has been done to increase the simulation speed of FEA by reducing the model complexity. In the proposed method, the rotor and stator models are calculated in the FEA program separately. Moreover, the rotor model contains only one slot pitch to limit the computational effort, and the stator model contains one pole pitch. The lumped parameters, which are then used to set up a LP steady-state model, can be therefore obtained within a short time. To incorporate the skew effect into the model, 3D FEA is usually used, which takes much more time than 2D FEA. To represent a rotor in 2D models, one can use a set of non-skewed 2D models, each representing a section of rotor at different positions along the machine axis. The continuously skewed rotor is then approximated as multiple slices. Care must be taken in this technique to ensure that the currents in the rotor bars are consistent on every slice.

### *2.3. Structural Design of Laboratory IM in FEA software*

In order to understand and design a fault diagnostic method two similar IM have been used in this study. Although the machine developed and used for testing is on industrial motors but the study done can be extended to traction application. One has been the healthy IM and the other is the IM with stator-inter turn fault. Both are the same motors of 7.5 hp motors. In order to understand the behavioural difference in the two motors, extensive experimentation have been conducted on both the motors. Once the results have been recorded which will be presented in the consequent chapters, the healthy motor was dismantled to understand the design of the motor. The windings were taken out to understand the way the stator winding was done and the rotor was cut to find the design of the rotor slots and the dimensions. On taking out the windings, it was found that the stator has single layer concentric winding distribution whose layout has been shown in Table 2.1.



The stator dimensions were taken to re-create the machine in a finite element software as shown in Fig. 2.1. Similarly, the rotor was cut as shown in order to find the design layout and the dimensions as shown in Fig. 2.2. In Fig. 2.3, the resemblance of the cut rotor to the designed rotor in FEA has been done to indicate the similarity of the FEA designed software to be as close to the machine being tested. The main objective has been to understand the motor performance and what happens to the motor when there is a slight inter-turn fault from design perspective. The complete motor was designed both in 2-D FEA as shown in Fig. 2.4 as well as 3-D FEA as shown in Fig. 2.5. But for analysis of results the 2-D FEA model was used because of it faster computational time and decent accuracy in results when compared with experimental results.

TABLE 2.1  
WINDING DISTRIBUTION IN THE STATOR OF THE IM UNDER STUDY

Slot	1	2	3	4	5	6	7	8	9	10	11	12	13	14	15	16
Phase	A	A	A	A	-C	-C	-C	-C	B	B	B	B	-A	-A	-A	-A
Slot	17	18	19	20	21	22	23	24	25	26	27	28	29	30	31	32
Phase	C	C	C	C	-B	-B	-B	-B	A	A	A	A	-C	-C	-C	-C
Slot	33	34	35	36	37	38	39	40	41	42	43	44	45	46	47	48
Phase	B	B	B	B	-A	-A	-A	-A	C	C	C	C	-B	-B	-B	-B

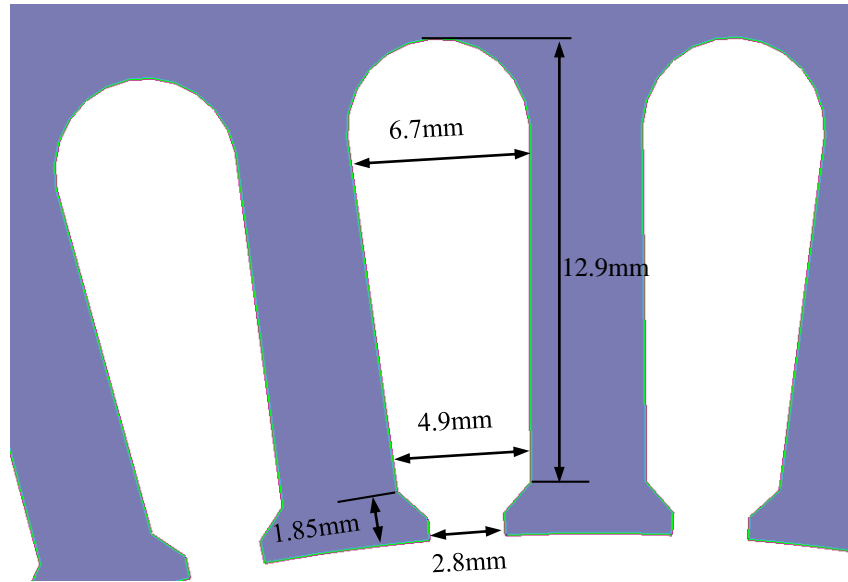


Fig. 2.1. Stator slot dimension as measured to be used as inputs for FEA design.

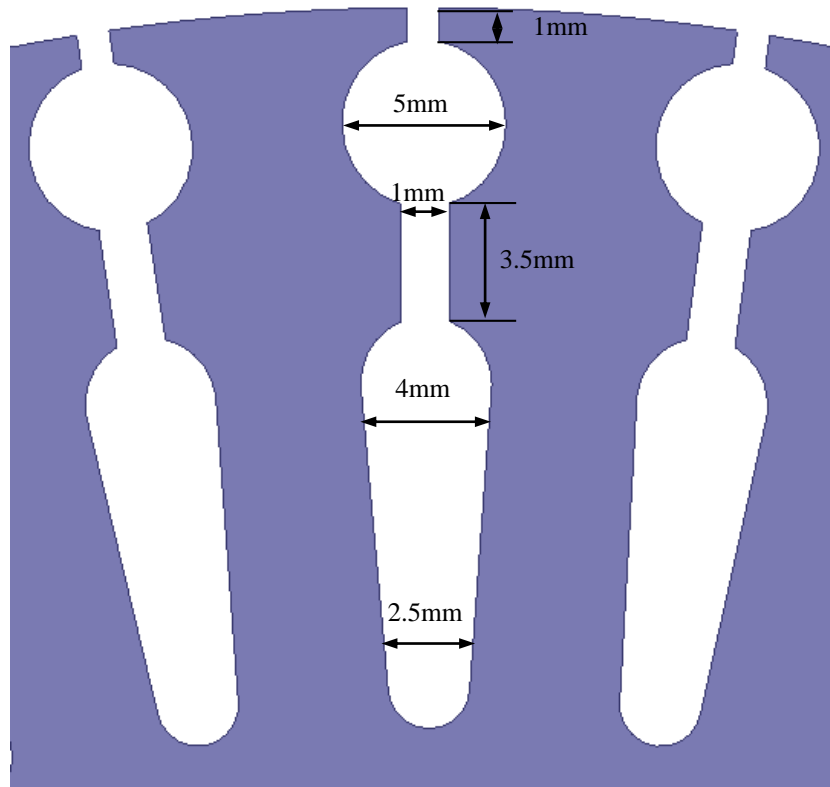
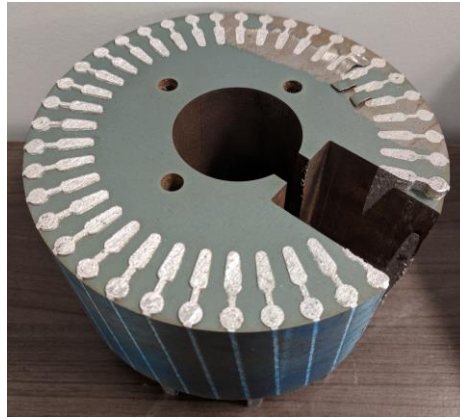


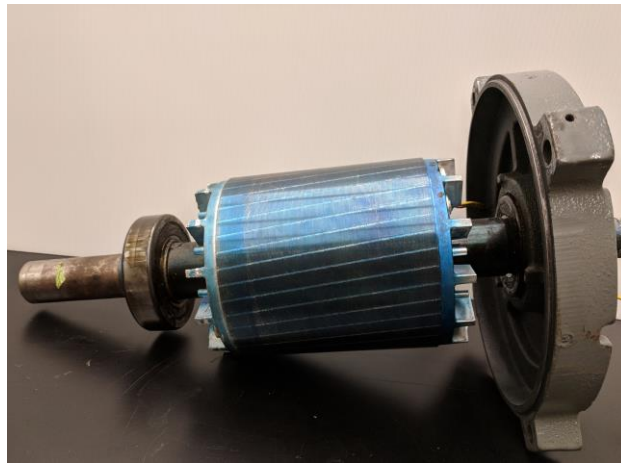
Fig. 2.2. Rotor slot dimensions as measured and used as input for FEA designing.



(a)



(b)



(c)



(d)



(e)

Fig. 2.3. Faulty IM under test. (a) Rotor cross-section to understand and find the dimensions of the rotor slots. (b) Opened stator for dimension measurement. (c) Just the rotor taken out of the motor. (d) Complete faulty IM. (e) Rotor placed inside the stator.

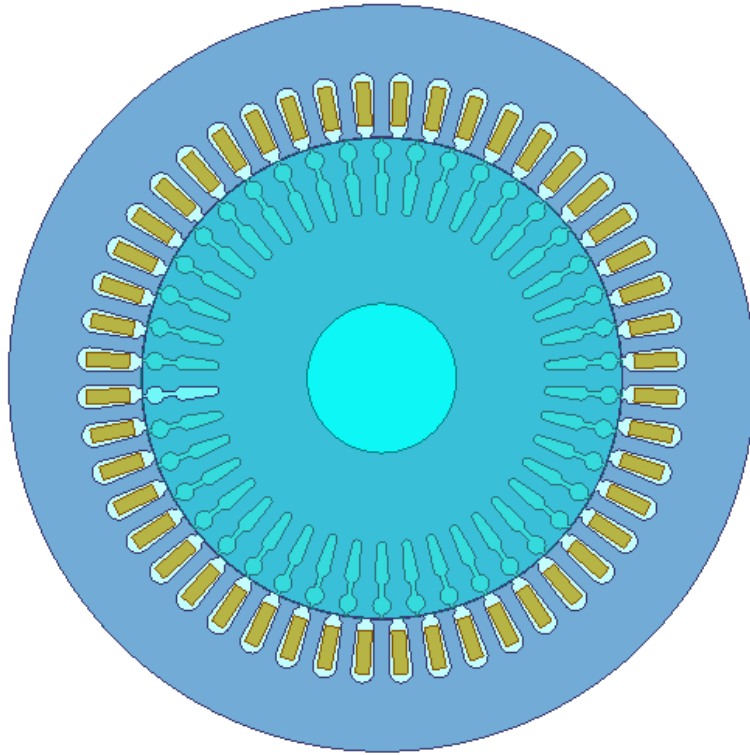


Fig. 2.4. 2-D FEA modelling of the 7.5 hp motor.

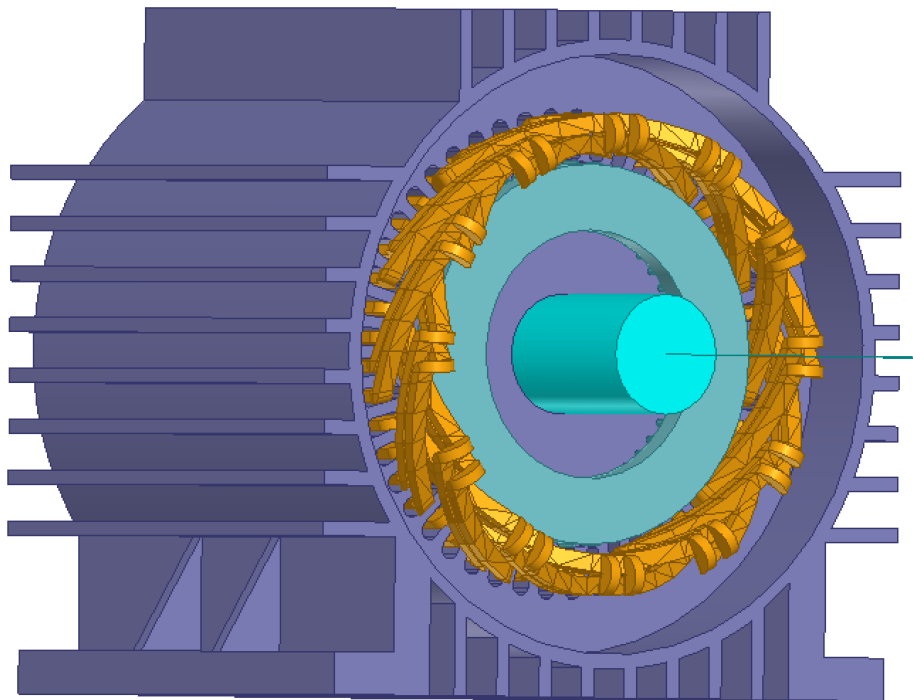


Fig. 2.5. 3-D FEA modelling of the motor under investigation.

TABLE 2.2

PARAMETERS OF THE ALUMINUM ROTOR INDUCTION MOTOR UNDER TEST

Equivalent Circuit Parameters		Rated Parameters	
$R_s$	0.180 $\Omega$	$P_{out}$	7.5 hp
$R_r$	0.590 $\Omega$	$V_{rms}$	200 V
$X_{ls}$	0.570 $\Omega$	$I_{rms}$	20.9 A
$X_{lr}$	0.860 $\Omega$	Speed	1,750 rpm
$X_m$	22.67 $\Omega$	Pole Pairs	2
$\omega$	376.8 rad/s	Rotor Slots	42

#### 2.4. Performance Analysis of IM under Different Operating Conditions

During FEA, the IMs both the faulty and healthy IM have been given the same operating conditions. Both have been operated in voltage and current excitation for better understanding. The results presented here are for the motor being operated at line-to-line voltage of 208 V. As it can be seen in Fig. 2.6 (a), the healthy IM has even distribution in the current waveform whereas in Fig 2.6 (b), it can be seen that the behaviour of phase A is different in amplitude compared to the other two phases since the fault occurrence is in that phase. Similarly, when comparing the induced voltages in the stator windings as shown in Figs. 2.7. (a) and (b), the faulty phase not only has lesser amplitude but also disturbs the consequent phases. Figs. 2.8 (a) and (b) represents the motor performance in terms of flux linkage where in healthy conditions, the flux linkage induces in all phases is even at 0.8 Wb, whereas in the faulty IM for phase A it is at 0.6 Wb while phase B and C are at 0.76 Wb. This indicates why having current voltage and flux are important features for fault detection. The fault also affects the torque performance with increase ripples as in Fig. 2.9.

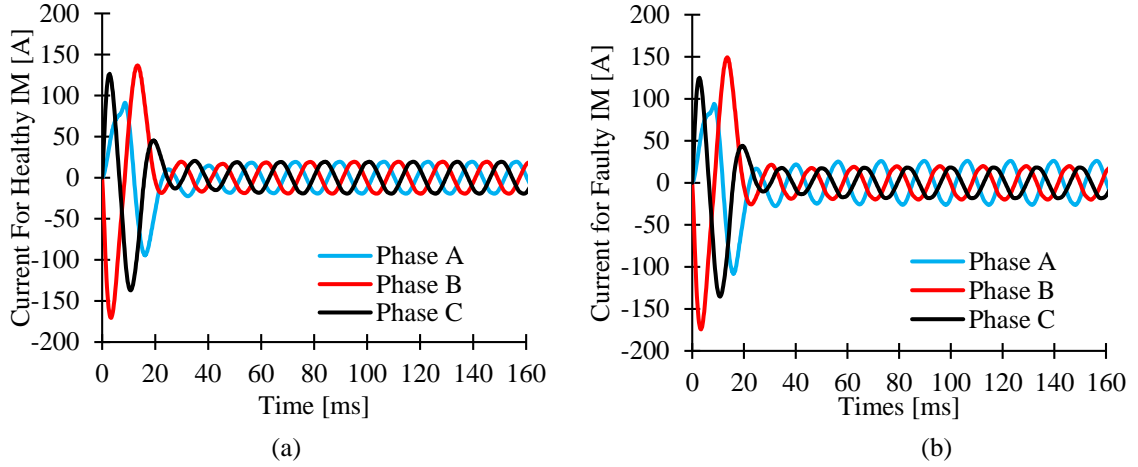


Fig. 2.6. The stator current waveform as generated in FEA software. (a) Healthy IM. (b) IM with incipient stator winding fault.

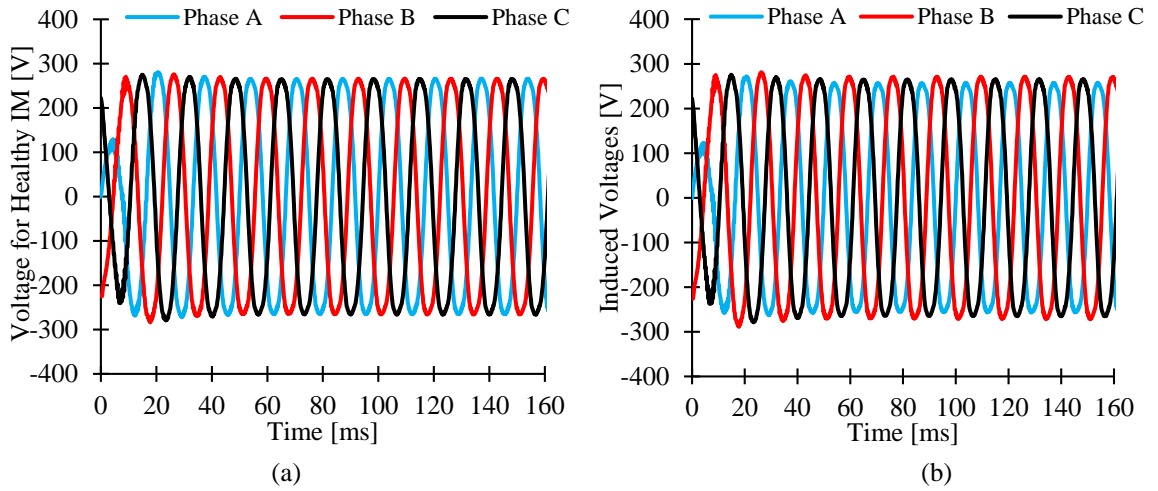


Fig. 2.7. The induced voltage in the windings of all the phases of IM. (a) Healthy IM. (b) IM with incipient stator winding fault.

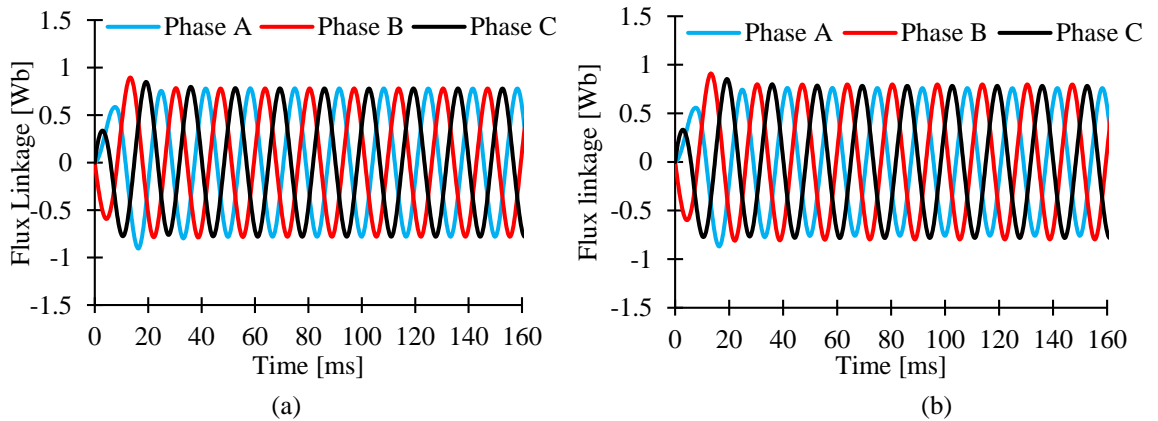


Fig. 2.8. The flux linkage as generated in the windings of all the phases of IM. (a) Healthy IM. (b) IM with incipient stator winding fault.

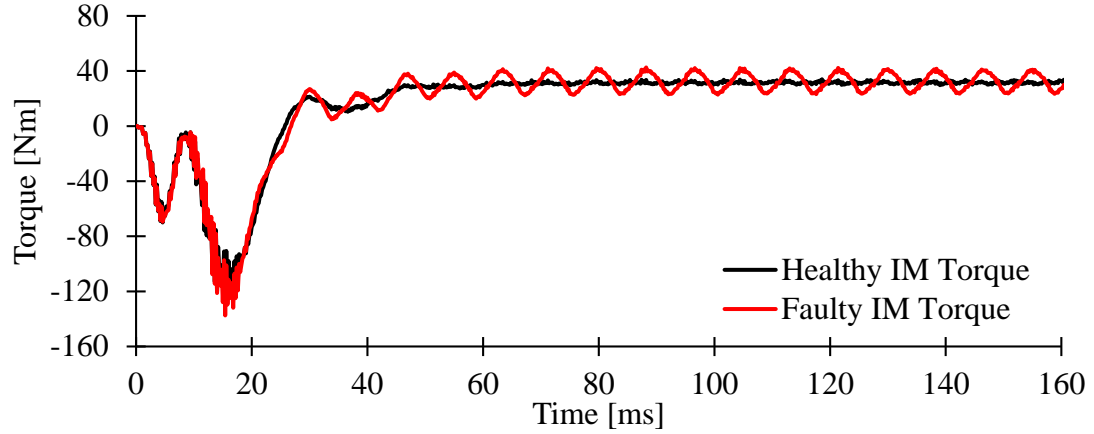


Fig. 2.9. Torque generated in IM with incipient fault has more torque ripple when compared with the healthy IM condition.

## 2.5. Fundamentals of Heat Transfer in Electric Machines

This section overviews the theory behind fluid dynamics and heat transfer [4]. This is the theory behind the simulations done for investigating thermal distribution of electric machines.

### A. Heat Transfer in Electric Machines

Heat transfer always occurs through a temperature gradient in a system. According to the second law of thermodynamics, the entropy of a system always increases over time or remains constant in a steady state. In an electric motor, heat sources are losses in the machine, which generate heat that transfers to the machine casing. In an electric machine, heat transfer has equal importance as electromagnetics because the temperature rise of the machine determines the total power output. The problem of temperature rise can be seen in two ways, removal of heat from the motor or distribution of the heat inside the machine. In transients of the motor, heat is also distributed differently than in steady state conditions.

Conduction is the transfer of heat through some medium. This only occurs when a temperature gradient is present. The rate that the heat transfers through a material depends on the temperature and thermal conductivity of the material. This can be expressed by the following equation:

$$q = -k \frac{dT}{dx} \quad (2.13)$$

where  $q$ [W/mK] is the heat flux, and  $k$  is called thermal conductivity. Conduction can be described as the quantity of heat transmitted in time through a distance. The property of  $k$  can change the rate it can conduct and this property can also be dependent on temperature. Typically, in metallic substances, thermal conductivity decreases while temperature rises. In comparison, the thermal conductivity of an insulator increases as temperature increases.

#### *B. Losses in Traction Electric Machines*

Losses in the electric machine can directly be related to the heat generated in a motor. The losses can be characterized in the following types - core losses or iron losses, stator coil winding losses (copper losses), friction and windage losses (mechanical losses), and stray load losses. Understanding these losses can help in understanding the sources of heat and areas of concern in the machine layout.

Iron losses are losses that occur in the core of the machine itself. These losses depend on the geometry, manufacturing processes and construction of the laminations. Losses in the iron can be split into two types, hysteresis losses and eddy current losses. Hysteresis loss comes from the alternating flux in the iron core, but the alternating flux also induces a voltage that induces eddy currents. This is reduced by laminations or high resistivity compounds. The iron losses can be shown in the equation below:

$$P_{Fe} = \sum K_h f B_p^n + K_e (f B_p)^2 \quad (2.14)$$

Stator losses are the resistive losses in the conductors of the machine. Resistive losses come from the actual windings of the machine. Since there are only windings on the stator of the machine, all of the resistive losses are on the stator. This makes the simulations and the calculations simpler, as only one part has to be solved for. The power loss that occurs in the windings can be described by the following equation:

$$P_{Cu} = I^2 R_{AC} \quad (2.15)$$

where  $R_{AC}$  is the AC resistance of the phase winding.



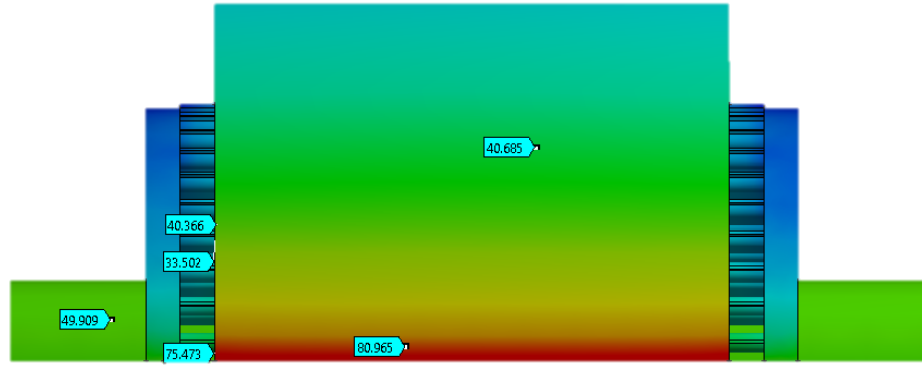
### *C. Other Mechanical Losses in the Machine*

Some of the losses come from the bearing themselves. This comes from the friction in the rolling elements to the sealing for the grease of the bearing. These losses are very small and have relatively no impact on the machine thermally. One of the other mechanical losses is windage, this comes from the rotor spinning and acting as an inefficient fan. This actually has a positive impact on thermal management of the system as it creates moving air inside the machine. This does not have a great effect on the overall thermal management of the machine.

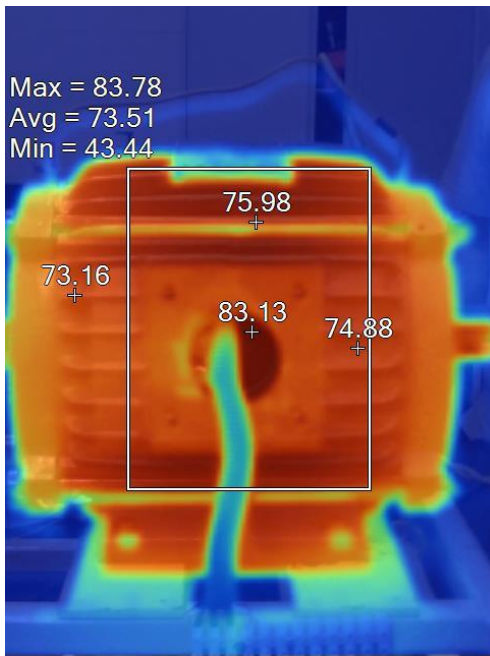
### *D. CFD Analysis of Electric Machine at Steady State*

Computational fluid dynamic (CFD) simulations are important for understanding heat extraction from the machine. The original design of the machine was meant to be air cooled by ambient air. This is just air that is around the machine and there is no forced air cooling involved. This type of cooling is the easiest to implement as there are no additional parts for the machine and this method is the most reliable as there are no moving parts for cooling. This type cooling, however, is insufficient for current electric machine design and additional cooling needs to be added for optimal performance characteristics. This type of air cooling will be simulated through CFD to see the flow around the machine. The purpose of this simulation is to observe the nature of air as it becomes lighter and rises as the temperature increases. This air is then replaced by cool air from below the machine. The simulation is done to observe this air cooling effect and to determine how much current can be applied while keeping the temperature of the machine below its limits. This was performed to mimic the steady state condition where the air around the machine is heated from the motor itself. The internals of the machine are also filled with air, but are in an enclosed space similar to the actual machine. The purpose of the simulation with CFD of the machine is to identify the heat distribution of the machine with natural air flow. All of the information from electromagnetic analysis is used in the following simulations. These will include all of the factors of the machines, including all of the heat generation of the machine. At high current loads, the dominant heat generation comes from the coils in resistance heating. As it can be seen in Fig. 2.10 (a) the motor gets extremely high in certain region indicating the fault occurrence. The CFD results indicating temperature rise as high

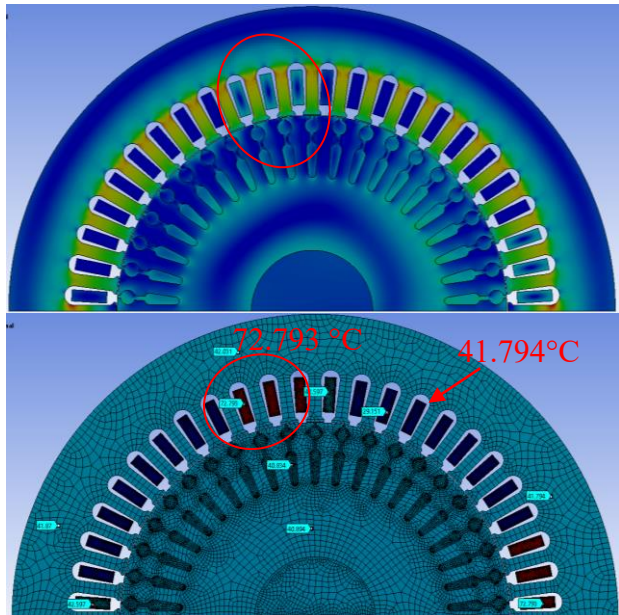
as  $80.965^{\circ}\text{C}$  complied with the experimental results as shown in Fig. 2.10 (b) where the temperature rises to around  $83.13^{\circ}\text{C}$



(a)



(b)



(c)

Fig. 2.10. Temperature rise in Faulty IM. (a) Thermal analysis. (b) Experimental results. (c) Heat flux and temperature variation as studied in FEA thermal analyser

## 2.6. Feature Selection for Developing Machine Learning for Fault Diagnosis

As seen in Section 2.4, the motor performance varies slightly when there is a change in an incipient stator winding fault. As the fault gradually changes to a major stator fault, the

motor performance changes drastically show the dangers of having such a motor in a vehicle can cause the safety of passengers to be at risk. From Sections 2.2 and 2.3, it can be said that flux and temperature are can be used to understand the occurrence of incipient fault. An incipient stator winding fault causes a variation in the balanced air-gap. The unbalance in air-gap causes the rotor to rotate in an uneven manner thereby worsening the situation. This air-gap flux can be studied and the variation can be used as an indication of fault occurrence. Even a harmonic tracking of the flux and current is a definitive indication of stator fault which will be presented in Chapter 4. Temperature is usually a result of continuous monitoring over a period of time to see any significant change. Thus temperature has been used as a feature which is more long term and definitive representative of the area of fault occurrence since the region cause more heat with increase in losses. As usual in a field-oriented control of IM the motor, the existing voltage and current sensors used for controlling the motor can also be used as feature which indicate if there is a fault due to change in the waveform of the result. In the consequent chapters, it will be shown how flux and temperature are used and the data analysis done to use them as feature for fault prediction machine learning algorithm.

## 2.7. References

- [1] S. Teymoori, A. Rahideh, H. Moayed-Jahromi, and M. Mardaneh, "2-D Analytical Magnetic Field Prediction for Consequent-Pole Permanent Magnet Synchronous Machines," *IEEE Transactions on Magnetics*, vol. 52, no. 6, pp. 1-14, June 2016.
- [2] M. Ojaghi, and S. Nasiri, "Modeling Eccentric Squirrel-Cage Induction Motors with Slotting Effect and Saturable Teeth Reluctances," *IEEE Transactions on Energy Conversion*, vol. 29, no. 3, pp. 619-627, Sept. 2014.
- [3] K. Komeza, and M. Dems, "Finite-Element and Analytical Calculations of No-Load Core Losses in Energy-Saving Induction Motors," *IEEE Transactions on Industrial Electronics*, vol. 59, no. 7, pp. 2934-2946, July 2012.
- [4] G. J. Li, J. Ojeda, E. Hoang and M. Gabsi, "Thermal-Electromagnetic Analysis of a Fault-tolerant Dual-Star Flux-Switching Permanent Magnet Motor for Critical Applications," *IET Electric Power Applications*, vol. 5, no. 6, pp. 503-513, July 2011.

## **CHAPTER 3**

### **MODEL BASED TEMPERATURE FEATURE PREDICTION UNDER INCIPIENT FAULT CONDITION**

#### *3.1. Introduction*

In this chapter, temperature has been considered as one of the primary features to identify any occurrence of stator winding fault for traction motor. A change in temperature in the stator windings can be a clear indication of the occurrence of some fault in the motor which causes additional increase in losses which is usually dissipated in the form of heat. This is a direct indication of the effect of incipient stator fault on the IM. When connected to a drive, the increase of losses is more causing further increase in thermal conditions of the motor. It is of utmost importance to understand the change in machine parameters caused during a stator fault, since it negatively affects the drive performance and degrades the motor performance even more. Initially, the temperature variation of a 15 kW copper rotor induction motor (CRIM) has been studied which is a scaled down traction motor and the variation of stator parameters in the form of resistance has been evaluated as well as estimated using a mild artificial intelligence namely, an Improved Swarm Particle Optimization (IPSO) technique to be used for determining any stator fault occurrence. This proposed method has been key in developing machine learning algorithms. Once established that stator fault causes huge variation in temperature, a novel Duplex Neural-Lumped Thermal Network (DNLTN) has been developed to predict temperature as well as fault in relation to temperature variation. This duplex lumped thermal model with machine learning has been presented in the later half of this chapter.

Several algorithms have been proposed in literature to estimate the stator and rotor resistance [1]–[4] from mathematical models using only stator voltage and current measurements. However, inclusion of precise temperature measurement has not been studied in detail. The parameters, when estimated independent of temperature, do not give a comprehensive understanding of how the stator resistance might change with increase in temperature due to continuous running of the machine. The robustness of various

algorithms can clearly be improved when observed from the perspective of temperature measurement [5], [6]. The IPSO technique is proposed in conjunction with the two axis model of an IM in order to precisely determine the variation of stator resistance occurring due to temperature rise. Subsequently, the accuracy of the estimated model based stator resistance is determined with the help of experimental verification using a 15 kW CRIM as shown in Fig. 3.1. This section hereby, provides a mild artificial intelligence method for accurately determining the temperature dependent stator resistance thereby determining the possibility of a stator failure. This estimated stator resistance can be fed back to the motor drive for better control of the motor under fault conditions. Thus, the ideology of an accurate drive fed machine is achieved.

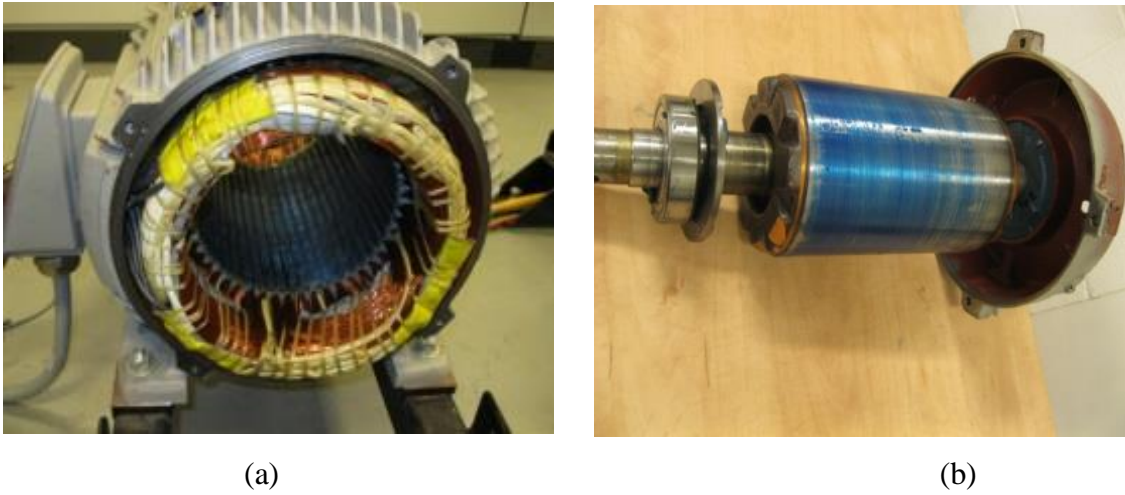


Fig. 3.1. The investigated motor under test. (a) Stator. (b) Rotor.

### 3.2. *Mathematical Model of Copper Rotor Induction Motor*

Since the machine under test is an induction machine, it has been modeled accordingly based on the two-axis theory [7]. The stator resistance,  $R_s$  is taken as an unknown variable. Since a squirrel cage IM is used, the rotor currents of the q-axis and the d-axis namely,  $I_{qr}$  and  $I_{dr}$  cannot be directly measured and the rotor voltages,  $V_{qr}$  and  $V_{dr}$  are zero as the rotor ends are shorted. In order to evaluate the rotor speed ( $\omega_r$ ) of the IM, the formula used is expressed as in (3.1)

$$\frac{d\omega_r}{dt} = \frac{P}{2J} (T_e - T_L) \quad (3.1)$$

where  $T_e$  and  $T_L$  are the electromagnetic and load torques of the machine respectively.  $T_L$  is the load torque that would be provided to the machine externally, while  $T_e$  needs to be formulated as in (3.2) where  $L_m$  is the mutual inductance in terms of current in two-axis.

$$T_e = \frac{3}{2} \frac{P}{2} L_m (i_{qs} i_{dr} - i_{ds} i_{qr}). \quad (3.2)$$

$$\begin{bmatrix} v_{qs} \\ v_{ds} \\ 0 \\ 0 \end{bmatrix} = \begin{bmatrix} R_s + pL_s & \omega L_s & pL_m & \omega L_m \\ -\omega L_s & R_s + pL_s & -\omega L_m & pL_m \\ pL_m & (\omega - \omega_r)L_m & R_r + pL_r & (\omega - \omega_r)L_r \\ -(\omega - \omega_r)L_m & pL_m & -(\omega - \omega_r)L_r & R_r + pL_r \end{bmatrix} \begin{bmatrix} i_{qs} \\ i_{ds} \\ i_{qr} \\ i_{dr} \end{bmatrix} \quad (3.3)$$

Using (3.1)-(3.3) the machine model has been developed in a high level analytical and numerical program keeping in mind the data of the CRIM which was obtained from the datasheet and nameplate of the motor as summarised in Table 3.1.

TABLE 3.1  
CRIM DATA SHEET

Manufacturer	Siemens	Min. Efficiency	0.924
Output Power	20 hp	Ambient Temp.	40°C
Rater Power	14.92 kW	Insulation Class	F
Rated Voltage	200/400 V	Temp. Rise Class	B
Rated Current	57.0/28.5 A	NEMA Design	B
Rated Speed	1,475 rpm	Frame	256 T
Number of Poles	4	Weight	341 lbs.

### *3.3. Investigation of Online Stator Resistance using Thermal Resistance*

#### *A. Experimental Evaluation of Stator Resistance*

The experiment is performed on a 15 kW, totally enclosed fan-cooled CRIM as shown in the Fig. 3.2. In the conducted experimental evaluation, the CRIM is made to run at a rated speed of 1,500 rpm with varying load conditions. The motor is driven by an inverter-fed PLC based drive system which can be tested for both encoder-less and encoder-based drive system. The encoder-less drive system is an open-loop slip speed controlled variable frequency drive (VFD) system. On the other hand, the encoder based system is a closed-loop speed control VFD with a PID control for the feedback loop. The experiment was performed initially keeping the fan of the induction motor so that the machine is provided with appropriate cooling. The experiment was repeated after removing the fan in order to measure temperature rise leading to the measurement of change in stator resistance.

The experimental setup in Fig. 3.3 illustrates that the test motor is driven by a variable frequency drive and a dynamometer is used as a load. The motor control unit controls the speed and torque settings of the dynamometer and the test motor respectively used as a load. The motor control unit controls the speed and torque settings of the dynamometer and the test motor respectively. A torque transducer is used to measure the torque of the test motor and the dynamometer. Two four-wire resistance temperature detectors (RTD) have been installed at stator end-windings to measure the temperature rise. Data acquisition (DAQ) system controller unit records the temperature measurements using RTDs as shown in Fig. 3.3. The experiment on the motor has been performed with and without the fan cooling to investigate the temperature rise at the stator end-winding. The final results are taken for investigation when the motor is operating at full load conditions with a speed of 1,500 rpm delivering a torque of 60 Nm at 50 Hz. Fig. 3.4 presents the experimental results obtained for stator end-winding temperature rise in case of 75% loading condition. It is demonstrated for both with fan cooling and without fan cooling. The deviation in the temperature in the both cases shows that heating in CRIM is a serious issue which affects machine parameters to a considerable difference. This has been shown for the CRIM running for a period of 2 hours.

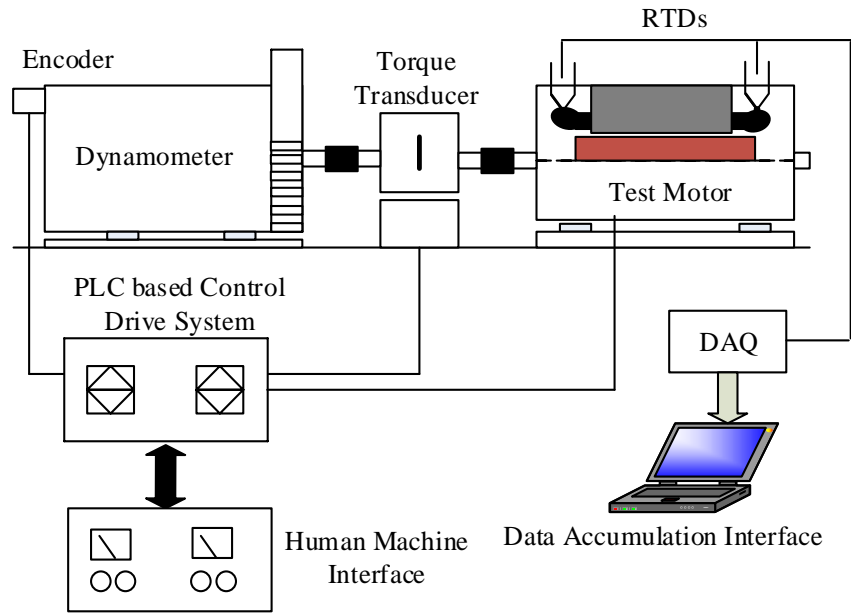


Fig. 3.2. Schematic representation of the experimental test setup

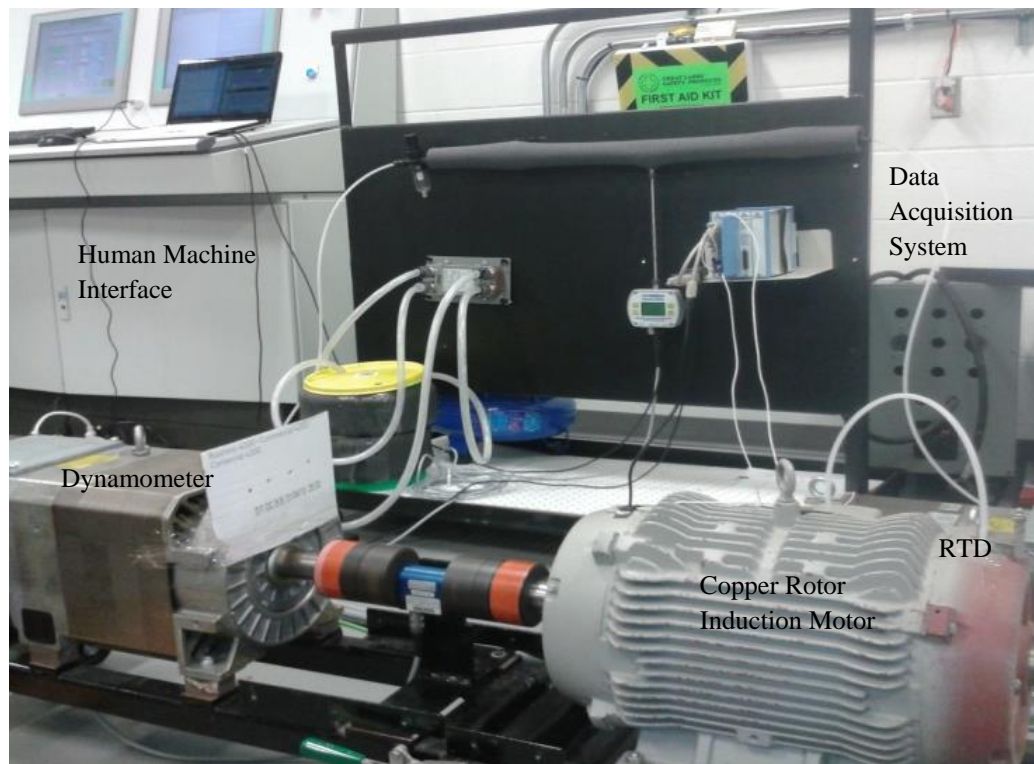


Fig. 3.3. Machine under test and instrumentation layout.



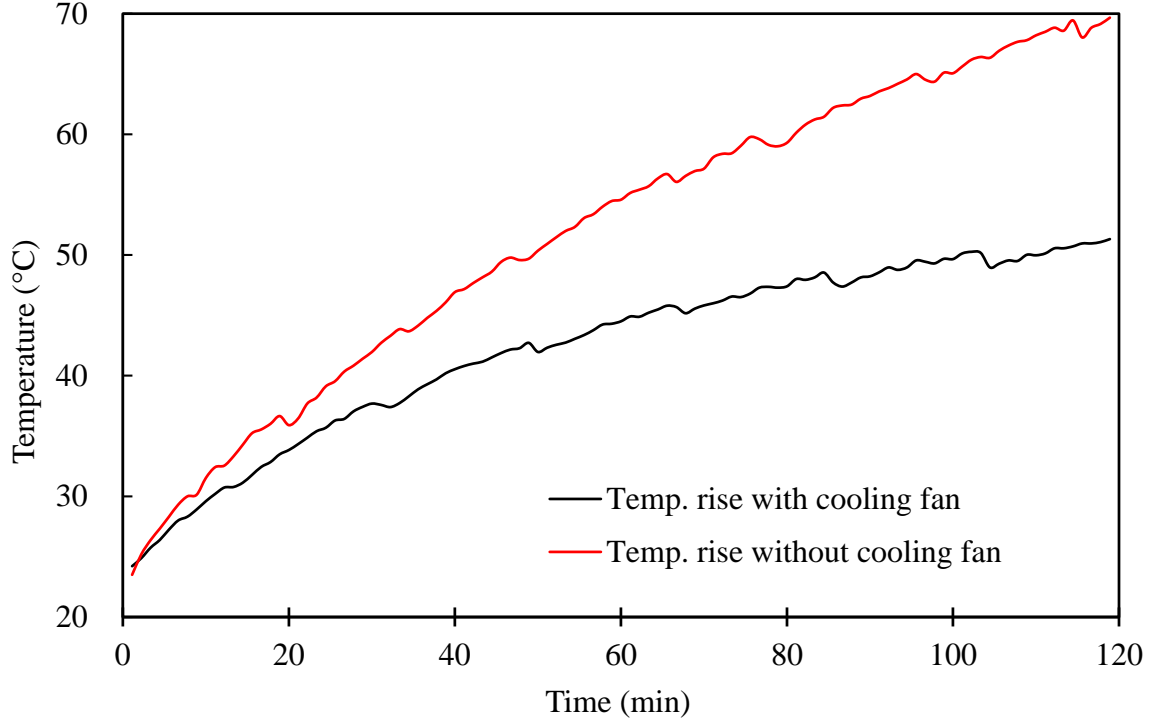


Fig. 3.4. Measured temperature over a period of time with & without cooling fan.

### B. Estimation of Stator Resistance

The stator coil resistance is found to increase with a small increase in temperature. This effect is formulated by (3.4):

$$R_T = R_0 \times (1 + \alpha \Delta T) \quad (3.4)$$

where,  $R_T$  is the value of stator coil resistance at temperature  $T$ ,  $R_0$  is the value of resistance at a reference temperature, and  $\alpha$  is the temperature coefficient for copper, and  $\Delta T$  is the temperature rise at the stator end-winding.

$$R_T = R_0 \times \left[ 1 + \alpha \times \left\{ T_{\max} \times \left( 1 - e^{-t/\tau} \right) \right\} \right] \quad (3.5)$$

The formulation of (3.4) can be expressed exponentially as in (3.5) with  $R_0$ ,  $\alpha$  and  $T_{\max}$  being constant values as it is more comprehensive and result oriented when compared to the requirement of this research manuscript. Steady-state temperature rise analysis is used

to compare the cooling effects on the stator end-windings under different cooling arrangements. For transient thermal behavior for the end-winding, temperature rise can be expressed as in (3.6):

$$\Delta T = T_{\max} \times \left(1 - e^{-t/\tau}\right) \quad (3.6)$$

where,  $\Delta T$  is the temperature rise ( $^{\circ}\text{C}$ ),  $T_{\max}$  is the maximum steady state temperature in  $^{\circ}\text{C}$ ,  $\tau$  is a heating time constant and  $t$  is the time which depends on the convection heat transfer coefficients, end-winding surface area, end-winding mass and heat capacity [8]. By using (3.6) the best value for each of the experimentally found stator end-winding temperature results for different cooling arrangements is taken along with the maximum steady state temperature  $T_{\max}$  and the values are presented in Table 3.2.

TABLE 3.2  
STEADY STATE TEMPERATURE RISE AT 1,500 RPM

Cooling Types	50% load	75% load	88% load
With fan cooling	45.53 $^{\circ}\text{C}$	51.32 $^{\circ}\text{C}$	64.98 $^{\circ}\text{C}$
Without fan cooling	61.57 $^{\circ}\text{C}$	69.67 $^{\circ}\text{C}$	104.87 $^{\circ}\text{C}$

### 3.4. Calculation of Stator Resistance Using Particle Swarm Optimization

To estimate the online resistance of an induction, motor the two-axis modeling is applied to the CRIM. According to [9]-[12], in PSO, the potential solutions, called particles, move through the problem space with a velocity  $v$  by following the current optimum particles. Each particle keeps track of its coordinates in the problem space which are associated with the best solution it has achieved so far which is indicated as  $P_b$ . Apart from  $P_b$ , taking into account the neighborhood of the particle, another best value is kept in track by the optimizer.

When a particle takes all the population as its topological neighbors, the best value is a global best and is called  $G_b$  [13]-[17]. The velocity of particle  $i$  at iteration  $m$ ,  $v_i^m$  can be expressed as in (3.7)

$$v_i^{m+1} = wv_i^m + c_1 \times rand_1 \times (P_{bi} - s_i^m) + c_2 \times rand_2 \times (G_{bi} - s_i^m) \quad (3.7)$$

where,  $C_j$  is the weighting co-efficient,  $rand_j$  is a random number between 0 and 1,  $s_i^m$  is the current position of the particle  $i$  at iteration  $m$ , and is equal to vector  $[R_{si}^m, R_{ri}^m]$  in this condition.  $C_1$  and  $C_2$  normally are two positive constants, called the cognitive and social parameters respectively. In this study, these parameters are considered to be dynamic in nature with initial and final values for  $C_1$  as 1.5 and 2.5 respectively while 2.5 and 1.5 respectively for  $C_2$  [10], [11]. The weighing function  $w$  of the (3.8)

$$w = w_{\max} + \left[ \frac{w_{\max} - w_{\min}}{iter_{\max}} \times iter \right] \quad (3.8)$$

The objective function is designed based on finding the rotor and stator resistance expressed in two parts. The initial step taken by IPSO is to minimize the error of the measured current from the test and current as formulated by the machine model. There is a need to consider the measured stator resistance due to thermal effect as a part of the required research activity. Another part is added to the objective function in order to satisfy the error of stator and rotor resistance ( $R_s, R_r$ ). Therefore, the final objective function can be expressed as in (3.9).

$$obj(r_s, r_r) = Min \left[ \begin{array}{l} Error(i_{measured}, i_{calculated}) \\ + Error(r_{s,thermal}, r_{s,IPSO}) \end{array} \right]. \quad (3.9)$$

The improved particle swarm optimization as developed can be expressed using the flowchart depicted in Fig. 3.5. 100 iterations have been performed so that the best results obtained are as close to the expected and measured values.

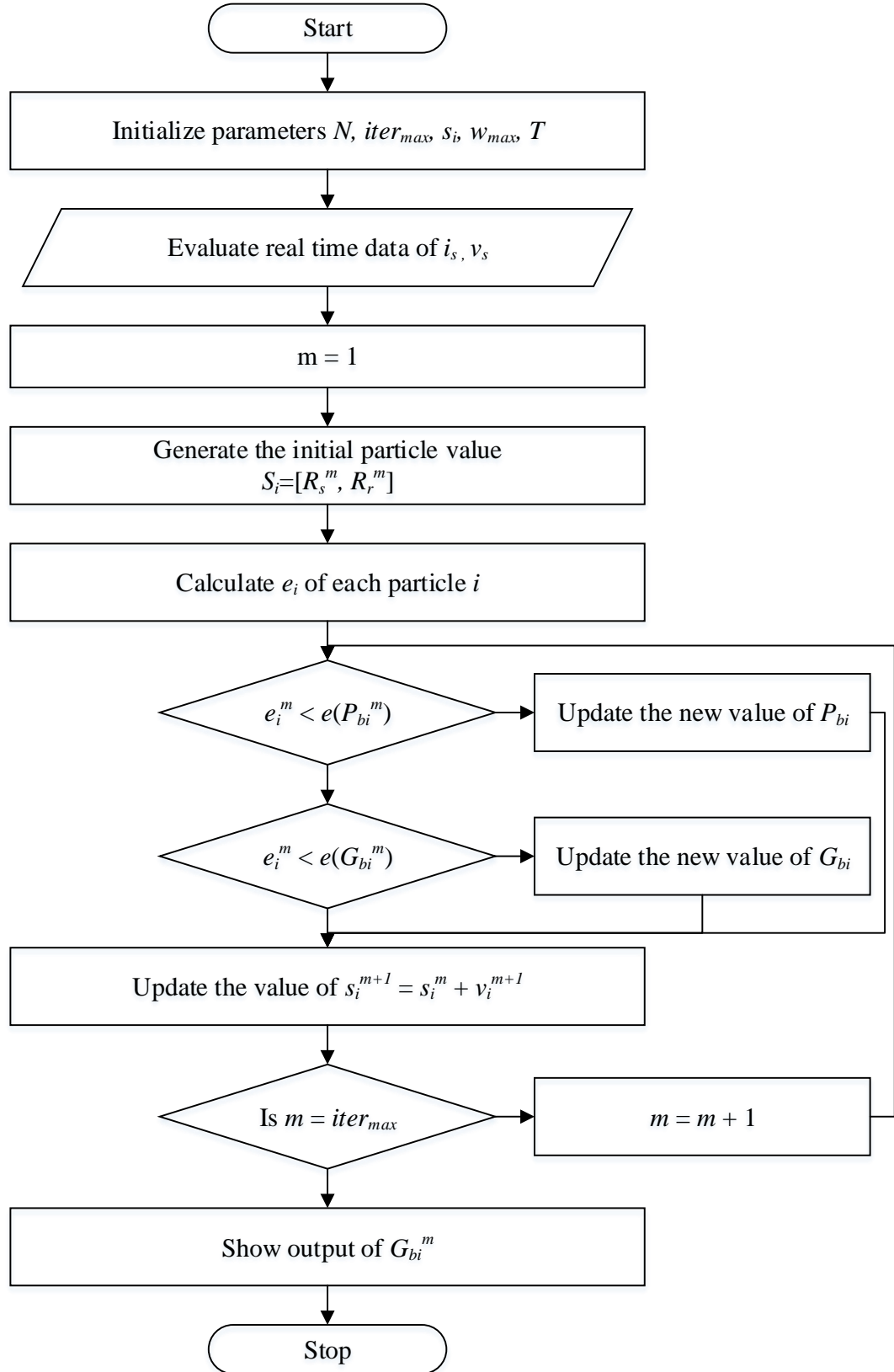


Fig. 3.5. Flowchart to show each step of process used in finding stator resistance.

### 3.5. Numerical Investigation of Copper Rotor Induction Motor

The machine model as established in section II has been developed in a technical computer programming language used for data analysis. The developed IPSO is then integrated with the machine model which analyses each result till the optimized value is obtained. Fig. 3.6 depicts the performance of IPSO and indicates the convergence of the fitness function to the optimized result. 30 samples for each of the 100 iterations was used to find the best value at the fastest converging point. The DC test, no load test and the blocked rotor test were respectively performed on the machine in order to find the parameters of the 20 hp copper-rotor induction motor values. The values obtained have been presented in Table 3.3. The values of the stator resistance as retrieved from the numerical investigation was compared with those obtained from the thermal measurement of resistance and the test of DC injection into the stator windings.

TABLE 3.3  
EQUIVALENT CIRCUIT PARAMETERS OF CRIM

Parameters	Values	Parameters	Values
$R_s$	0.35625 $\Omega$	$X_m$	28.20 $\Omega$
$R_r$	0.12 $\Omega$	$\omega$	314.159
$X_{ls}$	1.71 $\Omega$	$P_{cu(stator)}$	94.43 W
$X_{lr}$	1.71 $\Omega$	$P_{rotational}$	355.40 W

Fig. 3.7 (a) presents the relative analysis of experimental results obtained for stator end-winding temperature rise with fan cooling and the estimated value as produced by the developed PSO. It shows a definite stray of the estimated resistance value from the experimentally measured value. Fig. 3.7 (b) represents a similar investigation for the machine under test without any aided cooling system. It is seen that under both cases, the experimental value is in close correspondence with the values obtained from numerical

investigation. From the figures, it is evident that the stator resistance increases with time and temperature. In order to take care of the overall efficiency of the CRIM when taking temperature into account, skin effect of the conductor bars in the machine has to be taken into account. The flow of alternating currents in close proximity to a conducting material induces eddy currents in the material. This induced eddy current density varies exponentially with depth. The skin depth  $\delta$  of the conducting material depends on magnetic and electric permeability and frequency of the magnetizing current,  $f$  shown as in (3.10)

$$\delta = 1 / \sqrt{\pi \mu f \sigma} . \quad (3.10)$$

Due to the increase in skin effect, the effective stator and rotor resistance gets modified with time. There is an existence of ferromagnetic materials in the machine whose magnetic domain changes or they tend to lose magnetic properties due to rise in temperature. The atoms in the domain are excited enough to remain pointed in one direction over a longer period of time as a result of rise in temperature. This also affects the motor at the material level [18].

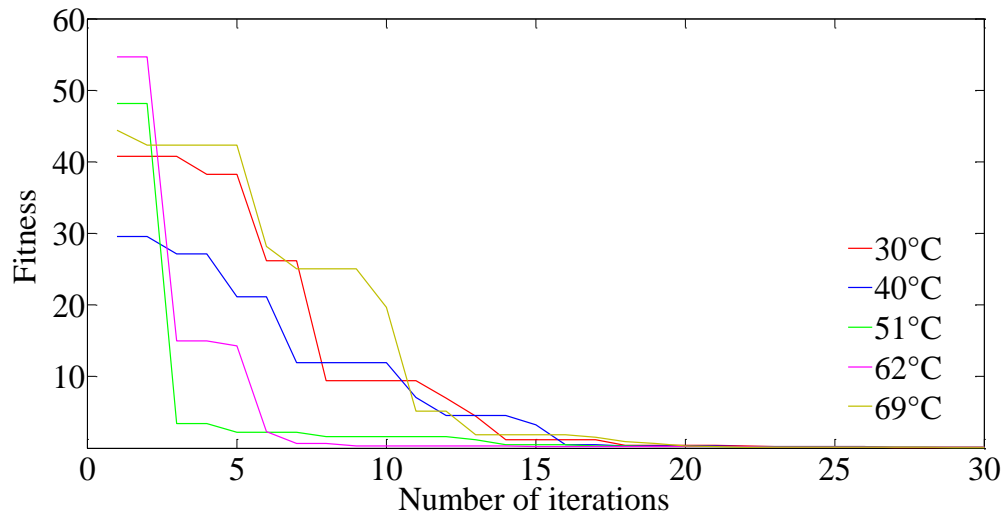
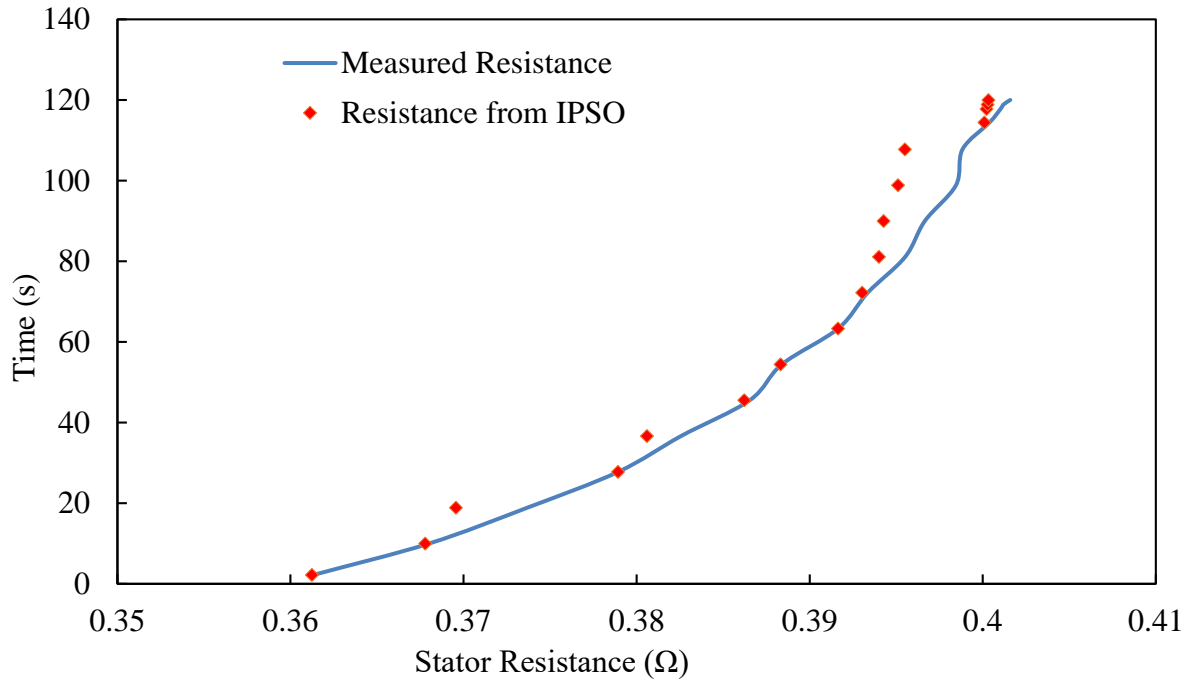
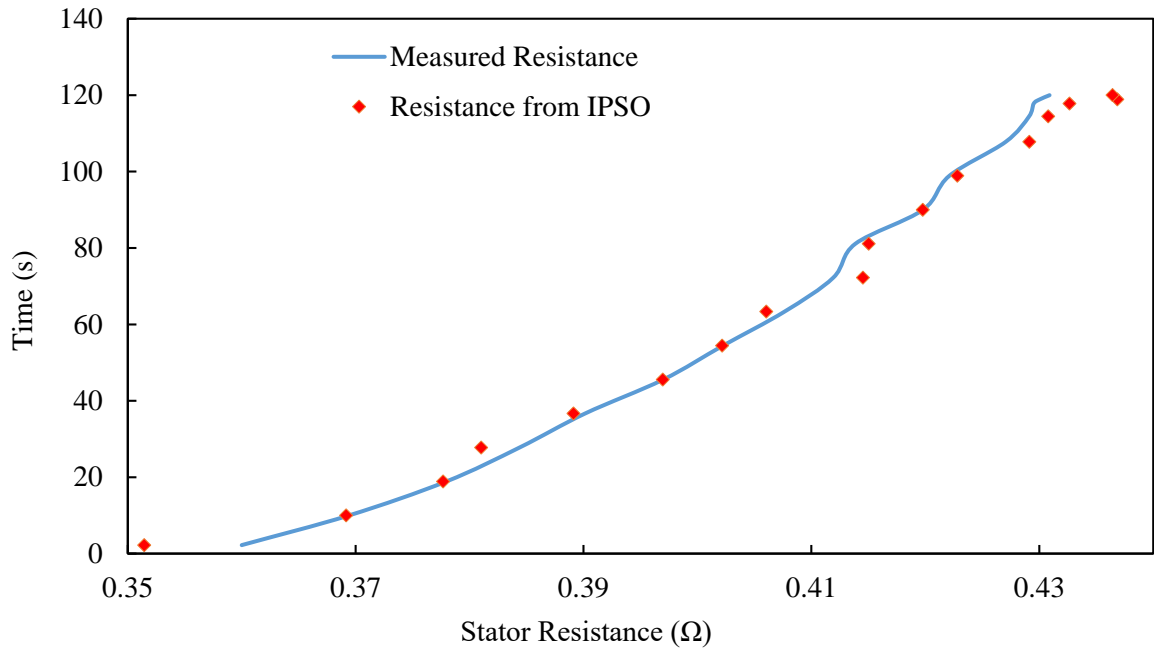


Fig. 3.6. Convergence diagram of the IPSO for the CRIM.



(a)



(b)

Fig. 3.7. Comparative results for IM under investigation. (a) With fan cooling as obtained from the experimental setup and the output of the PSO. (b) Without fan cooling as obtained from the experimental setup and the output of the PSO.

### 3.6. Re-Modelling of Faulty IM for DNLTN Method

Once temperature has been found to be a useful feature for detection of variation in machine performance, a novel method of online parameter estimation along with loss calculation using Duplex Neural-Lumped Parameter Thermal Network (DNLTN) is done to create a robust self-governing system using deep capture over a period of time. Current, voltage, flux and temperature are used as feedback to the duplex network model which is trained inorder to recognize pattern change for fault diagnosis and compute the changed parameters, providing a more comprehensive, precise and reliable online parameter estimator with condition monitoring. This DNLTN method has been implemented on the 7.5 hp aluminum rotor induction motor (ALIM) which has been designed in Chapter 2.

#### A. Mathematical Model

The ALIM has been modeled using Steinmetz equivalent circuit based on the two-axis rotating reference frame theory expressed as in (3.11). The major difference in ALIM and CRIM is the value of rotor resistance. This model is chosen over the conventional voltage-current two-axis model because when current is taken as the state variable, the model contains two derivatives of current in the  $d$ - $q$  voltage equations. While considering flux linkage as the state variable, there is only one derivative of flux linkage. This makes computation and modelling of ALIM easier in terms of extracting the flux.

$$\begin{bmatrix} v_{qs} \\ v_{ds} \\ v_{qr} \\ v_{dr} \end{bmatrix} = \begin{bmatrix} \frac{X_r' r_s}{D} + \frac{p}{\omega_b} & \frac{\omega}{\omega_b} & -\frac{X_M r_s}{D} & 0 \\ -\frac{\omega}{\omega_b} & \frac{X_r' r_s}{D} + \frac{p}{\omega_b} & 0 & -\frac{X_M r_s}{D} \\ -\frac{X_M r_r}{D} & 0 & \frac{X_s' r_r'}{D} + \frac{p}{\omega_b} & \frac{\omega}{\omega_b} - \frac{\omega_r}{\omega_b} \\ 0 & -\frac{X_M r_r}{D} & -\frac{\omega}{\omega_b} + \frac{\omega_r}{\omega_b} & \frac{X_s' r_r'}{D} + \frac{p}{\omega_b} \end{bmatrix} \begin{bmatrix} \psi_{qs} \\ \psi_{ds} \\ \psi_{qr} \\ \psi_{dr} \end{bmatrix} \quad (3.11)$$

where  $D = X_s X_r - X_m^2$

If current is chosen as the independent variable, the voltage-flux equations get expressed as (3.12). The parameters of IM, namely, the measured voltage, current and flux, can be calculated as defined in (3.11) and (3.12).



$$\begin{bmatrix} i_{qs} \\ i_{ds} \\ i_{qr} \\ i_{dr} \end{bmatrix} = \frac{1}{D} \begin{bmatrix} X_r' & 0 & -X_M & 0 \\ 0 & X_r' & 0 & -X_M \\ -X_M & 0 & X_s & 0 \\ 0 & -X_M & 0 & X_s \end{bmatrix} \begin{bmatrix} \psi_{qs} \\ \psi_{ds} \\ \psi_{qr} \\ \psi_{dr} \end{bmatrix} \quad (3.12)$$

### B. Loss Calculation and Estimation

In an induction traction motor three-phase electrical power changes to mechanical power. The input power to the IM  $P_{in}$  is in the form of three-phase electric voltages and currents. The first losses encountered in the machine are copper losses in the stator windings which is stated as the stator copper loss  $P_{SCL}$ . Some amount of power is lost as hysteresis and eddy currents in the stator core  $P_{core}$ . The power remaining at this point is transferred to the rotor of the machine across the air gap between the stator and rotor. This power is called the air-gap power  $P_{AG}$  of the machine. After the power is transferred to the rotor, some of it is lost as aluminium losses namely the rotor aluminium loss  $P_{RAL}$ , and the rest is converted from electrical to mechanical form as  $P_{conv}$ . Finally, friction and windage losses  $P_{F\&W}$  and stray losses  $P_{misc.}$  are subtracted. The remaining power is the output of the motor  $P_{out}$ . The core losses do not always appear in the power-flow diagram at the point shown in Fig. 3.8. Because of the nature of core losses, where they are accounted for in the machine is somewhat arbitrary. The core losses of the IM motor come partially from the stator circuit and partially from the rotor circuit. Since an IM motor normally operates at almost synchronous speed, the relative motion of the magnetic fields over the rotor surface is quite slow, and the rotor core losses are very tiny compared to the stator core losses. Since the largest fraction of the core losses comes from the stator circuit, all the core losses are lumped together at that point on the diagram. These losses are represented in the equivalent circuit by the resistor  $R_c$ . If core losses are just given by a number instead of as a circuit element they are often lumped together with the mechanical losses and subtracted at the point on the diagram where the mechanical losses are located. The higher the speed of the IM motor, the higher its friction, windage, and stray losses. These factors needed to be considered while modelling the loss profile of the motor. On the other hand, the higher the speed of the motor, the lower its core losses. Therefore, these three categories of losses are sometimes lumped together. The total rotational losses of a motor are often considered

to be constant with changing speed, since the component losses change in opposite directions with a change in speed [19].

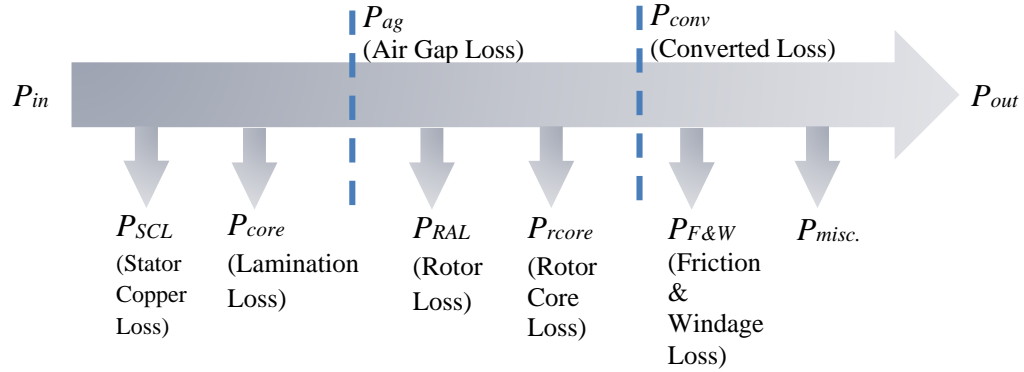


Fig. 3.8. The power flow and losses as generated in the induction motor

The losses in IM can be divided into stator copper loss, rotor copper loss, core losses at stator and rotor teeth, core losses due to leakage flux, and additional stray losses which can be due to friction of motor coupling, bearings, overheating or some other mechanical losses. The overall losses in IM can be estimated as shown in (3.13) – (3.15).

$$P_{input} - P_{output} = P_{cu\_stator} - P_{cu\_rotor} - P_{core} - P_{misc} \quad (3.13)$$

$$P_{cu\_stator} = 3I_s^2 R_s; P_{cu\_rotor} = 3I_r^2 R_r; P_{out} = \tau_{load} \omega_r \quad (3.14)$$

$$P_{input} = \sqrt{3} V_s I_s \cos \theta \quad (3.15)$$

Using the parameters as calculated from the model explained in Section 3.6 A,  $P_{cu\_stator}$ ,  $P_{cu\_rotor}$ , and  $P_{input}$  can be estimated. Since the speed and load torque are measured,  $P_{out}$  can be estimated. The miscellaneous losses are considered as 2% of  $P_{out}$ . Since no real-time measurement of core resistance and inductance is done here,  $P_{core}$  is evaluated using the method of elimination. These calculated losses are used in the lumped parameter model in

order to predict the temperature rise in the machine. During faulty conditions, the change in parameters due to change in magnetic flux, are incorporated, to calculate the losses and further utilised in the LPTN model. Hence, online parameter estimation enables prediction of temperature rise in the machine during operation of motor under faulty conditions.

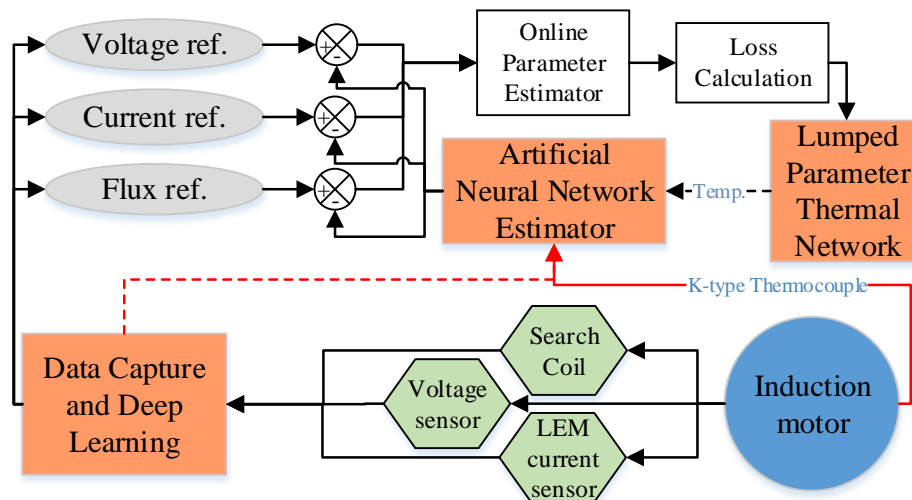


Fig. 3.9. Schematic flow of novel DNLTN method for parameter and loss estimation.

### 3.7. Duplex Neural — Lumped Thermal Network Development

#### A. Neural Network Parameter Estimator

Artificial neural networks (ANNs) can be used to identify and control the nonlinear dynamic systems because they can approximate a wide range of nonlinear functions to any desired degree of accuracy. Moreover, they can be implemented in parallel and therefore, shorter computational time can be achieved. In addition, they have immunity to harmonic ripples and have fault-tolerant capabilities [20].

A three-layer feed-forward neural network, as shown in Fig. 3.10, has been used – input, hidden and output layers. Each of these is made of artificial neurons. Input layer is composed of measured values of voltage, current and flux density from the motor. This is

defined by  $x_j$  which is the input value of the  $j^{\text{th}}$  neuron. This  $x_j$  now enters the hidden layer where it is multiplied by a weight  $w_{kj}$ . Sometimes if needed a bias  $b_k$  can be added to it.  $v_k$  is the linear combination output of the input signals with their corresponding neuron weights as shown in (3.16). Output layer is defined by  $y_k$  which is the equivalent of activation function of  $v_k$  with a bias of  $b_k$  as defined in (3.17).

$$v_k = \sum_{j=1}^m w_{kj} \cdot x_j \quad (3.16)$$

$$y_k = \varphi(v_k + b_k) \quad (3.17)$$

One of the main properties of neural network is the ability to be trained in order to optimize the values which it gathers from deep learning method. Then the trained results are validated and tested before producing the best fitted value. All the experimentally measured values are fed into this artificial neural network along with the model calculated values in order to get the best fitted values for voltage, current and flux density.

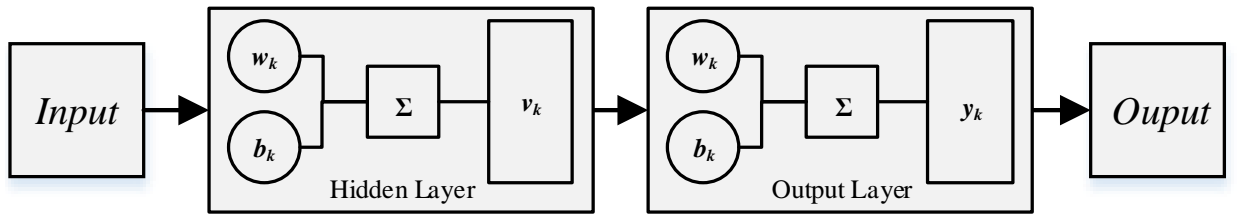


Fig. 3.10. Design of neural network used in application of parameter estimation.

### B. Lumped Parameter Thermal Network (LPTN)

The principle of the nodal method consists of dividing the machine into basic thermal elements that represent a combination of conduction, convection and radiation heat transfer processes. Lumped elements are chosen on the basis of thermal and physical uniformity. The part of the winding with maximum temperature is usually inaccessible. The proposed LPTN model for a faulty condition is shown in Fig. 3.11.

$P_{cu-S}$ ,  $P_{cu-R}$  and  $P_{core}$  represent the copper losses of stator and rotor and the core losses.  $R$  and  $C$  represent the thermal resistances and conductances due to conduction and convection heat transfer.  $T_n$  shows the temperature rise at the  $n^{\text{th}}$  node in the machine. The losses calculated in Section 3.6 B are incorporated in (3.18) showing increase in temperature  $T$  over period of time  $p$ .

$$T_{p+1} = T_p + \left[ \left\{ \frac{P_{motor-loss} + h_{conv} A_{conv} (T_{conv} - T_{ref}) + \sigma \epsilon A_{rad} (T_{rad}^4 - T_{ref}^4) + \kappa A_{cond} (T_{cond} - T_{ref})}{\rho c V} \right\} \times (dt) \right] \quad (3.18)$$

where  $\rho$  denotes density of air,  $\sigma$  is Stefan-Boltzman constant,  $\kappa$  is thermal conductivity of air,  $\epsilon$  is emissivity,  $c$  is specific heat capacity of air,  $V$  is volume,  $h_c$  is convection coefficient of air,  $\tau$  is total time,  $A_{conv}$ ,  $A_{cond}$ , and  $A_{rad}$  is convection, conduction and radiation area,  $T_{conv}$ ,  $T_{cond}$ ,  $T_{rad}$ , and  $T_{ref}$  are convection, conduction, radiation and reference temperatures respectively.

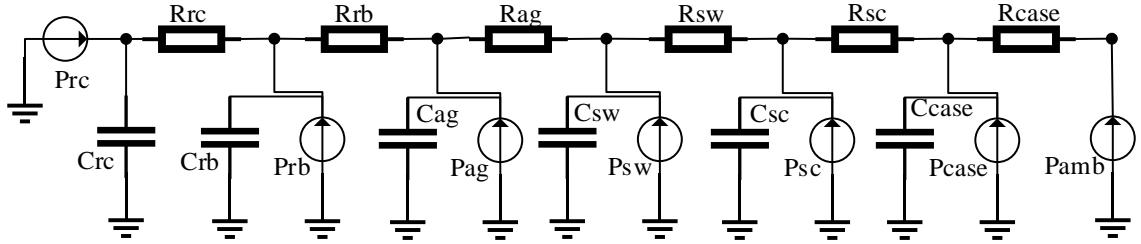


Fig. 3.11. Proposed lumped parameter thermal network for the fault IM.

### 3.8. Experimental Validation of Proposed Novel Duplex Network

The IM with stator inter-turn fault is connected to the DC machine as a load as shown in Fig. 3.12. The test was performed at different speeds and loading conditions. A high

performance 32-bit microcontroller capable of real-time control is used to run the IM. This control board is capable of handling a large amount of data capture which is sent to the local computer for storing during each test. It triggers the proposed duplex model running on the board and results are displayed on the computer.

For magnetic flux measurement, a search coil has been wound on the previously detected faulty phase of the ALIM. Unlike other fault condition monitoring methods where search coil is placed at the end-windings, it has been placed along the entire length of stator tooth for more uniform result of the magnetic flux which changes the desired results to a great extent.

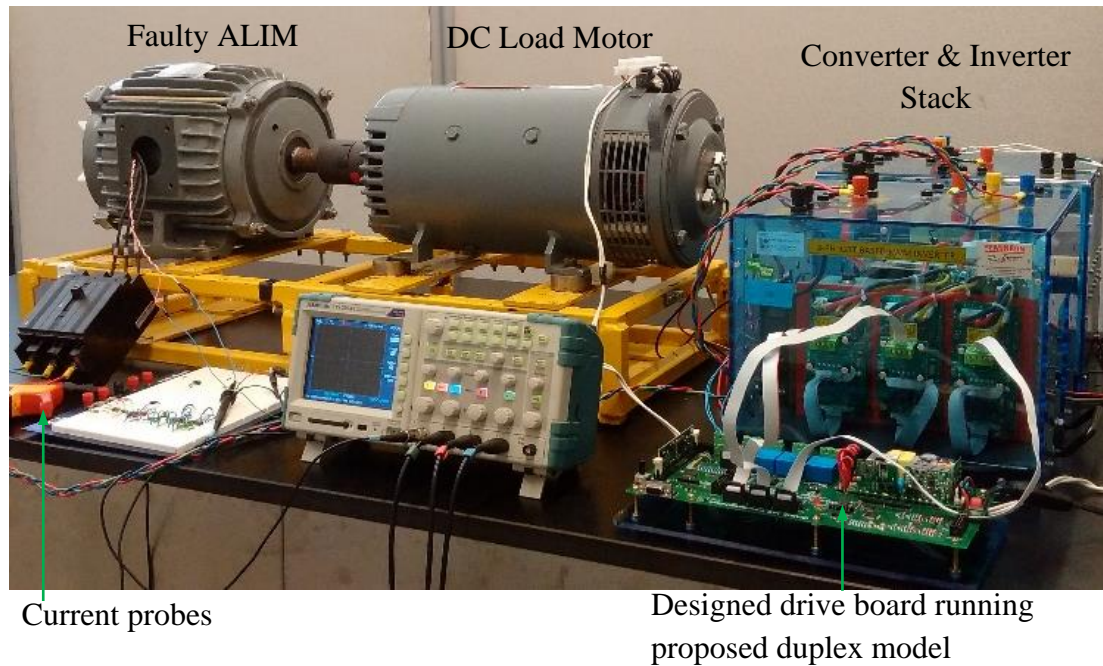


Fig. 3.12. Set up for experimental validation of the proposed duplex neural-lumped thermal network.

The current, voltage and flux values are measured and fed into the control board. K-type thermocouples have been placed inside to find out the experimental temperature values. This is an invasive method of estimation which increases the robustness of the DNLTN.

### 3.9. Proposed Duplex Model Result Analysis

The duplex neural-lumped parameter thermal model has been implemented on the 7.5 hp faulty aluminium rotor IM. It has been studied under various speeds and loads in order to check the reliability of the proposed model. The DNLTN model estimates the temperature of the motor and then calculates the parameters of the motor. In Fig. 3.13, it has been shown how the calculated resistance using DNLTN is compared to the experimental values. Although there is a steady increase in resistance due to fault but the values of predicted resistance is close to the experimental value. Figs 3.14 show the thermal condition of the faulty IM over a period of operation which has been measured using RTD and infrared temperature sensor. Fig 3.14 (a) indicates the distribution of heat over the IM with the overlay of the IM below to have a clear picture of excess heating. Fig. 3.14 (b) shows how the loading DC motor is cool although the IM is getting excessively heated due to fault occurrence. Fig. 3.14 (c) show the temperature and condition of the motor at room temperature of 24.69°C whereas Fig 3.14 (d) shows how heated up the IM becomes and it reaches a temperature of 83.78°C. The IM was stopped at 90 °C to stop the insulations from breaking down further.

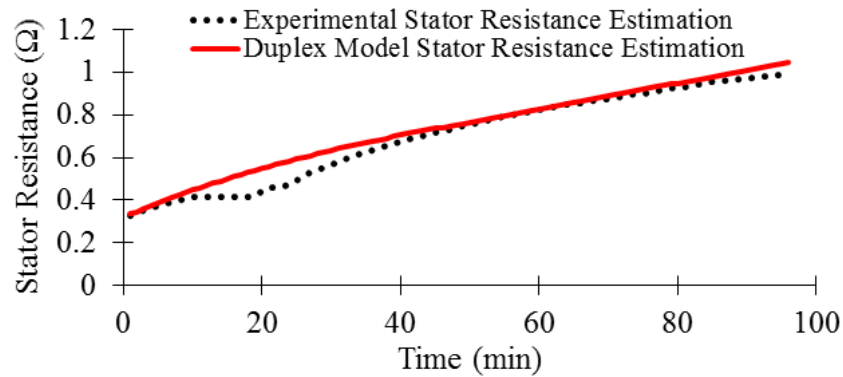
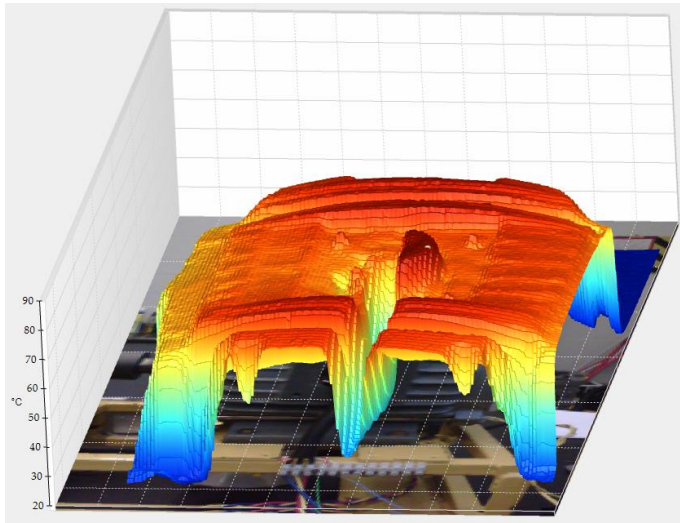
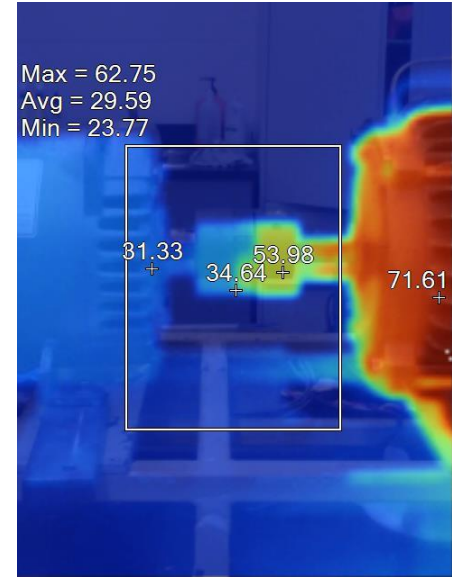


Fig. 3.13. Comparison of experimental and duplex model based change in stator resistance.

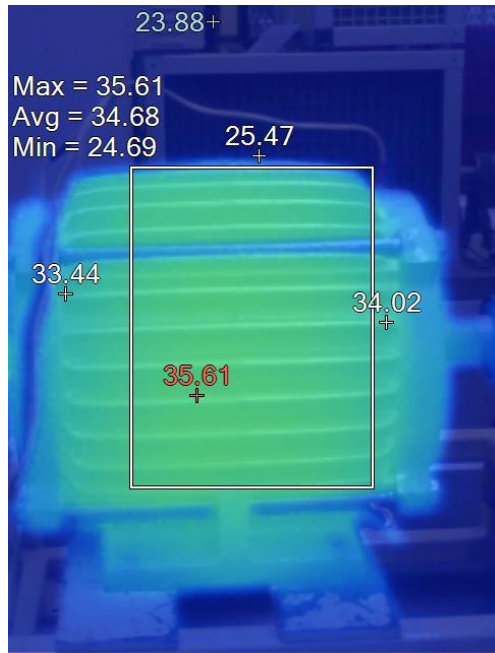




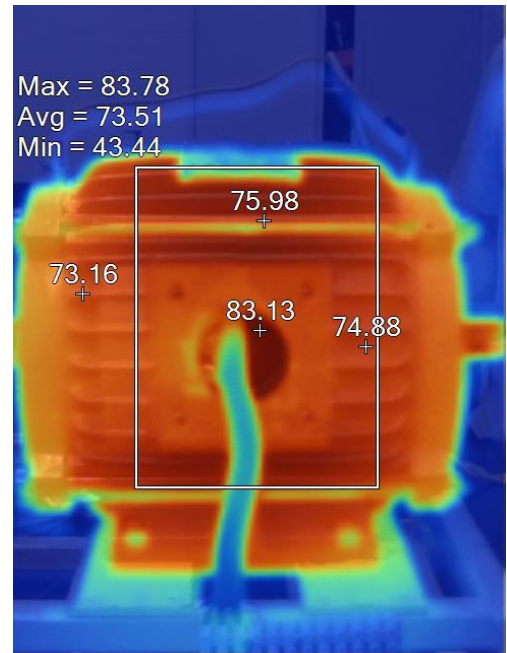
(a)



(b)



(c)



(d)

Fig. 3.14. Motor thermal condition as measured using IR sensor. (a) Distribution of temperature over various parts of the motor with the image of IM as x-axis to indication the locations. (b) DC load motor remains cool unlike the faulty IM indicating that fault cause undue heat at same ambient conditions. (c) Faulty IM before starting the experiment. (d) Faulty IM condition after 30 minutes of operation.



### 3.10. Conclusion

The research done in this chapter presents IPSO as a predictive method which can provide an effective online tuning of stator resistive parameters using temperature as a vital feature. The necessity of online parameter estimation has also been highlighted. The improved algorithm makes the system more reliable and fast at different loading condition and temperature, thereby making it flexible to be used for EV/HEV motor drive application. The novel Duplex Neural-Lumped Thermal Network model which uses a trained neural network along with lumped thermal model operating at same time for consideration of thermal issue as a single learning body for online parameter estimation and loss calculation of a faulty IM with a higher accuracy and reliability as compared with IPSO. This model also uses deep learning to verify the fault trend occurrence as pattern recognition method which is fundamental for eventual machine learning algorithm developed in this dissertation. Both the methods can be used for condition monitoring as well as designing a fault-tolerant control drive for IM which will be implemented for future work. This also calls for a predictive drive control system to prevent hazards caused due to overheating of the motor in EV/HEV application which has been developed and proposed in later sections. As an additional outcome, these methods can also be used to design an adaptive cooling system which increases the cooling rate of the motor to assist during the occurrence of stator fault.

### 3.11. References

- [1] S. F. Farag, and M. K. Jhaveri, "Intelligent Microprocessor based Devices Provide Advanced Motor Protection, Flexible Control and Communication in Paper Mills," *IEEE Transactions on Industry Applications*, vol. 33, pp. 840–847, May/June 1997.
- [2] J. L. Kirtley, Jr., J. G. Cowie, E. F. Brush, D. T. Peters, and R. Kimmich, "Improving Induction Motor Efficiency with Die-Cast Copper Rotor Cages," in the *Proc. of Power Engg. Society General Meeting*, pp.1-6, June 2007.
- [3] J. L. Zamora and A. Garcia-Cerrada, "Online estimation of the stator parameters in an induction motor using only voltage and current measurements," *IEEE Transaction on Industry Applications*, vol. 36, no. 3, pp.805-816, 2000.

- [4] K. D. Hurst, and T. G. Habetler, "A Thermal Monitoring and Parameter Tuning Scheme for Induction Machines," in the Proc. of *Thirty-Second IAS Annual Meeting of IEEE Industry Applications*, vol.1, pp.136-142 Oct. 1997.
- [5] S. F. Farag, R. G. Bartheld and W. E. May, "Electronically Enhanced Low Voltage Motor Protection and Control," *IEEE Transactions on Industry Applications*, vol.30, no.3, pp.776-784, May/Jun 1994.
- [6] K. L. V. Iyer, X Lu, K. Mukherjee, and N. C. Kar, "Online Stator and Rotor Resistance Estimation Scheme Using Swarm Intelligence for Induction Motor Drive in EV/HEV," in the Proc of *IEEE Electric Drives Production Conference*, pp.202-207, 2011.
- [7] P. C. Krause, O. Wasynczuk, and S. D. Sudhoff, "*Analysis of Electric Machinery and Drive Systems*" NJ, USA: IEEE Press, 2002.
- [8] A. Boglietti and A. Cavagnino, "Analysis of the Endwinding Cooling Effects in TEFC Induction Motors," *IEEE Transactions on Industry Applications*, vol. 43, no. 5, pp. 1214-1222, Sept.-Oct. 2007.
- [9] X. Hu, Y. Shi, and R. Eberhart, "Recent Advances in Particle Swarm," in the Proc of *IEEE Congress on Evolutionary Computation*, vol.1, pp.90-97, 2004.
- [10] Y. Wu and H. Gao, "Optimization of Fuel Cell and Supercapacitor for Fuel-Cell Electric Vehicles," *IEEE Transaction on Vehicular Technology*, vol. 55, no. 6, pp. 1748-1755, Nov. 2006.
- [11] Y. Del Valle, G. K. Venayagamoorthy, S. Mohagheghi, J.-C. Hernandez, and R. G. Harley, "Particle Swarm Optimization: Basic Concepts, Variants and Applications in Power Systems," *IEEE Transaction on Evolutionary Computation*, vol.12, no. 2, pp. 171–195, Apr. 2008.
- [12] H. Tajima; G. Guidi; and H. Umida, "Consideration about Problems and Solutions of Speed Estimation Method and Parameter Tuning for Speed Sensorless Vector Control of Induction Motor Drives," in the Proc. of *IEEE Industry Applications Conference*, vol.3, pp.1787-1793, 2000.

- [13] E. M. Tofighi, A. Mahdizadeh, and M. R. Feyzi; "Online Estimation of Induction Motor Parameters Using a Modified Particle Swarm Optimization Technique", in the Proc of *IEEE Industrial Electronics Society*, pp. 3645-3650, 2013.
- [14] Boyd, and Vandenberghe, "*Convex Optimization*," Cambridge University Press, Cambridge, UK, 2004
- [15] Z. Gao; T.G. Habetler; R.G. Harley; and R.S. Colby, "A Novel Online Rotor Temperature Estimator for Induction Machines based on a Cascading Motor Parameter Estimation Scheme," in the Proc. of *IEEE International Symposium on Diagnostics for Electric Machines, Power Electronics and Drives, SDEMPED 2005*, pp.1-6, Sept. 2005.
- [16] O. Sundstrom and C. Binding, "Flexible Charging Optimization for Electric Vehicles Considering Distribution Grid Constraints," *IEEE Transactions on Smart Grid*, vol.3, no.1, pp.26-37, March 2012.
- [17] Ju. H. Zhao; F. Wen, Z. Y. Dong, Y. Xue, and K. P. Wong, "Optimal Dispatch of Electric Vehicles and Wind Power Using Enhanced Particle Swarm Optimization," *IEEE Transactions on Industrial Informatics*, vol.8, no.4, pp.889-899, Nov. 2012
- [18] K. Hafiz, G. Nanda, and N. C. Kar, "Performance Analysis of Aluminum- and Copper-Rotor Induction Generators Considering Skin and Thermal Effects," *IEEE Transactions. on Industrial Electronics* , vol.57, no.1, pp.181-192, Jan. 2010.
- [19] N. Hildebrand and H. Roehrdanz, "Losses in Three-Phase Induction Machines Fed by PWM Converter," *IEEE Transactions on Energy Conversion*, vol. 16, no. 3, pp. 228-233, Sep 2001.
- [20] M. Barzegaran, A. Mazloomzadeh, and O. A. Mohammed, "Fault Diagnosis of the Asynchronous Machines Through Magnetic Signature Analysis Using Finite-Element Method and Neural Networks," *IEEE Transactions on Energy Conversion*, vol. 28, no. 4, pp. 1064-1071, Dec. 2013.
- [21] T. Ince, S. Kiranyaz, L. Eren, M. Askar, and M. Gabbouj, "Real-Time Motor Fault Detection by 1-D Convolutional Neural Networks," *IEEE Transaction on Industrial Electronics*, vol. 63, no. 11, pp. 7067-7075, Nov. 2016.

## **CHAPTER 4**

### **DESIGN OF HARMONICS ANALYSIS BLOCK FOR FLUX FEATURE PREDICTION**

#### *4.1. Introduction*

Once temperature has been established as a prime feature for detecting fault in motor, it has also been observed that rate of change in temperature is a much slower process for fault detection when it comes to traction application. On the other hand, using flux as a feature has been found to be much faster in predicting fault. In order to achieve that, a novel harmonic analysis block has been modelled using magnetic equivalent circuit (MEC) to determine the variation in air-gap flux developed due to unbalanced motor condition. Further, in order to verify the developed MEC and also distinguish between harmonics induced from the inverter side and the motor inter-turn fault condition, an observer search coil technique (OSC) has been implemented on the 7.5 hp ALIM with incipient stator turn burnout under investigation. In the OSC technique, a search coil has been wound along the entire tooth of stator in order to estimate effective air-gap flux from the machine including effects from both the stator and rotor. The advantage of the developed OSC technique is low cost, simplicity, and ease in implementation. The developed MEC is first analyzed under healthy motor conditions without any faults and verified using experimental data from the search coil. Further, the MEC is updated for a stator inter-turn fault condition and implemented in the harmonic analysis block. Thus, the flux obtained from the MEC during healthy motor condition acts as a flux reference and any abnormal changes in this air-gap flux will indicate a fault occurrence in the motor. Since, input to the MEC is the machine three-phase currents, any time harmonics induced from the inverter can easily be taken into account. Based on the flux waveforms obtained from the MEC under both healthy and faulty conditions, harmonic analysis and modeling is also included in the novel harmonic block which can be used in a fault-tolerant control including harmonic compensation and stator-flux based control. The design of the harmonic block has been shown in Fig. 4.1.

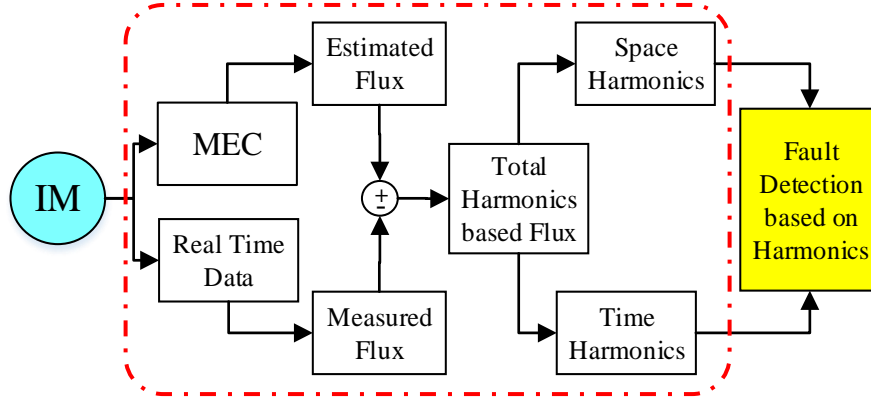


Fig. 4.1. MEC network as used for the proposed modelling.

#### 4.2. Modelling of Harmonics Analysis Block

The proposed method uses both MEC and real time data for fault detection and implements harmonic modeling to evaluate the harmonic orders induced during faults. In order to further develop a fault-tolerant control of the motor, knowledge about the harmonic orders induced during healthy condition is of prime importance as well. The MEC of a healthy ALIM is initially developed and the flux waveform obtained is verified with the experimental results obtained from the search coil. In order to clearly distinguish between inverter induced harmonics, the MEC is modeled for time harmonics as well. Thus, the initial healthy condition flux waveform obtained from MEC acts as a reference and in case of any inter-turn fault occurrence or any fluctuations in the order of harmonics is observed, faster classification of faults is achieved. In such a case, a MEC of ALIM with stator inter-turn fault is implemented to obtain the flux waveform and harmonic modeling is performed to understand and model a fault-tolerant control methodology.

##### A. Magnetic Flux Density Estimation using Observer Search Coil Method

In order to get the real time flux value, a flux sensor which is an observer search coil in this case, is wound along the previously detected faulty phase of the ALIM as shown in Fig. 4.2. Usually, most researchers use search coils at the end windings of the stator since it is easy in installation and lower in cost [1]. However, in the test motor under consideration, the search coil is wound along entire tooth for increased accuracy and

uniformity in measurement of magnetic flux. The magnetic flux can be calculated as (4.1) where  $B$  is the magnetic flux density

$$\int_s \nabla \times E \cdot dS = -\frac{d}{dt} \int_s B(t) \cdot dS = \int_s \frac{-dB(t)}{dt} \cdot dS \quad (4.1)$$

The calculated flux density value is used for detecting any variation in the flux and estimating the amount of variation when an inter-turn fault occurs. The only disadvantage with this method is that it is invasive and not all motors are designed with a search coil placed inside.



Fig. 4.2. Search coil placed on the phase of detected unbalance

### *B. Modelling of Unbalanced IM in dq-Axis Frame*

The 3-phase IM under test has been modelled using two-axis rotating reference frame as shown in (4.2). The fault occurrence in the stator winding has been considered as creating a variation in the stator side of the mathematical model. The change in stator resistance  $r_s$  has been considered as an addition effect of  $r_f$  resistance. Similarly, for stator inductance an additional effect of  $X_f$  is considered which occurs due to stator winding fault. This flux model is chosen over the conventional voltage-current two-axis model since the model contains two derivatives of current in conventional d-q voltage equations when current is considered as the state variable. But while considering flux linkage as the state variable, there is only one derivative of flux linkage [2]. This makes computation and

modelling of ALIM easier in terms of extracting the flux. The measured voltage, current and flux are fed into this model to calculate the parameters of IM. The difference in healthy and faulty condition has been taken care of by  $r_f$  and  $X_f$ .

$$\begin{bmatrix} v_{qs} \\ v_{ds} \\ v_{qr} \\ v_{dr} \end{bmatrix} = \begin{bmatrix} \frac{X'_r(r_s \pm r_f)}{D} + \frac{p}{\omega_b} & \frac{\omega}{\omega_b} & -\frac{X_M(r_s \pm r_f)}{D} & 0 \\ -\frac{\omega}{\omega_b} & \frac{X'_r r_s}{D} + \frac{p}{\omega_b} & 0 & -\frac{X_M(r_s \pm r_f)}{D} \\ -\frac{X_M r_r}{D} & 0 & \frac{(X'_s \pm X'_f) r'_r}{D} + \frac{p}{\omega_b} & \frac{\omega}{\omega_b} - \frac{\omega_r}{\omega_b} \\ 0 & -\frac{X_M r_r}{D} & -\frac{\omega}{\omega_b} + \frac{\omega_r}{\omega_b} & \frac{(X'_s \pm X'_f) r'_r}{D} + \frac{p}{\omega_b} \end{bmatrix} \begin{bmatrix} \psi_{qs} \\ \psi_{ds} \\ \psi_{qr} \\ \psi_{dr} \end{bmatrix} \quad (4.2)$$

where  $D = (X_s + X_f).X_r - X_m^2$

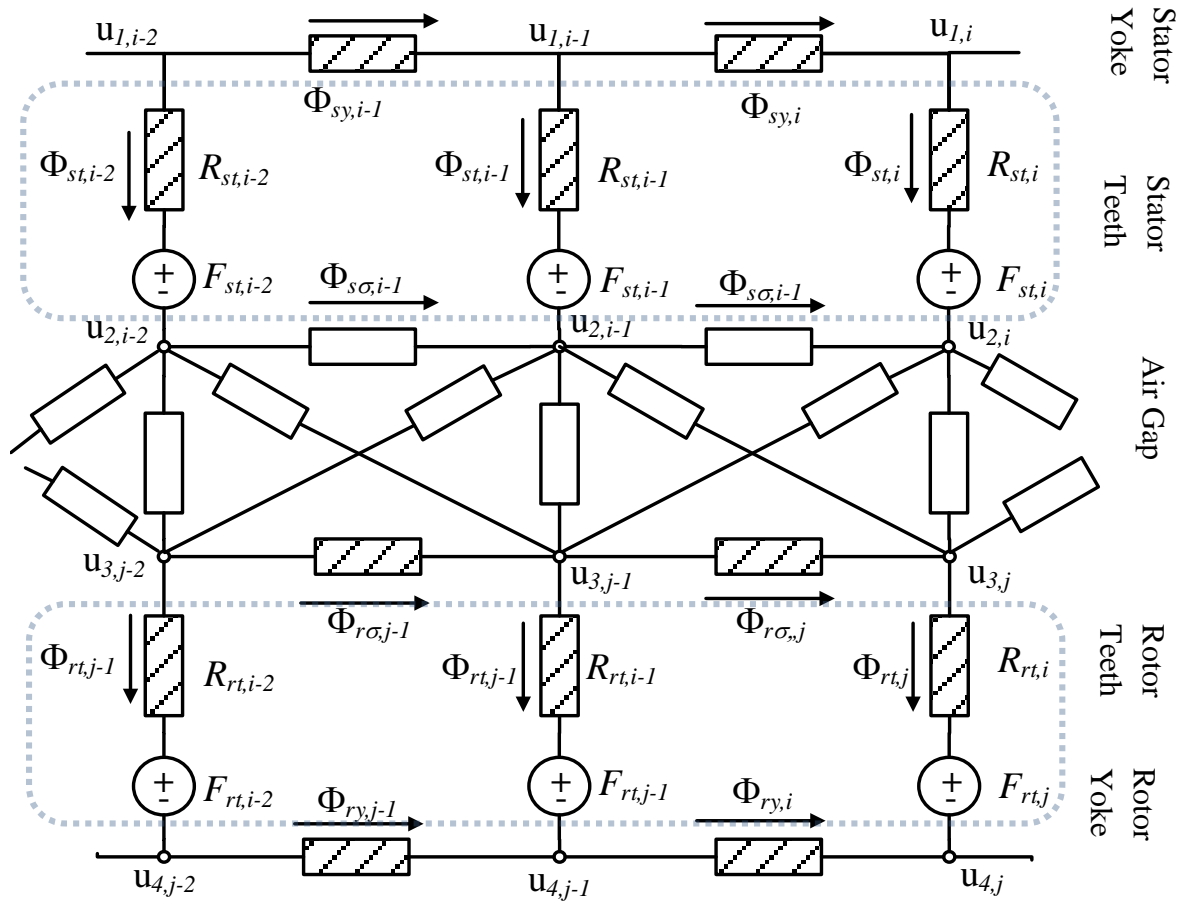


Fig. 4.3. MEC network as used for the proposed modelling.

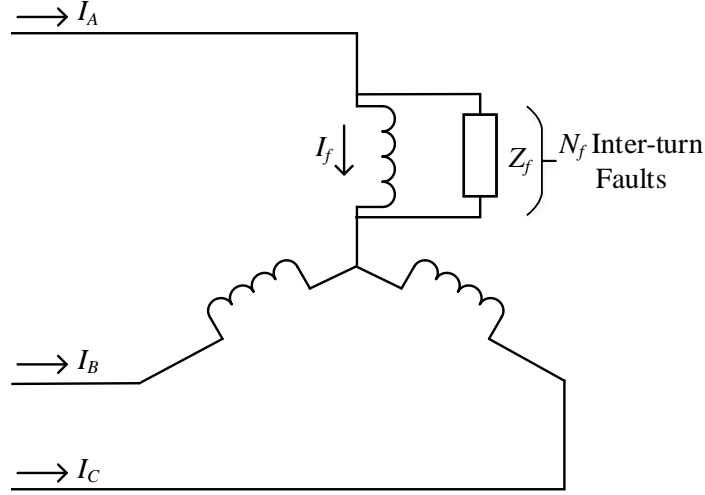


Fig. 4.4. MEC network variation due to inter-turn fault.

### C. Magnetic Equivalent Circuit Modelling of Faulty IM

During a stator inter-turn fault, the spatial magnetic field distribution in the machine is significantly affected. While the input parameters and operating conditions of the machine under consideration remains the same, the geometrical aspect of the machine is compromised. Thus, MEC model is implemented to investigate the magnetic field distribution of the IM during stator inter-turn fault conditions. Although the MEC model developed is for the 7.5 hp ALIM but it has been developed keeping in mind traction application. The model takes into account the stator and rotor slotting effects, saturation and slot leakage effects [3].

Using relevant geometrical data, details of winding configuration and material properties, a portion of the MEC model of the healthy ALIM without any faults has been developed as in Fig. 4.3. As seen from the figure, the magnetic scalar potential ( $u_n$ ) at 4 nodes identified as the stator yoke, stator tooth, rotor tooth and rotor yoke are to be determined for particular values of stator fluxes ( $\Phi_{st}$ ) and rotor fluxes ( $\Phi_{rt}$ ). In the model, the stator yoke reluctance ( $R_{sy}$ ), stator tooth reluctance ( $R_{st}$ ), rotor bar reluctance ( $R_{rt}$ ), rotor yoke reluctance ( $R_{ry}$ ), air-gap reluctance ( $R_{ij}$ ) and corresponding stator slot ( $R_{s\sigma}$ ) and rotor slot ( $R_{r\sigma}$ ) leakage reluctances associated with each part of the machine can be easily determined using geometric dimensions at each part. Further, permeance matrices ( $A_{ij}$ )



between various nodes can be easily determined. For a machine with  $N_s$  stator slots,  $N_r$  rotor bars and  $p$  poles,  $0 < i < N_s$  and  $0 < j < N_r$ . Applying nodal analysis, the following system of equations is obtained

$$\begin{bmatrix} A_{11} + (A_{11}R_{st} + I)A_{22} & (A_{11}R_{st} + I)A_{23} & 0 & 0 \\ 0 & A_{32} & A_{33} & 0 \\ 0 & 0 & A_{44} & 0 \\ 0 & 0 & 0 & -M_{rtmmf}^{-1} \end{bmatrix} \begin{bmatrix} u_2 \\ u_3 \\ u_4 \\ i_b \end{bmatrix} = \begin{bmatrix} -A_{11}F_{st} \\ -\phi_{rt} \\ \phi_{rt} \\ R_{rt}\phi_{rt} \end{bmatrix} \quad (4.3)$$

where  $F_{st}$  the stator tooth mmf matrix,  $M_{rtmmf}$  is the rotor tooth mmf matrix and  $i_b$  is the rotor bar matrix. The stator mmf can be calculated for a particular magnitude of current with or without any additional harmonics from the inverter side as well. For a particular current input, the induced rotor fluxes can be calculated to further obtain the rotor bar currents [4]. Thus, knowing the magnetic potentials, the air-gap flux density,  $B_g$  can be calculated for any rotor position,  $\theta$  of the IM using (4.4).

$$B_g(\theta) = \frac{u_2(\theta)}{[R_{ij}(\theta) \times A_g(\theta)]} \quad (4.4)$$

In case of fault condition, the turns per phase of the machine is disturbed and the corresponding stator tooth mmf matrix, rotor flux matrix and stator permeance matrices are modified. In order to account for the fault conditions, additional phase impedance component ( $Z_f$ ) can be included across any of the three phase impedance as shown in Fig. 4.4 and the air-gap flux density can be computed for the faulty IM. However, it is important to note that any change in the flux distribution of the faulty IM when compared to the healthy machine can be attributed to change in spatial harmonics caused by inter-turn faults only and has no contribution from the associated time harmonics from inverter side. Thus, MEC can be adapted to detect fault and also estimate the effective air-gap flux during inter-turn fault in IM.

#### D. Magnetic Harmonics Modelling of IM

In order to understand the harmonic order of the machine flux during both healthy and inter-turn fault condition to assist in developing a fault-tolerant control, harmonic modeling

of the IM is explained in this section. Current with fundamental frequency ( $\omega$ ) flows in the stator wound with  $P$  pairs of poles as in (4.5). Subscript  $m$  represents the peak value of the corresponding parameters.

$$I_s = I_{1m} \cos(P\theta - \omega t) \quad (4.5)$$

If the number of pole-phase groups of the stator winding is  $Z$ , the stator fluxes produced by the current will have the same frequency, but the number of pairs of poles are increased by  $v_s Z$ , where  $v_s$  is the order of stator space harmonics.  $\Phi_{sslot}$  is the flux produced due to stator slot opening, where  $v_{slot}$  is the stator slot harmonics

$$\left. \begin{aligned} \phi_s &= \sum_{v_s=1,2,3..}^{\infty} \phi_{smv_s} \cos((P + v_s Z)\theta - \omega t) + \phi_{sslot} \\ \phi_{sslot} &= \sum_{v_{slot}=kS \pm P} \phi_{sslotm} \cos((P + v_{slot} S)\theta - \omega t) \end{aligned} \right\} k = 1, 2, 3.. \quad (4.6)$$

The stator flux produces rotor currents, which have the same pairs of poles and the same frequency. This rotor current is written as in (4.7) where  $\omega_r$  is the speed of the rotor

$$I_r = \sum_{v_s=1,2,3..}^{\infty} I_{1rm} \cos((P + v_s Z)\theta - (\omega - (P + v_s Z)\omega_r)t) \quad (4.7)$$

If the number of rotor bars is  $S_r$ , then the rotor fluxes produced by rotor currents have the same frequency but the number of pole pairs is increased by  $v_r S_r$ . where  $v_r$  is rotor space harmonics.  $\Phi_{rslot}$  is the flux produced due to rotor slot opening [5].

$$\left. \begin{aligned} \phi_r &= \sum_{v_s=1,2,3..}^{\infty} \phi_{rmv_r} \cos((P + v_s Z + v_r S_r)\theta - (\omega - (P + v_s Z)\omega_r)t) + \phi_{rslot} \\ \phi_{rslot} &= \sum_{v_{slot}=kS_r \pm P} \phi_{rslotm} \cos((P + v_{slot} S_r)\theta - (\omega - v_r S_r \omega_r)t) \end{aligned} \right\} k = 1, 2, 3.. \quad (4.8)$$

Time harmonics are developed due to the inverter side of the drive system when there is a distorted voltage supply to the motor. The voltage and current can be expressed as

$$v = V_{1m} \sum_{\mu=1}^{\infty} C_{fv\mu} \cos(\mu\omega.t + \varphi_{v\mu}) \quad (4.9)$$

$$i = I_{1m} \sum_{\mu=1}^{\infty} \frac{C_{fv\mu}}{|Z_{\mu}|} \cos(\mu\omega.t + \varphi_{v\mu} + \theta_{\mu}) \quad (4.10)$$

where  $\mu$  is the order of the time harmonics voltage,  $V_{1m}$  and  $I_{1m}$  are the maximum values of the fundamental voltage and fundamental current respectively,  $C_{fv\mu}$  is the ratio of the amplitude of the  $\mu^{\text{th}}$  time harmonics voltage to the amplitude of the fundamental voltage,  $\omega$  is the angular frequency of the fundamental voltage,  $t$  is the time,  $\varphi_{v\mu}$  is the phase angle of the  $\mu^{\text{th}}$  time harmonics voltage,  $\theta_{\mu}$  is the phase angle between the  $\mu^{\text{th}}$  time harmonic voltage and current,  $\theta_1$  is the fundamental power factor angle [6].

The harmonic modeling block for fault diagnosis operates on the Fourier series for the magnetic flux density waves as expressed in (4.11) where  $B_p$ ,  $B_{\mu}$  represent time harmonics and  $B_{\lambda}$ ,  $B_{\lambda e}$  represent slot harmonics.

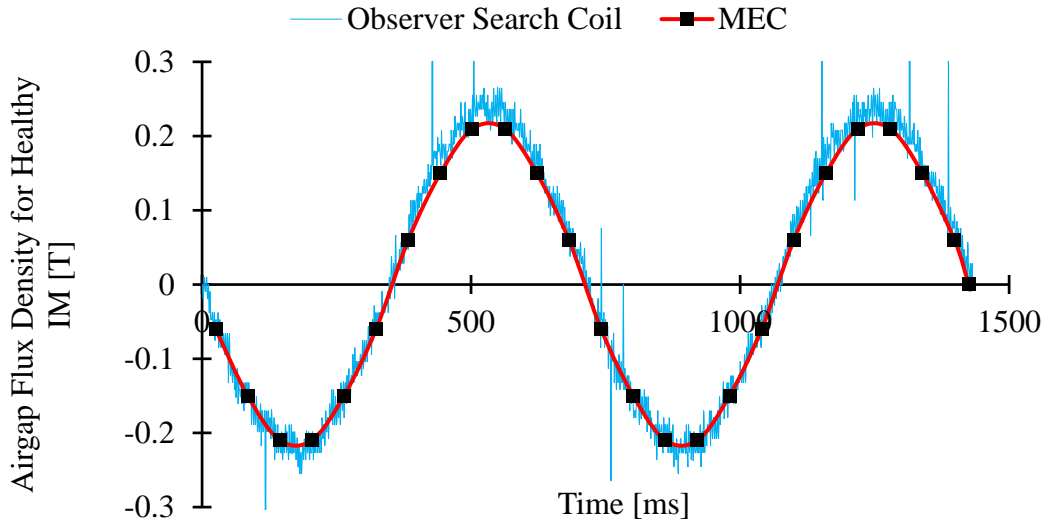
$$\begin{aligned} B(x, t) = & \sum_v B_p v \cos(px - v\omega_v t - \psi_v) + \sum_{\mu} B_{\mu} v \cos(\mu p x - v\omega_{\mu} t - \psi_{\mu}) \\ & + \sum_{\lambda} B_{\lambda} \cos(\lambda p x - \omega_{\lambda} t - \psi_{\lambda}) + \sum_{\lambda e} B_{\lambda e} \cos(\lambda_e p x - \omega_{\lambda e} t - \psi_{\lambda e}) \end{aligned} \quad (4.11)$$

### 4.3. Experimental Verification of Proposed Harmonic Block

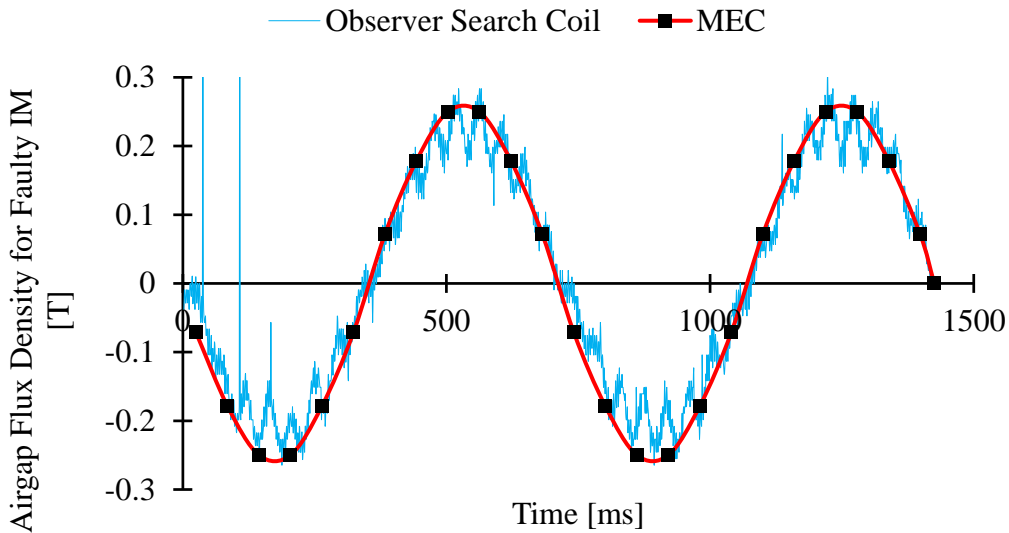
The proposed harmonics block implements the developed magnetic circuit model along with experimental results of faulty ALIM in order to get the real time data. The ALIM used is a 7.5 hp motor with winding inter-turn shorting on one of the phases. Another similar motor with same specifications has been used to get the healthy motor results.

The air-gap flux waveforms obtained from the search coil and the MEC of the healthy motor at a rated speed of 1,750 rpm and per phase current of 20.9 A are indicated in Fig. 4.5 (a). Similarly, the flux waveforms obtained from both the MEC and the search coil during the occurrence of an inter-turn fault at the same speed of 1,750 rpm, are illustrated in Fig. 4.5 (b). However, since the tests were performed during the fault condition, the currents were limited to only around 4 A. It is clearly seen that the results obtained from

MEC are in close agreement with the experimental data during both healthy and faulty operations. Also, the flux waveforms highlight the drastic changes in the flux values during fault occurrence from the reference flux obtained during healthy condition.



(a)

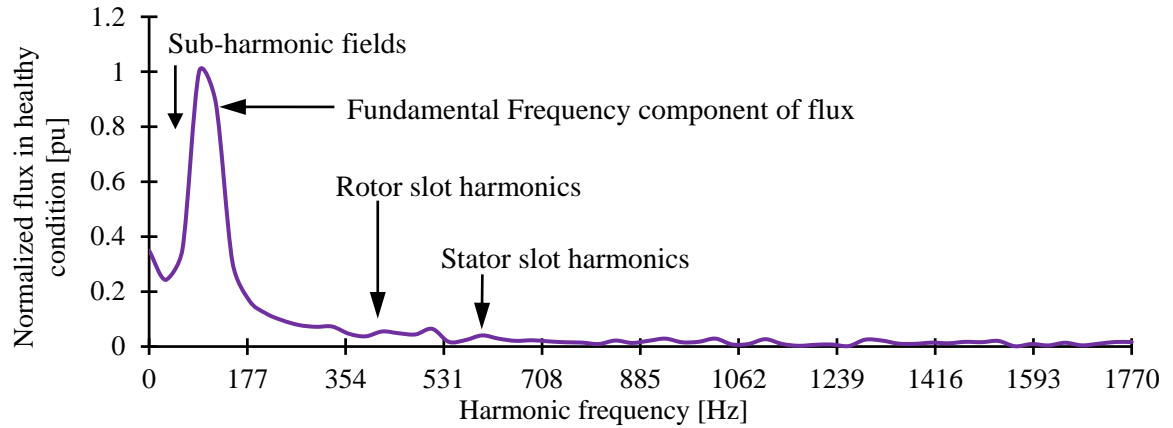


(b)

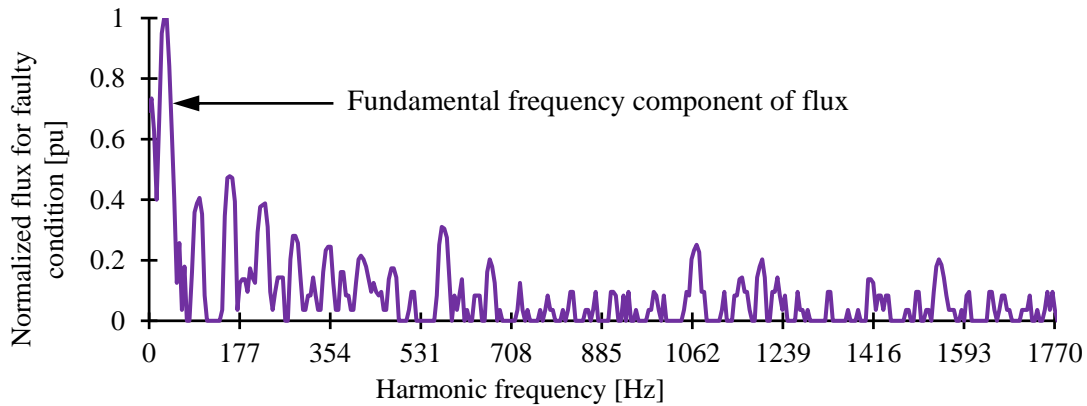
Fig. 4.5. Comparative results of flux obtained from MEC and OSC. (a) Healthy IM flux. (b) Faulty IM flux.

#### *4.4. Result Analysis of the Proposed Harmonic Block for Flux Feature Prediction*

Understanding the harmonic spectra of flux during healthy and faulty condition is vital for fault detection technique. A Fourier transform of flux obtained is performed for both healthy and faulty conditions and are illustrated in Figs.4.6 (a) and (b) respectively. The harmonic analysis is plotted for cycles per  $2\pi$  mechanical radians. If  $\nu$  is the order of flux harmonics as illustrated in Fig. 4.6, the fundamental torque producing component is  $\nu = P$  in the mechanical domain and hence is the fundamental rotor frequency corresponding to the machine speed. The machine under test consists of 4-poles and hence, the fundamental torque producing component is of 2<sup>nd</sup> order. The main harmonic is synchronous with the rotor speed; all the other harmonics are at asynchronous speed with respect to rotor inducing large rotor currents. Harmonics of order lower than  $\nu = P$  are sub-harmonic fields, which lead to parasitic effects in the machine such as rotor losses and noise and vibration. In case of the test machine, fundamental frequency component is the sub-harmonic field. The wavelength of sub-harmonics is higher than the corresponding wavelength of main harmonic leading to higher values of induced currents in the rotor. Stator and rotor slot harmonics are of the order  $\nu = kS \pm P$ , where  $S$  is the rotor or stator slots and  $k$  is any integer. For the machine under test, stator slot harmonics are of 50<sup>th</sup> and 46<sup>th</sup> orders and rotor slot harmonics are of 44<sup>th</sup> and 40<sup>th</sup> orders. The rotor and stator slot harmonics are caused due to non-uniform air-gap as a result of slotting and distribution of coils in the stator. During an inter-turn fault, the magnitude of rotor and stator slot harmonics is increased when compared to healthy operating conditions. It can be observed from the two figures that apart from the fundamental frequency component, sub-harmonic frequency components and slot harmonic components, a lot of other frequency components occur due to presence of faults, especially 5<sup>th</sup> and 7<sup>th</sup> order components including 11<sup>th</sup> and 17<sup>th</sup> orders, leading to additional torque ripple and losses in the machine. Thus, in order to develop a fault-tolerant control, these frequency components need to be compensated before completely shutting down the machine.



(a)



(b)

Fig. 4.6. Real time flux harmonic analysis of (a) Healthy motor condition (b) Faulty motor condition.

#### 4.5. Conclusion

The proposed harmonic analysis block uses MEC and real time data to detect fault and performs harmonic modeling and analysis to better understand the effects of inter-turn faults and further develop a fault-tolerant control. The added advantage of this model is that it can separate fault on motor side from that of inverter side by segregation of space and time harmonics and checking for any variation in harmonics from the normal healthy condition. This block can be used for designing a harmonic compensation block with adequate reference flux prediction so as to enable the safe operation of motor in incipient fault condition which means the EV can still be driven although there has been a fault. The driver shall be notified of the fault and the passengers can reach their destination safely.

#### 4.6. References

- [1] D. G. Dorrell, A. Salah, and Y. Guo, "The Detection and Suppression of Unbalanced Magnetic Pull in Wound Rotor Induction Motors Using Pole-Specific Search Coils and Auxiliary Windings," *IEEE Transactions on Industry Applications*, vol. 53, no. 3, pp. 2066-2076, May-June 2017.
- [2] G. Kron, "Equivalent Circuits of Electric Machinery," J. Wiley & Sons, 1951.
- [3] V. Ostovic, "Dynamics of Saturated Electric Machines," Springer Publications, 1989.
- [4] S. D. Sudhoff, B. T. Kuhn, K. A. Corzine, and B. T. Branecky, "Magnetic Equivalent Circuit Modeling of Induction Motors," *IEEE Transactions on Energy Conversion*, vol. 22, no. 2, pp. 259-270, June 2007.
- [5] Y. Ouazir, N. Takorabet, R. Ibtouen, and S. Mezani, "Consideration of Space Harmonics in Complex Finite Element Analysis of Induction Motors with an Air-Gap Interface Coupling," *IEEE Transactions on Magnetics*, vol. 42, no. 4, pp. 1279-1282, April 2006.
- [6] O. A. Mohammed, N. Y. Abed, and S. Ganu, "Modeling and Characterization of Induction Motor Internal Faults Using Finite-Element and Discrete Wavelet Transforms," *IEEE Transactions on Magnetics*, vol. 42, no. 10, pp. 3434-3436, Oct. 2006.
- [7] S. Mukundan, K. L. V. Iyer, H. Dhulipati, K. Mukherjee, J. Tjong, and N. C. Kar, "Response Surface Methodology based Optimization of Surface PM Machine Incorporating Stator Slotting and PM Sizing Effects to Extend the Operating Limits for Direct-Drive EV Application," in the *Proc. of XXII International Conference on Electrical Machines (ICEM)*, pp. 2045-2051, Lausanne, 2016.

## **CHAPTER 5**

# **FLUX FEATURE BASED ON-LINE HARMONIC COMPENSATION FOR FAULT-TOLERANT CONTROL**

### *5.1. Introduction*

This chapter proposes a field-oriented fault-tolerant control method to be used in traction application incorporating the developed methodology in Chapter 4. The space harmonics of magnetic flux is measured from the search coils wound around the stator slots and time harmonics is calculated from the measured currents and voltages of the induction motor. The measured values are represented/calculated in terms of magnetic flux and the error signal is processed as a reference to the drive system. The IM has been modelled in FEA as described in Chapter 2 with the parameters of machine-under-test in order to compare the healthy condition of the motor with the experimental results of faulty motor. The novelty of this procedure lies in highlighting the importance of reduction of both time and space harmonics developed simultaneously in an online compensation traction drive system.

### *5.2. Modelling of Harmonic Compensation Block*

#### *A. Slot Harmonic Modelling*

The slot harmonics in an induction motor arise from radial forces due to the magnetic flux density in the air gap which is dependent on the rotor speed. The influence of non-sinusoidal MMF and variation in magnetic permeance of air gap due to structural design of the IM such as the number of poles and slots, magnetic saturation of flux, non-linear faults and eccentricity of the rotor, leads to variation of the magnetic flux density. The slots produce an even distribution of air-gap permeance which interacts with magnetizing component of air-gap MMF even when the slip of IM is zero. When slip is greater than zero, there is a flow of rotor current producing slot MMF harmonics which also interacts with fundamental component of air-gap flux. Rotor eccentricity in the air gap flux originates due to difference in the regions of low and high reluctance causing air gap to be



maximum at one region and minimum on the other. These unbalances induce unstable voltages in the windings of the stator with change in rotor position [1].

Two harmonic components of frequencies  $Z/P(\omega_r \pm \omega_o)$ , where  $P$  is the number of pole pairs and  $Z$  is the rotor slots rotating at  $\omega_r$ , are produced at the air gap flux due to modulation of the rotor slots. This results in a sinusoidally distributed air-gap MMF which is expressed as (5.1)

$$B(\theta, t) = B_1 \cos(\omega_o t - P\theta) + B_{r1} \cos\left[\left(\frac{z}{P}\omega_r + \omega_o\right)t - (P+Z)\theta + \psi_{r1}\right] + B_{r2} \cos\left[\left(\frac{z}{P}\omega_r - \omega_o\right)t - (P-Z)\theta + \psi_{r2}\right] \quad (5.1)$$

where  $\psi_{r1}$  and  $\psi_{r2}$  are phase angles. The stator space harmonics is produced due to EMF in the stator windings induced by flux density. Generally, this air gap MMF is not perfectly sinusoidal since it contains space harmonics produced by spatial asymmetries, inverter supply and magnetic saturation [2]. This causes the rotor speed dependent harmonics to appear in the magnetic flux density of the air-gap represented as (5.2).

$$\omega_{sh} = \left(\frac{z}{P}\omega_r \pm k\omega_o\right) \quad (5.2)$$

where  $k$  is the positive order of the air-gap flux harmonic. The rotor speed frequency can be expressed in electrical Hz as

$$f_r = \frac{P}{z}(f_{sh} - kf_o) \quad (5.3)$$

### B. Time Harmonics Modelling

Time harmonics is developed from the inverter side of the drive system when the motor is supplied with a distorted voltage [3]. This leads to the frequency induced in the rotor to vary due to increased difference in fundamental and harmonic frequencies. The voltage and current can be expressed as

$$v = V_m \sum_{k=1}^{\infty} A_{vk} \cos(k\omega t + \phi_{vk}) \quad (5.4)$$

$$i = I_m \sum_{k=1}^{\infty} \frac{A_{vk}}{|Z_k|} \cos(k\omega t + \phi_{vk} + \theta_k) \quad (5.5)$$

where  $V_m$  and  $I_m$  are the maximum values of the fundamental voltage and current respectively,  $A_{vk}$  is the ratio of amplitude of  $k^{\text{th}}$  time harmonics voltage to fundamental voltage,  $\omega$  is the angular frequency of  $V_m$ ,  $\phi_{vk}$  is the phase angle of  $k^{\text{th}}$  time harmonics voltage,  $\theta_k$  is the phase angle between  $k^{\text{th}}$  time harmonic voltage and current. The novel compensation block incorporates the Fourier series of flux waveform as expressed in (5.6).

$$B(x, t) = \sum_v B_p v \cos(px - v\omega_v t - \psi_v) + \sum_{\mu} B_{\mu} v \cos(\mu p x - v\omega_{\mu} t - \psi_{\mu}) \\ + \sum_{\lambda} B_{\lambda} \cos(\lambda p x - \omega_{\lambda} t - \psi_{\lambda}) + \sum_{\lambda_e} B_{\lambda_e} \cos(\lambda_e p x - \omega_{\lambda_e} t - \psi_{\lambda_e}) \quad (5.6)$$

where  $B_p$ ,  $B_{\mu}$  represent time harmonics and  $B_{\lambda}$ ,  $B_{\lambda_e}$  represent slot harmonics.

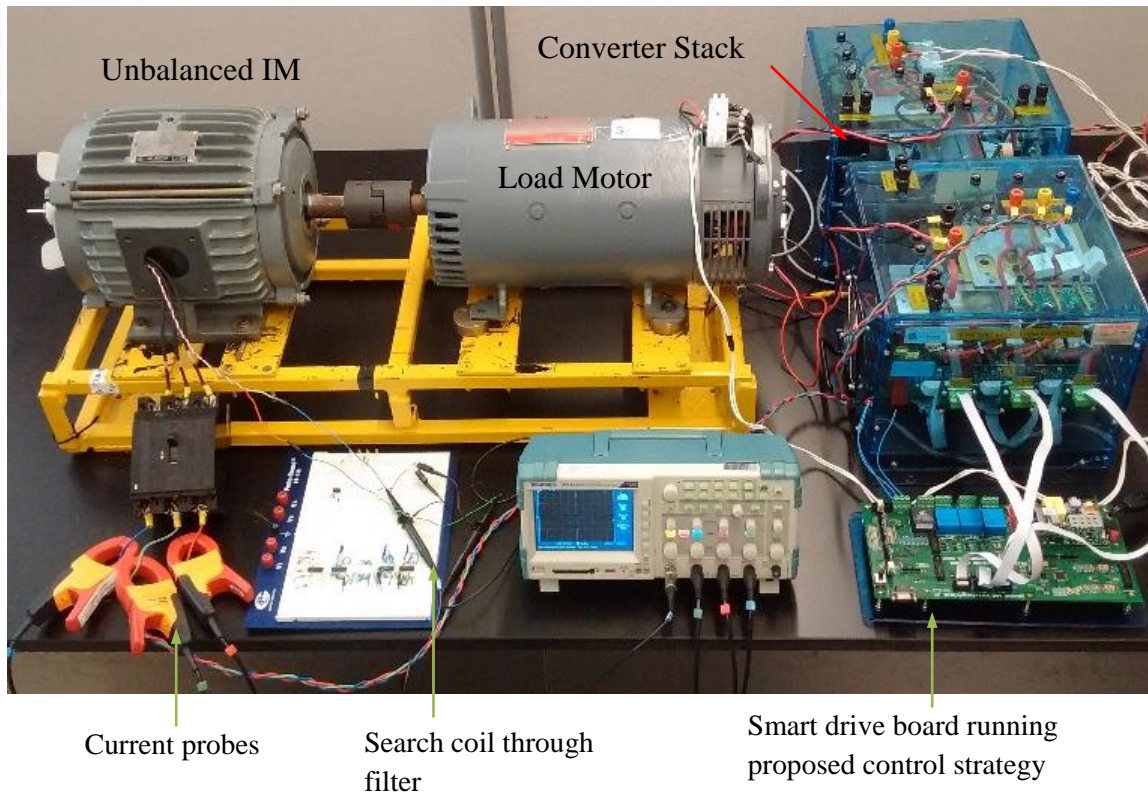


Fig. 5.1. Set up for experimental validation of the proposed compensation drive.

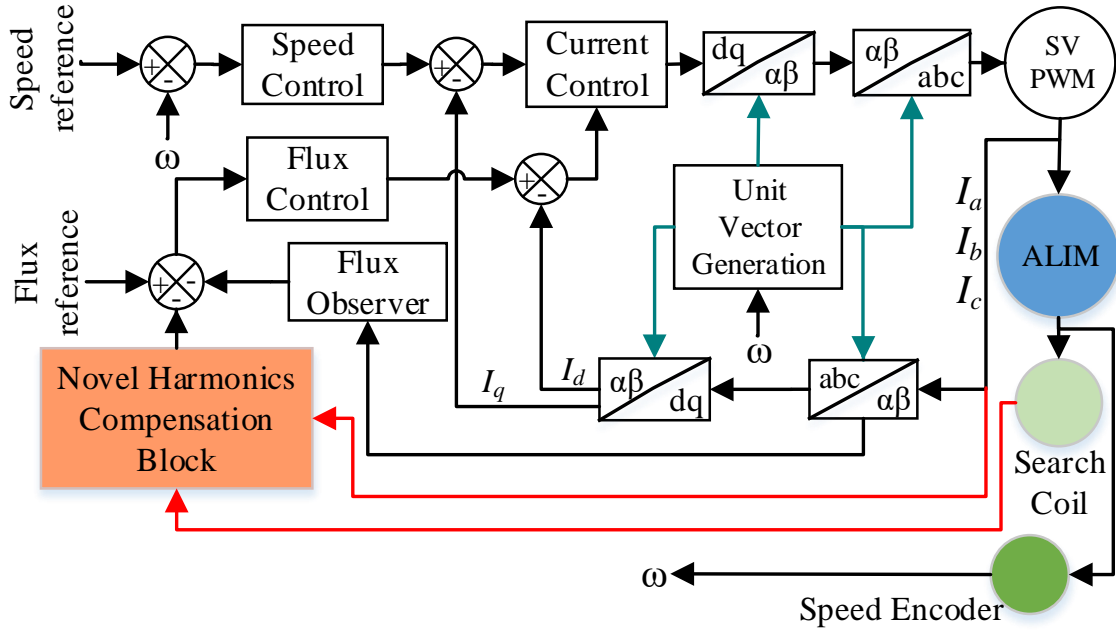


Fig. 5.2. Proposed novel control strategy with harmonic compensation block.

### 5.3. Experimental Validation of Proposed Harmonic Compensation Drive

#### A. Experimental Methodology

Comparative performance analysis was performed on a healthy 7.5 hp, laboratory totally enclosed fan-cooled aluminium-rotor induction motor (ALIM) and a faulty ALIM with the machine parameters as shown in Table 2.2. The test was performed at different speeds starting from 0 to the rated speed of 1,750 rpm. The faulty motor is driven by an inverter-fed, digital signal processor based drive system. The designed control logic has been implemented using high performance 32-bit microcontroller capable of real-time control. The complete setup with the control board running the proposed control strategy is shown in Fig. 5.1. The proposed drive system is a flux-oriented vector control which contains both current and speed feedback. The harmonic compensation block contains the mathematical formulation as explained. This block also uses a lookup table for magnetic flux based on values of flux as obtained from finite element analysis (FEA) and the experimental values for the healthy IM. The flow of operations is shown in Fig. 5.2.

### *B. Evaluation of Magnetic Air-gap Flux Density*

To measure the air gap flux density, search coils have been wound along the previously detected faulty phase of the ALIM as shown in Fig. 5.3. Traditionally the search coils are placed at the end windings of the stator. In order to obtain more accurate results search coil has been placed along the complete length of the tooth [4]-[6]. This gives a more uniform result of the magnetic flux along the entire stator length instead of just end windings which drastically changes the desired results. The search coil is designed using 22 AWG wire with 6 turns along the length of stator slot. The flux linkage can be calculated as (5.7)

$$\int_s \nabla \times E \cdot dS = -\frac{d}{dt} \int_s B(t) \cdot dS = \int_s \frac{-dB(t)}{dt} \cdot dS \quad (5.7)$$

where  $B$  is the magnetic flux density. The induced voltage measured at the search coil can be expressed using Maxwell Faraday's law of electromagnetism as (5.8)

$$e = -N \frac{d\Phi}{dt} \quad (5.8)$$

where  $N$  is the number of turns of the search coil.



Fig. 5.3. Search coil placed on the phase of detected fault.

### C. Slot and Time Harmonic Tracking

Since at no load  $f_r$  is same as  $f_o$ , rearranging (5.3) gives no load slot harmonic frequency  $f_{sh0}$  as (5.9) is used to define a search interval window as  $\Delta f_{sh}$  which tracks slot harmonics.

$$f_{sh0} = \left( \frac{z}{P} - k \right) f_o \quad (5.9)$$

The slip for  $k^{\text{th}}$  harmonics of the forward and backward rotating time harmonics is presented in terms of electrical synchronous speed and rotor speed as (5.10)

$$s_k = \frac{k\omega_{syn} \pm \omega_r}{k\omega_{syn}} \quad (5.10)$$

where  $\omega_{syn}$  is the synchronous speed of the motor. Since  $f_r$  can be related to the harmonics slip frequency which is in terms of the time harmonics, using (5.2), (5.3), (5.9) and (5.10), the stator slot harmonics can be estimated as

$$f_{sh} = f_{sh0} - \frac{z}{P} \left( \frac{1}{s_k} - 1 \right) f_r \quad (5.11)$$

here  $f_{sh}$  is the slot harmonics of the IM in terms of Hz. All the harmonics that are multiple of fundamental frequency of the inverter supply  $k.f_o$  is filtered out. This helps in defining  $\Delta f_{sh}$  as in (5.12). The harmonics of inverter supply are then considered for time harmonics tracking using the  $S_k$  from (5.10) and verified using (5.11) till the 37th harmonics for reasonable accuracy.

$$\Delta f_{sh} = f_o (1 - \omega_{syn}) \quad (5.12)$$

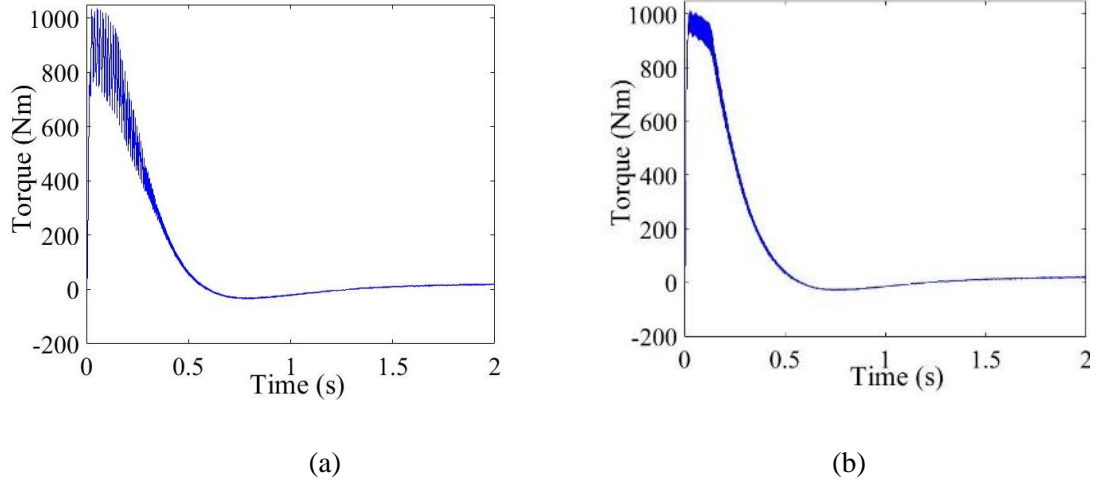


Fig. 5.4. Behavior of electromagnetic torque (a) Ripples caused in the unbalanced IM. (b) Decrease in ripples after balancing the IM.

#### *D. Control Strategy for On-line Harmonics Compensation*

The control drive was programmed to run the proposed control strategy as shown in Fig. 5.2. The harmonic compensation block takes back EMF of search coil and current from inverter supply as input, in order to work as an online data sampling module. This proposed control strategy, using speed and flux as references, is running continuously along with the conventional vector control. In case of the unbalanced motor, the online harmonics module computes the slot and time harmonics as explained in Section 5.2 C and gives flux, whose considered bandwidth is 2,160 Hz, as a feedback for the flux control. Spectral analysis using Fast Fourier Transformation (FFT) is done to extract harmonics from the search coil voltage. Since the FFT module in the drive uses 1024 sampling points in one period, theoretically FFT can be applied upto 512<sup>th</sup> harmonics. Figs. 5.4(a) and (b) illustrates harmonics effect on torque ripple.

### *5.4. Analysis of Time and Spatial Harmonics*

#### *A. Investigation Using Finite Element Model*

The 7.5 hp ALIM been designed using time stepping finite element analysis in this chapter following the steps in Chapter 2. Influence of both spatial and time harmonics is studied on the flux density distribution in the air-gap for the 48 stator slots and 42 rotor



bars IM. The flux density is calculated as a product of MMF function and permeance factor. Considering both the harmonics in MMF function, flux density distribution over one pole pair has been calculated using Maxwell equations. The difference in magnetic flux density for balanced and unbalanced induction machine have been compared in Fig. 5.5 for a slip of 0.0083. The inconsistency in flux lines of unstable IM due to increased harmonics in the air-gap is represented in a simulated IM and compared with the healthy motor.

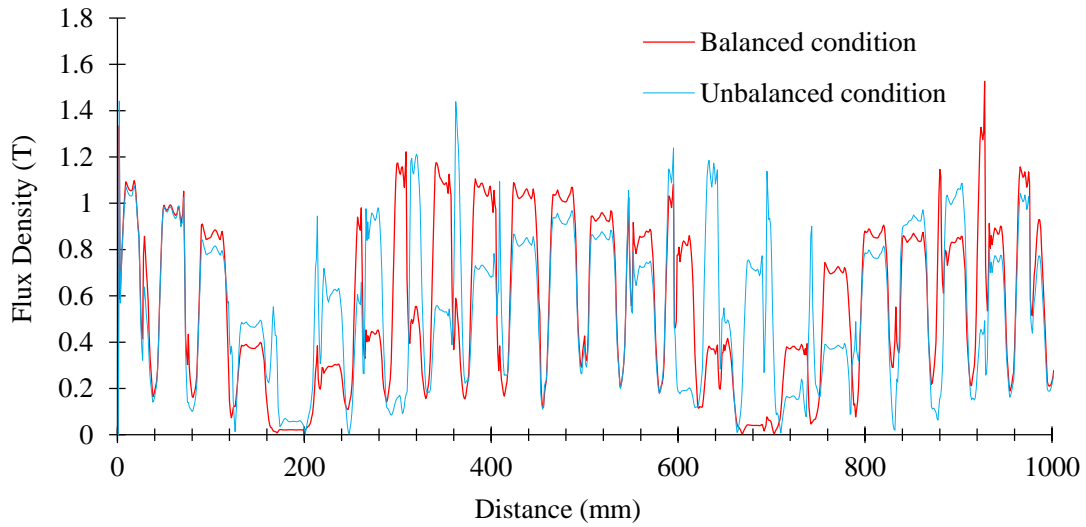


Fig. 5.5. The air gap magnetic flux density for healthy and unstable condition.

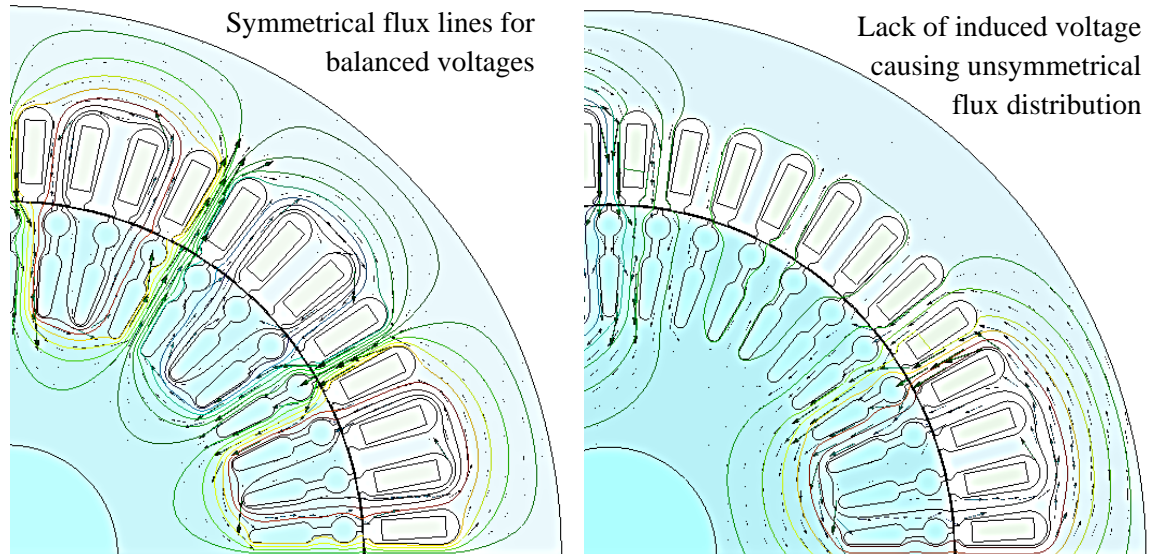
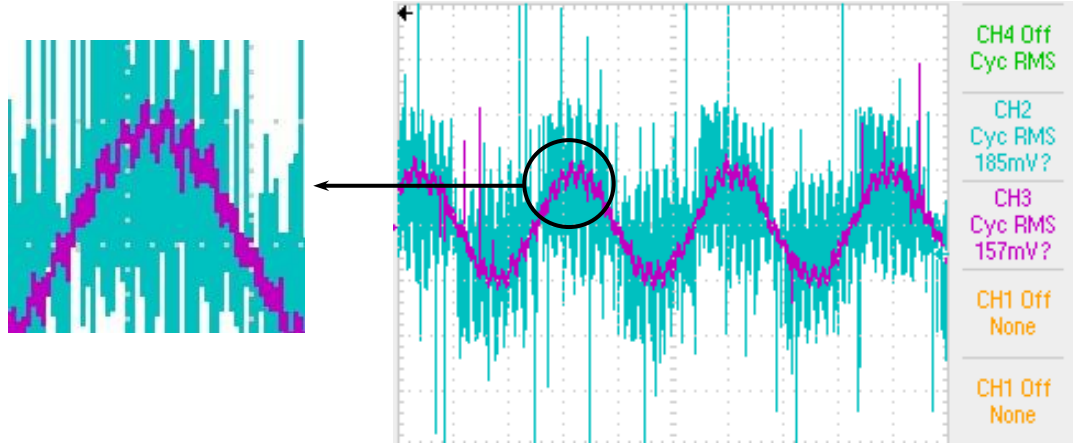
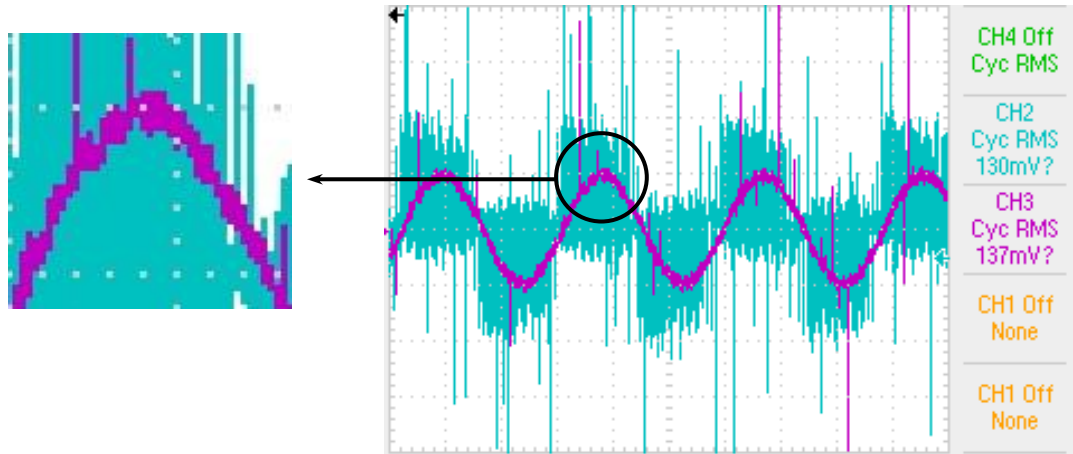


Fig. 5.6. Magnetic flux distribution for the IM. (a) Normal condition. (b) Unbalanced condition.



(a)



(b)

Fig. 5.7. Back EMF voltage as measured using search coil. (a) Eccentric condition of 157 mV for fundamental, 185 mV for harmonics. (b) After using the control 130 mV for fundamental, 137 mV for harmonics.

### *B. Evaluation of Experimental Results*

The back EMF of the stator search coil produced by the vector controlled induction motor under rated condition before and after implementation of online harmonic compression is shown Figs. 5.7(a) and (b) respectively. The ripple on the waveform is created due to slot and air gap harmonics. The higher-order harmonics can be obtained by filtering out the fundamental component. The voltage difference measure varies between



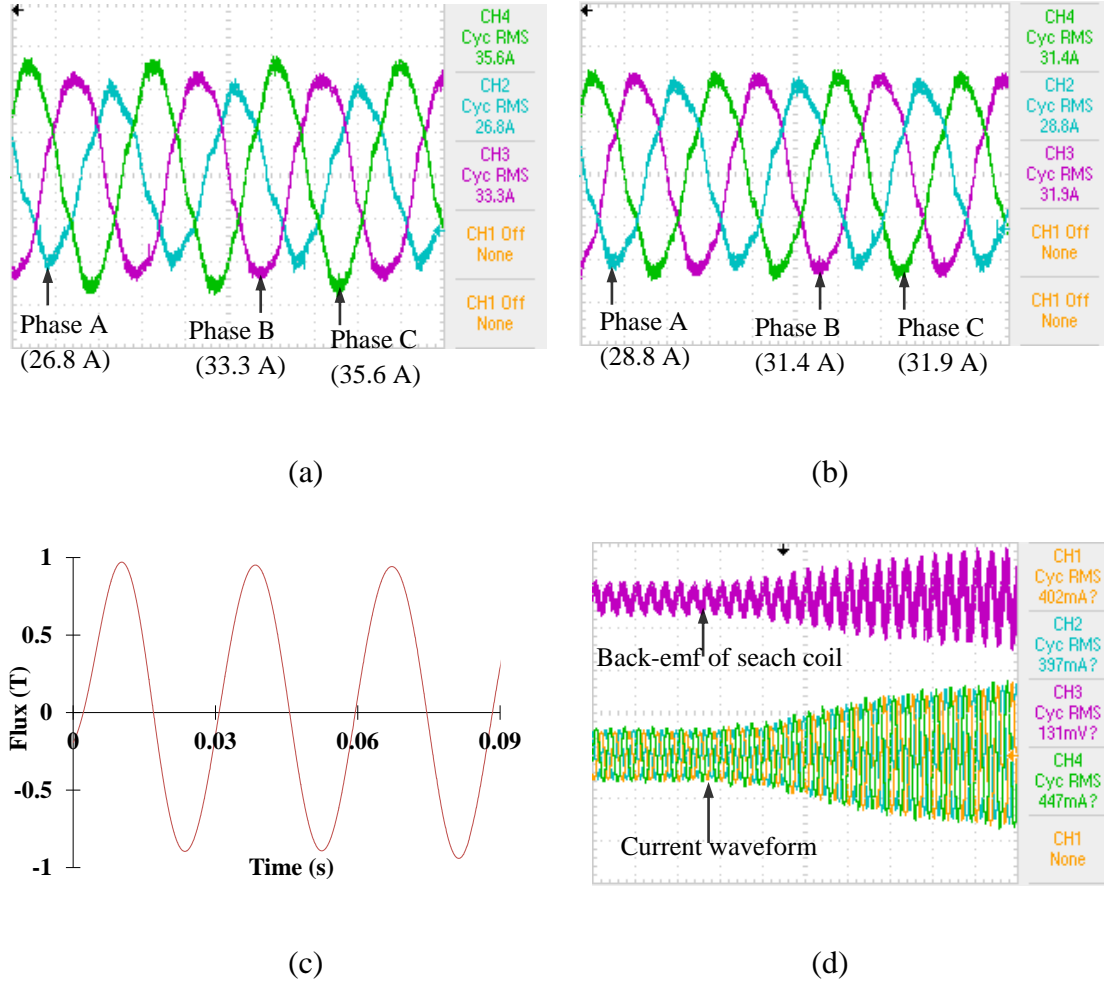


Fig. 5.8. The current waveform of the IM as measured. (a) Eccentric condition. (b) After using the control. (c) Reference flux input for the control. (d) Transient performance during speed change.

48mV and 100 mV. The value of air gap flux density as calculated and estimated by the controller in both with and without distorted harmonics differs by a value of 0.1. The average value of magnetic flux density varies between 0.45 and 0.7 T. It can be clearly seen that the fundamental voltage as shown in pink has more distortions before the control has been implemented. As shown in the Figs. 5.8(a) and (b), the three-phase current waveform is distorted due to unbalanced magnetic pull. The difference in the RMS value of current between A and C phase is 8.8 A while between B and C is 2.3 A. After balancing the motor with the designed drive the difference decreases to a minimum of 0.5 and

maximum of 2.6 A. To prevent inaccurate fault diagnosis due to interference of switching harmonics with magnetic slot harmonics, and consider them separately, a slot harmonic tracking window has been considered to exclude  $k.f_o$  while defining the search interval  $\Delta f_{sh}$  as given in Section 5.3 C. Fig. 5.8(c) indicates the reference flux input for the experiment performed. Fig. 5.8(d) presents a stable performance of the IM in terms of back-emf as well as current in transient condition when the speed is changed from 600 rpm to rated speed of 1,750 rpm. Although it is possible to stabilize the system using the feedback from the search coil, by taking the current distortion into consideration the drive control is made more fault tolerant.

### 5.5. Conclusion

This chapter proposes a new method to eliminate both time and space harmonics while the machine experiences a fault either due to the inverter or internal motor breakdown while driving the vehicle. Due to eccentricity in the rotating air-gap flux of the motor, asymmetric distribution of the magnetic flux is produced, causing an unbalanced magnetic pull. The online harmonics elimination control drive was simulated and results obtained from finite element analysis of the motor was compared with experimental results validating the proposed method. This process of estimation of reference flux can be made computationally faster with the help of model predictive algorithm or model reference adaptive system which has been developed and explained in later chapters.

### 5.6. References

- [1] H. Henao, C. Martis, and G. A. Capolino, "An Equivalent Internal Circuit of the Induction Machine for Advanced Spectral Analysis," *IEEE Transactions on Industry Applications*, vol. 40, no. 3, pp. 726-734, May-June 2004.
- [2] V. Climente-Alarcon, J. A. Antonino-Daviu, A. Haavisto, and A. Arkkio, "Diagnosis of Induction Motors Under Varying Speed Operation by Principal Slot Harmonic Tracking," *IEEE Transactions on Industry Applications*, vol. 51, no. 5, pp. 3591-3599, Sept.-Oct. 2015.

- [3] B. Akin, S. Choi, U. Orguner, and H. A. Toliyat, "A Simple Real-Time Fault Signature Monitoring Tool for Motor-Drive-Embedded Fault Diagnosis Systems," *IEEE Transactions on Industrial Electronics*, vol. 58, no. 5, pp. 1990-2001, May 2011.
- [4] D. Shah, S. Nandi, and P. Neti, "Stator-Interturn-Fault Detection of Doubly Fed Induction Generators Using Rotor-Current and Search-Coil-Voltage Signature Analysis," *IEEE Transactions on Industry Applications*, vol. 45, no. 5, pp. 1831-1842, Sept.-Oct. 2009.
- [5] S. M. Mirimani, A. Vahedi, F. Marignetti, and R. Di Stefano, "An Online Method for Static Eccentricity Fault Detection in Axial Flux Machines," *IEEE Transactions on Industrial Electronics*, vol. 62, no. 3, pp. 1931-1942, March 2015.
- [6] D. G. Dorrell, and O. Kayani, "Measurement and Calculation of Unbalanced Magnetic Pull in Wound Rotor Induction Machine," in *IEEE Transactions on Magnetics*, vol. 50, no. 11, pp. 1-4, Nov. 2014.
- [7] A. Sapena-Baño *et al.*, "Harmonic Order Tracking Analysis: A Novel Method for Fault Diagnosis in Induction Machines," *IEEE Transactions on Energy Conversion*, vol. 30, no. 3, pp. 833-841, Sept. 2015.
- [8] J. Faiz, B. M. Ebrahimi, B. Akin, and H. A. Toliyat, "Finite-Element Transient Analysis of Induction Motors Under Mixed Eccentricity Fault," *IEEE Transactions on Magnetics*, vol. 44, no. 1, pp. 66-74, Jan. 2008.
- [9] J. F. Bangura and N. A. Demerdash, "Diagnosis and Characterization of Effects of Broken Bars and Connectors in Squirrel-Cage Induction Motors by a Time-Stepping Coupled Finite Element-State Space Modeling Approach," *IEEE Transactions on Energy Conversion*, vol. 14, no. 4, pp. 1167-1176, Dec 1999.
- [10] R. Fiser and S. Ferkolj, "Application of a Finite Element Method to Predict Damaged Induction Motor Performance," *IEEE Transactions on Magnetics*, vol. 37, no. 5, pp. 3635-3639, Sep 2001.

# CHAPTER 6

## INTELLIGENT FLUX FEATURE PREDICTIVE CONTROL FOR FAULT-TOLERANT CONTROL

### 6.1. Introduction

In this chapter a new flux predictive control method has been proposed in which the flux of the rotating IM is monitored using flux sensor and the measured voltage and current are given as a feedback to the system. To increase the reliability and speed of the implemented vector control strategy, an improved stator-flux based predictive algorithm is used to obtain the flux reference thereby enhancing the overall stability of the control strategy. This method also improves the overall stability of the method. The IM under test has been modelled using finite element method (FEM) for both healthy and faulty conditions to get a detailed analysis of the behavior of flux distribution when inter-turn fault occurs. The proposed flux predictive control strategy has been implemented and tested to present the capabilities of the control method

### 6.2. Stator Flux Reference IM Model

Three-phase aluminum rotor induction motor (ALIM) has been modeled based on the two-axis rotating reference frame theory as expressed in (6.1).

$$V = A \times \Psi \quad (6.1)$$

Where

$$A = \begin{bmatrix} \frac{X'_r r_s}{D} + \frac{p}{\omega_b} & \omega_s & -\frac{X_M r_s}{D} & 0 \\ -\omega_s & \frac{X'_r r_s}{D} + \frac{p}{\omega_b} & 0 & -\frac{X_M r_s}{D} \\ -\frac{X_M r_r}{D} & 0 & \frac{X'_s r'_r}{D} + \frac{p}{\omega_b} & \omega_s - \frac{\omega_r}{\omega_b} \\ 0 & -\frac{X_M r_r}{D} & -\omega_s + \frac{\omega_r}{\omega_b} & \frac{X'_s r'_r}{D} + \frac{p}{\omega_b} \end{bmatrix} \quad V = \begin{bmatrix} v_{qs} \\ v_{ds} \\ v_{qr} \\ v_{dr} \end{bmatrix} ; \quad \Psi = \begin{bmatrix} \psi_{qs} \\ \psi_{ds} \\ \psi_{qr} \\ \psi_{dr} \end{bmatrix} ; \quad \omega_s = \frac{\omega}{\omega_b} ;$$

$$D = X_s X_r - X_M^2 ; \quad X_s = X_{ls} + X_M ; \quad X_r = X_{lr} + X_M$$

This model is chosen over the conventional voltage-current two-axis model because when current is taken as the state variable the model involves two derivative terms of current in the d-q voltage equations. But while considering flux linkage as the state variable, there is only one derivative of flux linkage [1]. This makes computation and modelling of ALIM easier in terms of the design for the novel flux predictive control.

Since a squirrel cage ALIM is used, the rotor currents of the  $q$ -axis and the  $d$ -axis namely,  $I_{qr}$  and  $I_{dr}$  cannot be directly measured and the rotor voltages,  $V_{qr}$  and  $V_{dr}$  are considered to be zero as the rotor ends are shorted. To evaluate the rotor speed  $\omega_r$  of the IM, the formula used is expressed as in (6.2).  $T_L$  is the load torque that would be provided to the machine externally, while  $T_e$  needs to be formulated as in (6.3).

$$\frac{d\omega_r}{dt} = \frac{P}{2J} (T_e - T_L) \quad (6.2)$$

$$T_e = \frac{3}{2} \frac{P}{2} L_m (i_{qs} \psi_{ds} - i_{ds} \psi_{qs}) \quad (6.3)$$

The stator current will affect both torque and flux of the machine. Thus using flux control technique, a decoupling between torque and flux is obtained. This decoupling method helps in the designing the stator flux based control logic. Using this two-axis model the following control, as explained, has been designed for the ALIM whose parameters are shown in Table 2.2.

### *6.3. Development of Proposed Flux-Oriented Control*

The novel fault-tolerant flux control running the ALIM is explained in this section through estimation of flux, fault detection, functioning of the proposed control and the operational test setup running the proposed control.

#### *A. Estimation of Magnetic Flux Linkage*

A flux sensor which is a search coil in this case is wound along the previously detected faulty phase of the ALIM as shown in Fig. 6.1, to measure the flux produced as a result of the rotating air-gap in the ALIM. In most cases, researchers place the search coils at the end windings of the stator for ease of installation and cheaper costs [2], [3]. For increased

accuracy in results search coil has been placed along the entire length of the tooth. This enables a more uniform result of the magnetic flux along the entire stator length instead of just end windings which changes the desired results to a great extent. The search coil has been designed using 22 AWG wire with 6 turns along the length of stator slot. The magnetic flux linkage can be calculated as (6.4)

$$\int_s \nabla \times E \cdot dS = - \frac{d}{dt} \int_s B(t) \cdot dS = \int_s \frac{-dB(t)}{dt} \cdot dS \quad (6.4)$$

where  $B$  is the magnetic flux density. The induced voltage measured at the search coil can be expressed using Maxwell Faraday's law of electromagnetism as (6.5) where  $N$  is number of turns of the search coil. The calculated flux  $\phi$  value is used for detecting the change in variation in the flux and estimating the amount of variation when an inter-turn fault occurs. This is an invasive method of estimation which increases the robustness of the control.

$$e = -N \frac{d\Phi}{dt} \quad (6.5)$$

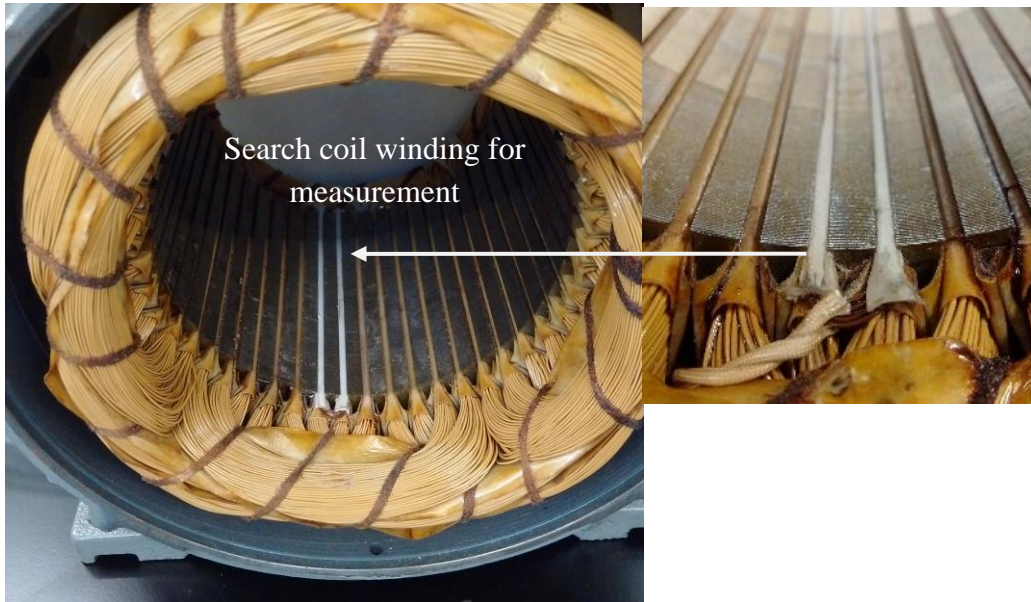


Fig. 6.1. Search coil placed on the phase of detected unbalance.

### B. Fault Detection using Space and Time Harmonic Measurement

The flow of current through the concentric windings of the healthy ALIM produces an even distribution of air-gap flux which interacts with magnetizing component of air-gap even when the slip of IM is zero. When the motor starts rotating, the slip is greater than zero, there is a flow of rotor current producing space harmonics which also interacts with fundamental component of air-gap flux. When a stator winding fault occurs, there is an immediate eccentricity in the air gap flux. This originates due to difference in the regions of low and high reluctance due to uneven distribution of current flow in the stator of the ALIM causing air gap to be maximum at one region and minimum on the other. The air gap magneto motive force (MMF) is not perfectly sinusoidal since it contains space harmonics produced by spatial asymmetries, inverter supply and magnetic saturation [4]. Thus proper detection of harmonics is needed to differentiate the inter-turn stator fault from the voltage unbalance.

Detection of the harmonics is done using both invasive and noninvasive method. Detection of space harmonics involves the detection of the flux linkage using the search coil as explained in Section 6.3 B, thus making it an intrusive method. On the other hand the time harmonics is detected by taking the measurement from the current sensor. This is done from outside the motor thus a non-intrusive method.

The space harmonics of the rotating magnetic flux can be presented as in (6.6) where  $\omega_{sh}$  is the speed of the space harmonics of the angular MMF and  $k$  is the positive order of the flux space harmonics [5].

$$\omega_{sh} = \left( \frac{z}{p} \omega_r \pm k \omega_o \right) \quad (6.6)$$

The rotor speed frequency  $f_r$ , in terms of space harmonics can be expressed in electrical Hz as in (6.7) where  $f_{sh}$  is the space harmonics frequency of the ALIM in terms of Hz.

$$f_r = \frac{p}{z} (f_{sh} - k f_o) \quad (6.7)$$

At no load,  $f_r$  becomes equal to  $f_o$ . The no load space harmonic frequency  $f_{sh0}$  can be obtained by rearranging (6.7) to get (6.8). The slip for  $k^{\text{th}}$  harmonics of the forward and

backward rotating time harmonics is presented in terms of electrical synchronous speed and rotor speed as in (6.9)

$$f_{sh0} = \left( \frac{z}{P} - k \right) f_o \quad (6.8)$$

$$s_k = \frac{k\omega_s \pm \omega_r}{k\omega_s} \quad (6.9)$$

The harmonic slip frequency is in terms of the time harmonics. Adding up equation (6.6) - (6.9) the following expression (6.10) can be derived which give the window for space harmonics as well as time harmonics tracking.

$$f_{sh} = f_{sh0} - \frac{z}{p} \left( \frac{1}{s_k} - 1 \right) f_r \quad (6.10)$$

### C. Control Scheme for Fault Detection and Flux Estimation

Using the machine model as explained in Section 6.2 A, a stator flux oriented vector control is designed. Since the motive of this chapter is to detect the stator fault, it calls for a vector control using stator flux for higher accuracy in detection. For vector control, the natural decoupling comes when  $i_{ds}$  is aligned with  $\psi_r$  in case of rotor flux control [6]. But for stator flux control, in order to get  $i_{ds}$  aligned with  $\psi_s$  and torque component along  $i_{qs}$ , the coupling effect produced has to be substituted with a decoupling compensation method. For decoupling control, the stator flux reference control model is based on aligning the stator flux linkage with the synchronously rotating d-axis thereby leading to  $\psi_{ds} = \psi_s$  and  $\psi_{qs} = 0$ . Thus for decoupling control the q-axis stator flux equation can be presented as in (6.11)

$$\left( 1 + \frac{D}{L_s R_r} \right) i_{ds-qs} - \frac{D}{L_s R_r} \cdot \omega_{sl} \cdot i_{ds-qs} = 0 \quad (6.11)$$

where  $\omega_{sl}$  can be expressed as (6.12)



$$\omega_{sl} = \frac{\left(1 + \frac{D}{L_s L_r}\right) \cdot i_{qs} \cdot R_r}{\psi_{ds} \cdot L_r - D \cdot i_{ds}} \quad (6.12)$$

Combining equations (6.11) and (6.12) the decoupling current can be obtained. This decoupling current is a function of  $\psi_{ds}$ ,  $i_{qs}$ , and  $i_{ds}$  as shown in (6.13)

$$i_{ds\_qs} = \frac{D \cdot i_{qs}}{\psi_{ds} \cdot L_r - D \cdot i_{ds}} \quad (6.13)$$

Since  $\psi_{qs}=0$ , the torque component from (6.14) can be represented as

$$T_e = \frac{3}{2} \frac{P}{2} \cdot \psi_{ds} \cdot i_{qs} \quad (6.14)$$

This stator flux control with the decoupling method is implemented in the block of improved flux observer as indicated in the control schematic as in Fig. 6.2. This control needs accurate calculation of  $i_{ds\_qs}$  which is directly related to machine parameters especially stator resistance. Any fault in the stator winding, no matter how small it is, will affect the accuracy of estimation in the flux observer.

The proposed control drive was programmed to a control board as shown in Fig. 6.3. The detection block takes back EMF of search coil and current and voltage from inverter supply as input, in order to work as an online data sampling module. This block not only detects the variation in normal functioning of the ALIM by the change in current but also has a Fast Fourier Transformation (FFT) module which does spectral analysis to detect the fault via the change in space and time harmonics pattern from normal functioning condition. The harmonics calculation has been presented in Section 6.3 C. The FFT module in the drive uses 1024 sampling points in one period. FFT can be applied upto 512<sup>th</sup> harmonics but only till 37<sup>th</sup> harmonic has been taken for measurable accuracy. This estimated flux reference block takes the input from the detection block in order to find the best value for the flux to control the ALIM. The calculation behind this intelligent prediction block is presented in the next section.

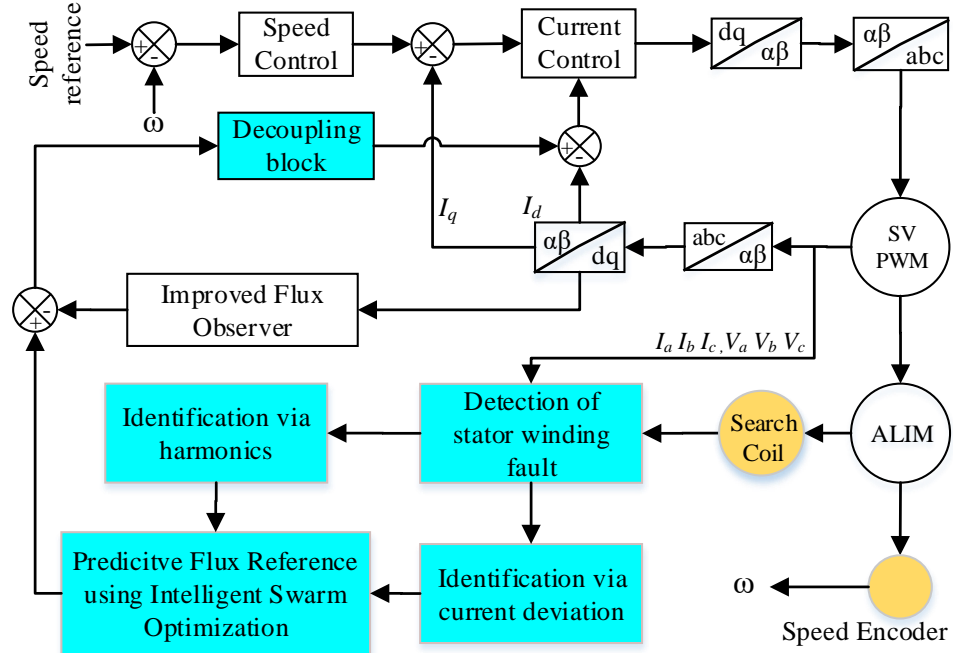


Fig. 6.2. Schematic flow for stator inter-turn fault detection with stator-flux oriented control.

#### D. Test Bench for Fault Detection and Proposed Control Implementation

Two 7.5 hp, laboratory totally enclosed fan-cooled aluminium-rotor induction motors were used for the experimental setup. One is the healthy motor, which was used to find parameters of the motor as shown in Table 2.2 using load test, no-load test and DC test and to understand the healthy motoring conditions. While the other ALIM with identical parameters, is the faulty motor with a small stator inter-turn fault. Both the motors were operated at varying speeds from 0 to rated speed of 1,750 rpm. The faulty motor was not run at rated speed for a longer time in order to protect the motor from complete breakdown due to winding short-circuit. Both the motors are driven by an inverter-fed, digital signal processor based drive system.

A high performance 32-bit microcontroller capable of real-time control is used to implement the designed control. The complete setup with the control board running the proposed control strategy is shown in Fig. 6.3. The proposed drive system is a stator flux-

oriented control using current, voltage, flux and speed as feedback. The stator inter-turn fault is detected in control logic by measuring the flux using flux sensor and time and space harmonic tracking as explained in Section 6.3 B, which is running continuously along with the stator-flux oriented vector control with the decoupling effect.

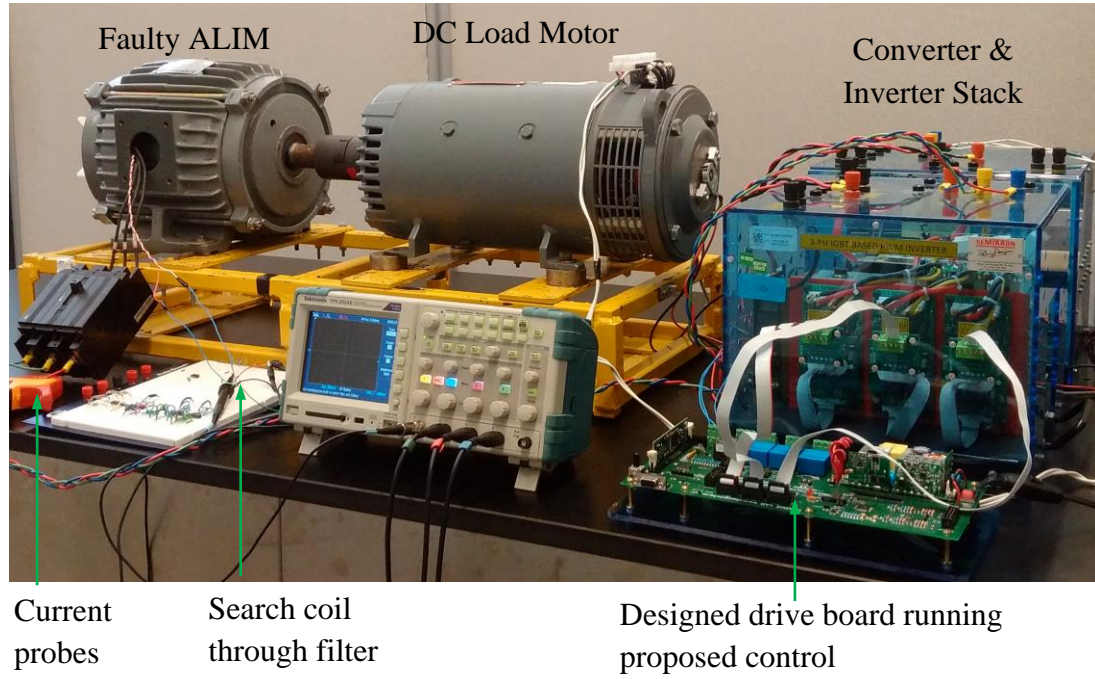


Fig. 6.3. Set up for experimental validation of the proposed fault tolerant control drive.

#### 6.4. Intelligent Swarm Optimization for Reference Flux Calculation

Since inter-turn stator fault affects the parameters of the ALIM, it is important to track the change in parameters of the stator winding. The fault causes a change in the stator resistance. To estimate flux linkage of the induction motor the two-axis modeling as explained in Section III is applied to the ALIM. In particle swarm optimization, particles are considered to be potential results which move in the problem space following the perfect particle with a velocity  $V$ . The particles keep track of their co-ordinate system. The best particle co-ordinates are saved as  $P_{best}$  [8]. Along with  $P_{best}$  the neighbour particles are also kept track of. In this way the best particle solution can be achieved. When a particle takes all the population as its topological neighbors, the best value is a global best  $G_{best}$ .

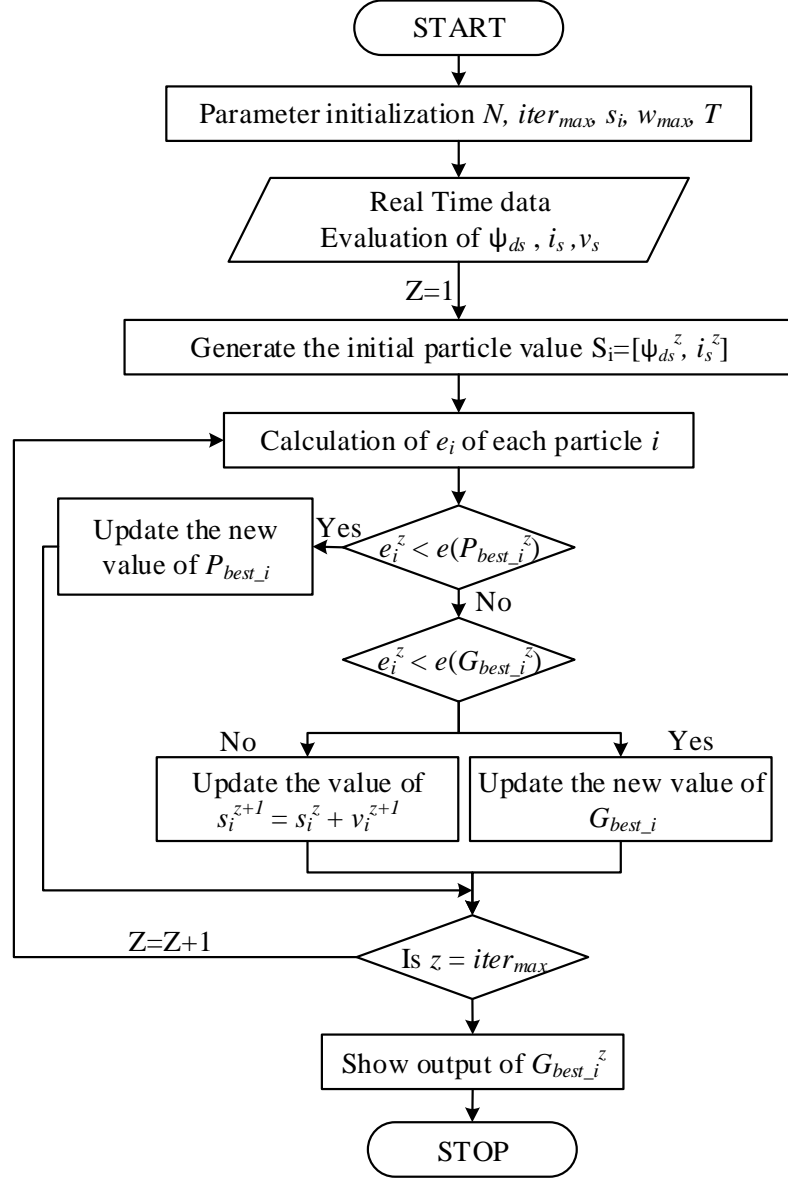


Fig. 6.4. Flowchart presenting the how the proposed algorithm uses to the best value of flux in order to predict accurately.

The velocity of particle  $i$  at iteration  $z$ ,  $V_i^z$  can be expressed as in

$$V_i^{z+1} = W V_i^z + c_1 \times rand_1 \times (P_{best\_i} - s_i^z) + c_2 \times rand_2 \times (G_{best\_i} - s_i^z) \quad (6.15)$$

where,  $C_j$  is the weighting co-efficient,  $rand_j$  is a random number between 0 and 1,  $s_i^z$  is the current position of the particle  $i$  at iteration  $z$ , and is equal to vector  $[\psi_{ds}^z, i_s^z]$  in this

condition.  $C_1$  and  $C_2$  normally are two positive constants, called the cognitive and social parameters respectively. In this study, these parameters are considered to be dynamic in nature with initial and final values for  $C_1$  as 1.0 and 3.0 respectively while 3.0 and 1.5 respectively for  $C_2$ . The weighing function  $w$  is defined as (6.16)

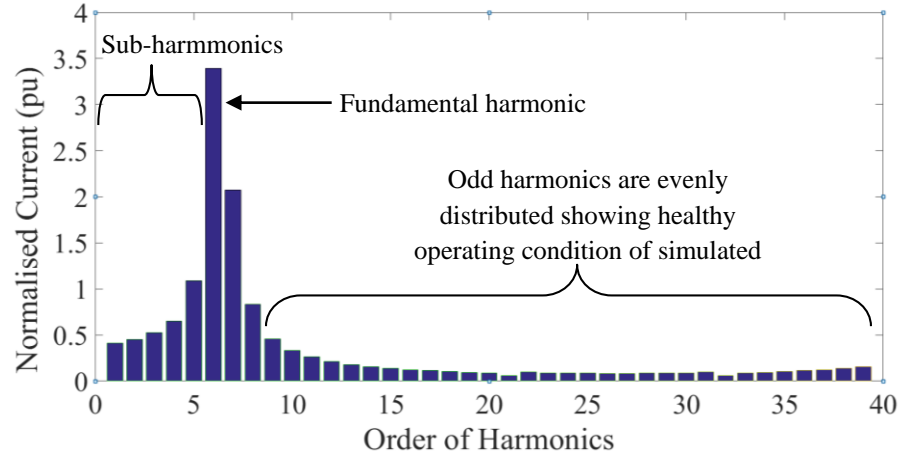
$$W = W_{\max} + \left[ \frac{W_{\max} - W_{\min}}{iter_{\max}} \times iter \right] \quad (6.16)$$

$$obj(\psi_{ds}, i_s) = Min \left[ \begin{array}{l} Error(\psi_{ds\_measured}, \psi_{ds\_PSO}) \\ + Error(i_{s\_measured}, i_{s\_calculated}) \end{array} \right] \quad (6.17)$$

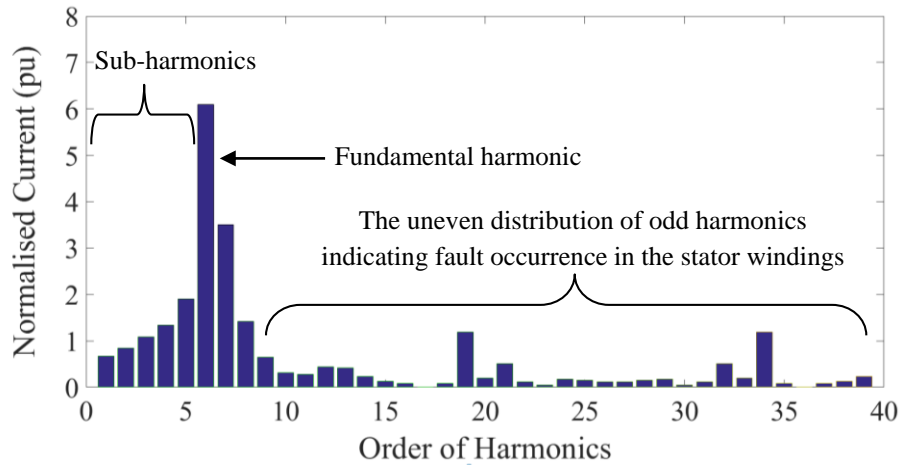
The objective function of the optimizer is formulated in two parts. The first part is to minimize the error between the measured flux from the search coil and the flux obtained from the real- time machine model. Second part of the objective function is to satisfy the error occurrence in the stator current during faulty condition as a deviation from stator current during healthy machine operation ( $i_{s\_faulty}$ ,  $i_{s\_healthy}$ ). Therefore the final objective function can be expressed as in (6.17). The developed model-specific intelligent particle swarm optimization can be expressed using the flowchart shown in Fig. 6.4.

### 6.5. Investigation of ALIM with Stator Winding Fault Using FEM

Geometrical and electrical parameters of an existing in house three-phase aluminum rotor bar IM is taken as mentioned in Table 2.2 to simulate IM using time stepping finite element analysis. Influence of spatial and time harmonics on distribution of the flux density in the air-gap is investigated for three case studies: 1) healthy; 2) short circuit fault; and 3) complete breakdown in stator winding. The magnetic flux density distribution in the ALIM varies due to the difference in per phase equivalent circuit parameter because of variation in the length of winding in stator resistance calculation and hence the current is slightly higher in case of inter-turn stator fault. On the other hand, harmonic magnitude is increasing due to rise in space and time harmonics. Accordingly phase current acts as a major affected characteristic of faulty condition is provided for both healthy conditions along with spectrum analysis of phase current.



(a)



(b)

Fig. 6.5. Fast Fourier Transformation of the current flowing through the stator windings for ALIM with (a) No winding fault. (b) Small stator winding fault.

From Fig 6.5(a) it can be clearly seen that the odd harmonics of the ALIM are at the same per unit value unlike in Fig 6.5(b) which clearly demarcates the uneven distribution of the odd harmonics and even increase in the value of the fundamental harmonics. The inconsistency in flux lines of faulty ALIM due to uneven distribution of flux in the magnetic air-gap is represented in a simulated induction machine and compared with the healthy motor. Fig. 6.6(a) presents the flux line distribution in a healthy ALIM. It can be seen that the flow of the flux lines is even in each phase of the motor. When a small inter-turn stator winding fault is introduced in the IM, the flux lines decrease. On the other hand

harmonic magnitude resulting in increase in flux lines in the neighboring phases which is shown in Fig. 6.6(b). In this case the ALIM rotates with the rotor moving more towards the direction of higher flux density creating an eccentricity in the air-gap flux. This is the reason of the beginning of the eccentricity in the motor. This FEM helps in getting a clear understanding of what the fault in the motor could lead to if not taken care of.

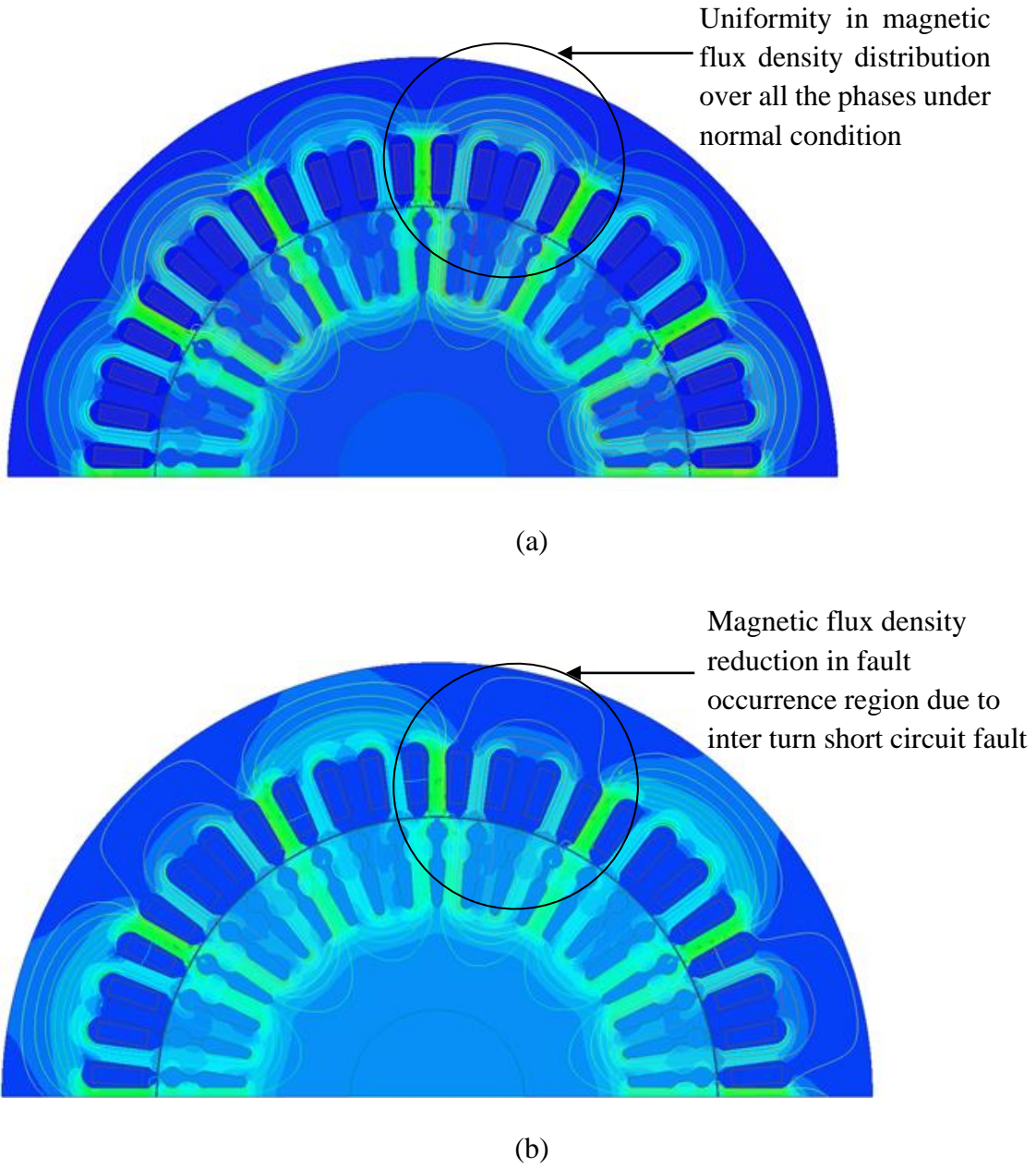


Fig. 6.6. Study of magnetic flux distribution for ALIM. (a) Normal operating condition. (b) With small stator winding fault on phase A.



## 6.6. Numerical and Experimental Investigation of Proposed Control

The fault tolerant flux predictive control drive was tested on the 7.5 hp ALIM. It was tested under various loads and speeds to emulate an EV drive cycle. The results presented are at rated speed. Fig 6.7(a) shows the distorted current waveform on the Phase A of the motor due to slight stator winding fault. Several tests were performed at the same operating conditions, and it was found that the difference in the RMS value of the current between phase A and C is 8.5 A and between phases B and C is 2.0 A. After running the faulty ALIM with the control the current waveform obtained is shown in Fig. 6.7(b). As indicated all the three phases of the motor are balanced with a maximum deviation between two phases as 0.8 A while minimum was 10 mA. As mentioned before not just current was used for detection of the fault. The results from the installed search coil on the stator of the faulty ALIM gave a better idea considering it shows the real flux value of the rotating motor. Figs. 6.8(a) and (b) shows how the back EMF of the motor varies before and after implementation of the predictive flux control. When the motor has a very small stator winding fault, flux generated gets deformed. But due to the harmonics it cannot be clearly estimated the extent of distortion created. By adding a filter, the sub-harmonics are filtered out leaving behind only the fundamental component. For proper understanding, a comparative waveform graph presenting the distortion in flux waveform and corrected waveform as obtained from the experimental results is shown in Fig. 6.9. The average value of the magnetic flux reference was about 0.6 T.

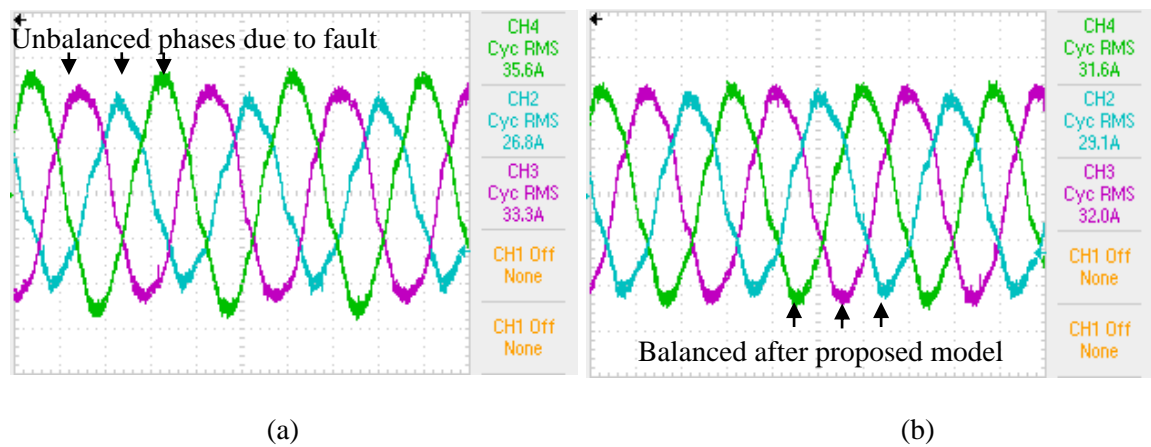


Fig. 6.7. Current waveform for ALIM (a) with incipient stator winding fault (b) after the proposed control has been implemented.



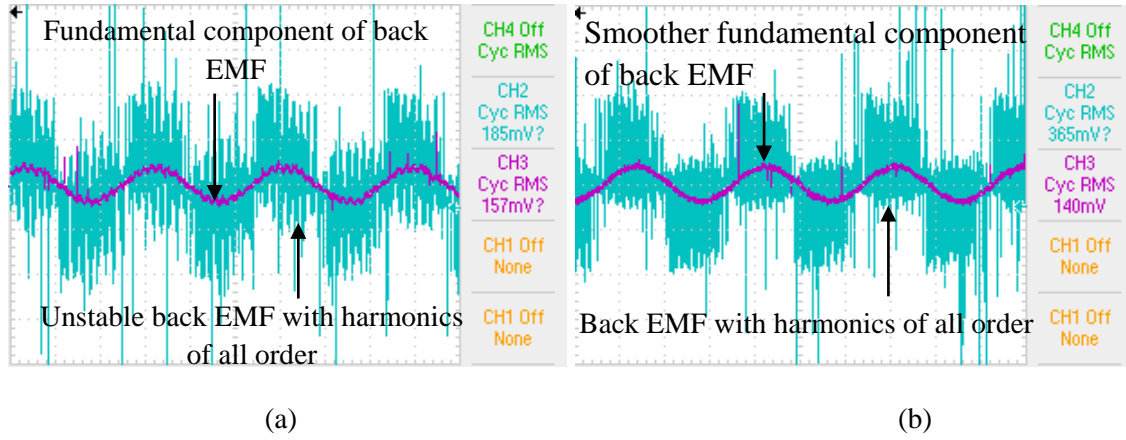


Fig. 6.8. The back EMF voltage as measured using the search coil. (a) With stator inter-turn fault (b) After proposed control has been implemented.

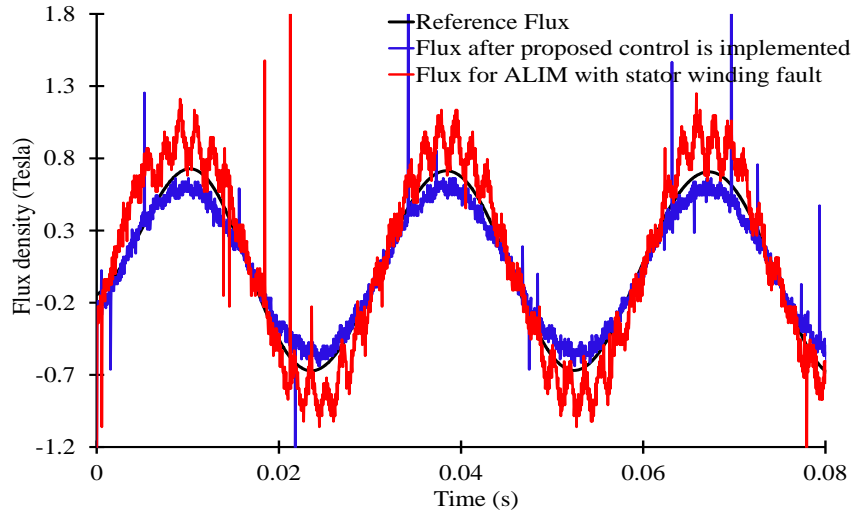


Fig. 6.9. Comparative experimental flux waveform of flux with stator-inter-turn fault (red), predicted reference flux (black), modified flux after the control (blue) to present how the flux waveform is modified.

## 6.7. Conclusion

This chapter proposed a new method to control a faulty traction motor using intelligent flux predictive method. This method can detect a fault occurring due to stator winding short circuit or unbalance in inverter supply, at an incipient stage, thereby preventing the complete breakdown of the EV motor. The eccentricity in behavior of the motor due to any fault leads to asymmetric distribution of the magnetic flux produced thereby causing an unbalanced magnetic pull. The predictive stator flux control drive was first simulated in a

technical computer programming language used for data analysis and finite element analysis of the ALIM was done before the implementation. The results obtained were then compared with experimental results validating the proposed method. This process of estimation of reference flux can be tested using machine learning algorithms for faster and more robust fault-tolerant vector control which is done in the next chapter.

## 6.8. References

- [1] B. K. Bose, "Modern Power Electronics and AC Drives," *Prentice Hall PTR*, 2002.
- [2] D. G. Dorrell and A. Salah, "Detection of Rotor Eccentricity in Wound Rotor Induction Machines Using Pole-Specific Search Coils," *IEEE Transactions on Magnetics*, vol. 51, no. 11, pp. 1-4, Nov. 2015.
- [3] A. Grosz, E. Paperno, S. Amrusi and B. Zadov, "A Three-Axial Search Coil Magnetometer Optimized for Small Size, Low Power, and Low Frequencies," *IEEE Sensors Journal*, vol. 11, no. 4, pp. 1088-1094, April 2011.
- [4] C. Yang *et al.*, "Screening of False Induction Motor Fault Alarms Produced by Axial Air Ducts Based on the Space-Harmonic-Induced Current Components," in *IEEE Transactions on Industrial Electronics*, vol. 62, no. 3, pp. 1803-1813, March 2015.
- [5] K. Saad and G. Mirzaeva, "Space-Time Representation of the Main Air Gap Flux of a Three Phase Squirrel Cage Induction Motor and its Application to Detect Eccentricity," in the Proc. of *IEEE International Electric Machines & Drives Conference (IEMDC)*, pp. 1466-1472, Coeur d'Alene, ID, 2015.
- [6] G. Liu, J. Lu, and H. Zhang, "A Stator Flux-oriented Decoupling Control Scheme for Induction Motor," *IEEE International Conference on Control and Automation*, pp. 1701-1704, Guangzhou, 2007.
- [7] R. J. Wai, K. L. Chuang, and J. D. Lee, "On-Line Supervisory Control Design for Maglev Transportation System via Total Sliding-Mode Approach and Particle Swarm Optimization," *IEEE Transactions on Automatic Control*, vol. 55, no. 7, pp. 1544-1559, July 2010.

## CHAPTER 7

# INTRODUCTION TO MACHINE LEARNING AND ITS APPLICATION FOR FLUX REFERENCE PREDICTION

### 7.1. Introduction

In this chapter, the harmonics compensation block based flux reference control for traction motor has been improved by introducing a novel DNN predictive magnetic flux reference method for control as shown in Fig. 7.1 in addition to the novel harmonic compensation block. This allows continuous operation of the faulty traction motor to a certain extent even after the occurrence of incipient stator winding fault. This shall prevent passengers from getting stranded in the middle of the highway or any such location where immediate actions cannot be taken. The proposed flux predictive control consists of three major parts. First, the detection block of unbalanced magnetic pull (UMP) in the machine which uses current, voltage as well as magnetic flux as a feedback to the system. Secondly, an on-line harmonics compensation block is designed which makes the control a more fault-tolerant one. Finally, a deep neural network optimization method has been introduced as a feedforward block in order to predict flux with higher accuracy.

### 7.2. Modelling of IM with UMP for DNN

The 7.5 hp aluminum rotor IM which has a slight inter-turn fault has been used in order to implement the proposed method. Several conducted experiments have shown that the motor is faulty. It can be clearly seen in Figs. 7.1(a) and (b), the imbalance in current feedback of the IM with the phase A being more in magnitude than phases B and C.

#### A. State Space Modelling of Unbalanced IM

The faulty ALIM has been modelled with consideration of an additional circuit  $f$ . The stator to stator and stator to rotor mutual inductances will have additional terms with suffix  $f$  to incorporate the effect of shorted windings. Taking into effect all the changes in the motor due to faulty condition can be presented in a state space model as (7.1). It has been

assumed here that the stator fault has occurred in phase A of the machine.

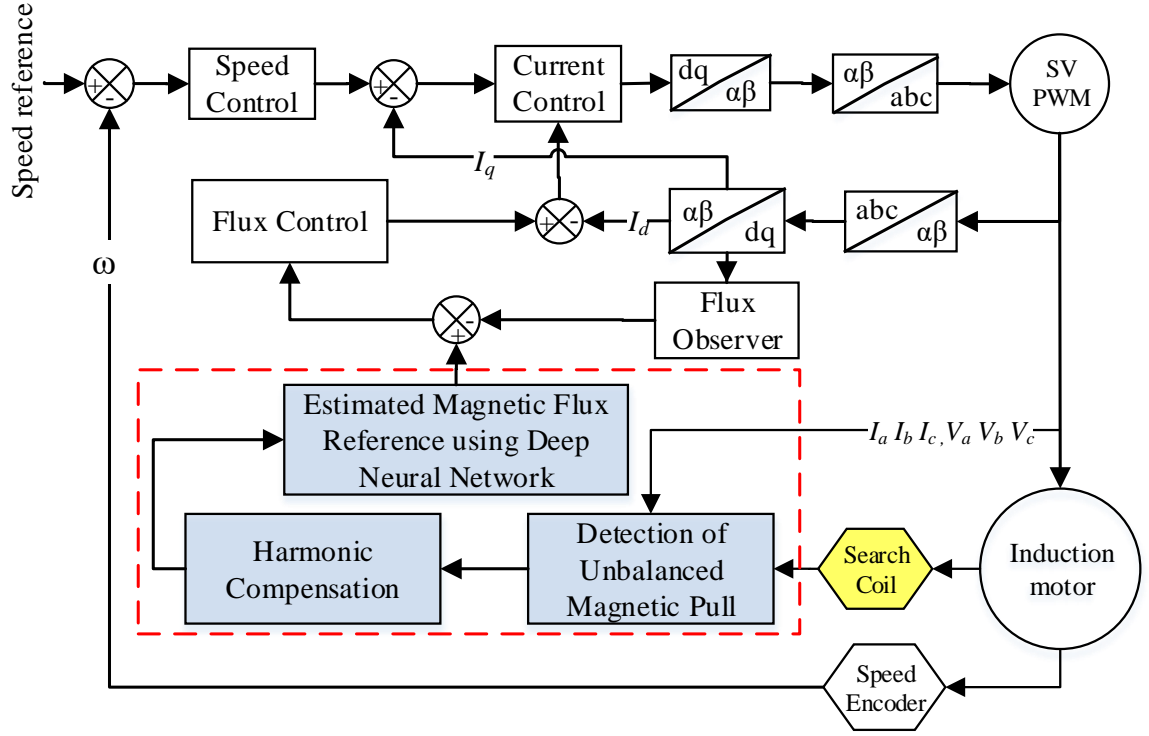


Fig. 7.1. Schematic flow of novel DNN based harmonic compensation method.

$$\dot{x} = -ABx + Bu \quad (7.1)$$

where

$$x = [i_{fs} \quad i_{as} \quad i_{bs} \quad i_r \quad \omega \quad \theta]^t \quad (7.2)$$

$$u = \left[ 0 \quad v_{ab} \quad v_{bc} \quad 0 \dots 0 \quad \frac{(T_m - T_l)}{J} \quad 0 \right]^t \quad (7.3)$$

$$A = \begin{bmatrix} R_{fs} & 0 & 0 & \omega \frac{\partial L_{fr}}{\partial \theta} & 0 & 0 \\ 0 & R_{as} & -R_{bs} & \omega \frac{\partial (L_{ar} - L_{br})}{\partial \theta} & 0 & 0 \\ 0 & R_{cs} & (R_{bs} + R_{cs}) & \omega \frac{\partial (L_{br} - L_{cr})}{\partial \theta} & 0 & 0 \\ \omega \frac{\partial L_{rf}}{\partial \theta} & \omega \frac{\partial (L_{ra} - L_{rc})}{\partial \theta} & \omega \frac{\partial (L_{rb} - L_{rc})}{\partial \theta} & R_r & 0 & 0 \\ 0 & 0 & 0 & 0 & 0 & 0 \\ 0 & 0 & 0 & 0 & -1 & 0 \end{bmatrix} \quad (7.4)$$

$$B = \begin{bmatrix} L_{ff} & (L_{fa} - L_{fc}) & (L_{fb} - L_{fc}) & L_{fr} & 0 & 0 \\ (L_{af} - L_{bf}) & \begin{pmatrix} L_{aa} - L_{ac} \\ -L_{ba} + L_{bc} \end{pmatrix} & \begin{pmatrix} L_{ab} - L_{ac} \\ -L_{bb} + L_{bc} \end{pmatrix} & (L_{ar} - L_{br}) & 0 & 0 \\ (L_{bf} - L_{cf}) & \begin{pmatrix} L_{ba} - L_{bc} \\ -L_{ca} + L_{cc} \end{pmatrix} & \begin{pmatrix} L_{bb} - L_{bc} \\ -L_{cb} + L_{cc} \end{pmatrix} & (L_{br} - L_{cr}) & 0 & 0 \\ L_{rf} & (L_{ra} - L_{rc}) & (L_{rb} - L_{rc}) & L_r & 0 & 0 \\ 0 & 0 & 0 & 0 & 1 & 0 \\ 0 & 0 & 0 & 0 & 0 & 1 \end{bmatrix} \quad (7.5)$$

As defined in the matrices, the variables with suffix  $f$  are used to describe the faulty parameters of the motor.  $R_{fs}$  is added resistance in the motor due to stator inter-turn fault whereas  $L_{af}$ ,  $L_{bf}$ , and  $L_{cf}$  are the effect of mutual inductance between the faulty inductance and the 3-phases  $\omega$  is defined as the electrical speed of the motor. The current flowing through the faulty arm is written as  $i_{fs}$ . The resistance in phase A,  $R_{as}$  will not be equal to  $R_{bs}$  or  $R_{cs}$ . So will the inductance of phase A different from that of the other 2 phases [1].

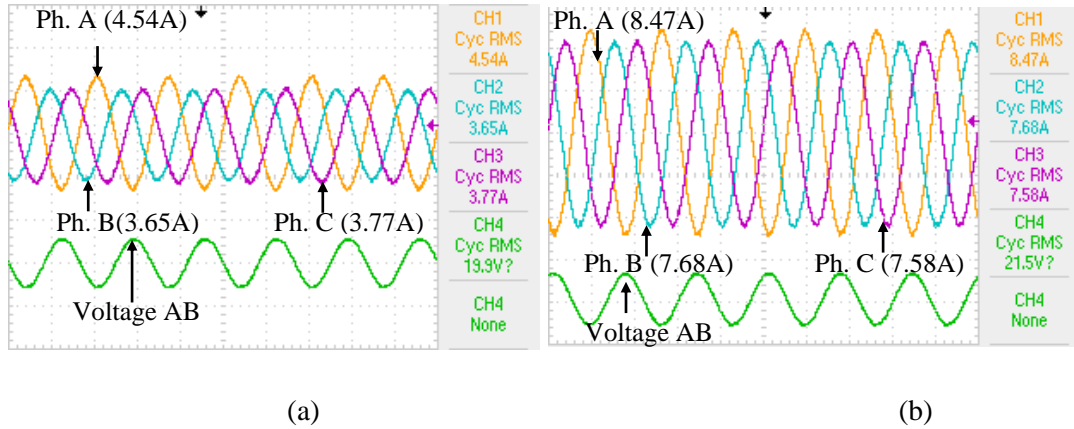


Fig. 7.2. The current and voltage waveforms of faulty IM at (a) Rated load. (b) Rated speed.

### B. Space and Time Harmonic Modelling for Faulty IM

As explained in Section 5.4, space harmonics arise from radial forces due to the magnetic flux density in the air gap. The variation of the magnetic flux density is due to varied influences of non-sinusoidal MMF and variation in magnetic permeance of air gap due to structural design of the IM [2].

The sinusoidally distributed air-gap MMF which is expressed as (7.6) where the harmonic components of frequencies is  $Z/P(\omega_r \pm \omega_o)$ ,  $P$  is pole pairs and  $Z$  is rotor slots rotating at  $\omega_r$  and  $\psi_{r1}$  and  $\psi_{r2}$  are phase angles.

$$B(\theta, t) = B_1 \cos(\omega_o t - P\theta) + B_{r1} \cos\left[\left(\frac{Z}{P} \omega_r t + \omega_o t\right) - (P + Z)\theta + \psi_{r1}\right] \\ + B_{r2} \cos\left[\left(\frac{Z}{P} \omega_r t - \omega_o t\right) - (P - Z)\theta + \psi_{r2}\right] \quad (7.6)$$

MMF in the stator windings induced by flux density leads to production of stator current harmonics. Spatial asymmetries, unbalanced inverter supply and magnetic saturation leads to distortion in space harmonics and thereby the air-gap MMF [3].

When the voltage supply to motor is distorted there is increase in time harmonics developed from the inverter side of the drive system. The voltage and current can be expressed as (7.7) and (7.8) respectively.

$$v = V_m \sum_{k=1}^{\infty} A_{vk} \cos(k\omega t + \phi_{vk}) \quad (7.7)$$

$$i = I_m \sum_{k=1}^{\infty} \frac{A_{vk}}{|Z_k|} \cos(k\omega t + \phi_{vk} + \theta_k) \quad (7.8)$$

Fourier series of magnetic flux density waveform as shown in (7.9) is used for designing the harmonic compensation block where  $B_p$ ,  $B_\mu$  represent time harmonics and  $B_\lambda$ ,  $B_{\lambda e}$  represent slot harmonics.

$$B(x, t) = \sum_v B_p v \cos(px - v\omega_v t - \psi_v) + \sum_\mu B_\mu v \cos(\mu p x - v\omega_\mu t - \psi_\mu) \\ + \sum_\lambda B_\lambda \cos(\lambda p x - \omega_\lambda t - \psi_\lambda) + \sum_{\lambda e} B_{\lambda e} \cos(\lambda_e p x - \omega_{\lambda e} t - \psi_{\lambda e}) \quad (7.9)$$

### C. Harmonic Search-Interval Tracking Window

To design the harmonic tracking/search-interval window, no load space harmonic frequency  $f_{sh0}$  and rotor frequency  $f_r$  is used to define  $\Delta f_{sh}$  which tracks space harmonics estimated as

$$f_{sh} = f_{sh0} - \frac{Z}{P} \left( \frac{1}{s_k} - 1 \right) f_r \quad (7.10)$$

Multiples of fundamental frequency harmonics of the inverter supply  $k.f_o$  is filtered out leading to define  $\Delta f_{sh}$  as in (7.11). For practical accuracy, harmonics of inverter supply was taken till the 37th harmonics.

$$\Delta f_{sh} = f_o (1 - \omega_{syn}) \quad (7.11)$$

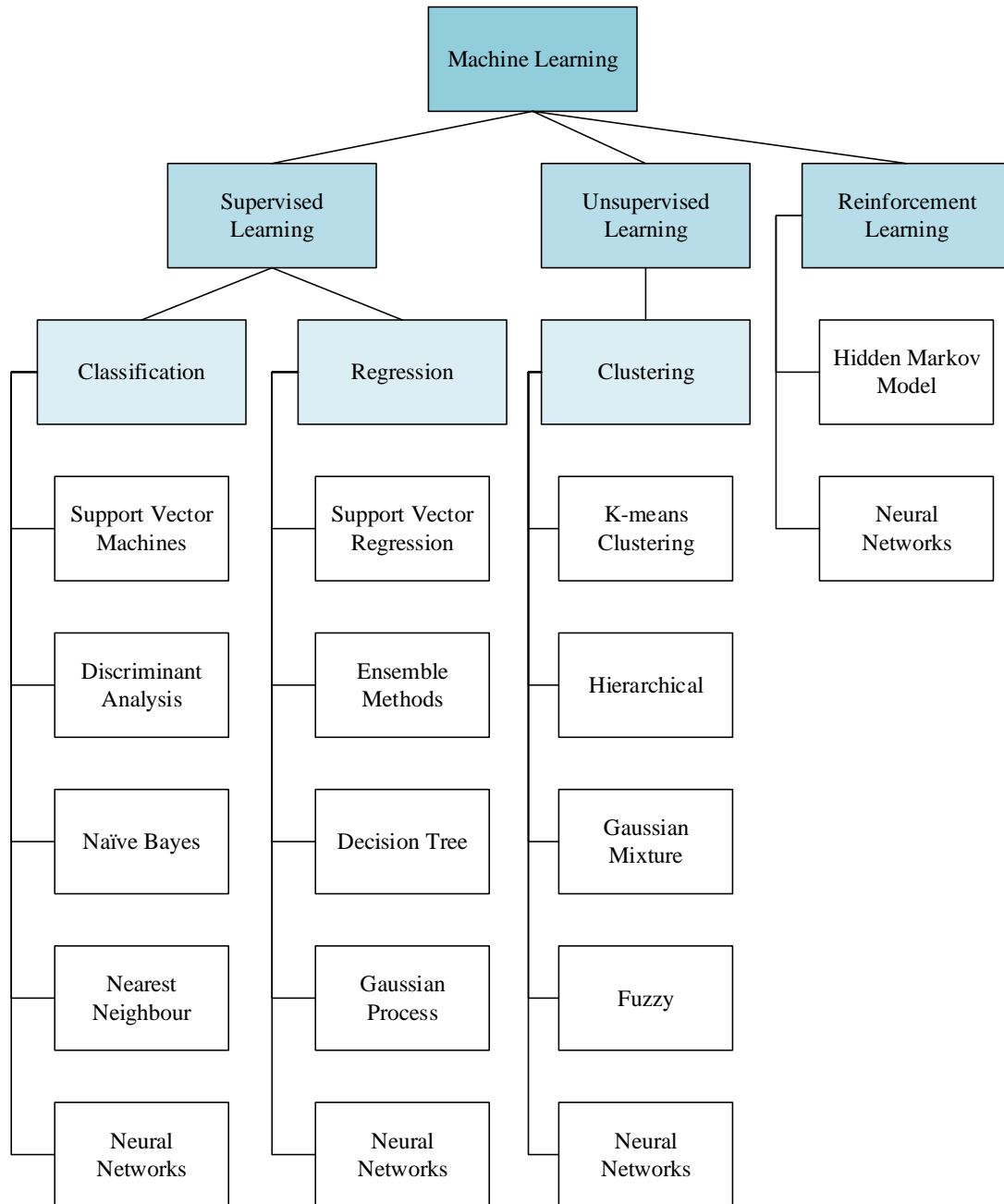


Fig. 7.3. Various types of machine learning techniques.

### 7.3. Machine Learning for Flux Prediction

The definition of machine learning in 1959 by Arthur Samuel is the field of study that gives computers the ability to learn without being explicitly programmed. Samuel wrote a checkers playing program, to learn to play the game, which played huge number of games and learnt over a period of time and became better than a human player. A more recent

definition by Tom Mitchell, university professor at Carnegie Mellon, has proven more useful in terms of engineering, as a computer program is said to learn from experience  $E$ , with respect to some task  $T$ , and some performance measure  $P$ , if its performance on  $T$  as measured by  $P$  improves with experience  $E$ . There are several types of machine learning as shown in Fig. 7.3. It can be broadly classified as supervised, unsupervised learning and reinforcement learning [4]. In supervised learning, the machine is taught to learn explicitly using data which has clearly defined output. It has a feedback loop in order to make it learn even better. Usually any kind of classification or regression problems are solved using this. In unsupervised learning, the machine learns the data by identifying patterns and structures. The output result of this method is usually qualitative or indirect and cannot predict to a very specific output. In reinforcement learning, which is very close to human brain learning, is a reward based machine learning method using positive or negative reinforcement as learning to act to certain environment.

For the purpose of fault diagnosis via prediction of magnetic flux, a supervised learning method is needed for proper estimation of flux values which is used as the reference value for control [5]. To create such an autonomous system capable of deep learning and developing preventive actions from the data captured over a period of time, a neural network based magnetic flux estimator is of paramount importance. Artificial neural networks (ANN) are the most versatile when it comes to machine learning since they can be used for supervised, unsupervised as well as reinforcement learning. ANN can be used to identify and control the nonlinear dynamic systems because they can approximate a wide range of nonlinear functions to any desired degree of accuracy. Moreover, they can be implemented in parallel and therefore, shorter computational time can be achieved. In addition, they have immunity to harmonic ripples and have fault-tolerant capabilities

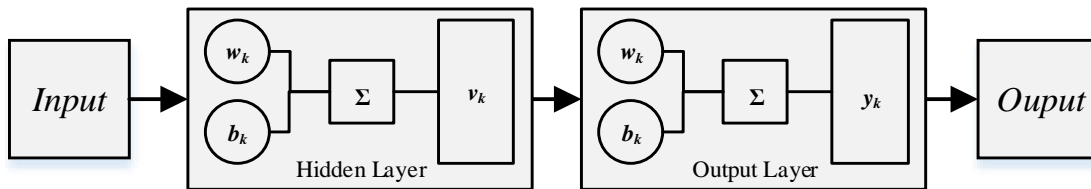


Fig. 7.4. Design of neural network used in application of harmonic compensation.

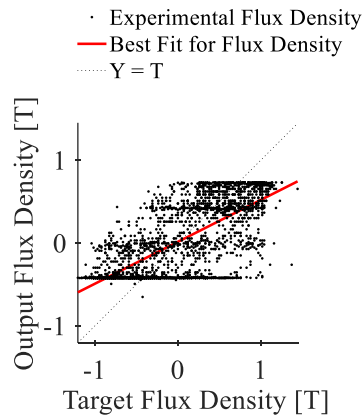


The development of neural network using equations (7.12) and (7.13) has been explained in Section 3.7 A. DNN has the ability to be trained in order to optimize the values which it gathers from deep learning method. Then the trained results are validated and tested before producing the best fitted value.

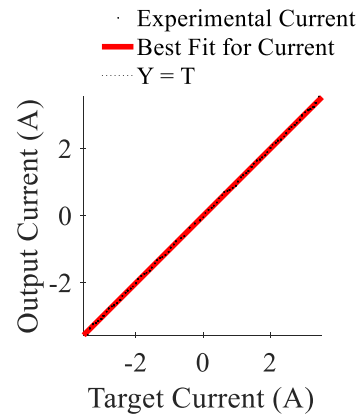
$$v_k = \sum_{j=1}^m w_{kj} \cdot x_j \quad (7.12)$$

$$y_k = \phi(v_k + b_k) \quad (7.13)$$

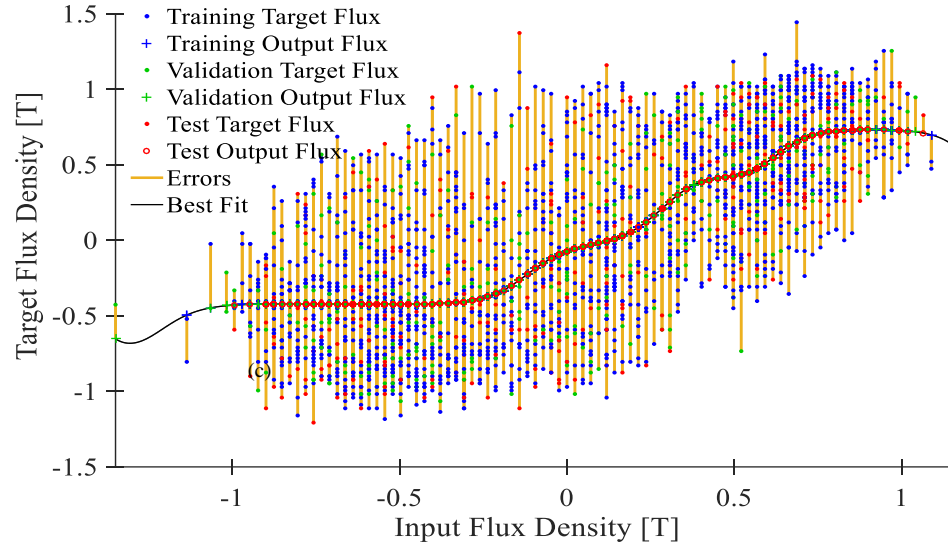
All the experimentally measured values of flux are fed into this deep neural network along with the model calculated values in order to get the best fitted values for flux density. Since a deep neural network has been used the number of hidden layers have been kept at 16 so as to enable higher accuracy with a bit more computational time. A single layer neural network can be used but in order to detect incipient stator fault via change in harmonics a deep neural network is used which differentiates from a single-hidden-layer neural networks by their depth; that is, the number of node layers through which data passes is a multistep process. In deep neural nets each layer of node trains on a discrete set of features based on previous layer. This leads to detect far more complexed indistinguishable harmonic changes as compared to general measurement. There is a trade off when compared to a single layer neural network with lesser computational time and much lesser in terms of accuracy in prediction of flux.



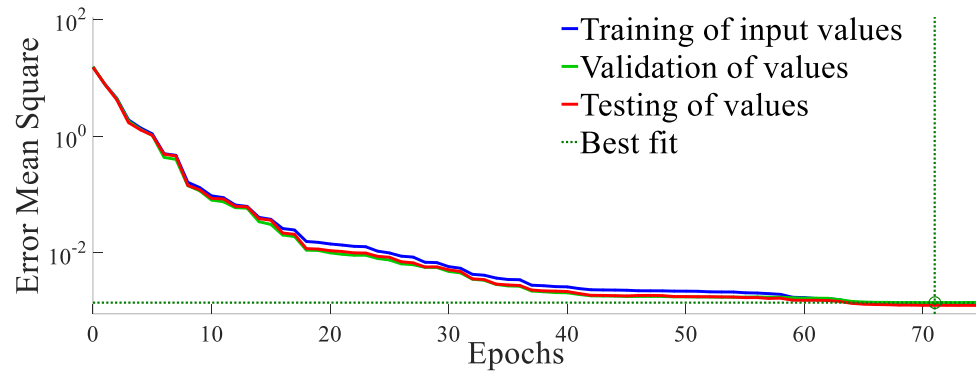
(a)



(b)



(c)



(d)

Fig. 7.5. DNN based prediction results. (a) Regression plot for output vs target flux density. (b) Regression plot for output vs target current. (c) Fitness plot for flux density. (d) Performance plot of DNN upto 77 epoch.

Figs. 7.5(a) and (b) show the regression plot for flux density and current for 27 Nm loading condition. The output and the target values are compared for getting the best fit. A sample of the fitness plot for input flux density with target values showing the amount of error and the results during the training, validation and testing period is shown in Fig. 7.5(c). Once the DNN is trained, a much lesser time is needed for establishing the best value. Fig. 7.5(d) represents the graph of mean squared error plotted against the number of epochs for all the 3 conditions where finally at epoch 71, the best fit value is reached thereby stopping the training of the neural network.

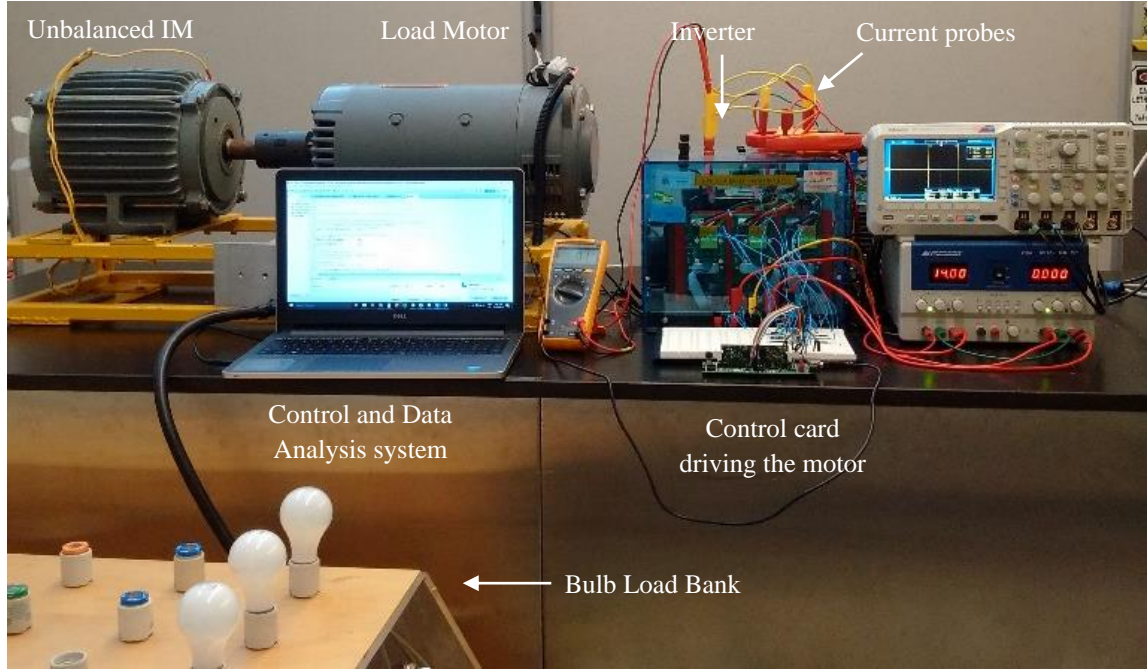


Fig. 7.6. Experimental setup to investigate the proposed DNN predictive method.

#### 7.4. *Experimental Validation of Proposed Novel DNN based Harmonic Compensation Block*

The implementation of proposed DNN based magnetic flux reference method has been explained in this section. The IM with stator inter-turn fault is connected to the DC machine as a load which is in-turn connected to a bulb load bank as shown in Fig. 7.6. The test was performed at different speeds and loading conditions. A high performance 32-bit microcontroller capable of real-time control is used to run the IM. This control board is capable of handling a large amount of data capture which is sent to the local computer for storing during each test. It triggers the proposed DNN predictive magnetic flux reference control running on the board and results are displayed on the computer.

For magnetic flux measurement, an observer search coil has been wound on the previously detected faulty phase of the ALIM as explained previously in Section 5.3. The current, voltage and flux values are measured and fed into the control board in order to design the vector control of IM. The measured flux is then analysed in order to detect any change in harmonics on spatial or time harmonics in order to find the fault in machine or inverter side. This analysis block is then passed through a compensation block in which

the harmonics are minimized in order to generate a better flux reference for operating the faulty IM. As previously suggested, a deep neural network block has been introduced in order to enable the flux required by the control to be predicted in a feedforward manner. This enables the system to be ready for any fault occurrence on motor or inverter side.

### 7.5. Investigation Using Finite Element Model

This section presents the dynamic model of ALIM using time stepping FEA. The model of a three- phase, 4 pole, 7.5 hp, with 200 V line to line voltage with detailed geometrical parameters as shown in Table 2.2 is analysed for both normal and inter-turn stator winding fault. Detailed analysis of radial and tangential components of magnetic flux density with a voltage excitation is performed for both balanced and unbalanced ALIM. Analysis shows that under fault condition magnetic flux lines are disturbed around the faulty phase winding and are calculated using (7.15) - (7.17) where  $A$ ,  $B$ ,  $V_s$ ,  $V_{ind}$  and  $l$  are the magnetic vector potential, magnetic flux density, induced and supply voltage, and stack length of IM respectively.  $\sigma$  and  $\mu$  are conductivity and permeability of material. Due to inter-turn stator winding fault, one phase resistance of the stator winding changes drastically. This leads to local saturation in adjacent stator slots of the other phases as well as rotor bars due to interaction of the stator and rotor MMFs. The electromagnetic torque is calculated as an average value over the whole air-gap surface defined as (7.18) where  $B_r$ ,  $B_\theta$ ,  $l_{ag}$  and  $s_{ag}$  are radial, tangential flux density, air-gap length and surface area of the air-gap and  $p$  is the number of pole pairs. Increase in local saturation effects the performance characteristics such as torque production [4].

$$V_s(t) = R_s i_s(t) + L_{end} \frac{di_s(t)}{dt} + V_{ind} \quad (7.15)$$

$$\frac{\partial}{\partial x} \frac{1}{\mu} \left( \frac{\partial A_z}{\partial x} \right) + \frac{\partial}{\partial y} \frac{1}{\mu} \left( \frac{\partial A_z}{\partial y} \right) = -\sigma \frac{V_s}{l} \quad (7.16)$$

$$\vec{B} = \left( \frac{\partial A_z}{\partial y} \right) \hat{x} + \left( -\frac{\partial A_z}{\partial x} \right) \hat{y} \quad (7.17)$$

$$T = \frac{l}{l_{ag} \mu_0} p \iint_{s_{ag}} r B_r B_\theta ds \quad (7.18)$$

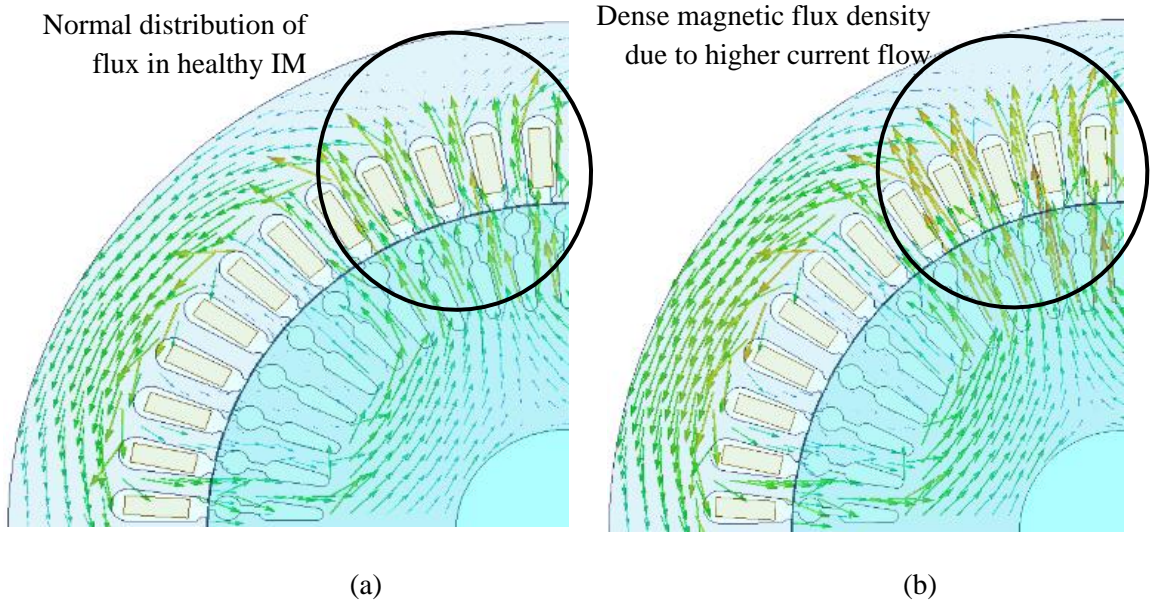


Fig. 7.7 . Magnetic flux vector distribution for IM in normal and unbalanced condition.

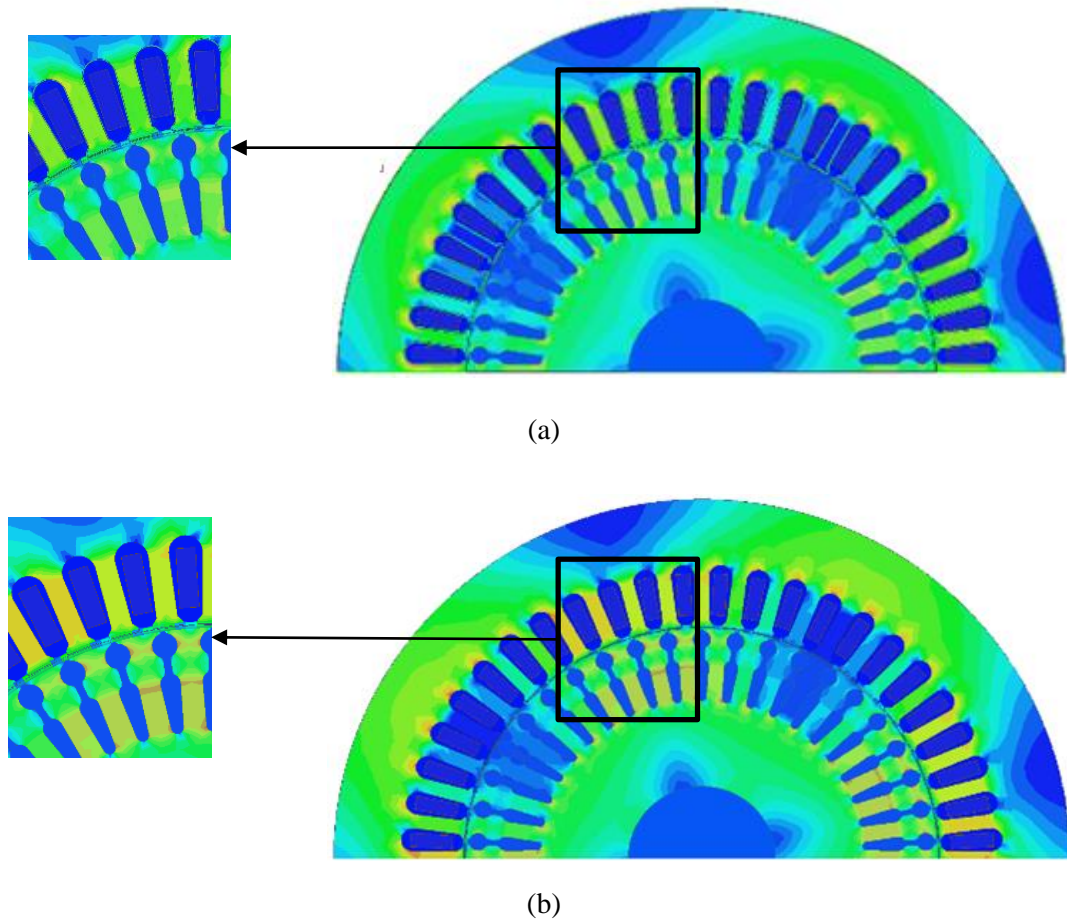
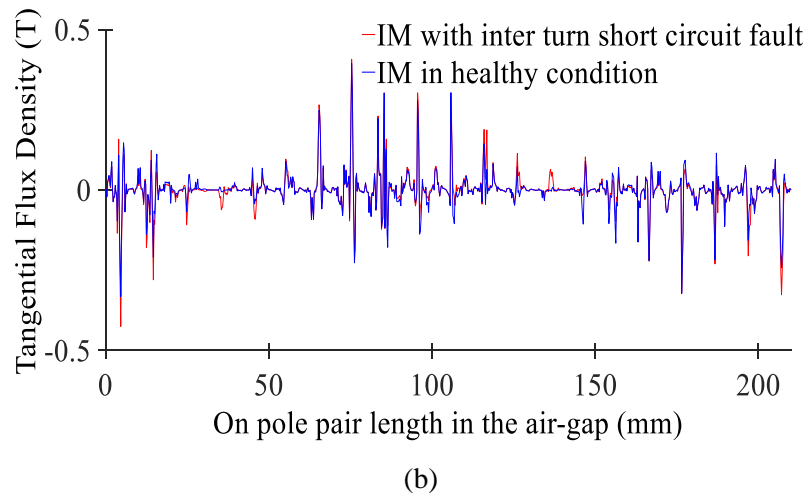
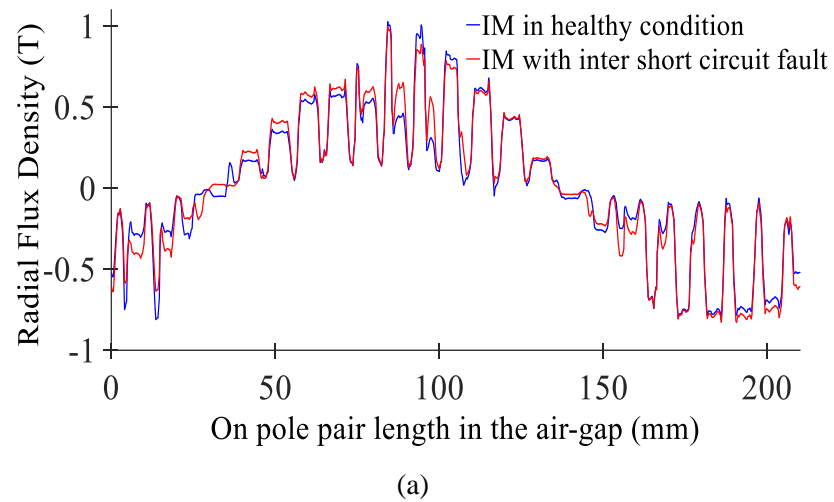
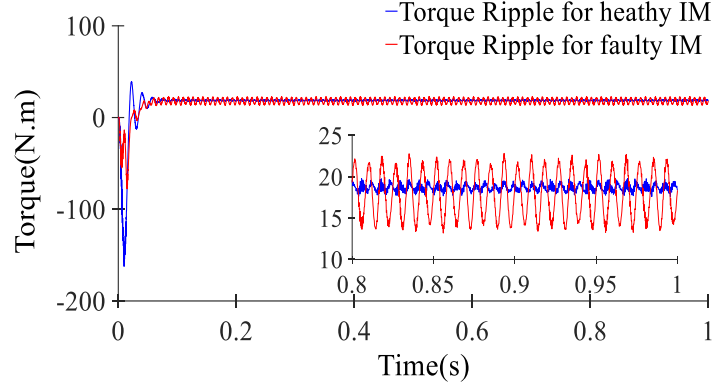


Fig. 7.8. Scalar and Vector distribution of magnetic flux density. (a) Healthy IM. (b) Faulty IM.



Fig. 7.8 shows condensed vectorial distribution of flux lines in the area of faulty phase. Figs. 7.9. (a) and (b) presents the magnetic flux distribution in a healthy and faulty ALIM. Electromagnetic analysis of both machines are observed to have a dissimilarity of flux distribution due to variation in circuit parameters. Unequal machine parameters in all 3-phase leads to flow of higher current which leads to saturation in corresponding phase. On the other hand, Figs. 7.10(a) and (b) presents increase in radial and tangential flux density harmonics for the one with fault. Furthermore, increase in electromagnetic torque fluctuation production due to excessive harmonics computed using (7.18) is shown in Fig. 7.10(c). The torque is calculated for both healthy and faulty conditions. It is observed that torque ripple in case of faulty condition increases significantly which leads to extreme vibration and noise in the machine.



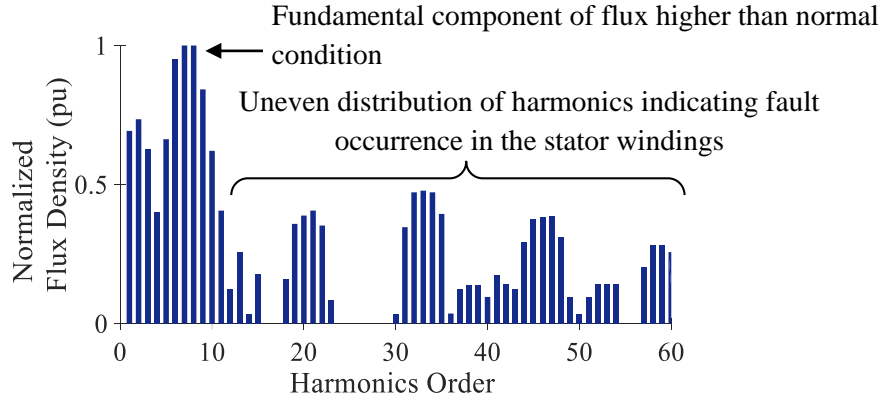


(c)

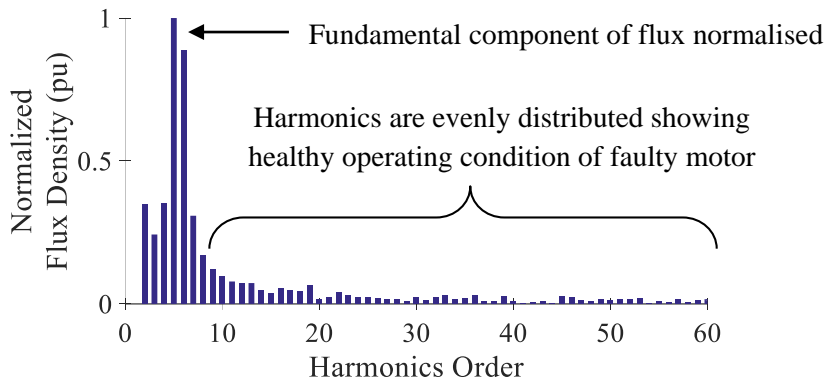
Fig. 7.9. Air-gap flux density over one pole pair. (a) Radial flux density. (b) Tangential flux density for both healthy and faulty condition flux density. (c) Electromagnetic torque fluctuation as shown due to deviation of IM from its healthy condition to stator.

### 7.6. Proposed Deep Neural Network Predictive Model Result Analysis

After modelling and simulating the faulty IM in FEA, it was clear how the magnetic flux density in air-gap is affected as well as the torque ripple and other performance factors of the machine. The novel DNN based harmonic compensation block on the 7.5 hp faulty aluminium rotor IM has been studied under various speeds and loads in order to investigate the reliability of the proposed methodology. In Fig. 7.10, fast Fourier transformation on the measured flux at rated speed was performed in order to understand the magnitude of space harmonics and higher order harmonic fields before and after implementing the proposed DNN predictive model. The higher order harmonics of measured flux was reduced to a great extent after proposed method was implemented. This indicates that the proposed predictive method was functioning precisely as modelled and simulated. The stator inter turn fault has a great impact on stator and rotor slot harmonics. Slot harmonics are of the order  $k=mQ_s \pm P$  where  $Q_s$  and  $P$  are the number of slots and pole pairs of the IM respectively and  $m$  is any integer. A significant decrease of 63% and 54% in stator and rotor space harmonics respectively was observed as shown in Fig. 7.10(b) when the proposed predictive model was implemented for faulty condition. Fig 7.2(a) shows the current unbalance in the phases and the voltage waveform of the machine operating at rated speed of 1,750 rpm. The average rms current value is 3.5 A.



(a)

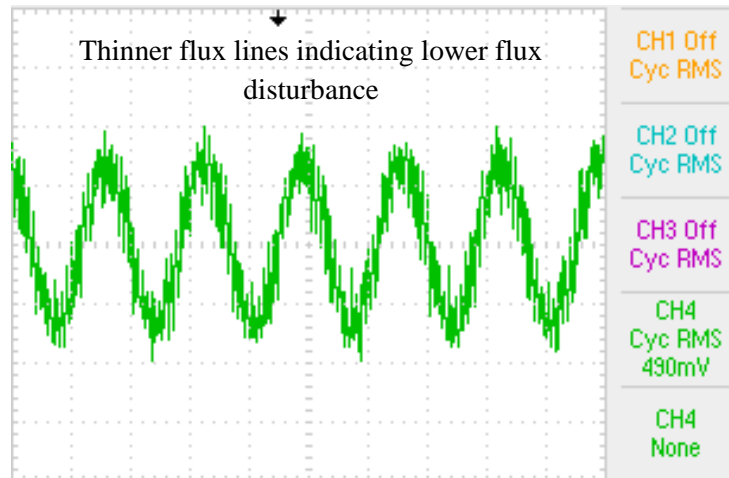


(b)

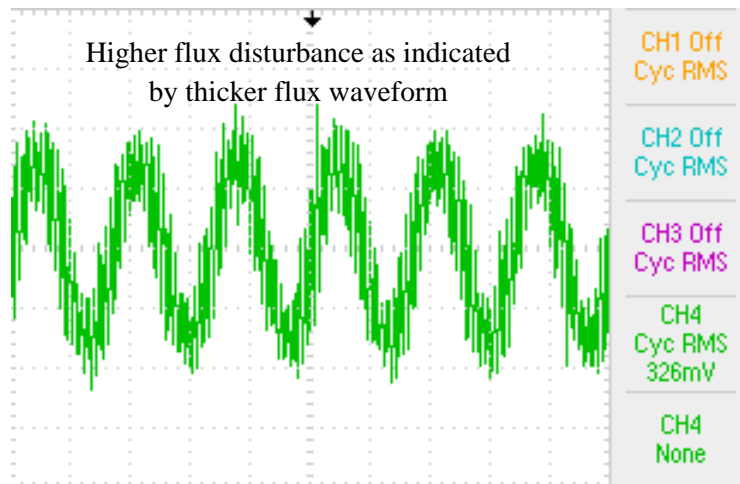
Fig. 7.10. Real time flux harmonic analysis. (a) Healthy motor condition. (b) Faulty motor condition.

The faulty IM is then run at 90% of the rated load in which the motor starts to draw more current as shown in Fig. 7.2(b) at an average rms of 8.2 A. Figs. 7.11(a) and (b) show the flux waveform as obtained from search coil at rated speed and load respectively. This DNN based model feeds the measured flux back to the control. Fig. 7.11(c) also shows the balanced current waveform due to implementation of control. Fig. 7.11(c) was observed with a attenuation scale of 10X in order to study the waveform closely. It was observed that the phase A current changed from 4.5 A rms to 3.16 A rms, closer to other phase current values during faulty condition on implementation of DNN predictive model. The final real time flux in faulty condition and after running it with the DNN predictive model is shown as Fig. 7.11(d). The DNN predicted magnetic flux forces the IM drive to operate in more close to healthy condition, thereby enforcing drive to operate in a condition which compensates the faulty IM parameters in the drive as opposed to a non-fault tolerant drive.

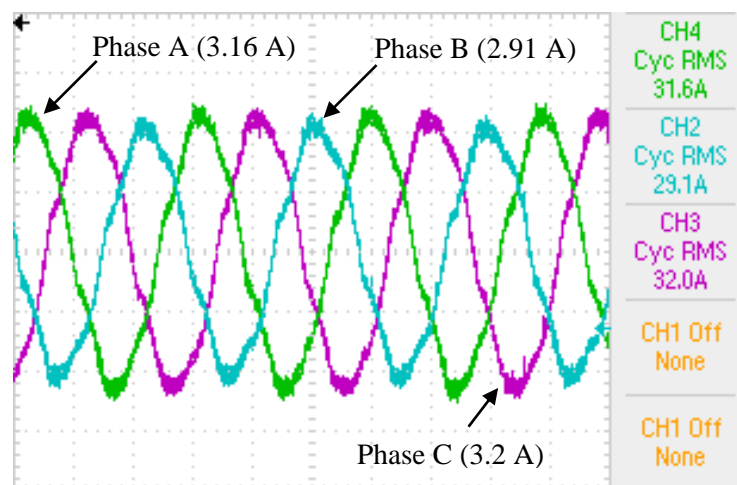




(a)



(b)



(c)

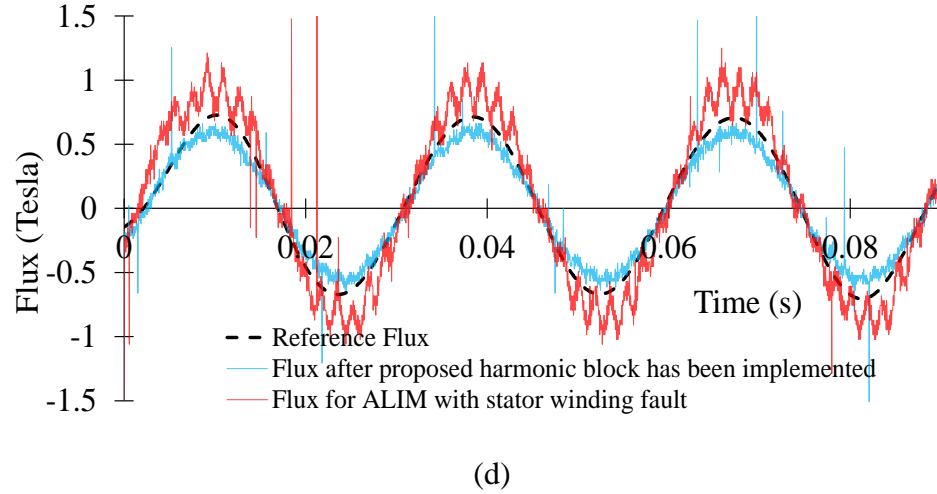


Fig. 7.11. Experimental validation. (a) Flux density at rated load for faulty IM (b) Flux density at rated speed for faulty IM. (c) Uniformity in current waveform after DNN predictive model implementation. (d) Comparison of experimental and DNN predictive harmonic.

## 7.7. Conclusion

This chapter proposed a novel method to control a faulty traction motor using a deep neural network predictive method for magnetic flux reference. This method can detect a fault occurring due to stator winding short circuit or unbalance in inverter supply, at an incipient stage, thereby preventing the complete break-down of the motor. The eccentricity in behavior of the motor due to any fault leads to asymmetric distribution of the magnetic flux produced thereby causing an UMP. This can be detected earlier by harmonic analysis of the magnetic air-gap flux. This DNN predictive harmonics compensated control drive was first simulated in a technical computer programming language used for data analysis and finite element analysis of the ALIM was done before the implementation. The results obtained were then compared with experimental results validating the proposed method. For future work, a model reference adaptive system will be designed using the magnetic equivalent circuit model of the faulty IM in order to differentiate fault occurrence due to distortion in time harmonics produced by unbalanced voltage supply and space harmonics distortion occurring due to fault inside the motor along with harmonics compensation for safer and more reliable fault-tolerant EV motor drive.

## 7.8. References

- [1] C. Lai, A. Balamurali, V. Bousaba, K. L. V. Iyer, and N. C. Kar, "Analysis of Stator Winding Inter-Turn Short-Circuit Fault in Interior and Surface Mounted Permanent Magnet Traction Machines," *IEEE Transportation of Electrification Conference and Expo (ITEC)*, Dearborn, MI, 2014.
- [2] A. Mollaeian, S. M. Sangdehi, A. Balamurali, G. Feng, J. Tjong, and N. C. Kar, "Reduction of Space Harmonics in Induction Machines Incorporating Rotor Bar Optimization Through a Coupled IPSO and 3-D FEA Algorithm," *XXII Inter. Conf. on Electr. Machines (ICEM)*, Lausanne, 2016.
- [3] K. Saad, and G. Mirzaeva, "Space-Time Representation of the Main Air Gap Flux of a Three Phase Squirrel Cage Induction Motor and its Application to Detect Eccentricity," in the Proc. of *IEEE International Electric Machines & Drives Conference (IEMDC)*, pp. 1466-1472, Coeur d'Alene, ID, 2015.
- [4] O.Chapelle, B.Schölkop, and A.Zien, "Semi-Supervised Learning", MIT Press, 2006
- [5] T. Boukra, A. Lebaroud, and G. Clerc, "Statistical and Neural-Network Approaches for the Classification of Induction Machine Faults Using the Ambiguity Plane Representation," *IEEE Transactions on Industrial Electronics*, vol. 60, no. 9, pp. 4034-4042, Sept. 2013.
- [6] D. G. Dorrell, A. Salah, and Y. Guo, "The Detection and Suppression of Unbalanced Magnetic Pull in Wound Rotor Induction Motors Using Pole-Specific Search Coils and Auxiliary Windings," *IEEE Transactions on Industry Applications*, vol. 53, no. 3, pp. 2066-2076, May-June 2017.

# CHAPTER 8

## DUAL MEMORIZATION AND GENERALIZATION MACHINE LEARNING BASED FLUX REFERENCE PREDICTION FOR FAULT DIAGNOSIS

### 8.1. *Introduction*

The work done in this chapter is an extension of the previous chapter by the development and application of a faster and more reliable dual memorization and generalization machine learning (DMG-ML) for magnetic flux reference prediction which can be used in a fault-tolerant control for EV as shown in Fig. 8.1. For any machine learning algorithm to be able to predict better, it needs a memorization of feature interactions along with generalization which requires more feature engineering effort. But if less feature engineering is needed, deep neural networks (DNN) are better in generalizing unseen feature combinations with the help of low-dimensional dense embeddings learned for the sparse features. However, DNN with embeddings tend to over-generalize and recommend less relevant flux values when the feature interactions are sparse and high-rank. This lead to combine generalization, memorization and deep neural networks to predict magnetic flux references with sparse dataset of voltage and current input and achieve a higher accuracy prediction rate. Since in a traction application estimation of flux is vital for control, the precision of flux predicted value needs to be higher in a lesser computational time. The proposed state-of-the-art DMG-ML for magnetic flux reference based fault diagnosis method achieves a significant improvement when compared with other direct learning and traditional methods.

### 8.2. *IM Model with Stator Winding Fault for DMG-ML*

The major cause of stator winding faults as discussed previously is short circuits between inter-turn of a phase winding or between two phases. Undetected incipient inter-turn stator fault may gradually develop to a major short circuit leading to destructive effects on stator windings. It can be stated that axial leakage flux from stator windings can be used to detect and locate stator inter-turns. If a search coil is placed near the middle of the machine shaft, the induced voltage in the search coil would be directly proportional to flux

component of the machine. Spectral analysis of this voltage is used to detect inter-turn stator fault. If there is a short circuit occurrence, the phase winding has less impedance due to fewer active turns thereby having less magneto motive force (MMF) in the machine. It is also possible to monitor the amplitude of phase currents to detect stator short circuit which is a very popular method of fault detection termed as motor current signature analysis (MCSA) [1], [2]. To design an adequate fault diagnostic strategy, it is important to understand the physical problem of stator winding fault associated and its affect in the machine mathematical model that considers the inclusion of stator fault effects. In the proposed model, 3-phase currents, voltage and flux of the motor are the required signals to compare healthy and faulty motor behavior. Models with fault inclusion, display a trade-off between complexity and accuracy. Most models have shortcomings, since it is not possible to include all non-idealities that exist in a real faulty induction machine. the proposed DMG-ML based flux prediction method has been implemented on the 7.5 hp ALIM with slight inter-turn stator fault.

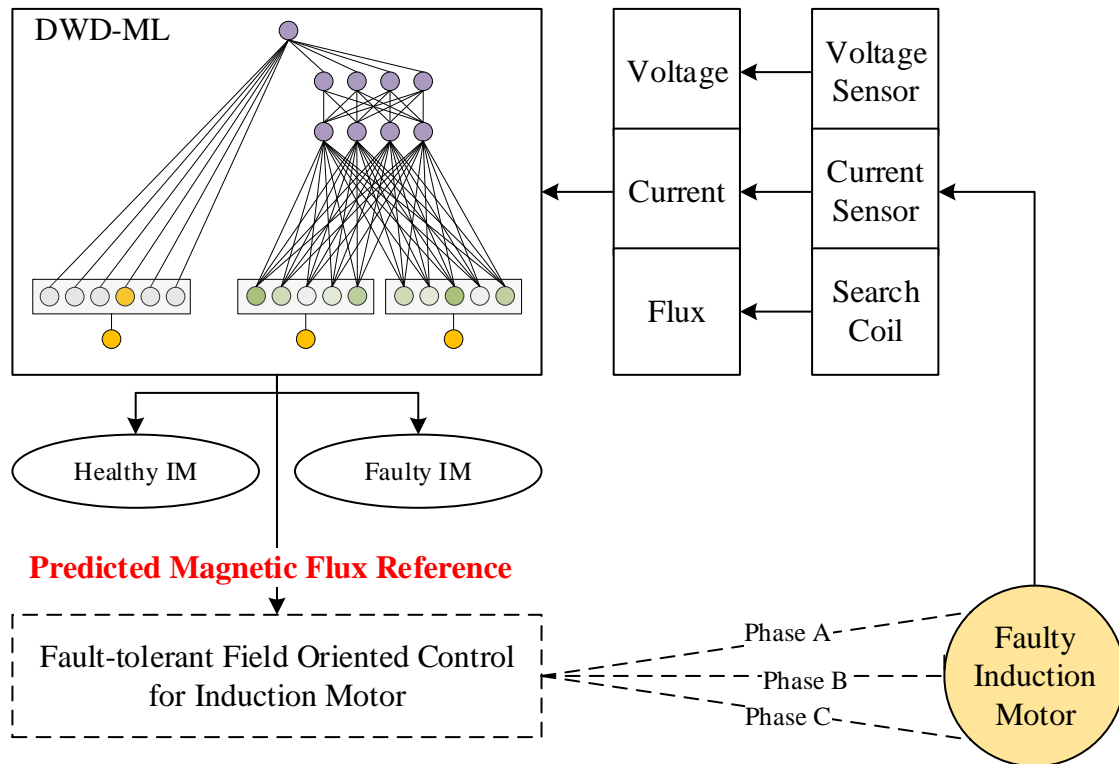


Fig. 8.1. Schematic flow of novel DMG-ML based flux reference and fault prediction.

Extensive experimental investigations have been conducted to verify the severity of the fault in the motor. In Figs. 8.2(a) and (c), the unbalance in current feedback of the IM with the phase A being more in magnitude than phase B and C. In Figs. 8.2(b) and (d) the deviation of flux is shown when the loading on the faulty machine is increased. It has been indicated in [3] and [4] that considering an unbalanced Park's model for stator fault diagnosis of induction motor is impractical. A deviation of IM electrical parameters used to be a definite indication that there has been a deviation in machine performance but according to recent research findings in fault diagnosis, it has been seen that such a deviation can occur due to unwanted temperature rise or a change in magnetic state of IM. Localization of faults can be done using Fast Fourier's analysis but estimation of electrical parameters is not a proper solution to understand the severity of the fault. This requires to model the IM in such a way that not only detection but also localization of the stator winding fault can be done

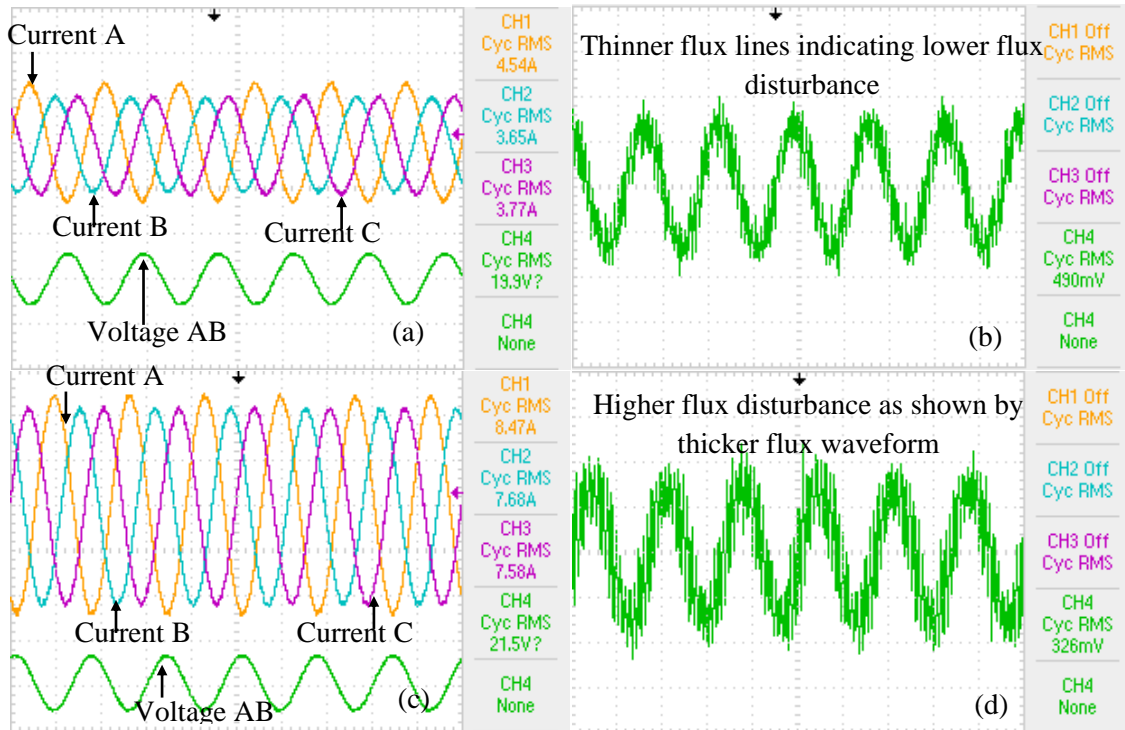


Fig. 8.2. Experimental analysis of faulty IM indicating (a) Current and voltage waveform at rated speed of 1,750 rpm with faulty phase A. (b) Magnetic flux density at rated speed. (c) Current and voltage at rated load of 70 Nm with faulty phase A. (d) Magnetic flux density at rated load.

An initial model was proposed in [3] which took into account the inter-turn short circuit fault in IM stator windings. The model consists of a supplementary shorted winding in a three-phase axis. The winding fault induces in stator a new short circuited winding  $A_{sc}$  and localized according to phase A by the angle  $\theta_{sc} = 0$  rad. Two new parameters have been introduced in the conventional machine model to define the stator faults – localization parameter  $\theta_{sc}$  and detection parameter  $\theta_{sc}$ . Localization parameter  $\theta_{sc}$ , is the angle between the inter-turn faulty stator winding and the first stator-phase axis (phase A). This determines which phase winding the fault has occurred and can have the values of 0,  $2\pi/3$ , or  $4\pi/3$ , respectively for the fault occurrences on the stator phases A, B, or C. Detection parameter  $\theta_{sc}$  can be defined as (11).  $\theta_{sc}$  helps in enumerating the unbalance occurred and figure out the number of inter-turns in the short circuit [5].

Due to fault in the stator, an additional short-circuited winding  $A_{sc}$  appears in the stator. Because of this winding, a stationary magnetic field  $H_{sc}$ , is developed which is oriented according to the faulty winding. The current flowing through this inter-turn short-circuit  $i_{sc}$  generating a short-circuit flux  $\phi_{sc}$ . Voltage and flux equations for faulty model of induction machine referred to the stator can be written as (8.1)-(8.9) where  $R_{sc}$ ,  $i_{sc}$  and  $\theta_{sc}$  are the current and flux for the short-circuit.  $\theta$  is rotor angular position.  $X_p$  and  $X_f$  are principal and global leakage inductance as referred to stator respectively.

$$\left. \begin{aligned} R_s i_s + \frac{d}{dt} \phi_s &= V_s ; & R_r i_r + \frac{d}{dt} \phi_r &= 0 ; \\ R_{sc} i_{sc} + \frac{d}{dt} \phi_{sc} &= 0 \\ X_s i_s + X_{sr} i_r + X_{s-sc} i_{sc} &= \phi_s , & X_{rs} i_s + X_r i_r + X_{r-sc} i_{sc} &= \phi_r \\ X_{sc-s} i_s + X_{sc-r} i_r + X_{sc} i_{sc} &= \phi_{sc} \end{aligned} \right\} \quad (8.1)$$

$$X_s = \begin{bmatrix} X_p + X_f & -\frac{X_p}{2} & -\frac{X_p}{2} \\ -\frac{X_p}{2} & X_p + X_f & -\frac{X_p}{2} \\ -\frac{X_p}{2} & -\frac{X_p}{2} & X_p + X_f \end{bmatrix} \quad (8.2)$$

$$X_r = \begin{bmatrix} X_p & -\frac{X_p}{2} & -\frac{X_p}{2} \\ -\frac{X_p}{2} & X_p & -\frac{X_p}{2} \\ -\frac{X_p}{2} & -\frac{X_p}{2} & X_p \end{bmatrix} \quad (8.3)$$

$$X_{sr} = L_p \begin{bmatrix} \cos(\theta) & \cos\left(\theta + \frac{2\pi}{3}\right) & \cos\left(\theta - \frac{2\pi}{3}\right) \\ \cos\left(\theta - \frac{2\pi}{3}\right) & \cos(\theta) & \cos\left(\theta + \frac{2\pi}{3}\right) \\ \cos\left(\theta + \frac{2\pi}{3}\right) & \cos\left(\theta - \frac{2\pi}{3}\right) & \cos(\theta) \end{bmatrix} \quad (8.4)$$

$$X_{s\_sc} = \eta_{sc} X_p \begin{bmatrix} \cos(\theta) \\ \cos\left(\theta - \frac{2\pi}{3}\right) \\ \cos\left(\theta + \frac{2\pi}{3}\right) \end{bmatrix} \quad (8.5)$$

$$X_{r\_sc} = \eta_{sc} X_p \begin{bmatrix} \cos(\theta_{sc} - \theta) \\ \cos\left(\theta_{sc} - \theta - \frac{2\pi}{3}\right) \\ \cos\left(\theta_{sc} - \theta + \frac{2\pi}{3}\right) \end{bmatrix} \quad (8.6)$$

$$X_{sc} = \eta_{sc}^2 (L_p + L_f) \quad (8.7)$$

$$X_{rs} = [X_{sr}]^T \quad X_{r\_sc} = [X_{sc\_r}]^T \quad X_{sc\_s} = [X_{s\_sc}]^T \quad (8.8)$$

$$\eta_{sc} = \frac{\eta_{sc}}{\eta_s} = \frac{\text{Number of interturn short - circuit winding}}{\text{Total number of interturn in healthy phase}} \quad (8.9)$$

### 8.3. Motor Condition in-terms of Flux under Fault Condition

The IM under test needed to be modelled in finite element analysis software in order to investigate the motor in both prior to fault and faulty condition. Two identical machines have been investigated by the authors as tabulated in Table 2.2. Since the motor under test is an aluminum die-casted rotor induction motor, determining the exact size and design of



the rotor slots is not possible to understand from outside the rotor. To successfully model the motor under investigation in FEA, out of the two motor, the healthy motor was cut to study the stator and rotor slot shape and size. After extensive measurement of all the required parameters, the motor was designed in 2D and 3D FEA models. In Fig. 8.3(a), one of the rotors which was cut for the purpose of measurement of dimensions has been indicated. For stator, since most part is exposed, it was fairly easier to take the measurements. Once the measurements were taken, the motor under study was recreated in finite element software as shown in Fig. 8.3(b).

Detailed analysis of the designed motor in FEA with a voltage and current excitation was performed for both balanced and unbalanced IM. Analysis exhibited that under fault conditions magnetic flux lines are disturbed around the faulty phase winding. One phase resistance of the stator winding changes drastically due to the inter-turn stator fault. This leads to local saturation in adjacent stator slots of the other phases as well as rotor bars due Figs.8.4(a) and (b) show the variation in flux linkage in the 3 phases. For the healthy IM as shown in Fig 8.4(a), all the three phases have the same waveform. But if there is inter-turn fault at Phase A of the machine, the flux decreases at that phase and also affects the corresponding phases. Figs. 8.5(a) and (b) presents the magnetic flux distribution in a healthy and faulty IM. Finite element analysis of the machines led to the observation of dissimilarity of flux distribution due to variation in machine parameters. Imbalanced parameters in the three phases led to flow of higher current which leads to saturation in corresponding phase as shown in Fig. 8.5(b).

TABLE 8.1

VARIATION IN FLUX IN 3-PHASES FOR HEALTHY AND FAULTY IM UNDER FEA

<b>Phase Flux Linkage</b>	<b>Healthy IM</b>	<b>Faulty IM</b>
Phase A	1.3964 Wb	0.3318 Wb
Phase B	1.3905 Wb	0.5254 Wb
Phase C	1.3964 Wb	1.3838 Wb

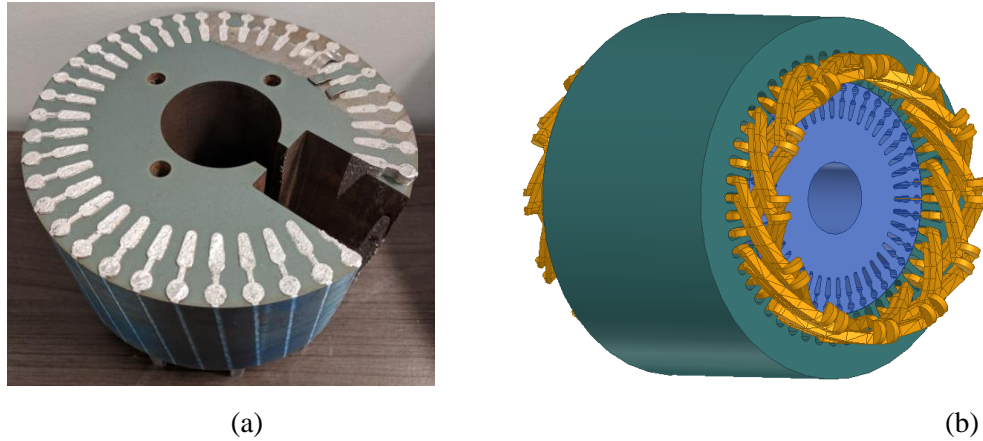


Fig. 8.3. FEA modelling of IM under test for understanding of the motor in healthy and unhealthy conditions. (a) Cross-sectional cut of rotor for design purpose. (b) 3D FEA Model.

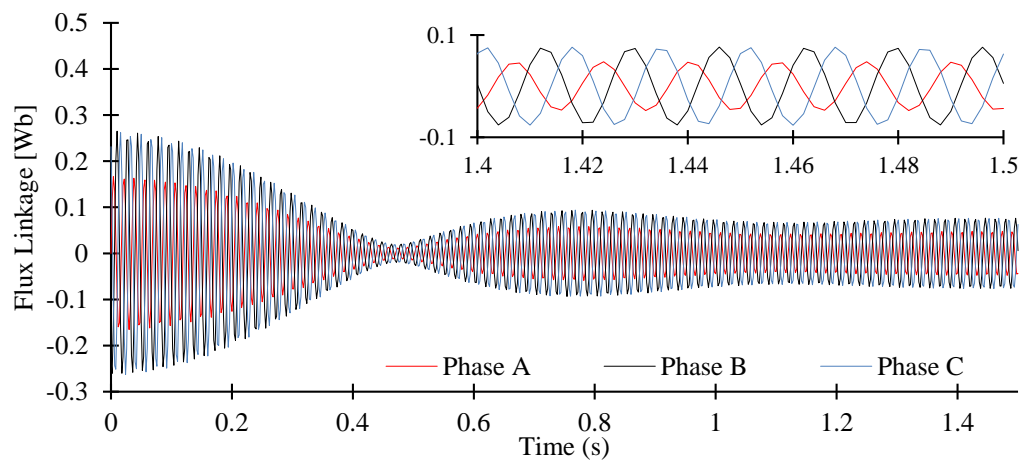
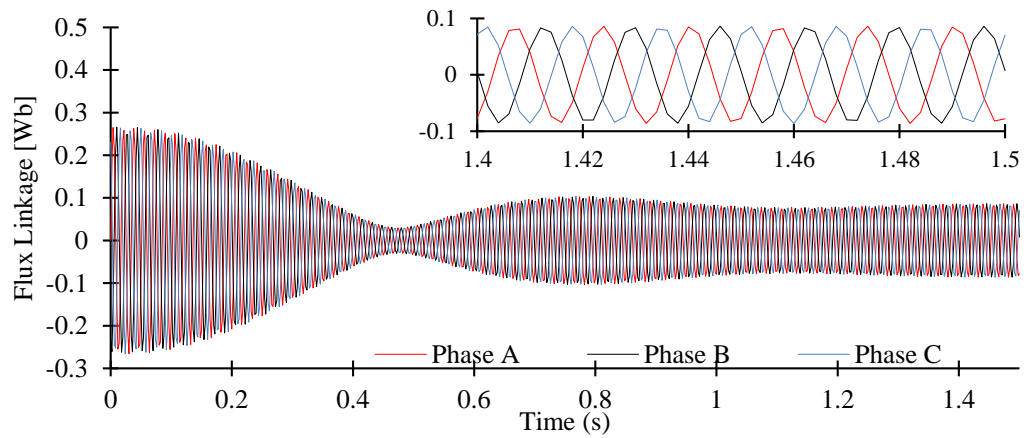


Fig. 8.4. Flux linkage as observed using finite element method to evaluate flux variation in different conditions. (a) Healthy IM. (b) Fault IM.

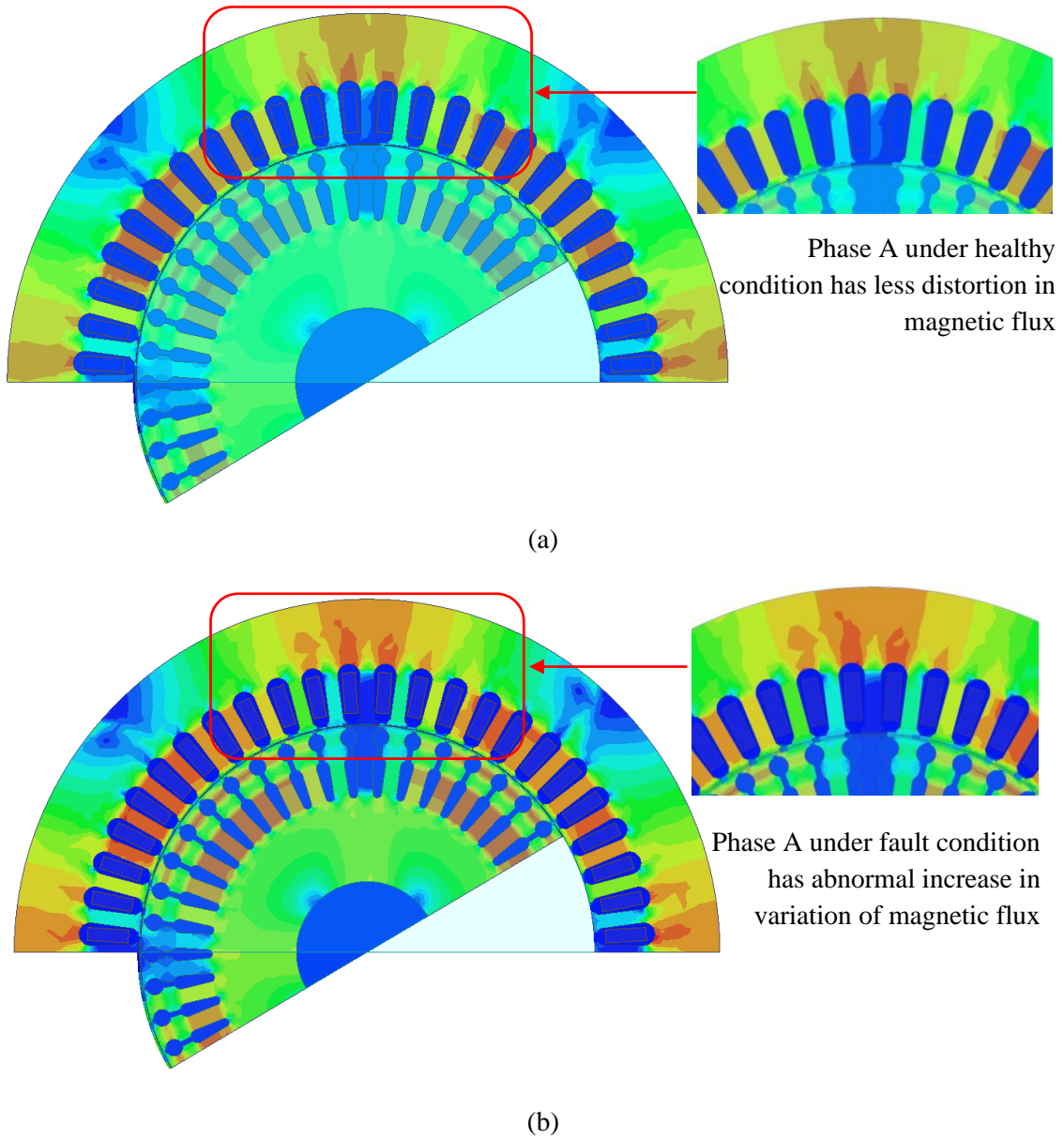


Fig. 8.5. Variation in scalar and vector magnetic flux density. (a) Healthy IM. (b) IM with inter-turn fault.

#### 8.4. Dual Memorization and Generalization Machine Learning for Magnetic Flux Reference Estimation

##### A. Classification

Classification is a core problem of machine learning. Machine learning is a field that grew out of artificial intelligence within computer science, and the goal is to teach

computers by example. For example, if the computer program needs to recognize images of dogs, then the computer shall be given a dataset containing images of things with 4 legs and taught which ones are dogs and which ones are not. In this way supposedly, the computer learns to recognize dogs, even ones it hasn't seen before. It is important to be considered that the human perception of what a dog looks like is very different from how a computer recognizes a dog. Since machine learning is closely linked to statistics; in today's world the gap between predictive statistics and machine learning is being bridged more than ever.

The example problem just mentioned is a classification problem where according to the requirement the computer tries to identify dogs. The problem to be solved needs a training set of observations, such as labeled images in this case, and a test set that is only for evaluation. The training set is used to learn the model of what a dog is, and the test set are images that are not in the training set and are used to make predictions on those as to whether or not each image is a dog. It is also highly likely that some of the labels on the training set might be noisy. If there isn't too much noise, the program should still be able to learn a model for a dog; it just would have some difficulty to classify perfectly. In general, some prediction problems are just much harder than others. As long as there is a considerable amount of good training data, such kind of noise data wouldn't affect the prediction results a lot. In terms of training data for machine learning world, it can be aptly said – the more the merrier. In general for solving a machine learning problem, each observation in the training and test sets needs to be represented as a vector of numbers, and a label, represented by a number, is also needs to be defined. For the example problem all dog images in the training set can be labelled as 1 and the rest as -1. Thus, the computer program now learns to coordinate the large vector of numbers with the labels in order to identify the classification problem.

Since, a classification problem has been defined and explained, not all classification problems are so easily programmable. Most classification problems have feature intense and all the features needs to be interlinked. Computationally, it is easier if a fewer features dataset is used, but then there is a risk leaving out information which is a trade-off right there. In order to defined it more clearly each observation is represented by a set of features  $x$ , also called predictors, co-variant, explanatory or independent variables and labels  $y$ ., For

a given training set of feature label pairs  $(x_i, y_i)$ , where  $i = 1, 2, 3 \dots n$ , a classification model  $f$  that can predict a label  $y$  or a new  $x$ . For instance, if an event has 2 features  $x_1$  and  $x_2$ . Each observation of that event can be represented as a two-dimensional graph, thus giving the ability to plot it in the graph as shown in Fig.8.6. The function  $f$  divides the space into two parts,— on one side of the decision boundary the predicted condition will be considered as an event occurrence, and on the other side of the decision boundary, the predicted condition will be no event. So this decision boundary is actually just the equation where the function is 0.

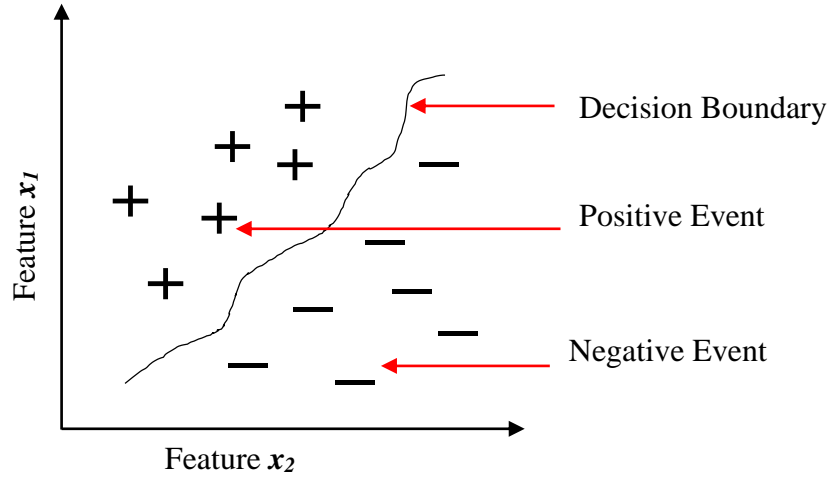


Fig. 8.6. Event classification for a set of features.

The machine learning algorithm creates the function  $f$ , and no matter how complicated that function  $f$  is, the way to use it is not very complicated. The way to use it is just like this: the predicted value of  $y$  for a new  $x$  that is not observed before is just the sign of that function  $f$ .

#### B. Loss Function

Loss function of a machine learning algorithm is the decision factor that differentiates one machine learning method from another. It quantifies how accurately the predictions are done based on the outputs. If it is considered that the classification error is such as (8.10), it will be computationally difficult to minimize the error.

$$\text{Classification Error} = \frac{1}{n} \sum_{i=1}^n [y_i \neq \text{sign}(f(x_i))] \quad (8.10)$$

### C. Statistical Principle of Supervised Learning

The key principle in statistical learning theory is the principle of Ockham's razor. The principle states that the best models are simple models that fit the data well. It was named after the English friar and philosopher Ockham, who had stated that among different hypothesis that predict equally well the one with the fewest assumptions should be chosen. Now let's assume that there a way to measure model complexity, and with increase in complexity of the model, over-fitting and under-fitting becomes an issue.

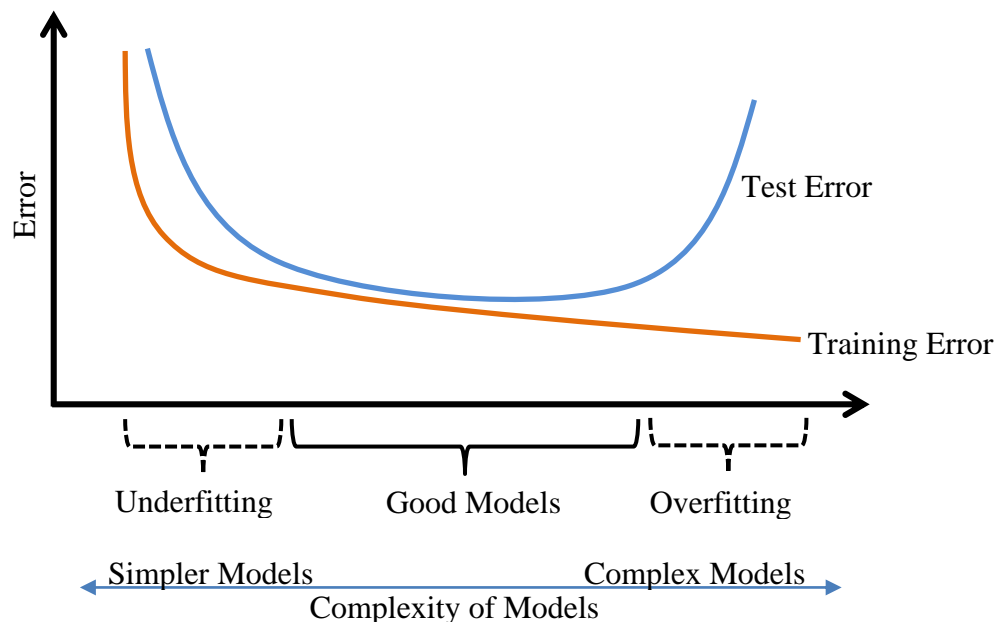


Fig. 8.7. Statistical understanding of model fitting

As shown in Fig. 8.7 below, the plot is key to understanding machine learning theory. It can be seen in the plot that as the models grow more and more complex, the training error continues to decrease since it can over-fit more and more. But at the same time the test error gets worse and worse. If it is under-fit, then the model won't do well for either training or test. Thus it can be rightly said that the sweet spot is in the middle of the plot. This understanding of the plot it holds true for classification, regression and most other machine learning algorithms. Best models are simple models that fit the data well. Thus it is important to strike a balance between accuracy and simplicity. The most common

machine learning algorithms choose their function  $f$  in such a way that it minimizes training error and model complexity, thereby trying to thwart the curse of dimensionality. Thus to find the adequate model that's both simple, low complexity and has low training error; is the exact principle of Ockham's razor.

$$Best Model = \frac{1}{n} \sum_{i=1}^n l(y_i, f(x_i)) + Complexity(f) \quad (8.11)$$

Simplicity of model is measured in several different ways, and is usually referred as regularization of machine learning. So the main foundation of machine learning is about creating functions that not only minimizes the loss, but also keeps the model simple. Different machine learning methods have different loss functions and they have different regularization terms. It is of utmost importance to understand the problem in hand and create the machine learning algorithm accordingly.

#### D. *Logistic Regression or Maximum like hood perspective*

Logistic regression is one of the simplest and oldest algorithm. It is fast as well as can compete with the best machine learning algorithm. It will explained in details in Section 8.4 G. Logistic regression uses the loss function as shown in (8.12). It minimizes the function which is the average loss on the training points

$$Loss Function = \min_{models f} \frac{1}{n} \sum_{i=1}^n \log(1 + e^{-y_i f(x_i)}) \quad (8.12)$$

Let's consider a linear model which is a weighted sum of the features such as (8.13)

$$f(x_i) = \beta_1 x_{i1} + \beta_2 x_{i2} + \beta_3 x_{i3} + \dots + \beta_p x_{ip} = \sum_{j=1}^p \beta_j x_{ij} \quad (8.13)$$

$f$  is the sum of the weighted features which in this case is voltage, and current, where the weights are called  $\beta$  coefficients. So here. Using (8.12) and (8.13), the minimization problem for logistic regression can be defined. This will try to find the weights that minimize the sum of the training losses. In short, this is what logistic regression does, just chooses the coefficients  $\beta$  to minimize the loss.

$$Loss Function = \min_{\beta_1, \beta_2, \beta_3, \dots} \frac{1}{n} \sum_{i=1}^n \log \left( 1 + e^{-y_i \sum_{j=1}^p \beta_j x_{ij}} \right) \quad (8.14)$$

The performance of logistic regression can be improved by adding a regularization term

$$ObjectiveFunction = \frac{1}{n} \sum_{i=1}^n l(y_i(f(x_i))) + C \times Regularization(f) \quad (8.15)$$

where  $f(x)$  is defined as (8.13) and  $Regularization(f)$  can be defined as (8.16)

$$Regularization(f) = \beta_1^2 + \beta_2^2 + \beta_3^2 + \dots + \beta_p^2 = \|\beta\|_2^2 \quad (8.16)$$

#### E. Evaluation Methods for Classifiers

Lets consider for a given model with observations, having features  $x$  and labels  $y$ . Then the machine learning algorithm comes along and it gives a number to each observation, which is sort of what the algorithm thinks is going on defined as  $f(x)$ , indicating how far away from the decision boundary the observation is. The sign of  $f(x)$  is predicted label  $y'$ . Now if the machine learning algorithm is good, the label  $y$  and predicted label  $y'$  should agree for most of it.

In short, True Positive (TP), True Negative (TN), False Positive (FP) and False Negative (FN) are the terms which help in defining the performance of the algorithm as shown in Fig. 8.9 where

**True Positive** can be defined as the value where label  $y$  is +1 but predicted label  $y'$  is +1

**True Negative** can be defined as the value where label  $y$  is -1 but predicted label  $y'$  is -1

**False Positive** can be defined as the value where label  $y$  is -1 but predicted label  $y'$  is +1

**False Negative** can be defined as the value where label  $y$  is +1 but predicted label  $y'$  is -1

If a classifier algorithm is pretty good then there are no errors and TP and TN are good. But if there is a misclassification error, which means some of the observations are classified incorrectly and the count for FN and FP are high. Misclassification error can be defined as (8.17)

$$\frac{FP + FN}{n} = \frac{1}{n} \sum_{i=1}^n 1_{[y_i \neq y'_i]} \quad (8.17)$$



This is where the terms **Sensitivity** and **Specificity** come into play which are the statistical measures of the performance of classification function.

- **Sensitivity** is also known as True Positive Rate (TPR), or the recall, or probability of detection, measures the proportion of positive labels that have been correctly identified.
- **Specificity** is also called the true negative rate (TNR), measures the proportion of negative labels that are correctly identified.

True Positive Rate can be defined as

$$TPR = \frac{TP}{P} = \frac{\sum_i^n 1_{[y_i = y'_i \text{ and } y_i = 1]}}{\sum_i^n 1_{[y_i = 1]}} \quad (8.18)$$

True Negative Rate can be defined as

$$TNR = \frac{TN}{N} = \frac{\sum_i^n 1_{[y_i = y'_i \text{ and } y_i = -1]}}{\sum_i^n 1_{[y_i = -1]}} \quad (8.19)$$

Precision or Positive Predicted Value (PPV)

$$PPV = \frac{TP}{TP + FP} = \frac{\sum_i^n 1_{[y_i = y'_i \text{ and } y_i = 1]}}{\sum_i^n 1_{[y_i = 1]}} \quad (8.20)$$

F1-score

$$F1 = \frac{PPV \times TPR}{PPV + TPR} \quad (8.21)$$

The accuracy of the model is defined as

$$Accuracy = \frac{TP + TN}{(TP + TN + FP + FN)} \quad (8.22)$$

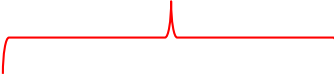

		Predicted	
			
Actual		True Positive (TP)	False Negative (FN)
		False Positive (FP)	True Negative (TN)

Fig. 8.8. Confusion Matrix for statistical measurement of results

The importance of understanding these metrics is needed later in order to figure out the accuracy of the machine learning algorithm as developed for the application of detection of motor fault

#### F. Managing Imbalanced Data

Imbalanced data can be understood as a sea of negative observations with a few little positive observations around. This is one of the possibilities which is highly likely when gather data from a running faulty machine. In this case the machine learning algorithm would consider everything negative thus classification of data is meaningless though there will be a very high accuracy in prediction because only 1% of the observations are positive. In other words, getting TP right is way more important and better than getting TN right

In usual conditions the objective function for classification machine learning algorithm can be defined as

$$ObjectiveFunction = \frac{1}{n} \sum_{i=1}^n l(y_i(f(x_i))) + Regularization(f) \quad (8.23)$$

But in an imbalanced data model, where the positives need to be given more importance than negatives, the objective function can be redefined as (8.24) where  $i$  is considered positives and  $k$  the negatives. Each positive is  $C$  times more important than negative.

$$ObjectiveFunction = \frac{1}{n} \left[ C \sum_{i=1}^n l(y_i(f(x_i))) + \sum_{k=1}^n l(y_k(f(x_k))) \right] + Regularization(f) \quad (8.24)$$

In machine learning classifier defining parameter  $C$  plays a great role is classifying imbalanced data

## *G. Regression*

### *(i) Linear Regression*

Simple regression is used to examine the relationship between one dependent and one independent variable. After performing an analysis, the regression statistics can be used to predict the dependent variable when the independent variable is known. Regression goes beyond correlation by adding prediction capabilities.

The simplest form is Linear Regression which estimates label  $y$  for a new  $x$ . The linear model can be expressed as (8.25) where  $b_0$  and  $b_1$  are constants chosen for expressing the feature  $x_i$  in order to minimize the total error on the training set.

$$f(x_i) = b_0 + b_1 x_i \quad (8.25)$$

Adding up all the errors is called sum of squares error. This determines the quality of the regression model. Thus, Sum of Squared Error/Mean Squared Error (SSE/MSE) or Mean Absolute Error (MAE) is used to determine the distance between the truth and the prediction values

$$SSE = \sum_{i=1}^n ((f(x_i) - y_i))^2 \quad (8.26)$$

$$MAE = \sum_{i=1}^n |f(x_i) - y_i| \quad (8.27)$$

The regression line, also known as the least squares line, is a plot of the expected value of the dependent variable for all values of the independent variable. Technically, it is the line that "minimizes the squared residuals". The regression line is the one that best fits the data on a scatterplot. The significance of the slope of the regression line is determined from the t-statistic. It is the probability that the observed correlation coefficient occurred by chance if the true correlation is zero. The standard error of the estimate for regression measures the amount of variability in the points around the regression line. It is the standard

deviation of the data points as they are distributed around the regression line. The standard error of the estimate can be used to develop confidence intervals around a prediction.

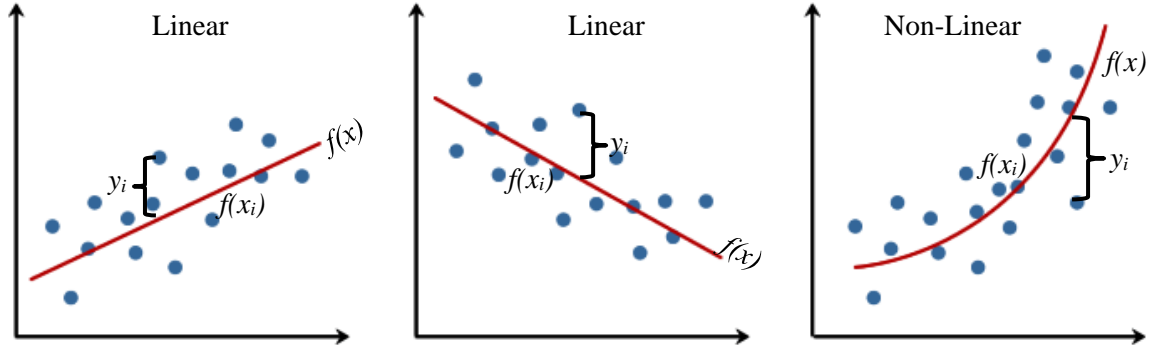


Fig. 8.9 Types of Regression model relationships

## (ii) Multiple Linear Regression

Simple regression model was of having a single feature. Let's consider a situation when there is more than one feature which determines the final results of the model. The model is still linear but just a weighted combination of all the factors. Thus making the model more complex.

$$f(x_i) = b_0 + b_1x_{i,1} + b_2x_{i,2} + b_3x_{i,3} + b_4x_{i,4} \quad (8.28)$$

Since it is a linear model, the method of least squares is simple - choose the coefficients  $b_i$ , to minimize the sum of squares error. the weights are learned from data. this is an optimization problem that's exactly the same as the one for simple linear regression, the only difference is that the function can take – has multiple terms in it. And this is called the method of least squares

$$SSE = \sum_{i=1}^n ((f(x_i) - y_i)^2 + \sum_{i=1}^n (y_i - (b_0 + b_1x_{i,1} + b_2x_{i,2} + b_3x_{i,3} + b_4x_{i,4} + \dots))^2 \quad (8.29)$$

The process is is to give the data and tell it to do least squares regression and done. The coefficient  $b$ 's can be used in the predictive model  $f$ . If there are too many variables in the model, optimization problem gets harder, and it run into recursive dimensionality issues.

Thus it is crucial to decide which are the potentially important factors to be taken in to account for the model. If model  $f$  has polynomials in it, it means the function would be kind of curvy as shown in Fig. 8.11 and which might seem interesting in terms of designing the optimization problem but there is a risk of over-fitting.

### (iii) Evaluating Regression Models

The difference between the observed value of the true value/observation  $y$  and the predicted value  $y'$  is called the residual. For a good optimization, the residual should be close to 0. If there is some sort of structure or pattern in these residuals, then it would mean there is more modeling. Plotting a histogram of all of the residuals will help in understanding the importance of residuals. In Fig. 8.11, histogram is higher is where most of the residuals are and ideally they are mostly close to 0. This is a very good model since most of the residuals are around 0 and there is no pattern in these residuals. But if the model looks like Fig. 8.11 (a) it is a bad model. In situations such as Fig. 8.12 (c), the other 2 bumps which are not close to 0, which means the modelling has not been correct and extra factors have to be included in the regression model. This concludes the fact that missing out a few important factors can drastically change the model. This is due to outliers which is explained in the next section.

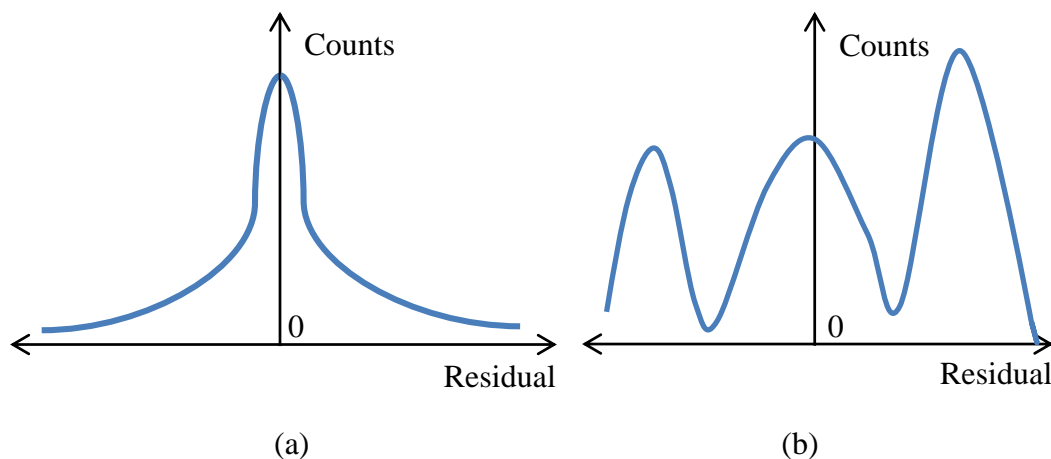


Fig. 8.10. Evaluating regression model. (a) When histogram is close to 0 with a definite pattern. (b) When histogram is close to 0 with no apparent pattern.

## H. Outliers

An influential point is one that changes the estimates of the error substantially when it is omitted. This is one of the major headaches for machine learning. As shown in Fig. 8.12 the solid red line is the way the model is supposed to look with everything nice and near the line. But then an influential point, as indicated in green, comes along and moves the whole line towards itself when trying to minimize the sum of squares errors. Thus the reason of the weird bumps in Fig. 8.11(b). Influential points steer the model away from the general truth, thereby, disrupting the prediction model. According to statistics of regression analysis, leverage is considered as a measure of how far away an independent observation is from the rest of other observations. Leverage point and influential points are two different things. High leverage points are not necessarily very influential and vice-versa is not true either.

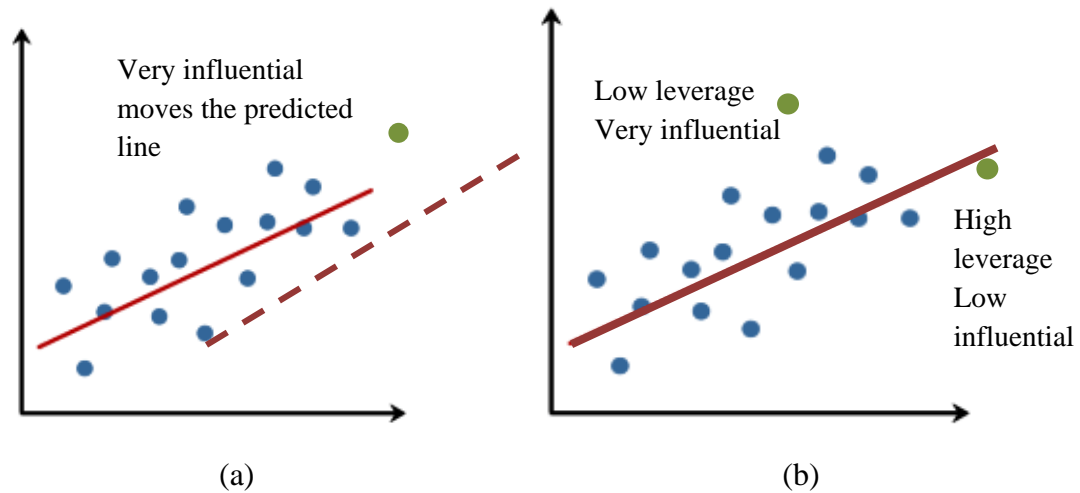


Fig. 8.11. Differentiating between outliers in terms of leverage and influence

## I. Deep Neural Network

To create an advanced fault detection algorithm capable of deep learning and be able to generate preventive actions from the data captured over a period of time, a neural network based parameter estimator is of dominating importance. Artificial neural networks (ANNs) have been used for a long time to detect and regulate the non-linearity in dynamic systems since ANN can estimate an extensive range of non-linear functions to varied degree of desired accuracy. They can be implemented in parallel to reduce computational time and

have immunity to noisy data which means for example, flux data with increased harmonic ripples [6]. To increase fault-tolerant capabilities of the algorithm, multi-layered neural network is used which is stated as deep neural network. The working principle of DNN has been explained in Section 7.3. The technique for DNN used here is the same except the purpose is different. The trained results can be retrained till adequate results are achieved. Finally, they are validated and tested before producing the best predicted value [7].

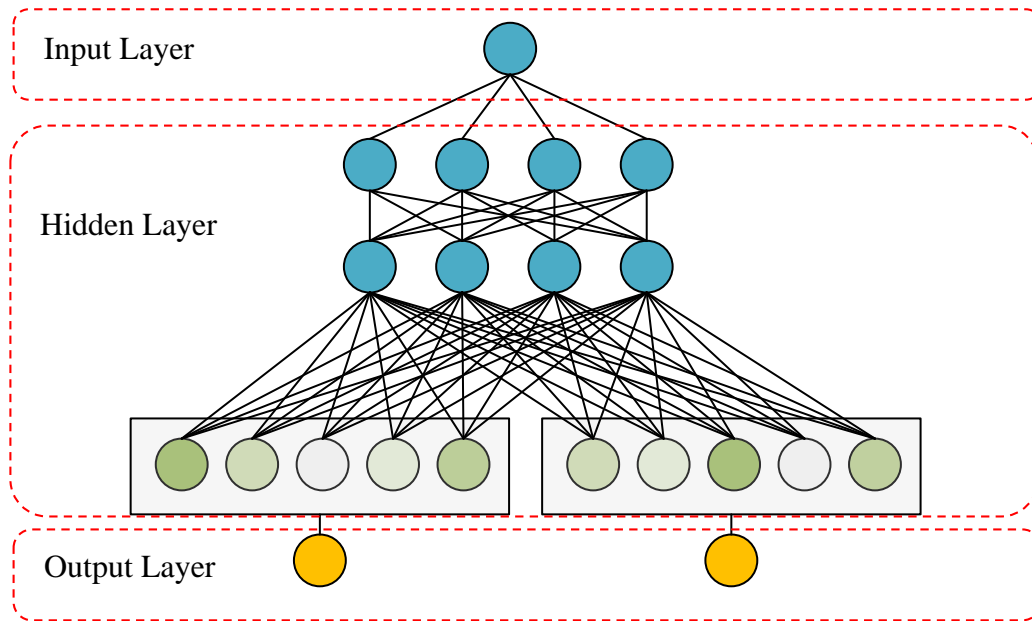


Fig. 8.12. Deep Neural Network with dense embedding.

#### *J. Dual Memorization and Generalization Machine Learning Algorithm Development*

Linear models are faster in terms of processing time considering they have less complexities. But with the inclusion of non-linear features like variation of flux values of the motor due to imbalance condition, the detection algorithm can no longer be used as a regression and classification problem with sparse inputs.

The Memorization and Generalization neural network uses both linear model combined with a Generalization neural network classifier/regressor to predict the target values of a set of data. A linear model uses a single weighted sum of features to make a prediction, opposed to a neural network, which uses multiple weighted connections. The network

operates by combining the weighted sum of output log odds of the Memorization and Generalization components, then this value is put through to a single logistic loss function to enable joint training; the values from the back propagation are also put through both components of the model, thus reinforcing the idea of a combined model.

The linear model, referred to as the Memorization component as illustrated in the left side of Fig. 8.14 can be expressed as (8.30).

$$y = m^T x + b \quad (8.30)$$

where  $y$  is the predicted value which in this case is the flux values,  $x$  is a vector of  $n$  features which includes voltage and current,  $m$  is the array of parameters as defined whereas  $b$  is the bias used in deep neural network as explained in Section 8.4 I. Voltage and current are regarded as feature inputs for the DMG-ML. Interaction of these feature can be considered voltage and current features are directly related to flux. Repeatedly cross-featuring done while training the algorithm leads to memorization of cross-feature interactions. These cross-features ultimately lead to the prediction of likelihood of the flux values are good or bad. Since the machine model is non-linear, the dataset can have millions or trillions of data to process. This needs less manual cross-feature engineering which is accomplished by the Generalization component.

The Generalization component, which is a feed-forward deep neural network, as shown in the right half of Fig. 8.14 includes the hidden layer and dense embeddings [8]. For categorical features, the original inputs are feature values of voltage and current from the machine under test. Each of these sparse input of voltage and current, high-dimensional categorical features are converted into a low-dimensional and condensed real-valued vector, called dense embedding vector. The dimensionality of the embeddings are of varying order depending on the amount of data collected from the running motor. Initially, embedding vectors are assigned random values which are trained to minimize the loss function of the predicted flux reference during model training. These dense embedding vectors are then fed into the hidden layers of the deep neural network. Each hidden layer performs the following computation as in (8.31).

$$a^{(n+1)} = f(W^n a^n + b^n) \quad (8.31)$$



where  $f$  is the activation function.  $a^n$ ,  $b^n$ , and  $w^n$  are the activations, bias, and model weights for  $n$ -th layer. The Generalization component in short generalizes the predictions which needs less specific data input values for proper prediction. But it needs more feature engineering. If there is less feature engineering, deep neural networks of the Generalization component can generalize better to unseen feature combinations through low-dimensional dense embeddings learned from the sparse features. Deep neural networks with embeddings tends to over-generalize and recommend less relevant flux values. Dual Memorization and Generalization learning jointly train wide linear models and deep neural networks to combine the benefits of memorization of the sparse data used as a part of deep learning and generalization of flux prediction values to achieve similar values at much lesser computational time. If the training was disjoint, each individual model size would need larger computational space and time.

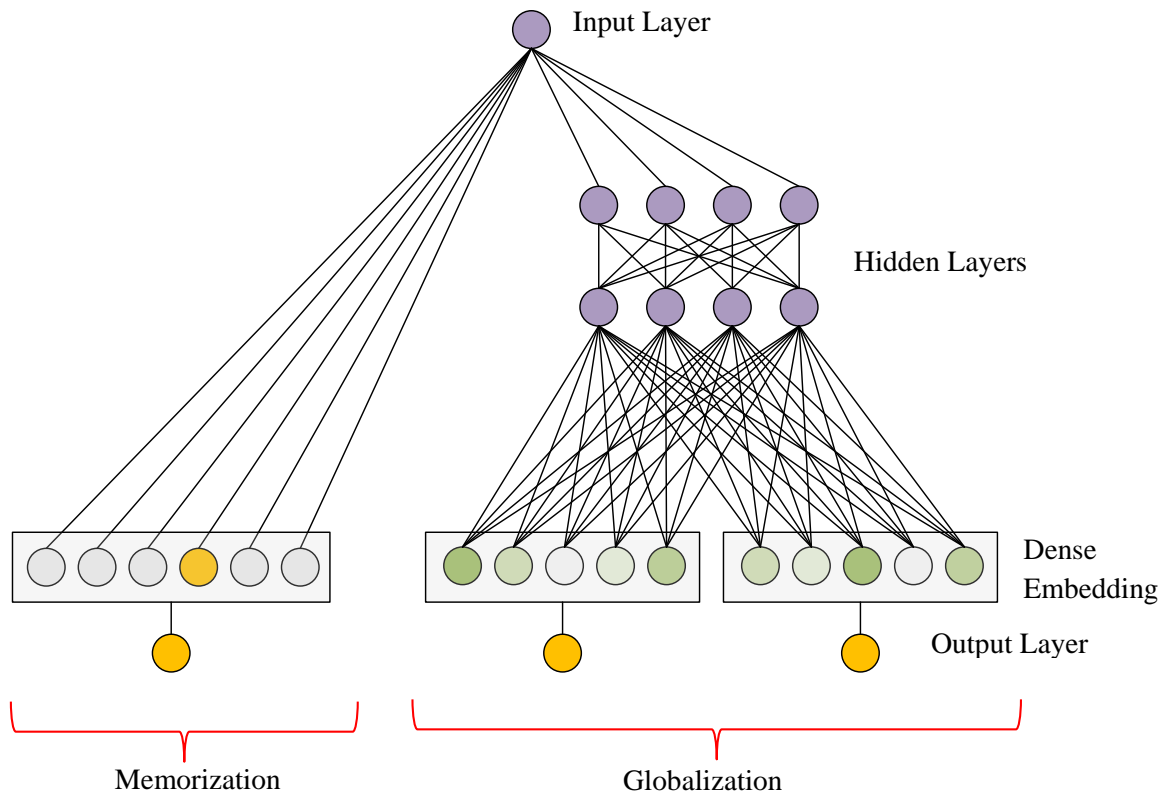


Fig. 8.13. Dual memorization and generalization machine learning used for flux prediction.

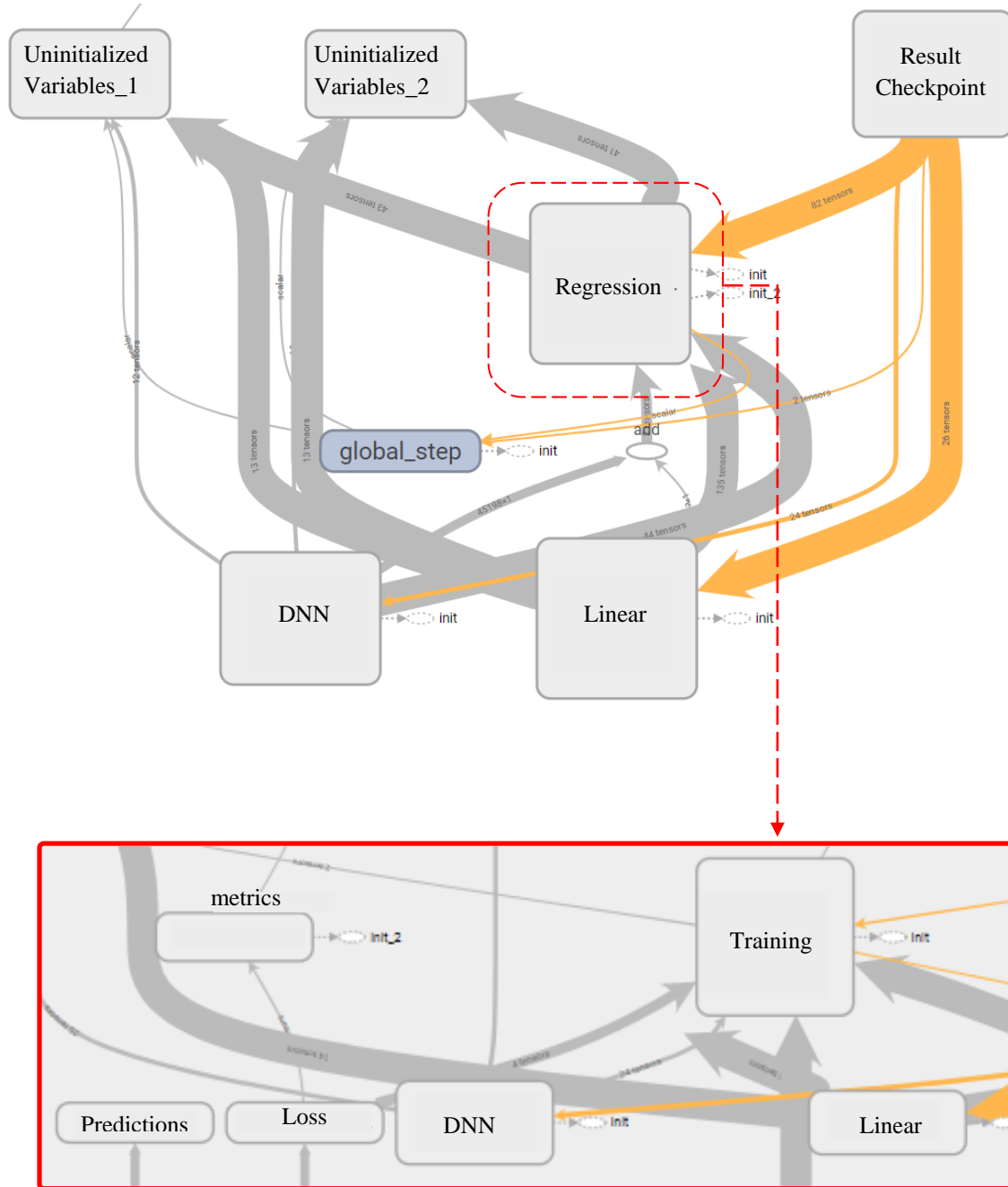


Fig. 8.14. Complete flow of dual memorization and generalization machine learning.

The weighted sum of predicted flux output of both Memorization and Generalization components are one common logistic loss function for joint training. In usual hybrid neural network based algorithms, individual models are trained independently and then their predictions are combined only at the output but not during training. Joint training of DMG-ML has the advantage of optimizing parameters of both models simultaneously. Another

advantage of joint training is the Memorization part only needs to supplement the weaknesses of the Generalization part with a small number of cross-product feature transformations and vice versa, rather than a full-size dual separate model. Thus saving on computational time. Joint training of this DMG-ML is done by back-propagating the gradients from the output to both the Memorization and Generalization part of the model simultaneously using mini-batch stochastic optimization. The overall DMG-ML was monitored by Follow-the-regularized-leader (FTRL) algorithm [9] with L1 regularization as the optimizer for the Memorization part of the model, and AdaGrad [10] for the Generalization part. Thus the Memorization and Generalization model can be summed with the model's prediction as (8.32)

$$P(Y = n | X) = w_{memorization}^T [x, \phi(x)] + w_{generalization}^T a^{n_f} + b \quad (8.32)$$

where  $Y$  is the binary class label,  $\phi(x)$  are the cross product transformations of the original features  $x$ , and  $b$  is the bias term.  $W_{memorization}$  is the vector of all Memorization model weights, and  $w_{generalization}$  are the weights applied on the final activations  $a^{n_f}$  [11].

### 8.5. Experimental Validation and Result Analysis

The implementation of proposed DMG-ML based magnetic flux reference method has been explained in this section. The stator inter-turn fault based IM is connected to a DC machine as a load which is in-turn connected to a load bank as shown in Fig. 8.16. This load bank helps in loading the faulty machine to different levels. Several tests were performed at different operating conditions such as variable speed and loading conditions. A high performance 32-bit microcontroller capable of real-time control is used to run the IM. The flux, voltage and current as shown in Fig. 8.2 are the features used as data capture and fed to the control board which converts into digital signal and feds to the computer which is running the DMG-ML. The system can handle a large amount of data capture for storing during each test. It triggers the proposed DMG-ML algorithm which finally leads to prediction of magnetic flux reference and results are displayed on the computer. The experiments have been performed with and without inverter to neglect the effect of any inverter fault that might be present. For measuring the magnetic flux of the motor, an observer search coil has been wound on the previously detected faulty phase of the IM.

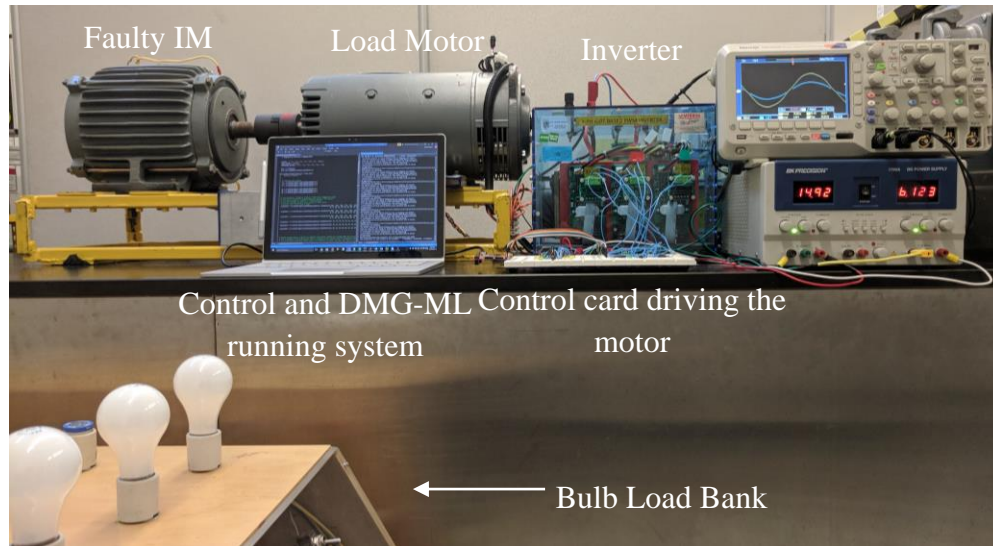
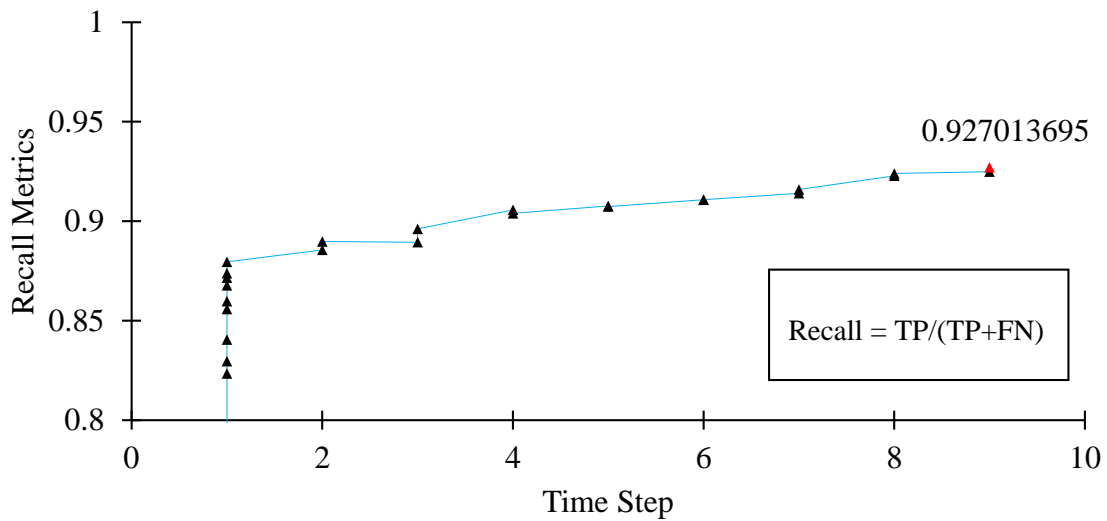


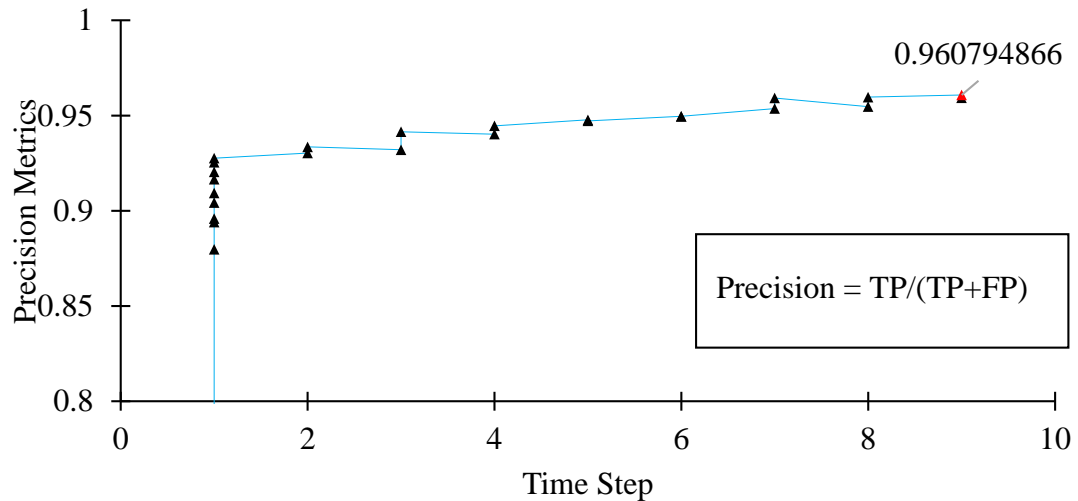
Fig. 8.15. Experimental setup using faulty IM for voltage and current feature extraction for input along with flux input for validation of DMG-ML.

After modelling and simulating the faulty IM in FEA, it was clear how the magnetic flux density in air-gap is affected as well as other performance factors of the machine. The novel DMG-ML based magnetic flux reference prediction for the 7.5 hp faulty aluminum rotor IM has been studied and compared with real-time flux values under various speeds and loads in order to investigate the reliability of the proposed advanced methodology. Initial predictions for flux by DMG-ML was extremely low when compared with the search coil values. But after repetitive training, the algorithm started adjusting the lower embedding values to high dimensional dense embedding values which in-turn led to better prediction. Thereby, overall model was improved and a significant increase in accuracy was noticed. The accuracy of the DMG-ML algorithm as defined by (8.22) is at 92.2% when both Memorization and Generalization models are operating jointly. The progressive increase in accuracy as increase in iterations of training has been illustrated in Fig. 8.17(a). It can be clearly seen that initial training values had an accuracy of around 83% but with subsequent training, the accuracy kept increasing till it was stabilized. But if just the Memorization model is used then the accuracy of the algorithm drops to 90.5% and if only Generalization model is used, it drops to 88.2%. Since accuracy is not enough to determine the machine learning algorithm performance, the progressive precision as well as recall has been presented in Figs. 8.17(b) and (c).

Finally, the DMG–ML settled after being correctly trained. Now the algorithm operated in the good model condition as explained earlier. The best trained predicted flux reference was extremely close to the flux values as obtained from the experiment as shown in Figs. 8.18(a), (b) and (c). The proposed intelligent DMG–ML was trained in such a way that the magnetic flux reference can be predicted at any operating condition of the motor. Since this DMG–ML algorithm also knows the difference between good flux and bad flux values, indicating a fault occurrence in the motor using the predicted flux values is now a much less complex task and also does not need the incipient condition to notice fault occurrence.



(a)



(b)

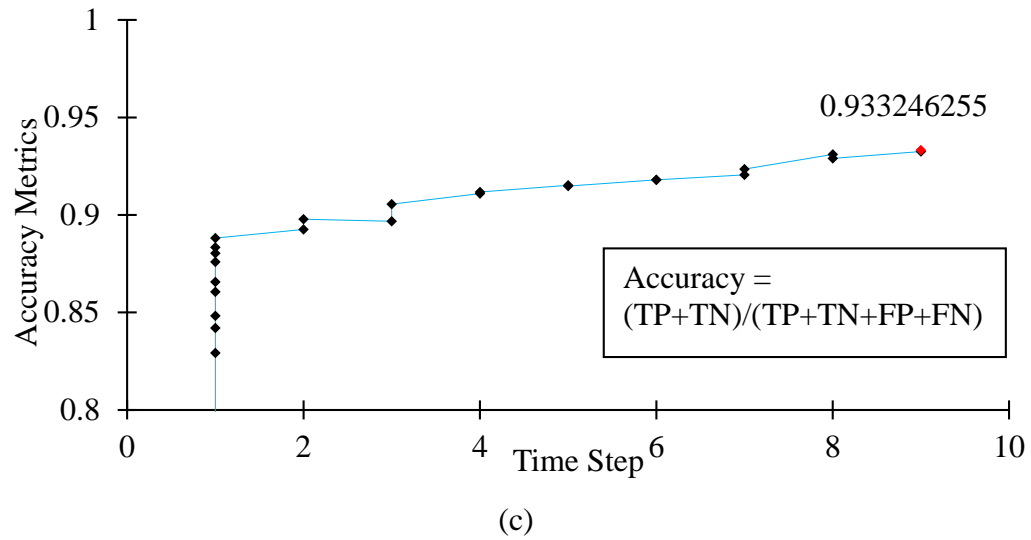
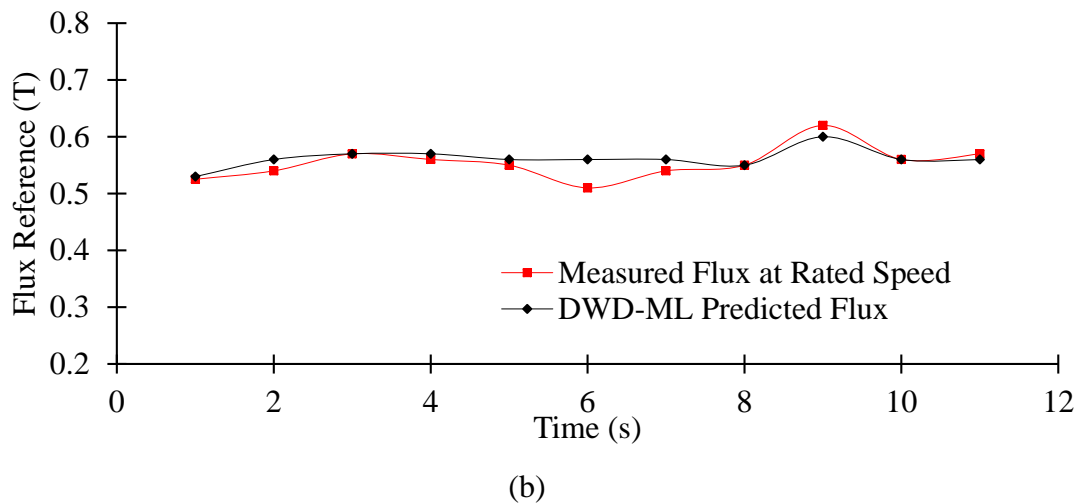
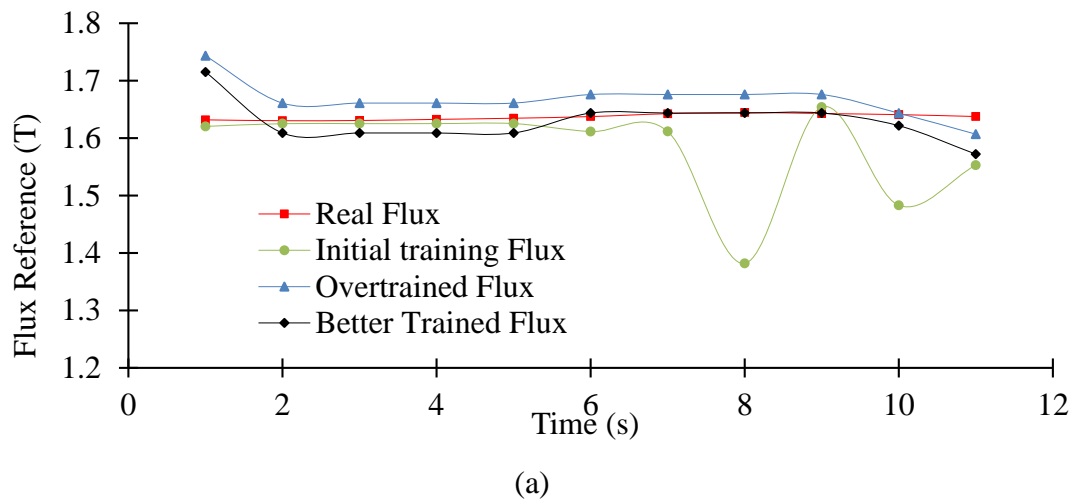


Fig. 8.16. DMG-ML metrics determining (a) Progressive Recall. (b) Progressive Precision. (c) Progressive Accuracy variation over repetitive iteration.



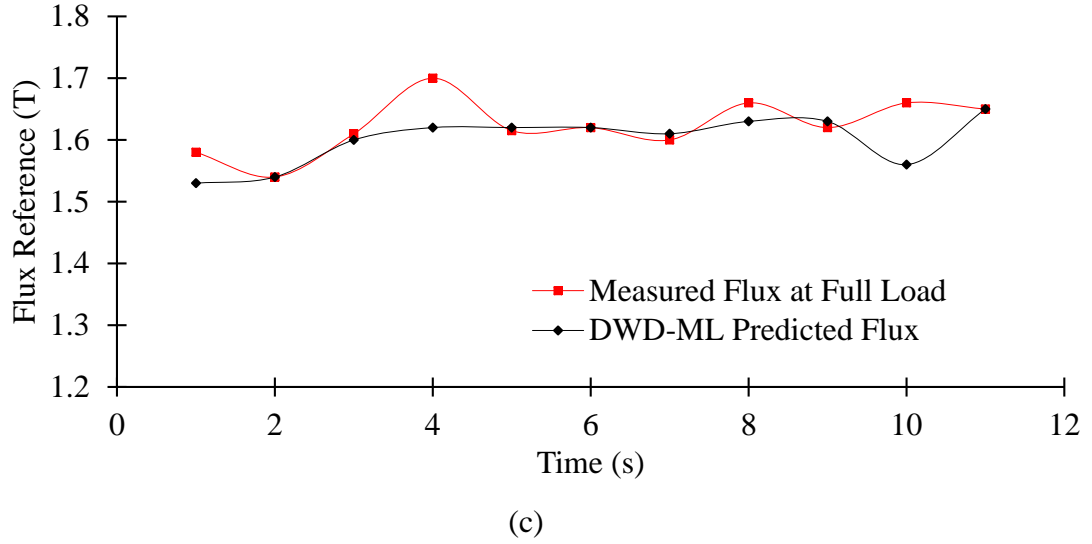


Fig. 8.17. DMG–ML based results. (a) Flux values as measured experimentally as well as during different training conditions and variation. (b) Comparison of magnetic flux reference at rated speed, and 10 Nm load. (c) Comparison of magnetic flux reference 300 rpm and rated load.

## 8.6. Conclusion

This chapter proposed a novel advanced Dual Memorization and Generalization Machine Learning algorithm for prediction of magnetic flux reference with increased accuracy and lower computational speed. This method can detect or predict a fault by predicting the flux values occurring due to stator winding short circuit before an incipient fault stage, evaluating its deviation from the real flux values and then classifying into flux values for healthy motor or faulty motor, thereby preventing the complete break-down of the motor while the EV is being driven on the road. The results obtained from the experimental were compared with the DMG-ML predicted flux reference validating the proposed method. Since this is an advanced machine learning algorithm, the prediction of flux reference which can be used for vector control of the motor, only gets better with time and increase in data capture.

## 8.7. References

- [1] T. Ince, S. Kiranyaz, L. Eren, M. Askar and M. Gabbouj, "Real-Time Motor Fault Detection by 1-D Convolutional Neural Networks," *IEEE Transactions on Industrial Electronics*, vol. 63, no. 11, pp. 7067-7075, Nov. 2016.

- [2] M. Eftekhari, M. Moallem, S. Sadri and M. F. Hsieh, "Online Detection of Induction Motor's Stator Winding Short-Circuit Faults," *IEEE Systems Journal*, vol. 8, no. 4, pp. 1272–1282, Dec. 2014.
- [3] M. Behrooz "Incipient Fault Diagnosis in Squirrel-Cage Induction Motors", Ph.D. dissertation, Dept. Elect. Eng., Marquette University, Wisconsin, 2005.
- [4] E. Schaeffer, "Diagnostic des Machines Asynchrones: Modèles et Outils Paramétriques Dédiés à La Simulation et à La Détection de Défauts," Ph.D. dissertation, Dept. Elect. Eng., Univ. Nantes, Nantes, France, 1999.
- [5] D. G. Dorrell, J. K. H. Shek, and M. F. Hsieh, "The Development of Indexing Method for the Comparison of Unbalanced Magnetic Pull in Electrical Machines," *IEEE Transactions on Industry Applications*, vol. 52, no. 1, pp. 145-153, Jan. 2016.
- [6] D. T. Tran, N. Ono, and E. Vincent, "Fast DNN Training Based on Auxiliary Function Technique," in the Proc. of *2015 IEEE International Conference on Acoustics, Speech and Signal Processing*, pp. 2160-2164, South Brisbane, 2015.
- [7] M. Barzegaran, A. Mazloomzadeh, and O. A. Mohammed, "Fault Diagnosis of the Asynchronous Machines Through Magnetic Signature Analysis Using Finite-Element Method and Neural Networks," *IEEE Transactions on Energy Conversion*, vol. 28, no. 4, pp. 1064-1071, Dec. 2013.
- [8] Y. He *et al.*, "Deep-Reinforcement-Learning-Based Optimization for Cache-Enabled Opportunistic Interference Alignment Wireless Networks," *IEEE Transactions on Vehicular Technology*, vol. 66, no. 11, pp. 10433-10445, Nov. 2017.
- [9] A. P. Ta, "Factorization Machines with Follow-The-Regularized-Leader for CTR Prediction in Display Advertising," in the Proc. of *2015 IEEE International Conference on Big Data (Big Data)*, pp. 2889-2891, Santa Clara, CA, 2015.
- [10] A. Senior, G. Heigold, M. Ranzato, and K. Yang, "An Empirical Study of Learning Rates in Deep Neural Networks for Speech Recognition," in the Proc. of *IEEE International Conference on Acoustics, Speech and Signal Processing*, pp. 6724-6728, Vancouver, BC, 2013.
- [11] H. Cheng, L. Koc, J. Harmsen, T. Shaked, T. Chandra, H. Aradhye, G. Anderson, W. Chai, M. Ispir, R. Anil, Z. Haque, L. Hong, V. Jain, X. Liu, and H. Shah, "Wide & Deep Learning for Recommender Systems", Cornell University Library, arXiv:1606.07792, June 2016.



## **CHAPTER 9**

### **CONCLUSION AND SUGGESTED FUTURE WORK**

#### *9.1. Conclusion*

This chapter is more of a summarization of the conclusions of the previous chapters which ultimately led to the development of a novel machine learning based magnetic flux prediction which can be used for fault diagnosis as well as for fault-tolerant control. A brief summary is presented here.

Chapter 1 showed how the market of electric vehicles is booming not only in North America but all over the world. As there is a rapid progress in manufacturing and development in EVs, there is a necessity for the safety of passengers. This culminates to the development of a fault diagnostic method so that the person driving an EV does not get stranded. Since most fault diagnostic methods have been for industrial purposes, a faster, more intelligent, more efficient method of fault diagnosis for motors used in EV has been proposed.

Chapter 2 presented an approach to design the fault motor under test so as to identify and understand the stator fault occurred and motor performance from the design aspect. This study has been vital to understand which features would be best needed to develop a machine learning algorithm to detect fault faster. The study concluded with current, temperature and flux as the prime features for machine learning.

Chapter 3 presented IPSO as a predictive method which provides an active online tuning of stator resistive parameters using temperature as a vital feature. This showed how swarm optimization predicted temperature can be used for predicting parameters and any deviation in those parameters is an indication of incipient fault. This temperature feature based fault detection was extended by developing a novel Duplex Neural-Lumped Parameter Thermal Model which used neural networks in collaboration with thermal model to predict temperature and fault faster than the swarm optimization method. This showed how artificial intelligence can be more reliable compared to old predictive methods.

Chapter 4 was the beginning of the prime focus of this dissertation where flux is used at the primary feature for stator inter-turn fault detection. Using magnetic equivalent circuit and harmonic analysis method, a novel harmonic block was developed which helped in developing a fault-tolerant control using the better predicted magnetic flux reference for the control.

Chapter 5 discussed about how the novel harmonic compensation block developed in the previous chapter helps in making the control more fault tolerant. The developed control was programmed into a 32-bit microcontroller which was used to run the faulty motor. The motor performance before and after the developed control has been shown proving how a well predicted flux reference can be used for predictive fault-tolerant control.

Chapter 6 extended the work done in the previous chapter by including the particle swarm optimization which was previously developed for using it with temperature as a feature. PSO based prediction of flux reference was helpful in reducing the delay caused in evaluating a new flux reference in Chapter 5. The values of predicted flux were compared with the results as experimentally obtained from the search coil placed along the tooth of the faulty phase.

Chapter 7 gave a brief explanation of what is machine learning and how it can be used for developing faster fault-tolerant control. The unbalanced magnetic pull created by the faulty IM developed an uneven flux in the air-gap. Deep neural network was used to predict the flux since PSO was a much slower and less reliable method. This chapter proves how the accuracy improved in flux prediction with the development of the DNN based flux reference method.

Chapter 8 is the conclusive chapter where the developed higher accuracy and more precise dual memorization and generalization machine learning technique has established. The DMG-ML had a accuracy of 93.3% and a precision in prediction of 96%. This developed technique was faster because it used memorization to find those obvious flux predicted values by repeating when it sees a similar trend, thus reducing the computational time while generalization was used to find new magnetic flux references while it came across some unknown features. This developed method is not yet ready to be implemented

in a vehicular environment due to lack of faster computational chips. But this DMG-ML is ready to be implemented in powerful chips like the upcoming chips like the Intel Nervana Neural Network Processor which can process data at 1TB/s.

## *9.2. Future Work*

- A. Implementation of DMG-ML based predicted flux reference in a model reference adaptive control system to operate on a traction motor. Repeat the complete scenario for a real EV motor and compare with the present driving condition.
- B. Implementation of this machine learning algorithm onto powerful chips which are deep learning ready like the upcoming chip Nervana Neural Network Processor from Intel which can process data at 1TB/s. Other companies like NVIDIA have driver's boards namely DRIVE Pegasus and DRIVE Xavier to take care of high power deep learning calculations. Even ARM just launched a new machine learning capable chip on February 13<sup>th</sup>, 2018 can be used for this work.
- C. Since motor control is developed on independent chips with is placed inside the motor drive unit, and if the fault protection machine learning algorithm is on a separate deep learning drive unit, a seamless communication protocol needs to be established to provide least amount of delay in communication after new flux parameters have been computed.
- D. Implementing the developed algorithm on several motors to have a much deeper learning and making the fault-tolerant drive universal.
- E. Prototype a drive board integrating both motor control as well as DMG-ML into one unit.
- F. Extend the limits of using this algorithm to detect other faults in the complete EV powertrain.
- G. Since most modern electric cars are moving to the development of self-driving capabilities, time sharing of different tasks along with the DMG-ML based control.

## **APPENDIX A: ABBREVIATIONS**

<b>Abbreviation</b>	<b>Explanation</b>
AC	Alternating Current
2D	Two Dimensional
3D	Three Dimensional
ALIM	Aluminium Rotor Induction Motor
ANN	Artificial Neural Networks
AWD	All-wheel Drive
AWG	American Wire Gauge
CFD	Computational Fluid Dynamics
CRIM	Copper rotor Induction Motor
DAQ	Data Acquisition
DC	Direct Current
DMG-ML	Dual Memorization and Generalization Machine Learning
DNLTN	Duplex Neural-Lumped Thermal Network
DNN	Deep Neural Network
EMF	Electro Motive Force
EPRI	Electric Power Research Institute
EV	Electric Vehicles
FEA	Finite Element Analysis
FEM	Finite Element Method
FFT	Fast Fourier Transformation
FN	False Negative
FN	False Negative
FP	False Positive
FTRL	Follow-the-regularized-leader

HEV	Hybrid Electric Vehicle
IEEE-IAS	IEEE Industry Applications Society
IM	Induction Motor
IPSO	Improved Swarm Particle Optimization
LIDAR	Light Detecting and Ranging
LP	Lumped Parameter
LPTN	Lumped Parameter Thermal Network
MAE	Mean Absolute Error
MCSA	Motor Current Signature Analysis
MEC	Magnetic Equivalent Circuit
MMF	Magneto Motive Force
MSE	Mean Squared Error
OSC	Observer Search Coil
PID	Proportional Integral Derivative
PMSM	Permanent Magnet Synchronous Machines
PSO	Particle Swarm Optimization
RMS	Root Mean Square
RTD	Resistance Temperature Detectors
SSE	Sum of Squared Error
TN	True Negative
TNR	True Negative Rate
TP	True Positive
TPR	True Positive Rate
UMP	Unbalanced Magnetic Pull
VFD	Variable Frequency Drive

## APPENDIX B: LIST OF PUBLICATIONS

### *Journals*

- [1] **E. Ghosh**, A. Mollaeian, S. Kim, J. Tjong and N. C. Kar, "DNN-Based Predictive Magnetic Flux Reference for Harmonic Compensation Control in Magnetically Unbalanced Induction Motor," *IEEE Transactions on Magnetics*, vol. 53, no. 11, pp. 1-7, Nov. 2017.
- [2] A. Mollaeian, **E. Ghosh**, H. Dhulipati, J. Tjong, and N. C. Kar, "3-D Sub-Domain Analytical Model to Calculate Magnetic Flux Density in Induction Machines with Semiclosed Slots Under No-Load Condition," *IEEE Transactions on Magnetics*, vol. 53, no. 6, pp. 1-5, June 2017.
- [3] **E. Ghosh**, A. Mollaeian, W. Hu and N. C. Kar, "A Novel Control Strategy for Online Harmonic Compensation in Parametrically Unbalanced Induction Motor," *IEEE Transactions on Magnetics*, vol. 52, no. 7, pp. 1-4, July 2016.
- [4] **E. Ghosh**, A. Mollaeian, J. Li, and N. C. Kar, "Dual Wide and Deep Machine Learning based Magnetic Flux Reference Prediction for Fault Diagnosis of Induction Motor," to be submitted to *IEEE Transactions on Industrial Informatics*, 2018.
- [5] **E. Ghosh**, A. Mollaeian, and N. C. Kar, "Prediction of Magnetic Flux Reference using DMG Machine Learning for Fault-tolerant Control of Magnetically Unbalanced Induction Motor," to be submitted to *IEEE Transactions on Industrial Electronics*, 2018.
- [6] **E. Ghosh**, S. Mukundan, H. Dhulipati, and N. C. Kar, "Design of Harmonics Analysis Block for Faulty Induction Motor Using Magnetic Equivalent Circuit and Observer Search Coil," to be submitted to *IET Electric Power Application*, 2018.
- [7] A. Mollaeian, **E. Ghosh**, S. Kim, J. Tjong and N. C. Kar, "Parametric and Sensitivity based Design Optimization to Extend Constant Power Speed Ratio of Induction Machine for EV Application," to be submitted to *IEEE Transactions on Transportation Electrification*, 2018.

## ***Conference***

- [1] F. Ahmed, **E. Ghosh**, S. Mukundan, H. Dhulipati, and N. C. Kar, "LPTN and FEA Modeling for Thermal Characterization of an Interior Permanent Magnet Synchronous Motor (IPMSM) for Electric Vehicle Application," in the Proc. of *2018 Energy & Sustainability Symposium*, Windsor, ON, June 2018.
- [2] A. Kundu, **E. Ghosh**, and N. C. Kar, "Survey of T-type Neutral Point Clamped Traction Drive for EV Application," in the Proc. of *2018 Energy & Sustainability Symposium*, Windsor, ON, June 2018.
- [3] A. Mollaeian, M. Mehdi, **E. Ghosh**, A. Edrisy, S. Kim, J. Tjong, and N. C. Kar, "Investigation of Electromagnetic Torque Capability Reduction of Induction Machine due to Magnetic Property Deterioration of Laminations due to Manufacturing," accepted in the Proc. of *International Conference on Magnetism*, July, 2018.
- [4] H. Dhulipati, **E. Ghosh**, S. Mukundan, J. Tjong, and N. C. Kar, "Adagrad Algorithm based Optimal Slot-pole Selection for Reduced Inductance Harmonics in Concentrated Wound Multiphase PMSM," in the Proc. of *IEEE International Magnetics Conference*, pp. 1-1, Singapore, 2018.
- [5] **E. Ghosh**, A. Mollaeian, S. Kim and N. C. Kar, "DNN Predictive Magnetic Flux Control for Harmonics Compensation in Magnetically Unbalanced Induction Motor," in the Proc. of *IEEE International Magnetics Conference*, pp. 1-1 Dublin, 2017.
- [6] **E. Ghosh**, A. Mollaeian, S. Kim, J. Tjong, and N. C. Kar, "Intelligent Flux Predictive Control Through Online Stator Inter-Turn Fault Detection for Fault-Tolerant Control of Induction Motor," in the Proc. of *IEEE International Conference on Industrial Technology (ICIT)*, pp. 306-311, Toronto, ON, 2017.
- [7] A. Mollaeian, **E. Ghosh**, H. Dhulipati, J. Tjong and N. C. Kar, "3-D Sub-Domain Analytical Model to Calculate Magnetic Flux Density in Induction Machines with Semi-Closed Slots Under No-Load Condition," in the Proc. of *2016 IEEE Conference on Electromagnetic Field Computation (CEFC)*, pp. 1-1, Miami, FL, 2016.
- [8] **E. Ghosh**, F. Ahmed, A. Mollaeian, J. Tjong and N. C. Kar, "Online Parameter Estimation and Loss Calculation Using Duplex Neural — Lumped Parameter

- Thermal Network for Faulty Induction Motor," in the Proc. of *IEEE Conference on Electromagnetic Field Computation (CEFC)*, pp. 1-1, Miami, FL, 2016.
- [9] **E. Ghosh**, A. Mollaeian, W. Hu and N. C. Kar, " A Novel Control Strategy for Online Harmonic Compensation in Parametrically Unbalanced Induction Motor," in the Proc. of *2016 IEEE International Magnetics Conference*, pp. 1-1, San Diego, 2016.
- [10] F. Ahmed, **E. Ghosh** and N. C. Kar, "Transient Thermal Analysis of a Copper Rotor Induction Motor Using a Lumped Parameter Temperature Network Model," in the Proc. of *IEEE Transportation Electrification Conference and Expo*, pp. 1-6, Dearborn, MI, 2016.
- [11] **E. Ghosh**, F. Ahmed, M. M. Sangdehi and N. C. Kar, "Temperature Influenced Online Stator Resistance Estimation Using an Improved Swarm Intelligence Technique for Induction Machine," in the Proc. of *IEEE Transportation Electrification Conference and Expo (ITEC)*, pp. 1-6, Dearborn, MI, 2015.



## APPENDIX C: LIST OF INDUSTRIAL PROJECTS AND SCHOLARSHIPS

### *Projects Undertaken*

1. *NSERC CRD project with MAGNA International Ltd.*
  - Study of various inverter topologies for traction application.
  - Modelling and investigation of multilevel traction converter drives for implementation with control algorithm for new high speed motor application.
  - Preparing EPT-150 for universal motor testing by developing base plate, developing and performing torque calibration system.
  - Development of cooling system for various motor under test.
  - Scripting of EPT system for automated testing.
2. *NSERC Engage project with TM4 Inc.*
  - Development of Loss Model for Lumped Parameter Thermal Network Model for Thermal Analysis of Surface Permanent Magnet Synchronous Machines for Application in Hardware-in-Loop Environment
3. *OCE Talent Edge project at D&V Electronics Ltd.*
  - Design and development of DC-DC Converter for bi-directional regenerative power unit under project entitled “Development of High-performance Bi-directional AC-DC Power Source”
  - Worked with company researchers and engineers “Development of a High Performance 48VDC Battery Simulator”
  - Worked with company researchers and engineers on “Modelling of existing RG-BS20,” as faster method to tune PID controller
  - Worked on the project “Programming and prototyping of Master Controller,” using low cost SoC devices.
4. *NSERC CRD project with Ford Motor Company Ltd. and D&V Electronics Ltd.*

- Motor prototype development for “Powertrain Components and Systems for Next-generation Electric Vehicles”
  - Equip the electric power train for testing with drives and drive cycle based testing
5. *ORF project with Ford Motor Company Ltd. and D&V Electronics Ltd.*
    - Build base plate, coupling, controls and test setup for testing the motors for “Multi-phase E-motor design for direct-drive applications,”
    - Test for efficiency map, loss map, parameter changes, temperature, etc.
  6. *Solar panel based electric golf cart with Unconquered Sun Solar Technologies Inc.*
    - Development of an optimally-sized powertrain system with built-in charger for electric golf carts
  7. *NSERC Engage project entitled with IGB Automotive Ltd.*
    - Investigation of noise reduction schemes for bldc motors in comfort seat ventilation module. Performance mapping of BLDC motors in car seat under various operating conditions

### ***Scholarships Received***

1. Research Scholarship received from Canada Research Chair Program in Electrified Transportation Systems, Centre for Hybrid Automotive Research and Green Energy, 2013 – 2018.
2. University of Windsor Graduate Teaching Assistance, 2013 – 2017.
3. Outstanding Graduate Student Scholarship honoured by Graduate Student Society, University of Windsor, March 2017.
4. Industry-Academic R&D Collaboration Fellowship honoured by Ontario Centres of Excellence, January 2016.
5. Outstanding Graduate Student Scholarship honoured by Graduate Student Society, University of Windsor, August 2014.

## APPENDIX D: PERMISSION FOR USING IEEE PUBLICATIONS

5/2/2018

RightsLink® by Copyright Clearance Center



RightsLink®

Home

Create Account

Help



**Title:** Temperature influenced online stator resistance estimation using an improved swarm intelligence technique for induction machine

**Conference Proceedings:** 2015 IEEE Transportation Electrification Conference and Expo (ITEC)

**Author:** Eshaan Ghosh; Firoz Ahmed; Mahdi Mousavi Sangdehi; Narayan C. Kar

**Publisher:** IEEE

**Date:** 14-17 June 2015

Copyright © 2015, IEEE

**LOGIN**

If you're a copyright.com user, you can login to RightsLink using your copyright.com credentials.

Already a RightsLink user or want to [learn more?](#)

### Thesis / Dissertation Reuse

**The IEEE does not require individuals working on a thesis to obtain a formal reuse license, however, you may print out this statement to be used as a permission grant:**

*Requirements to be followed when using any portion (e.g., figure, graph, table, or textual material) of an IEEE copyrighted paper in a thesis:*

- 1) In the case of textual material (e.g., using short quotes or referring to the work within these papers) users must give full credit to the original source (author, paper, publication) followed by the IEEE copyright line © 2011 IEEE.
- 2) In the case of illustrations or tabular material, we require that the copyright line © [Year of original publication] IEEE appear prominently with each reprinted figure and/or table.
- 3) If a substantial portion of the original paper is to be used, and if you are not the senior author, also obtain the senior author's approval.

*Requirements to be followed when using an entire IEEE copyrighted paper in a thesis:*

- 1) The following IEEE copyright/ credit notice should be placed prominently in the references: © [year of original publication] IEEE. Reprinted, with permission, from [author names, paper title, IEEE publication title, and month/year of publication]
- 2) Only the accepted version of an IEEE copyrighted paper can be used when posting the paper or your thesis on-line.
- 3) In placing the thesis on the author's university website, please display the following message in a prominent place on the website: In reference to IEEE copyrighted material which is used with permission in this thesis, the IEEE does not endorse any of [university/educational entity's name goes here]'s products or services. Internal or personal use of this material is permitted. If interested in reprinting/republishing IEEE copyrighted material for advertising or promotional purposes or for creating new collective works for resale or redistribution, please go to [http://www.ieee.org/publications\\_standards/publications/rights/rights\\_link.html](http://www.ieee.org/publications_standards/publications/rights/rights_link.html) to learn how to obtain a License from RightsLink.

If applicable, University Microfilms and/or ProQuest Library, or the Archives of Canada may supply single copies of the dissertation.

BACK

CLOSE WINDOW

Copyright © 2018 Copyright Clearance Center, Inc. All Rights Reserved. [Privacy statement](#). [Terms and Conditions](#).  
Comments? We would like to hear from you. E-mail us at [customer@copyright.com](mailto:customer@copyright.com)



# RightsLink®

[Home](#)
[Create Account](#)
[Help](#)


**Title:** Transient thermal analysis of a copper rotor induction motor using a lumped parameter temperature network model

**Conference Proceedings:** 2016 IEEE Transportation Electrification Conference and Expo (ITEC)

**Author:** Firoz Ahmed; Eshaan Ghosh; Narayan C. Kar

**Publisher:** IEEE

**Date:** 27-29 June 2016

Copyright © 2016, IEEE

## LOGIN

If you're a [copyright.com](#) user, you can login to RightsLink using your copyright.com credentials. Already a [RightsLink](#) user or want to [learn more?](#)

## Thesis / Dissertation Reuse

**The IEEE does not require individuals working on a thesis to obtain a formal reuse license, however, you may print out this statement to be used as a permission grant:**

*Requirements to be followed when using any portion (e.g., figure, graph, table, or textual material) of an IEEE copyrighted paper in a thesis:*

- 1) In the case of textual material (e.g., using short quotes or referring to the work within these papers) users must give full credit to the original source (author, paper, publication) followed by the IEEE copyright line © 2011 IEEE.
- 2) In the case of illustrations or tabular material, we require that the copyright line © [Year of original publication] IEEE appear prominently with each reprinted figure and/or table.
- 3) If a substantial portion of the original paper is to be used, and if you are not the senior author, also obtain the senior author's approval.

*Requirements to be followed when using an entire IEEE copyrighted paper in a thesis:*

- 1) The following IEEE copyright/ credit notice should be placed prominently in the references: © [year of original publication] IEEE. Reprinted, with permission, from [author names, paper title, IEEE publication title, and month/year of publication]
- 2) Only the accepted version of an IEEE copyrighted paper can be used when posting the paper or your thesis on-line.
- 3) In placing the thesis on the author's university website, please display the following message in a prominent place on the website: In reference to IEEE copyrighted material which is used with permission in this thesis, the IEEE does not endorse any of [university/educational entity's name goes here]'s products or services. Internal or personal use of this material is permitted. If interested in reprinting/republishing IEEE copyrighted material for advertising or promotional purposes or for creating new collective works for resale or redistribution, please go to [http://www.ieee.org/publications\\_standards/publications/rights/rights\\_link.html](http://www.ieee.org/publications_standards/publications/rights/rights_link.html) to learn how to obtain a License from RightsLink.

If applicable, University Microfilms and/or ProQuest Library, or the Archives of Canada may supply single copies of the dissertation.

[BACK](#)
[CLOSE WINDOW](#)

Copyright © 2018 [Copyright Clearance Center, Inc.](#) All Rights Reserved. [Privacy statement](#). [Terms and Conditions](#). Comments? We would like to hear from you. E-mail us at [customercare@copyright.com](mailto:customercare@copyright.com).



# RightsLink®

[Home](#)
[Create Account](#)
[Help](#)


**Title:** A Novel Control Strategy for Online Harmonic Compensation in Parametrically Unbalanced Induction Motor

**Author:** Eshaan Ghosh; Aida Mollaeian; Weusong Hu; Narayan C. Kar

**Publication:** Magnetics, IEEE Transactions on

**Publisher:** IEEE

**Date:** July 2016

Copyright © 2016, IEEE

**LOGIN**

If you're a [copyright.com](#) user, you can login to RightsLink using your copyright.com credentials.

Already a [RightsLink](#) user or want to [learn more?](#)

## Thesis / Dissertation Reuse

**The IEEE does not require individuals working on a thesis to obtain a formal reuse license, however, you may print out this statement to be used as a permission grant:**

*Requirements to be followed when using any portion (e.g., figure, graph, table, or textual material) of an IEEE copyrighted paper in a thesis:*

- 1) In the case of textual material (e.g., using short quotes or referring to the work within these papers) users must give full credit to the original source (author, paper, publication) followed by the IEEE copyright line © 2011 IEEE.
- 2) In the case of illustrations or tabular material, we require that the copyright line © [Year of original publication] IEEE appear prominently with each reprinted figure and/or table.
- 3) If a substantial portion of the original paper is to be used, and if you are not the senior author, also obtain the senior author's approval.

*Requirements to be followed when using an entire IEEE copyrighted paper in a thesis:*

- 1) The following IEEE copyright/ credit notice should be placed prominently in the references: © [year of original publication] IEEE. Reprinted, with permission, from [author names, paper title, IEEE publication title, and month/year of publication]
- 2) Only the accepted version of an IEEE copyrighted paper can be used when posting the paper or your thesis on-line.
- 3) In placing the thesis on the author's university website, please display the following message in a prominent place on the website: In reference to IEEE copyrighted material which is used with permission in this thesis, the IEEE does not endorse any of [university/educational entity's name goes here]'s products or services. Internal or personal use of this material is permitted. If interested in reprinting/republishing IEEE copyrighted material for advertising or promotional purposes or for creating new collective works for resale or redistribution, please go to [http://www.ieee.org/publications\\_standards/publications/rights/rights\\_link.html](http://www.ieee.org/publications_standards/publications/rights/rights_link.html) to learn how to obtain a License from RightsLink.

If applicable, University Microfilms and/or ProQuest Library, or the Archives of Canada may supply single copies of the dissertation.

[BACK](#)
[CLOSE WINDOW](#)

Copyright © 2018 [Copyright Clearance Center, Inc.](#) All Rights Reserved. [Privacy statement](#), [Terms and Conditions](#).  
Comments? We would like to hear from you. E-mail us at [customercare@copyright.com](mailto:customercare@copyright.com)



# RightsLink®

[Home](#)
[Create Account](#)
[Help](#)


**Title:** 3-D sub-domain analytical model to calculate magnetic flux density in induction machines with semi-closed slots under no-load condition

**Conference Proceedings:** Electromagnetic Field Computation (CEFC), 2016 IEEE Conference on

**Author:** Aida Mollaeian

**Publisher:** IEEE

**Date:** Nov. 2016

Copyright © 2016, IEEE

## LOGIN

If you're a [copyright.com](#) user, you can login to RightsLink using your copyright.com credentials. Already a RightsLink user or want to [learn more?](#)

## Thesis / Dissertation Reuse

**The IEEE does not require individuals working on a thesis to obtain a formal reuse license, however, you may print out this statement to be used as a permission grant:**

*Requirements to be followed when using any portion (e.g., figure, graph, table, or textual material) of an IEEE copyrighted paper in a thesis:*

- 1) In the case of textual material (e.g., using short quotes or referring to the work within these papers) users must give full credit to the original source (author, paper, publication) followed by the IEEE copyright line © 2011 IEEE.
- 2) In the case of illustrations or tabular material, we require that the copyright line © [Year of original publication] IEEE appear prominently with each reprinted figure and/or table.
- 3) If a substantial portion of the original paper is to be used, and if you are not the senior author, also obtain the senior author's approval.

*Requirements to be followed when using an entire IEEE copyrighted paper in a thesis:*

- 1) The following IEEE copyright/ credit notice should be placed prominently in the references: © [year of original publication] IEEE. Reprinted, with permission, from [author names, paper title, IEEE publication title, and month/year of publication]
- 2) Only the accepted version of an IEEE copyrighted paper can be used when posting the paper or your thesis on-line.
- 3) In placing the thesis on the author's university website, please display the following message in a prominent place on the website: In reference to IEEE copyrighted material which is used with permission in this thesis, the IEEE does not endorse any of [university/educational entity's name goes here]'s products or services. Internal or personal use of this material is permitted. If interested in reprinting/republishing IEEE copyrighted material for advertising or promotional purposes or for creating new collective works for resale or redistribution, please go to [http://www.ieee.org/publications\\_standards/publications/rights/rights\\_link.html](http://www.ieee.org/publications_standards/publications/rights/rights_link.html) to learn how to obtain a License from RightsLink.

If applicable, University Microfilms and/or ProQuest Library, or the Archives of Canada may supply single copies of the dissertation.

[BACK](#)
[CLOSE WINDOW](#)

Copyright © 2018 [Copyright Clearance Center, Inc.](#) All Rights Reserved. [Privacy statement](#). [Terms and Conditions](#). Comments? We would like to hear from you. E-mail us at [customercare@copyright.com](mailto:customercare@copyright.com)





# RightsLink®

[Home](#)
[Create Account](#)
[Help](#)


**Title:** Online parameter estimation and loss calculation using duplex neural — Lumped parameter thermal network for faulty induction motor

**Conference Proceedings:** Electromagnetic Field Computation (CEFC), 2016 IEEE Conference on

**Author:** Eshaan Ghosh

**Publisher:** IEEE

**Date:** Nov. 2016

Copyright © 2016, IEEE

## LOGIN

If you're a [copyright.com](#) user, you can login to RightsLink using your copyright.com credentials. Already a [RightsLink](#) user or want to [learn more?](#)

## Thesis / Dissertation Reuse

**The IEEE does not require individuals working on a thesis to obtain a formal reuse license, however, you may print out this statement to be used as a permission grant:**

*Requirements to be followed when using any portion (e.g., figure, graph, table, or textual material) of an IEEE copyrighted paper in a thesis:*

- 1) In the case of textual material (e.g., using short quotes or referring to the work within these papers) users must give full credit to the original source (author, paper, publication) followed by the IEEE copyright line © 2011 IEEE.
- 2) In the case of illustrations or tabular material, we require that the copyright line © [Year of original publication] IEEE appear prominently with each reprinted figure and/or table.
- 3) If a substantial portion of the original paper is to be used, and if you are not the senior author, also obtain the senior author's approval.

*Requirements to be followed when using an entire IEEE copyrighted paper in a thesis:*

- 1) The following IEEE copyright/ credit notice should be placed prominently in the references: © [year of original publication] IEEE. Reprinted, with permission, from [author names, paper title, IEEE publication title, and month/year of publication]
- 2) Only the accepted version of an IEEE copyrighted paper can be used when posting the paper or your thesis on-line.
- 3) In placing the thesis on the author's university website, please display the following message in a prominent place on the website: In reference to IEEE copyrighted material which is used with permission in this thesis, the IEEE does not endorse any of [university/educational entity's name goes here]'s products or services. Internal or personal use of this material is permitted. If interested in reprinting/republishing IEEE copyrighted material for advertising or promotional purposes or for creating new collective works for resale or redistribution, please go to [http://www.ieee.org/publications\\_standards/publications/rights/rights\\_link.html](http://www.ieee.org/publications_standards/publications/rights/rights_link.html) to learn how to obtain a License from RightsLink.

If applicable, University Microfilms and/or ProQuest Library, or the Archives of Canada may supply single copies of the dissertation.

[BACK](#)
[CLOSE WINDOW](#)

Copyright © 2018 [Copyright Clearance Center, Inc.](#) All Rights Reserved. [Privacy statement](#). [Terms and Conditions](#). Comments? We would like to hear from you. E-mail us at [customercare@copyright.com](mailto:customercare@copyright.com)



# RightsLink®

[Home](#)
[Create Account](#)
[Help](#)


**Title:** Intelligent flux predictive control through online stator inter-turn fault detection for fault-tolerant control of induction motor

**Conference Proceedings:** Industrial Technology (ICIT), 2017 IEEE International Conference on

**Author:** Eshaan Ghosh

**Publisher:** IEEE

**Date:** March 2017

Copyright © 2017, IEEE

## LOGIN

If you're a [copyright.com](#) user, you can login to RightsLink using your copyright.com credentials. Already a [RightsLink](#) user or want to [learn more?](#)

## Thesis / Dissertation Reuse

**The IEEE does not require individuals working on a thesis to obtain a formal reuse license, however, you may print out this statement to be used as a permission grant:**

*Requirements to be followed when using any portion (e.g., figure, graph, table, or textual material) of an IEEE copyrighted paper in a thesis:*

- 1) In the case of textual material (e.g., using short quotes or referring to the work within these papers) users must give full credit to the original source (author, paper, publication) followed by the IEEE copyright line © 2011 IEEE.
- 2) In the case of illustrations or tabular material, we require that the copyright line © [Year of original publication] IEEE appear prominently with each reprinted figure and/or table.
- 3) If a substantial portion of the original paper is to be used, and if you are not the senior author, also obtain the senior author's approval.

*Requirements to be followed when using an entire IEEE copyrighted paper in a thesis:*

- 1) The following IEEE copyright/ credit notice should be placed prominently in the references: © [year of original publication] IEEE. Reprinted, with permission, from [author names, paper title, IEEE publication title, and month/year of publication]
- 2) Only the accepted version of an IEEE copyrighted paper can be used when posting the paper or your thesis on-line.
- 3) In placing the thesis on the author's university website, please display the following message in a prominent place on the website: In reference to IEEE copyrighted material which is used with permission in this thesis, the IEEE does not endorse any of [university/educational entity's name goes here]'s products or services. Internal or personal use of this material is permitted. If interested in reprinting/republishing IEEE copyrighted material for advertising or promotional purposes or for creating new collective works for resale or redistribution, please go to [http://www.ieee.org/publications\\_standards/publications/rights/rights\\_link.html](http://www.ieee.org/publications_standards/publications/rights/rights_link.html) to learn how to obtain a License from RightsLink.

If applicable, University Microfilms and/or ProQuest Library, or the Archives of Canada may supply single copies of the dissertation.

[BACK](#)
[CLOSE WINDOW](#)

Copyright © 2018 [Copyright Clearance Center, Inc.](#) All Rights Reserved. [Privacy statement](#). [Terms and Conditions](#). Comments? We would like to hear from you. E-mail us at [customercare@copyright.com](mailto:customercare@copyright.com)





# RightsLink®

[Home](#)
[Create Account](#)
[Help](#)


**Title:** 3-D Sub-Domain Analytical Model to Calculate Magnetic Flux Density in Induction Machines With Semiclosed Slots Under No-Load Condition

**Author:** Aida Mollaeian

**Publication:** Magnetics, IEEE Transactions on

**Publisher:** IEEE

**Date:** June 2017

Copyright © 2017, IEEE

**LOGIN**

If you're a [copyright.com](#) user, you can login to RightsLink using your copyright.com credentials.

Already a [RightsLink](#) user or want to [learn more?](#)

## Thesis / Dissertation Reuse

**The IEEE does not require individuals working on a thesis to obtain a formal reuse license, however, you may print out this statement to be used as a permission grant:**

*Requirements to be followed when using any portion (e.g., figure, graph, table, or textual material) of an IEEE copyrighted paper in a thesis:*

- 1) In the case of textual material (e.g., using short quotes or referring to the work within these papers) users must give full credit to the original source (author, paper, publication) followed by the IEEE copyright line © 2011 IEEE.
- 2) In the case of illustrations or tabular material, we require that the copyright line © [Year of original publication] IEEE appear prominently with each reprinted figure and/or table.
- 3) If a substantial portion of the original paper is to be used, and if you are not the senior author, also obtain the senior author's approval.

*Requirements to be followed when using an entire IEEE copyrighted paper in a thesis:*

- 1) The following IEEE copyright/ credit notice should be placed prominently in the references: © [year of original publication] IEEE. Reprinted, with permission, from [author names, paper title, IEEE publication title, and month/year of publication]
- 2) Only the accepted version of an IEEE copyrighted paper can be used when posting the paper or your thesis on-line.
- 3) In placing the thesis on the author's university website, please display the following message in a prominent place on the website: In reference to IEEE copyrighted material which is used with permission in this thesis, the IEEE does not endorse any of [university/educational entity's name goes here]'s products or services. Internal or personal use of this material is permitted. If interested in reprinting/republishing IEEE copyrighted material for advertising or promotional purposes or for creating new collective works for resale or redistribution, please go to [http://www.ieee.org/publications\\_standards/publications/rights/rights\\_link.html](http://www.ieee.org/publications_standards/publications/rights/rights_link.html) to learn how to obtain a License from RightsLink.

If applicable, University Microfilms and/or ProQuest Library, or the Archives of Canada may supply single copies of the dissertation.

[BACK](#)
[CLOSE WINDOW](#)

Copyright © 2018 [Copyright Clearance Center, Inc.](#) All Rights Reserved. [Privacy statement](#), [Terms and Conditions](#).  
Comments? We would like to hear from you. E-mail us at [customercare@copyright.com](mailto:customercare@copyright.com)



# RightsLink®

[Home](#)
[Create Account](#)
[Help](#)


**Title:** DNN predictive magnetic flux control for harmonics compensation in magnetically unbalanced induction motor

**Conference Proceedings:** Magnetics Conference (INTERMAG), 2017 IEEE International

**Author:** E. Ghosh

**Publisher:** IEEE

**Date:** April 2017

Copyright © 2017, IEEE

## LOGIN

If you're a [copyright.com](#) user, you can login to RightsLink using your copyright.com credentials. Already a RightsLink user or want to [learn more?](#)

## Thesis / Dissertation Reuse

**The IEEE does not require individuals working on a thesis to obtain a formal reuse license, however, you may print out this statement to be used as a permission grant:**

*Requirements to be followed when using any portion (e.g., figure, graph, table, or textual material) of an IEEE copyrighted paper in a thesis:*

- 1) In the case of textual material (e.g., using short quotes or referring to the work within these papers) users must give full credit to the original source (author, paper, publication) followed by the IEEE copyright line © 2011 IEEE.
- 2) In the case of illustrations or tabular material, we require that the copyright line © [Year of original publication] IEEE appear prominently with each reprinted figure and/or table.
- 3) If a substantial portion of the original paper is to be used, and if you are not the senior author, also obtain the senior author's approval.

*Requirements to be followed when using an entire IEEE copyrighted paper in a thesis:*

- 1) The following IEEE copyright/ credit notice should be placed prominently in the references: © [year of original publication] IEEE. Reprinted, with permission, from [author names, paper title, IEEE publication title, and month/year of publication]
- 2) Only the accepted version of an IEEE copyrighted paper can be used when posting the paper or your thesis on-line.
- 3) In placing the thesis on the author's university website, please display the following message in a prominent place on the website: In reference to IEEE copyrighted material which is used with permission in this thesis, the IEEE does not endorse any of [university/educational entity's name goes here]'s products or services. Internal or personal use of this material is permitted. If interested in reprinting/republishing IEEE copyrighted material for advertising or promotional purposes or for creating new collective works for resale or redistribution, please go to [http://www.ieee.org/publications\\_standards/publications/rights/rights\\_link.html](http://www.ieee.org/publications_standards/publications/rights/rights_link.html) to learn how to obtain a License from RightsLink.

If applicable, University Microfilms and/or ProQuest Library, or the Archives of Canada may supply single copies of the dissertation.

[BACK](#)
[CLOSE WINDOW](#)

Copyright © 2018 Copyright Clearance Center, Inc. All Rights Reserved. [Privacy statement](#), [Terms and Conditions](#). Comments? We would like to hear from you. E-mail us at [customercare@copyright.com](mailto:customercare@copyright.com)



# RightsLink®

[Home](#)
[Create Account](#)
[Help](#)


**Title:** DNN-Based Predictive Magnetic Flux Reference for Harmonic Compensation Control in Magnetically Unbalanced Induction Motor

**Author:** Eshaan Ghosh

**Publication:** Magnetics, IEEE Transactions on

**Publisher:** IEEE

**Date:** Nov. 2017

Copyright © 2017, IEEE

## LOGIN

If you're a [copyright.com](#) user, you can login to RightsLink using your copyright.com credentials. Already a RightsLink user or want to [learn more?](#)

## Thesis / Dissertation Reuse

**The IEEE does not require individuals working on a thesis to obtain a formal reuse license, however, you may print out this statement to be used as a permission grant:**

*Requirements to be followed when using any portion (e.g., figure, graph, table, or textual material) of an IEEE copyrighted paper in a thesis:*

- 1) In the case of textual material (e.g., using short quotes or referring to the work within these papers) users must give full credit to the original source (author, paper, publication) followed by the IEEE copyright line © 2011 IEEE.
- 2) In the case of illustrations or tabular material, we require that the copyright line © [Year of original publication] IEEE appear prominently with each reprinted figure and/or table.
- 3) If a substantial portion of the original paper is to be used, and if you are not the senior author, also obtain the senior author's approval.

*Requirements to be followed when using an entire IEEE copyrighted paper in a thesis:*

- 1) The following IEEE copyright/ credit notice should be placed prominently in the references: © [year of original publication] IEEE. Reprinted, with permission, from [author names, paper title, IEEE publication title, and month/year of publication]
- 2) Only the accepted version of an IEEE copyrighted paper can be used when posting the paper or your thesis on-line.
- 3) In placing the thesis on the author's university website, please display the following message in a prominent place on the website: In reference to IEEE copyrighted material which is used with permission in this thesis, the IEEE does not endorse any of [university/educational entity's name goes here]'s products or services. Internal or personal use of this material is permitted. If interested in reprinting/republishing IEEE copyrighted material for advertising or promotional purposes or for creating new collective works for resale or redistribution, please go to [http://www.ieee.org/publications\\_standards/publications/rights/rights\\_link.html](http://www.ieee.org/publications_standards/publications/rights/rights_link.html) to learn how to obtain a License from RightsLink.

If applicable, University Microfilms and/or ProQuest Library, or the Archives of Canada may supply single copies of the dissertation.

[BACK](#)
[CLOSE WINDOW](#)

Copyright © 2018 Copyright Clearance Center, Inc. All Rights Reserved. [Privacy statement](#), [Terms and Conditions](#). Comments? We would like to hear from you. E-mail us at [customercare@copyright.com](mailto:customercare@copyright.com)

## VITA AUCTORIS

NAME:	Eshaan Ghosh
PLACE OF BIRTH:	Burnpur, West Bengal, India
YEAR OF BIRTH:	1990
EDUCATION:	Haldia Institute of Technology, India 2008 – 2012, B.Tech  Burnpur Riverside School, India 2006 – 2008  St. Patrick's H.S. School, India 1995 - 2008